Neuroprosthetic Technologies to Evaluate and Train Leg Motor Control in Neurologically Impaired Individuals

Thèse N° 9339

Présentée le 5 avril 2019

à la Faculté des sciences de la vie
Unité du Prof. Courtine
Programme doctoral en neurosciences

pour l'obtention du grade de Docteur ès Sciences

par

Camille Georgette Marie LE GOFF-MIGNARDOT

Acceptée sur proposition du jury

Prof. D. N. A. Van De Ville, président du jury
Prof. G. Courtine, directeur de thèse
Prof. S. J. Harkema, rapporteuse
Prof. F. Lacquaniti, rapporteur
Prof. F. C. Hummel, rapporteur

2019

ÉCOLE POLYTECHNIQUE
FÉDÉRALE DE LAUSANNE

La technique résout les problèmes et apporte des satisfactions mais elle n'est qu'un moyen et reste pauvre si on la sépare de l'esprit qui la guide.

Gaston Rébuffat

Thesis Abstract

Spinal cord injury (SCI) disrupts or even abolishes many essential sensorimotor and autonomic functions. Consequently, individuals with SCI can face decades with permanent disabilities. Advances in clinical management have decreased morbidity and improved outcome, but no clinical trial has yet demonstrated the efficacy of a repair strategy for improving recovery from SCI. In the past decade, Courtine's laboratory has developed neurotechnologies that restored volitional control of locomotion in animal models of SCI. The intervention acts over two-time windows. In the short-term, the delivery of epidural electrical stimulation (EES) targeting the posterior roots of the lumbar spinal cord with a timing that mimics the natural activation of the spinal cord enables stepping in otherwise paralyzed rats. In the long-term, the delivery of this targeted EES with intensive robot-assisted overground locomotor training triggers a re-organization of descending pathways that reestablished voluntary control of the previously paralyzed legs, even without electrical stimulation. These encouraging results in animal models led to a translational program that aims to transfer these neurotechnologies and concepts to clinical applications. My contribution to this translational research program forms the core of my thesis, which is articulated into three sections.

In the first section, I document a software that I developed in order to enable a comprehensive yet semi-automated analysis of kinematics and muscle activity underlying locomotor functions in humans. This toolbox allows to (i) evaluate gait features of individuals with neuro-motor deficits, (ii) quantify locomotor performance compared to healthy people or to monitor changes in locomotion in different experimental conditions or over the time course of interventions, and (iii) automatically generate comprehensive gait reports that are immediately understandable by scientists and clinicians.

The second section introduces a paradigm shift in robotic postural assistance: the gravity-assist. We demonstrated the detrimental impact of high levels of body weight support on gravity-dependent interactions during standing and walking. We developed a gravity-assist algorithm that fine-tunes the forward and upward body weight support to reestablish these interactions based on the residual capacities of

each patient. We validated this personalized gravity-assist in 30 individuals with SCI or stroke. Compared to other conditions of support, the gravity-assist enabled all the participants to produce locomotion with improved performance. This platform establishes refined conditions to train locomotor functions in a safe yet ecological environment that empowers overground locomotion.

The third section reports the development of targeted EES in three patients with chronic SCI, and the impact of an intensive 5-month rehabilitation program with gravity-assist and targeted EES on the recovery of motor functions. The key findings can be summarized as follows: (i) We established detailed procedures to configure targeted EES protocols that immediately enabled voluntary control of weak or paralyzed muscles, (ii) Targeted EES boosts the residual supraspinal inputs to the lumbar spinal cord, enabling all three participants to walk for extensive period of time and to accommodate their gait to task-specific requirements, (iii) Locomotor performance improved over the course of the rehabilitation program, (iv) All participants regained voluntary control over previously paralyzed muscles without stimulation, which translated into durable improvements in neurological function.

These combined results establish the proof-of-concept on the therapeutic potential of targeted EES and intensive rehabilitation enabled by a smart robotic postural assistance to restore locomotion after SCI. Together with similar results obtained in the United States in patients with severe SCI, our findings are establishing a pathway towards the development of a viable treatment to support motor functions and improve neurological recovery after SCI.

Keywords

Spinal cord injury, epidural electrical stimulation, human locomotion, leg motor control, neuroprosthetics, neuro-biomechanics, spatio-temporal neuromodulation, robotic postural assistance, gravity-assist, comprehensive gait analysis, translational research, targeted intervention.

Résumé de la Thèse

Les lésions traumatiques de la moelle épinière conduisant à la paraplégie ou tétraplégie affectent grandement la qualité de vie des personnes touchées. D'un jour à l'autre, certaines fonctions sensorielles, motrices ou autonomes sont partiellement ou totalement perdues. La moitié des personnes concernées ne pourront récupérer leurs fonctions en suivant les thérapies actuelles. Lors de cette dernière décennie, le laboratoire du professeur Courtine a développé des neuro-technologies permettant de retrouver le contrôle volontaire de la marche chez plusieurs modèles animaux de lésion de la moelle épinière. Des stimulations électriques épidurales mimant l'activité naturelle de la moelle épinière au niveau lombo-sacré permettent aux animaux paralysés de marcher. Ces stimulations combinées avec un entrainement intensif de la marche volontairement initiée pendant plusieurs semaines engendrent une récupération du contrôle volontaire de la marche grâce à une réorganisation des circuits neuronaux descendants. Ces résultats ont motivé le transfert des technologies et concepts vers une application clinique. Ma contribution à ce programme de recherche translationnel forme le coeur de ma thèse, articulée en trois sections.

La première section présente le software que j'ai développé afin de permettre une analyse à la fois complète et automatique de la cinématique et de l'activité musculaire durant la marche chez l'homme. Ce software permet (i) d'évaluer les caractéristiques de la marche des personnes ayant un déficit neuro-moteur, (ii) de la comparer à celles des personnes saines ou d'observer les changements dans la locomotion lors de différentes conditions expérimentales ou au cours d'une thérapie, et (iii) de générer automatiquement des rapports d'analyse quantifiée de la marche, directement compréhensible par les scientifiques et cliniciens.

La seconde section apporte une nouvelle approche dans le domaine de l'assistance posturale robotique : le "gravity-assist". Nous avons en effet démontré l'impact négatif du soutien corporel sur le comportement locomoteur lorsque l'assistance est uniquement donnée verticalement. En conséquence, j'ai développé un algorithme qui détermine le support vertical et horizontal approprié en fonction des capacités résiduelles propres à chaque individu, permettant ainsi de rétablir un comportement moteur naturel. Le "gravity-assist" a été validé chez une trentaine d'individus ayant

eu une lésion de la moelle épinière ou un accident vasculaire cérébrale. Comparé à d'autres conditions de support, le "gravity-assist" a permis aux individus les plus sévères de re-marcher et aux autres individus d'améliorer la qualité de leur marche. Ce système robotique offre les conditions nécessaires pour entrainer la fonction locomotrice dans un environnement écologique, offrant aux participants de se passer de leurs moyens auxiliaires d'aide à la marche.

La troisième et dernière section présente les résultats obtenus chez trois individus avec une lésion médullaire chronique ayant suivi un programme de réhabilitation intensif de cinq mois bénéficiant du "gravity-assist" combiné avec l'application de stimulations électriques épidurales. Lors de cette intervention, nous avons établi une procédure pour configurer le protocole de stimulation électrique ciblé qui a immédiatement élicité le contrôle volontaire des muscles affaiblis ou paralysés. Ce programme de stimulation a permis à chacun des participants de marcher pendant de longues périodes d'entrainement et d'adapter leur marche selon la tâche. Leur qualité de marche et leur endurance s'est améliorée au cours de la réhabilitation. Enfin, tous les participants ont amélioré leurs scores cliniques même sans stimulation électrique.

La combinaison de ces résultats établit la preuve de concept du potentiel thérapeutique des stimulations électriques ciblées combinées avec un programme de réhabilitation intensive afin de récupérer des fonctions locomotrices perdues à la suite d'une lésion médullaire. De concert avec des résultats rapportés récemment par des équipes nord-américaines avec des individus sévèrement atteints, nos observations ouvrent une nouvelle voie vers le développement d'un traitement viable pour améliorer la récupération des fonctions partiellement ou totalement perdues suite à une lésion médullaire.

Mots-clefs

Lésion de la moelle épinière, stimulation électrique épidurale, locomotion humaine, neuro-prosthétique, neuro-biomécanique, neuro-modulation spatio-temporelle, assistance posturale robotique, gravity-assist, analyse quantifiée de la marche, recherche translationnelle, intervention thérapeutique ciblée.

Acknowledgements

I first would like to express my gratitude to Prof. Courtine for opening me the doors of his laboratory and giving me the opportunity to carry out my PhD thesis in this outstanding, multidisciplinary environment. Over the past six years, Prof. Courtine has provided scientific guidance and transmitted his strong enthusiasm. I will always be impressed by all the achievements reached in his laboratory going from the rodents to the humans and all the energy and time he gives to bring our scientific findings out to the community. I had the incredible luck to arrive in the laboratory at the very beginning of an amazing adventure: the translation of the neuro-technologies and concepts developed on animal models to clinical application for humans.

My sincere thanks also goes to the second head of the clinical study, Prof. Bloch, our talented neurosurgeon, who let me enter the operating room; allowing me to follow our participants all the way from study enrolment, implantation surgery, numerous evaluations and rehabilitation.

I would like to thank my thesis committee: Prof. Harkema, Prof. Lacquaniti, Prof. Hummel and Prof. Van de Ville, for reading and revising this manuscript and for coming from various places to Geneva to examine my work.

My sincere thanks to Prof. Ijspeert, my mentor, for his valuable listening and precious time. We had the opportunity to collaborate on a passive walker model attached to the robotic-assistance, with his PhD student Jessica. Thank you for your help on this project.

Thank you to my master students: Fanny, Florian, Suzanne, Charlotte, who contributed to this journey. Thank you to Roman, who enhanced the automatic generation of the gait reports and adapted it to the small set of kinematic markers.

Naturally, I would like to thank the study core team, with whom I spent countless hours of recording and analysis. Good luck to the new(?), talented generation of PhD students, who are taking over the clinical study: Robin, Salif and Miro. Thank you to

Dr. Carda for his valuable help in patients' recruitment for the study about the robotic-assistance and for the clinical follow up of our implanted participants.

A huge thanks to Molywan, our amazing study nurse/Canadian, to Laura, our incredible technical assistant, and to the team of physiotherapists with whom I spent so much time and fun while training the patients: Isabelle, Muriel, Maryline, Manon, Moïra.

Thank you to all the people having directly or indirectly helped for the clinical study.

Special thanks to our participants. To the ones who tested for the first time the robotic-assistance, helped me to understand how it affects their gait behavior, and gave me so precious, warm feedback. To the pioneer ones who have accepted the challenge of five intensive months of rehabilitation paved with countless evaluations and have even ask for an extension to the rehabilitation program. Never stop fighting!

I also would like to thank Ed so full of energy, the future expert of the Parkinson's disease. It's a great pleasure to work with you on the data from Bordeaux. My sincere thanks to Prof. Bezard for supporting us on this work.

I would never forget to thank my friends for their smile, their constant attention, our passionate debate on everything and anything, their jokes enlightening my days. I would like to individually express them my gratefulness but I would then never finish on time! Thank you Camille, Ayah, Kat, Sibylle, Mica, Myriam, Sabry, Elodie, Jérôme, Léo, Laëti, Misha, Kay, Charlotte, Molywan, Anne, Moïra, Robin.

Special thought for my twin-in-lab, Selin.

My last and supreme thanks are for my family and family-in-law who always supports me at any hour of the day. Special thanks to my brother for his capacity to make visible concepts and his gift for piano, filling soundscape with classical music to which the coldest heart cannot remain insensitive. To my parents for their love, their concern, and their wise advice. Their trust in me gave me self-confidence, which is the most valuable gift they could offer me. To my grand-parents who offered me the perfect place where to write this thesis and prepare the oral presentation. To my father-in-law for his quince paste, a very precious help during this thesis. To my mother-in-law for her never-flagging positivity.

To my husband, my source of energy and so much more.

Table of Contents

Thesis Abstract 5

Résumé de la Thèse 7

Acknowledgements 9

List of Abbreviations 19

Background & State of the Art 21
- Spinal Cord Injury Problematic . . . 21
- Strategies for Locomotor Recovery . . . 24
- Reactivation of Dormant Spinal Networks . . . 25
- Activity-Based Rehabilitation . . . 26
- Robotic Postural Assistance . . . 27
- Clinical Studies . . . 28

Synopsis & Aims of the Thesis 31

1. Toolbox for Comprehensive Analyses 35
- Quantitative Gait Analysis . . . 36
- Multidimensional Analysis . . . 41
- Graphical User Interface . . . 43
- Automatic Gait Report Generation . . . 44
- Discussion . . . 46

2. Targeted Robotic Postural Assistance 49
- Abstract . . . 51
- Introduction . . . 52
- Materials and Methods . . . 54
  - Study Design . . . 54
  - Participants . . . 55
  - Neurorobotic Platform . . . 56

Data Acquisition and Analysis 60
Statistical Analysis 64
Extended Experimental Protocols 64
Results 70
Properties of the Neurorobotic Platform 70
Impact of Upward and Forward Forces on Posture and Gait 71
Gravity-Assist: Personalization of Upward Force 76
Gravity-Assist: Personalization of Forward Force 78
Gravity-Assist: Validation 78
Gravity-Assist: Improvement of Locomotor Performance after SCI and Stroke 81
Gravity-Assist: Improvement of Locomotor Performance after a one-hour Training Session 84
Gravity-Assist: Training of Skilled Locomotion and Dynamic Balance . 86
Discussion 88
Conclusion & Perspectives 91

3. Targeted Neuroprosthesis to Restore Walking 93
Abstract 95
Introduction 96
Materials & Methods 98
Clinical Study and Participants 98
Surgical Implantation 100
Personalised Computational Model 102
Single-Pulse EES 106
Evaluation of Single-Joint Torque Production 107
Technological Framework 108
Configuration of Targeted EES 111
Clinical Evaluations 115
Study Extension and Technologies for Home Use 117
Data Processing 120
Results 124
Targeted Neurotechnologies and Surgery 124
EES enables Control of Paralysed Muscles 127
EES modulates Cortical Activity 129
Spatiotemporal EES enables Walking 131
Continuous EES is poorly Effective 135
Rehabilitation improves Walking with EES 137

Neurological Recovery without EES 138
Support of Activities in the Community 141
Discussion 142
Conclusion & Perspectives 143

Integration & Perspectives 147

Publications & Contributions 167
Journal Publications 167
Conference Proceedings 169
Patent 170

A Gait parameters 173

B Gait report 177

List of Figures

1 Spinal cord organization 22
1.1 Spatio-temporal parameters 37
1.2 Joint and elevation angles 38
1.3 Trunk balance 38
1.4 Inter-limb coordination 39
1.5 Muscle activity 40
1.6 Principal component analysis 42
1.7 Toolbox for quantitative gait analysis 43
1.8 Quantitative gait analysis 45
2.1 A targeted robotic postural assistance to adapt external constraints to patient-specific residual abilities 49
2.2 Attachment to the robotic support system 58
2.3 Transparent mode of the robotic support system 59
2.4 Representation and processing of kinematic and muscle activity recordings 62
2.5 Technological framework of the multidirectional gravity-assist 70
2.6 Interaction between upward and forward forces during standing and walking 72
2.7 Impact of upward and forward forces on body kinematics and muscle activity 73
2.8 Interaction between upward and forward forces during locomotion on a treadmill 75
2.9 Design of the MGA algorithm 77
2.10 Validation of MGA algorithm in individuals with SCI or stroke 80
2.11 Performance of the MGA to enable or enhance locomotor control after SCI 82
2.12 Performance of the MGA to enable or enhance locomotor control after stroke 83
2.13 Gait training session overground with MGA or on a treadmill with upward support 85

2.14 The MGA allows training of skilled locomotor and postural activities . 87
2.15 RYSEN® 92
3.1 Surgical procedure 101
3.2 Identification of electrode configurations to target selected posterior roots 105
3.3 Technological framework 110
3.4 Configuration of spatiotemporal EES to enable walking 113
3.5 Targeted modulation of muscle activity during walking 115
3.6 Performance of closed-loop spatiotemporal EES to enable walking and cycling outside the laboratory 118
3.7 Technology and study design 124
3.8 Configuration of targeted EES 125
3.9 Spatial selectivity of targeted electrode configurations 127
3.10 Single-joint movements enabled by targeted EES 129
3.11 Modulation of EEG activity during volitional contraction of leg muscles 130
3.12 Configuration of spatiotemporal EES for walking 132
3.13 Voluntary control of adaptive and sustained locomotion 133
3.14 Volitional adaptations of walking during otherwise unchanged spatiotemporal EES 135
3.15 Comparison between continuous and spatiotemporal EES during overground walking 136
3.16 Rehabilitation program and evolution of walking capacity 137
3.17 Rehabilitation mediates neurological recovery 138
3.18 Changes in muscle mass and quality, and recovery of voluntary movements 140
3.19 Spatiotemporal EES in ecological settings 141

List of Tables

1 ASIA Impairment Scale 23
2.1 Characteristics of the subjects 56
2.2 List of parameters computed during walking and standing 61
3.1 Neurological status of the three participants 99
3.2 Muscle contributions 121
3.3 Coefficients $W_{i,j}$ 122

List of Abbreviations

AIS	ASIA Impairment Scale
ASIA	American Spinal Injury Association
BWS	Body Weight Support
CHUV	Centre Hospitalier Universitaire Vaudois – University Hospital of Vaud
CoM	Center of Mass
CoP	Center of foot Pressure
CSAs	Cross-Sectional Areas
CSF	Cerebrospinal Fluid
CT	Computed Tomography
EEG	Electroencephalography
EES	Epidural Electrical Stimulation
EMG	Electromyography
ERD	Event-related desynchronization
ERS	Event-related resynchronization
FIM	Functional Independence Measure
GRFs	Ground Reaction Forces
GUI	Graphical User Interface
HU	Hounsfield units
IMU	Inertial Measurement Unit
IPG	Implantable Pulse Generator
MGA	Multidirectional Gravity-Assist
MRI	Magnetic Resonance Imaging
NRPA	NEUWalk Research Programmer Application

PC	Principal Component
PCA	Principal Component Analysis
RMSE	Root Mean Square Error
SCI	Spinal Cord Injury
SPTM	Sensing Programmer Telemetry Module
SUVA	Swiss rehabilitation hospital in Sion
WISCI-II	Walking Index for Spinal Cord Injury II

Background & State of the Art

"The international symbol of disability is the wheelchair and the stereotype of a person with disability is a young man with paraplegia. While these images are very familiar, at the same time we know that this is not an accurate picture of the diversity of global disability. Whereas 15% of the population are affected by disability, less than 0.1% of the population have spinal cord injury. However, spinal cord injury is particularly devastating."

Preface of World Health Organization report on International Perspectives on Spinal Cord Injury [1].

Spinal Cord Injury Problematic

In Switzerland, 130 individuals per year incurred a traumatic spinal cord injury (SCI), 75% of these individuals are men [2]. The European estimates of annual traumatic SCI incidence for Switzerland is 18 per million population (95% confidence interval 16.9–19.2), which places the country at an intermediate position with respect to the other European countries – the lowest incidence is found in Denmark with 8.3 per million and the highest in Greece with 33.6 per million. In North America, the annual incidence rate is augmented to 39 per million [3]. Global prevalence ranges between 236 and 1,009 per million depending on the source [4]. Sports, leisure and transport-related injuries are the most common causes of traumatic SCI in young people – 16 to 30 years old, 25% of the injured population –, while falls is the main cause for the elderly with 11% of the injured population aged more than 75 years old [2].

Albeit rare compared to other neurological disorders, the traumatic SCI tremendously impacts the personal quality of life. From one day to the next, the sensory, motor or autonomic function are fully or partially impaired. Less than one percent of injured individuals undergo a complete neurological recovery by the time of hospital discharge. Depending on the location, shape and type of the lesion in the spinal

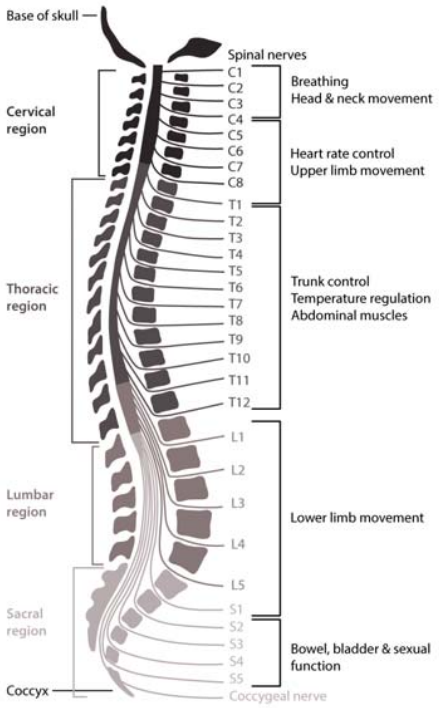

Figure 1 – Spinal cord organization along the backbone, with the major functions of the spinal nerves, adapted from World Health Organization report on International Perspectives on Spinal Cord Injury, 2013 [1].

cord, the resulting impairment is more or less incapacitating. The severity of spinal cord injury is characterized by lesion level and lesion completeness. The highest incidence rate is incomplete tetraplegia (45.8%), followed by incomplete paraplegia (20.9%), complete paraplegia (19.7%) and complete tetraplegia (13.2%) [5]. A lesion at cervical level leads to tetraplegia, while a thoracic, lumbar or sacral lesion leads to various degree of paraplegia (Figure 1). The American Spinal Injury Association (ASIA) developed the ASIA Impairment Scale (AIS) to assess the lesion severity. This scale ranges from AIS-A for motor and sensory complete impairment to AIS-D for motor incomplete impairment with a voluntary control of at least half of the key muscles or AIS-E for normal function of the sensory-motor system (Table 1). Key muscles are graded from 0, in case of total paralysis, to 5, if able to produce active movement, full range of motion against gravity and full resistance in a functional muscle position expected from an otherwise unimpaired person, to determine the motor subscores, while key sensory points are graded from 0, in case of absence of sensation to 2, in case of normal sensation, to determine the sensory subscores.

Following an injury graded AIS-C or D, the recovery is more substantial but highly variable compared to the most affected individuals (motor-complete, AIS-A and B). In average, the main spontaneous recovery happens during the three months post-injury, while a small amount of recovery can still be seen up to 18 months post-

AIS Scale	Definition	Description
AIS-A	Motor & sensory complete	No sensory or motor function is preserved in the sacral segments S4-5.
AIS-B	Sensory incomplete	Sensory but not motor function is preserved below the neurological level and includes the sacral segments S4-5, and no motor function is preserved more than three levels below the motor level on either side of the body.
AIS-C	Motor incomplete	Some motor preservation, but the majority of key muscles below the level of injury are graded less than 3.
AIS-D	Motor incomplete	Muscle grade is 3 or greater in the majority of muscles below the lesion.
AIS-E	Normal	Sensory and motor functions are normal.

Table 1 – ASIA Impairment Scale, adapted from Kirshblum et al. [6].

injury [7]. Roughly half of the individuals who start a rehabilitation with some residual movement capacity regains the ability to walk over short distances but is still dependent on assistive devices.

The resulting motor disorders leave the individuals facing various environmental and social constraints as they henceforth rely on assistive devices such as wheelchairs to get around. Besides this substantial reduction in their functional autonomy, these individuals have to cope with the loss of bowel and/or bladder control, exaggerated reflexes or spasticity, changes in sexual function and pain sensation. Due to their multisystem impairments, they can develop several complications, particularly infections, respiratory complications and pressure sores. Their life expectancy is lower than the normal population and they are at higher risk from age-related diseases, including cardiovascular disease and infection.

In addition to the dramatic loss in individual's quality of life, the social and medical cost is huge for the patient relatives and the society. Two-thirds of the SCI people have no employment 20 years after their injury [5]. For paraplegia (AIS-A, B and C), in the United States, the first year cost is estimated at 526 k$; 70 k$ are then required per subsequent year because of the everyday assistance needed for a lifetime. This represents an estimated lifetime cost of 2.3 million dollars for someone injured at aged of 25 [5]. Winslow et al. reported the fact that SCI is the second most expensive condition to treat, with mean acute-care hospital charges of 53 k$, behind the respiratory distress syndrome of infants [8].

Enhanced recovery in functional autonomy, such as walking capacity, would reduce the socio-economic cost and, in parallel, would increase the personal quality of life. A therapy allowing an improved recovery is therefore of primary interest.

Strategies for Locomotor Recovery

To date, chronic SCI is incurable. There are only minimally effective pharmacological and surgical procedures in place to treat it [9]. In Switzerland, following an accident, the injured individual is treated in emergency in a specialized center. The surgery aims to decompress the spinal cord, close the open wounds, and stabilize the backbone in the adequate position. A surgical reconnection or suturing of nervous circuits of the severed spinal cord is nowadays impossible. Therefore, very rigorous health care is needed to prevent from and treat immediate subsequent diseases and damages, in particular bloodstream instability, thrombosis, pneumonia, eschars, urinary tract infection, bowel obstruction, joint stiffening, muscular atrophy, osteoporosis and depression.

In a first attempt, rehabilitation sessions are started as early as possible to maintain and recover a maximum of functions, with professional and social integration as the main objective. However, even after these sessions of six to twelve months, more than half of the injured people keep using a wheelchair for the rest of their lives, while a significant number of the less severe cases suffers from important motor impairments [10]. When the situation turns out to be chronic, **autonomy** becomes the main goal of rehabilitation centers. Strong efforts are done on learning transfers between bed and wheelchair, preventing eschars and other skin issues, practicing bladder probing, and the auxiliary aids for daily life. Though, the primordial objectives for paraplegic people is to **regain control** over their body. Unfortunately, current therapies provide only limited solutions for the restoration of motor control and very few centers offer physical activity of the full body, including paralyzed limbs, in order to ensure a minimal level of activity to stimulate the different functions of the organism and reduce secondary effects. The Swiss Recovery Center is a unique center in Switzerland that proposes a long-term, post-rehabilitation follow-up with physical activity, two to three times per week with a minimum of 150 minutes per week as recommended by ESSA (Exercise and Sports Sciences Australia, 2017). With few other centers over the world, they respond to a lack in long-term follow-up of the injured individuals and meet the need of exercises engaging the full-body in order to maintain individual's residual capacities. Still, the actual rehabilitation programs offer limited improvement in individual's function.

Yet, numerous novel therapeutic approaches are emerging [11] in three axes of research: cell or stem-cells implantation (adult neural stem cells: Pathway study by StemCell Inc. (stopped), Neuralstem Inc. at Sanford Stem Cell Clinical Center, In-

Vivo Neuro-Spinal Scaffold by InVivo Therapeutics (halted in July 2017); olfactory cells and nerve graft (single participant) [11]; Schwann cells (clinical trial phase I completed) [12]; autologous bone-marrow mesenchymal stem-cells intrathecal injection (clinical trial phase II completed) [13]), neurotransmitter delivery [14] or scar and growth inhibitors reduction ([15, 16]; chondroitinase, to degrade the scar and promote growth [17]; NoGo Trap protein by ReNetX Bio (clinical trial phase I-II to be started late 2018)), and transcutaneous or epidural electrical stimulation [18, 19, 20]. All of these diverse approaches have the common goal of guiding the reestablishment of the communication in the central nervous system through the lesion. While some approaches require more time and research development to be translated to medical practice, electrical stimulation to re-activate dormant spinal networks seems promising [21].

Reactivation of Dormant Spinal Networks

After a severe lesion, communication between supraspinal centers and spinal circuits is disrupted and the spinal neuronal networks below the injury enter in a depressed state [14, 22]. Over the past years, a major research focus has been to promote the sprouting of spared fibers and the regeneration of the severed ones. Experiments on pre-clinical models with incomplete SCI evidenced that the injured spinal cord retains the potential for functional repair [23, 24, 25, 26, 27, 28, 29]. The dormant, disconnected spinal cord is still able to produce motor patterns to stand or walk [22, 30]. Rodents [24], non-human primates [28] as well as humans [31] show spontaneous recovery with partial spinal cord damage. However, the translation of cellular and molecular strategies from pre-clinical models with small SCI to people with severe paralysis may produce only small improvements insufficient to improve the quality of life and remains a challenge. Scar and growth inhibitors reduction strategies to improve regeneration such as Anti NogoA antibodies [29, 32] and the enzyme chondroitinase [33, 34] reach the growth of a limited number of neurons and over a limited distance. A recent and promising study [15] demonstrated in rodents that the combination of three factors is necessary for axon growth across a complete SCI: neuron intrinsic growth capacity, growth-supportive substrate and chemoattraction. The propriospinal axons regrew across the lesion core and formed functional synapses with the spared neural tissue below the lesion. But, for the moment, the link between regeneration and return of function remains unknown.

Still, spared fibers generally remain, connecting the spinal cord below the injury

to the supraspinal regions. Consequently, in the past decade, main hopeful efforts are focused on developing neuromodulation paradigms to strengthen the flow of information going through the residual connections and to tune the physiological state of spinal circuits to a level sufficient for standing or walking to occur. Standing and stepping were shown to be facilitated by strategies including electrical stimulations of the muscles [35, 36], electrical stimulation of the dorsal roots [37], epidural electrical stimulation (EES) of the spinal cord [38, 39, 40, 41], or intraspinal electrical stimulation [36, 37], and with pharmacological agents [19, 42, 43, 44, 45, 46]. Among these approaches, EES seems the most efficient and safest method to reactivate the dormant spinal networks [21].

EES delivered with an electrode array implanted over the lumbo-sacral region of the spinal cord enabled motor control in pre-clinical models and in humans with severe SCI [19, 30, 47]. Continuous EES[1] can produce stepping or enable standing in rats [44, 48], cats [49], and humans [30]. The mechanisms activated by EES to facilitate motor control are not yet fully understood but electrophysiological recordings [50] and computer simulations [51, 52, 53] suggest that EES recruits posterior root fibers at their entry into the spinal cord that, then, engage the spinal circuits.

Activity-Based Rehabilitation

Nonetheless, EES is not sufficient to help long-term recovery of locomotion alone, but coupling EES to activity-based rehabilitation can trigger long-term recovery. Indeed, activity-based therapies have been successful on cat models [54, 55] and were tested on humans with partial SCI [56, 57, 58, 59]. Activity-based therapies exploit two critical properties of the motor infrastructure. One property is the intrinsic capacity of the sensorimotor circuits within the lumbosacral spinal cord to generate effective postural and locomotor tasks [19, 54, 60, 61]. The second property is the ability of repetitive sensory patterns associated with physical training to steer useful functional plastic changes in caudal spinal networks and spared descending fibers [19, 47, 62]. However, from the best of our knowledge, functional improvement by locomotor training alone such as overground walking has been very limited in people with a low lower-limb motor score after their SCI, supposedly due to the insufficient engagement of the spinal circuits during manual assistance [31, 63].

[1] Continuous EES (also called tonic EES) is the delivery of a train of EES for which the intensity and frequency is maintained overtime, irrespective of the gait cycle phase. Its counterpart is spatio-temporal EES (also called targeted EES) where the intensity and frequency of the stimulation trains are modulated according to the phase of the gait cycle.

Consequently, a promising strategy to enhance the efficacy of activity-dependent rehabilitative therapy in severely affected individuals is to develop interventions to induce locomotor permissive states during training [19,30,47]. Indeed, a key study has tested EES in a pioneer individual with chronic motor complete paralysis [30] and has been confirmed by a second study including three more individuals [22]. While they received continuous EES, participants were asked to daily practice intentional movement during about one hour. Following the rehabilitation program, participants were able to stand for several minutes and to voluntarily move their legs, which suggest that continuous EES coupled to personalized training triggers plastic changes in people with chronic motor complete SCI. Additionally, there is strong evidence that gait rehabilitation should be performed overground with adequate support conditions to enable highly functional states [64].

Robotic Postural Assistance

To permit overground walking, robotic postural assistance brings a safe environment to people with neuro-motor disorders. Indeed, robot-mediated training plays a crucial role in the therapy as it provides the framework for free overground walking and active participation. Contrary to treadmill session, where an automated gait pattern is produced – the legs are mainly driven by sensory feedbacks or are actuated by a physiotherapist or an exoskeleton –, the robot-assisted overground session requires a more important involvement from the participant during the motor task. This approach engages cortical neurons and forces connections between the brain or brainstem and the spinal region below the lesion in order to start motion, as shown on the rodent model [65, 66].

A robotic postural neuroprosthesis for rats has been successfully developed by U. Keller and H. Vallery [67], immediately enabling skilled locomotion in SCI rats while promoting active participation during training. An analogous smart trunk support system, TheFLOAT®, was developed for rehabilitation in human beings [68]. This robotic device offers four degrees of freedom, enabling as well free walking in any direction as passing obstacles. It can deliver active body weight support for severely motor impaired subjects or simply act as a transparent safety belt. With the appropriate trunk support, the participants can be released from their habitual assistive device, enabling them to experience locomotion with free upper limb movements, dynamic balance regulation, and gravity-dependent gait interactions.

Clinical Studies

Nowadays, the challenge is to translate the developed strategies on pre-clinical models to prevailing human therapy in order to improve motor recovery after a SCI. While some strategies require more time and research development to be translated to medical practice, EES combined with an intensive, active, robot-assisted rehabilitation training seems promising. Over the past decade, electrochemical neuromodulation of spinal circuits along with robot-mediated training procedures have shown the ability to promote extensive and ubiquitous neuroplasticity that restored locomotion in pre-clinical models of SCI [69].

Several clinical studies are currently exploiting this approach. In the University of Louisville, Dr. Harkema combined a long period of intensive training with continuous EES in people with chronic, motor complete SCI (AIS-A or B). A pilot participant has regained voluntary motor control with EES [30], followed by three other participants [22]. More recently, she showed an improvement on overground locomotor performance in four participants with EES switched on, after an intensive training with continuous EES [70]. At the Mayo clinic (Minnesota), Dr. Zhao and Dr. Lee investigated multi-modal rehabilitation, i.e. dynamic task-specific training, with continuous EES on a participant with a chronic, complete SCI [71]. After 43 weeks of training, the participant was able to produce independent standing and stepping with EES switched on. Along the same path, Dr. Darrow is starting a study named E-STAND (NCT03026816), in which 100 participants with chronic, motor complete SCI (AIS-A or B) will be enrolled. The presumed improvement in autonomic function due to EES-enabled training of leg volitional movement will be evaluated.

In this context, our laboratory has prepared a clinical study (NCT02936453), combining also EES with intensive rehabilitation. Still, we explore a novel approach in EES delivery, closer to the natural activation of the spinal cord during complex motor tasks, such as walking, that requires different muscle synergies to be activated at different timing. For this purpose, we developed a neuroprosthesis enabling real-time spatio-temporal modulation of EES. Tested on the rodent and non-human primates [65, 72], we now translate this technology to human beings. Combining spatiotemporal EES with overground, robot-assisted neurorehabilitative and engaging physical training, we hypothesize that these synergistic technologies will improve standing and walking capacities in participants with chronic, incomplete SCI, who, even with the most intensive current rehabilitative treatments, have not recovered the ability to stand or walk independently.

Synopsis & Aims of the Thesis

Altogether, the epidural electrical stimulation (EES) of the spinal cord, the postural robotic assistance and a participative locomotion rehabilitation are essential to promote activity-dependent neuroplasticity after a traumatic spinal cord injury (SCI) leading to paraplegia. Accordingly, a novel therapeutic approach has been designed and refined in our laboratory. To assess its efficacy, a feasibility clinical study in humans with chronic spinal cord injury has started in July 2016: the STIMO study entitled *Efficacy of Spinal Epidural Electrical Stimulation (EES) in combination with Robot-assisted Neurorehabilitation in Patients with Spinal Cord Injury* (clinicaltrial.gov identifier: NCT02936453). Combining targeted epidural electrical stimulation with overground, robot-assisted neuro-rehabilitative and engaging physical training, we hypothesize that these synergistic technologies improve standing and walking capacities in our participants, who, even with the most intensive current rehabilitative treatments, had not recovered the ability to stand or walk independently.

This doctoral thesis is integrated within the preparation, the proceedings and the assessment of the STIMO study. The three next chapters gather the work I carried out for three main research goals. In the preparation process of the clinical study, my leading objectives were to design and develop an innovative neuroprosthetic environment to assess, enable and train motor recovery in neurologically impaired population, from which two research goals stemmed: (i) elaborate the toolbox for comprehensive analyses of gait to evaluate prior abilities of the tested subjects and monitor their performance over the time course of the rehabilitation program (Chapter 1), and (ii) decipher the impact of the robotic assistance on the gait behavior and define the optimal, personalized robotic support to deliver (Chapter 2).

AIM 1: Evaluating gait behavior within a comprehensive and uniform approach.

Our laboratory values integrative approach in the development of therapies for locomotion recovery. In this respect, trunk position and inter-limb coordination strategies are considered for gait analysis as well as the proper leg movements and muscles activity as they affect the locomotion too. Therefore, we take into account numerous parameters to obtain a comprehensive signature of the gait behavior of individuals with neuromotor disorders. In addition to standard spatio-temporal gait parameters such as the step length, gait cycle speed or step height, more elaborated gait parameters are analyzed to reveal compensation strategies that may involve trunk adjustments or abnormal coordination strategies. Besides this embracing approach, consistent analyses have to be conveyed in order to allow a proper comparison of different subjects between conditions, since cohorts of individuals are involved in the studies.

To respond to the need of comprehensive but also uniform analysis performed on human gait, I first aimed at designing and implementing a toolbox with a graphical user interface. This toolbox computes a large variety of gait parameters in addition to the standard ones and offers the possibility to be used by scientists or clinicians not familiar with programming environment. This work enables the diagnosis, high-level characterization and monitoring of the evolution of motor disorders before and during rehabilitation. Its first application was for the analysis of the human locomotion under a postural robotic assistance.

AIM 2: Uncovering the effect of body weight support on human gait.

Robotic assistance applied at the trunk level interacts with body mechanics. With the objective to allow the delivery of a body weight assistance with a minimal impact on the gait capacities of individuals with neuromotor disorders, I aimed at investigating the detrimental impact of body weight support on human gait. Indeed, Cochrane databases and other clinical guidelines advised to keep a low body weight support during rehabilitation but, from the best of our knowledge, nobody investigated why high body weight support impacted gait pattern. We hypothesized that a corrective force in the forward direction, tuned in function of the amount of body weight support, could alleviate this undesirable interaction. Based on this work, I designed and implemented an algorithm that guides the adjustment of the robotic assistance to the individual's residual capacities.

Once the conceptual and methodological framework has been established, I focused, in the course of the STIMO study, on a third research goal: investigate the ability of epidural electrical stimulation to improve lower limb motor control in spinal cord injured individuals on the short- and long-term time scale (Chapter 3).

AIM 3: Investigating the leg motor responses to targeted EES.

Based on recent knowledge (see Introduction), we hypothesized that an intensive, EES-enabled neuro-rehabilitation program would enhance leg motor control. We thus put in place the STIMO study, where individuals with a SCI received an electrode array to deliver EES at the lumbo-sacral spinal level. In the weeks following the implantation, we investigated how the electrical epidural stimulation affects the locomotor responses and what are the specific effects of the different stimulation parameters – frequency, amplitude and electrodes location. The study participants then underwent a 5-month rehabilitation period focused on locomotion training. On the long-term time scale, we evaluated the effects of the therapy in participant's neurobiomechanics, neurophysiology and clinical status.

1. Toolbox for Comprehensive Analyses

Comprehensive analysis of walking and other neuro-motor functions is ubiquitous in my research work. These extensive analyses allow getting an imprint of an individual's state for a particular condition and comparing it to other conditions or to the healthy imprint. They give the metrics to objectively quantify potential improvements or deteriorations of the individual's status following a treatment – may it be robotic support, medicine, electrical stimulation, training.

In order to guarantee the reproducibility of the analyses and to permit the comparison between participants from the same population or from different populations, the employed methods and algorithms needed to be kept unchanged thorough a study. Moreover, all users had to apply these methods and algorithms in the exact same fashion, be they engineers, medical doctors, or pure physiologists. A toolbox gathering these methods and algorithms under a graphical user interface responded to these needs. Once the codes have been implemented, the exact same analysis could be indefinitely conducted on large samples by any member from the laboratory or even outside the laboratory.

Several software on the market such as Polygon®, Gait Up®, Simi®, etc., processed raw data and edited reports, but they were bounded to a specific recording system belonging to their brand. Moreover, they either did not compare to a healthy database or did not permit to use an age-matched healthy database or a database of reference people having performed the same task in a similar environment. As a last point, they output the standard spatio-temporal gait parameters and couldn't be adapted to the specific requirements of our studies. In the light of these limitations, we were in the need to develop a more versatile software that could process raw data from different recording systems, that allowed the selection of a reference database matching the studied condition, and that could automatically generate a report gathering standard spatio-temporal parameters along with tailored analyses and parameters adapted to each of our study design.

Quantitative Gait Analysis

Our laboratory has implemented in the past a graphical user interface allowing the quantitative analysis of the gait in rodents. Having updated this former software, I designed and built its counterpart to provide tools for a comprehensive gait analysis in humans. Its conception was thought to permit the analysis of a broad range of individuals suffering from various neuromotor disorders. We indeed recorded the locomotion of individuals with a stroke, with a spinal cord injury, with a multiple sclerosis or with the Parkinson's disease. Each of these disorders produced a specific signature in the kinematic behavior. Standard spatio-temporal gait parameters are sometimes too restrictive to describe their locomotion, as they look mainly at the foot level: stride and step length, step width, speed, foot elevation, percentage of swing and stance in a gait cycle, etc.

To take into account the use of assistive device such as crutches that increased their base of support, or the dragging (when the foot slides forward on the floor instead of being lifted at the beginning of the swing phase), we added some parameters to the list of spatio-temporal parameters: percentage of dragging in a gait cycle, percentage of dragging in the swing phase, width of the base of support including assistive device or foot orientation on the floor during stance phase (Figure 1.1).

In addition to the computation of the standard spatio-temporal gait parameters, the elevation angle[1] of each body segments was measured along with the flexion-extension angle[2] of each joint. The evolution of the leg elevation angles during a gait cycle is an example of data not presented in common gait reports. Nonetheless, the covariation of the leg elevation angles gives an important insight in the walking strategy of a person [73, 74]. Indeed, the thigh, shank and foot elevation angles covary in a specific plan and, at each gait cycle, they shape a 2D ellipse that is learned by children and remains invariant in healthy adults [75, 76, 77]. When people with neuromotor disorders adopt a different locomotor strategy, the profile of their leg elevation angles is altered and/or less repeatable, suggesting a modification in the coordination of the leg segments (Figure 1.2). The study of the leg elevation angles can be used as a marker of the coordination pattern that indicates the strength and properties of inter-segmental coordination patterns, which is otherwise barely vis-

[1] The elevation angle is the angle between the body segment (e.g. the thigh) and the gravity vector in the sagittal plane [73, 74].

[2] Though the raw data permitted to also measure the abduction/adduction angle and the internal/external rotation of each joint, we didn't use them as the precision that we could achieve with our selected marker model was not high enough compared to the range of amplitude of the joints.

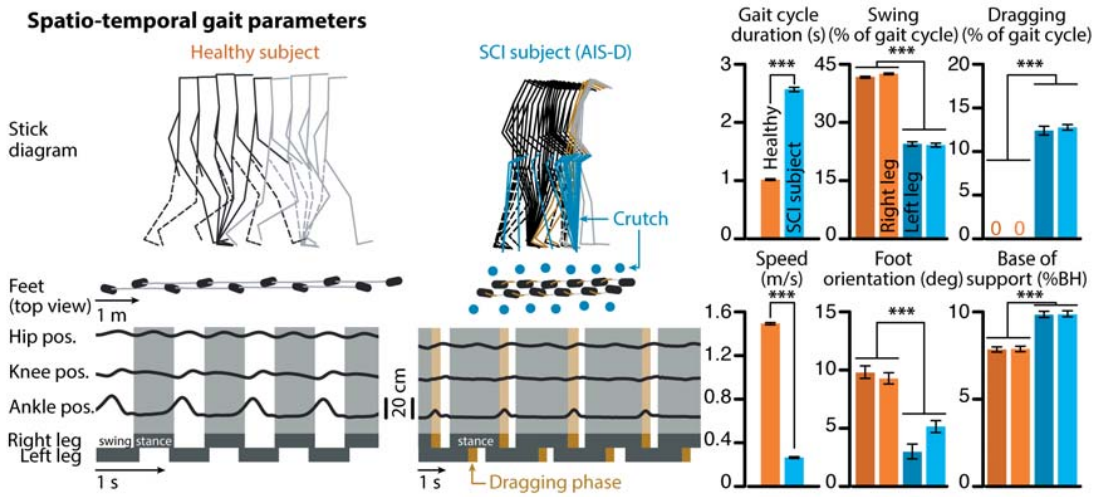

Figure 1.1 – **Spatio-temporal parameters.** Stick diagram decomposition (rate, 120ms) of the head, trunk and legs during the stance (dark) and swing (light) phases of a gait cycle; the brown color indicates the occurrence of dragging during the stance-to-swing transition. The filled and dashed lines respectively differentiate the right and left legs. The crutches are displayed as blue sticks. The feet positions on the floor (dark) are displayed with the continuous trajectories of the feet in the horizontal plane. A blue dot indicates a crutch placement on the floor. Temporal trajectories on the vertical axis are shown for the right hip, knee and ankle. Few spatio-temporal gait parameters are represented in bar plots. A healthy subject and a subject with SCI (AIS-D) are represented here as examples. The SCI subject drags at the beginning of the swing phase as shown in brown. The bar plots indicate that the swing phase was decreased to less than 30% of the gait cycle duration and about half of the swing phase the subject was actually dragging (top middle and right bar plots). Regarding feet placement, the SCI subject increased his base of support but his feet orientation during stance phase (i.e. the angle between foot and forward axis, in the floor plane) was less than a healthy subject, which could be a factor of instability (bottom middle and right bar plots).

ible to the naked eye. During long-term rehabilitation, for example, the profile of leg elevation angles could indicate whether the patient is going towards a healthy inter-segmental coordination strategy (shape and covariation plane formed by the leg elevation angles of the patient compared to the reference shape and covariation plane), and how much robust is the gait strategy (variability in shape and covariation plane for consecutive gait cycles). Several gait parameters were derived from the covariation plane and included in our gait analysis (see Appendix A).

Another aspect we considered was the movements of the trunk, in transversal and frontal planes, as well as the trajectory of its barycentre during each gait cycle (Figure 1.3). Indeed, the trunk posture affects the generation of gait patterns, for example the coordination between the leg segments is altered if the subject walks with a bent posture instead of the normal erect position [78]. Its balance during walk is therefore of main interest but is, however, poorly studied. In Chapter 2, we studied the impact of a trunk support system on the gait of healthy and neuromotor impaired people. Consequently, the parameters about trunk stability and displacement in the different anatomical planes were of key interest to compare different conditions of support.

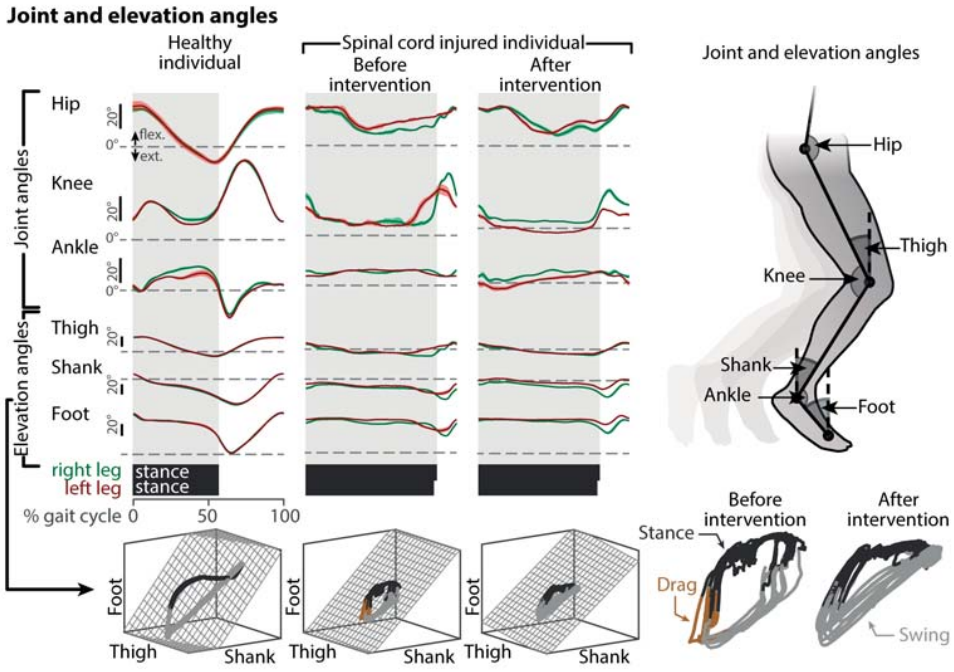

Figure 1.2 – Joint and elevation angles. Evolution of joint (hip, knee and ankle) and elevation (thigh, shank and foot) angles of the right and left legs averaged over several gait cycles for each leg. The 3D plot shows the successive gait loops obtained by plotting the thigh, shank and foot elevation angles (oscillations with respect to the direction of gravity) against each other. In a healthy individual, the gait loops lie close to an invariant plane of covariation. In the case of the individual with a SCI (AIS-C), the orientation of his covariation plane was altered, the variability between successive gait loops was increased compared to healthy adults and the ellipse shape of the loops was deteriorated. After intervention (several months of training), the ellipse shape improved and the variability was reduced.

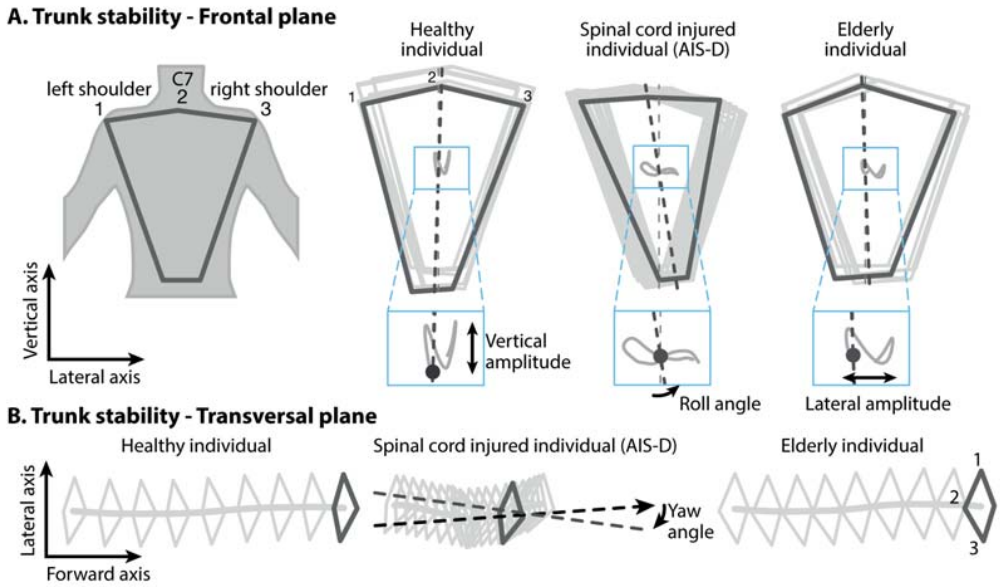

Figure 1.3 – Trunk balance. The successive positions of the trunk (rate, 120 ms) are shown together with the trajectory of the center of mass (CoM) of the trunk, in frontal (A) and transversal (B) planes. The healthy individual displayed the typical vertical displacement of the trunk with a light displacement on the lateral axis. The spinal cord injured individual (AIS-D) showed an important roll angle as well as a yaw angle, with less vertical displacement. Due to his injury, he swung more from one side to the other as he shifted his weight from one leg to the other. The elderly individual displayed a higher lateral amplitude, probably related to an increased base of support for a better stability.

In addition to the trunk balance, proper arm movements are crucial for proper walking behavior and suspected to be a remnant of quadrupedal locomotion [79]. Human walking uses out-of-phase arm movements for a smoother and more efficient locomotion [80] (Figure 1.4). Coordination between arm pendulum and leg movements as well as phase differences between the limbs highlight the compensatory behaviour produced by the arms when leg motor controls present deficits [81, 82]. These parameters were hence computed in order to obtain a full characterization of the gait behavior of our individuals with neuromotor disorders. The exhaustive list of computed gait parameters can be found in Appendix A.

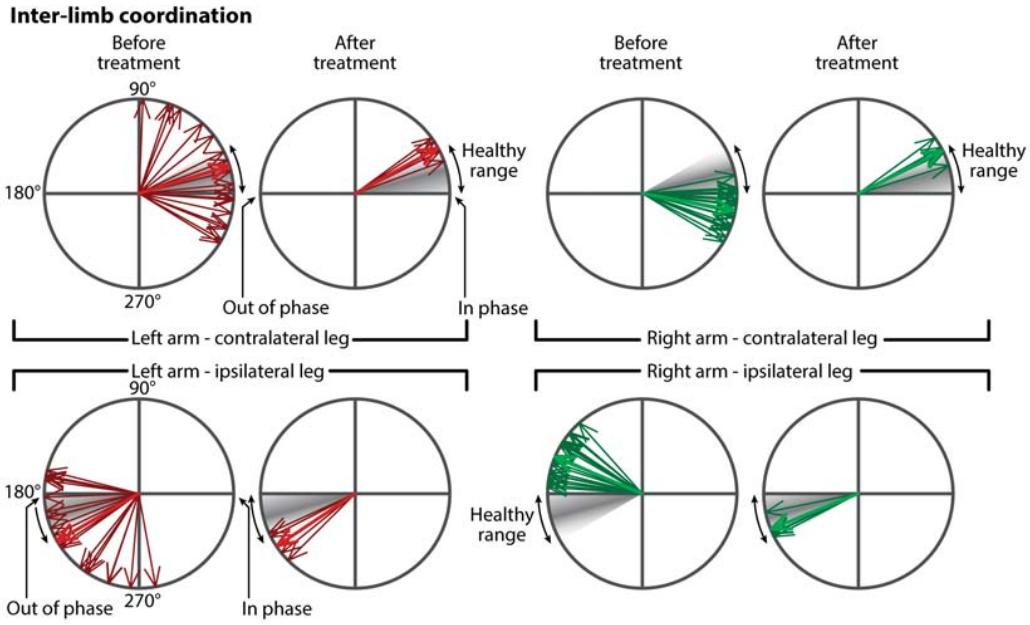

Figure 1.4 – **Inter-limb coordination.** Polar plots showing the coordination between each arm and leg. The represented individual had the Parkinson's disease and was asked to walk overground alone. Before treatment, arms and legs were not coordinated and varied a lot (phase between the left arm and a leg spanned a large range around the reference values, while the phase between the right arm and the ipsilateral leg appeared outside the reference range). After treatment (L-Dopa, a dopamine precursor able to cross the blood brain barrier and commonly used in Parkinson's disease treatment), the measured difference in phase were closer to the reference values and less variable.

Besides kinematic parameters, a suitable EMG processing was required for the extraction of muscle synergies and spatio-temporal representation of the leg alpha-motoneuron activity at the spinal cord level (Figure 1.5). These representations allow, respectively, the observation of muscles coordination and the lumbosacral activity over a gait cycle, which are important indicators of the stage of rehabilitation of the SCI patients [83]. In the Chapter 3, we tried to mimic the natural activity of the leg motoneuron at the spinal cord level in our participants with SCI using spatio-temporal epidural electrical stimulation. For this purpose, the map of motoneuron activity was

used to obtain the state of the participant's spinal cord before the intervention, determine the stimulation program to apply in order to mimic the reference map, and assess the efficacy of the chosen stimulation program.

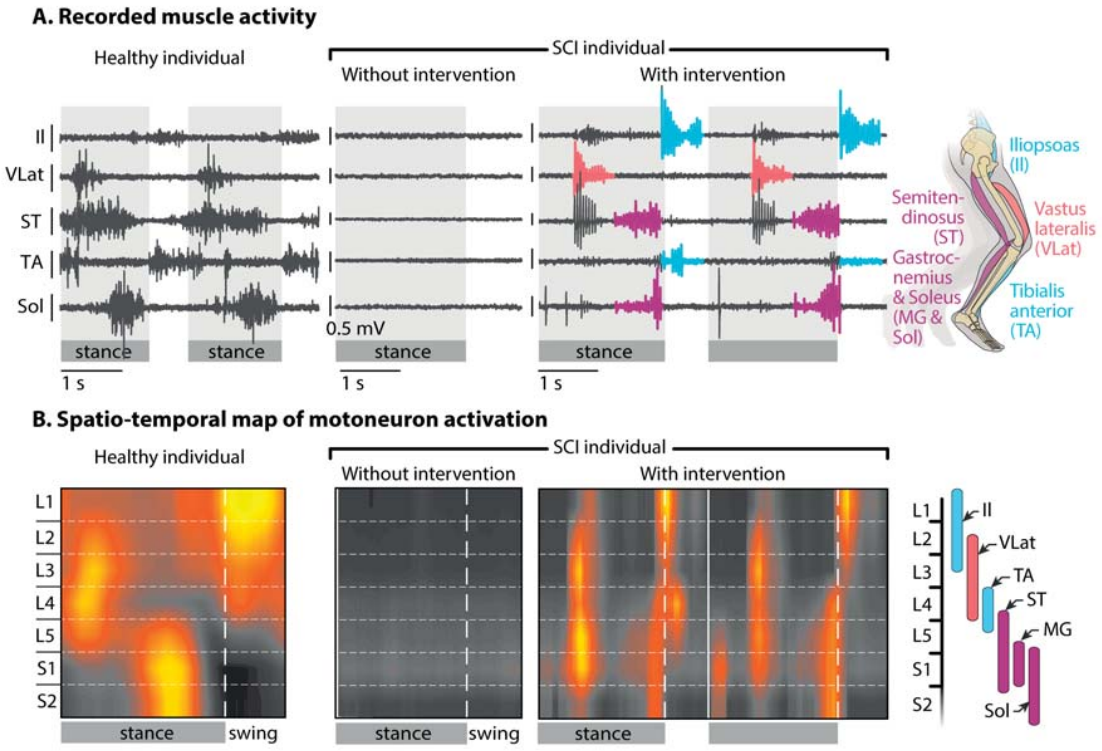

Figure 1.5 – **Muscle activity. A**, Recorded electromyographic (EMG) signals of some leg muscles during one or two steps. The horizontal bars indicate the stance and swing phases of the leg. The color code (cyan, magenta, salmon) corresponds to sequences of muscle activity detailed in Chapter 3, Figure 3.12. The recorded individuals were a healthy individual and a paraplegic individual (AIS-C) without intervention and with intervention (targeted EES, see Chapter 3). Without intervention, each recorded muscle of the SCI individual was inactive during stance and swing phases (manual assistance was provided here to enable locomotion pattern). With intervention, a pattern of EMG similar to the healthy one was obtained. **B**, Spatio-temporal map of motoneuron activation computed from the recorded muscles on the same two individuals and with the same intervention as (A). With intervention, the spatio-temporal map of the SCI individual displays the three "hotspots" (light orange spots) as observed in the healthy individual's map. For more details, see Chapter 3. Adapted from the figure 3 of our article presented in Chapter 3 [84].

Multidimensional Analysis

From this large amount of computed parameters, more advanced analyses can be performed over various conditions or populations to highpoint the gait parameters that are the most relevant to discriminate between the studied conditions or individuals. Feature extraction and dimensionality reduction can be achieved by principal component analysis (PCA). In the laboratory context, PCA, which looks for the direction of highest variance, is the standard practice as it enables to visualize high dimensional space of parameters in a two or three dimensional space of principal components. Most of the time, these two or three principal components grasp altogether the main meaningful variance in the dataset. From them we can easily retrieve which gait parameters characterize the best the differences in behavior, or compute a locomotor score to assess how far are the neuromotor impaired individuals from the reference persons (Figure 1.6).

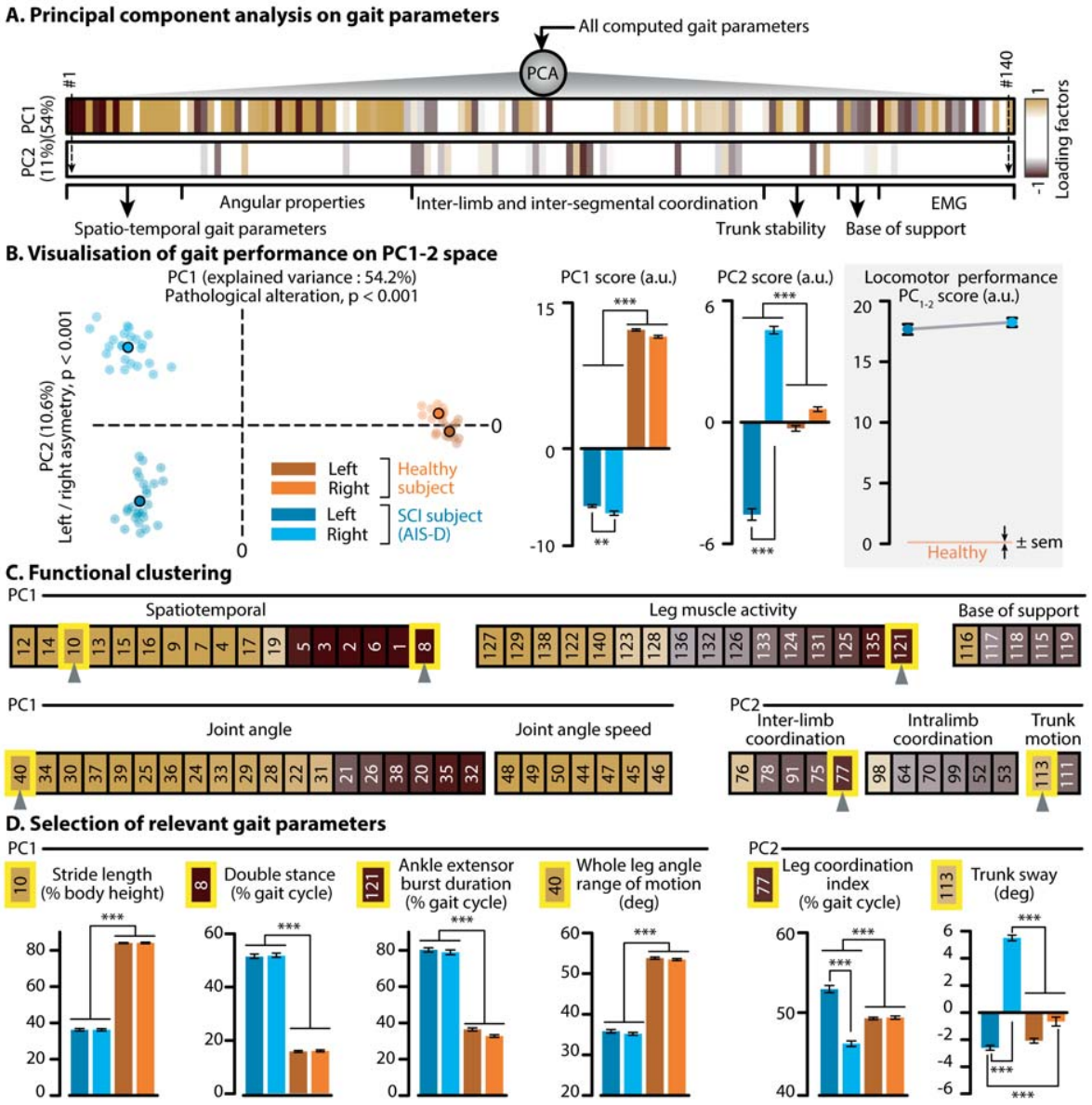

Figure 1.6 – Principal component analysis (PCA) on gait parameters. A, A PCA is applied to all the computed gait parameters to quantify locomotor performance and identify the most relevant parameters to explain differences between subjects or experimental conditions. The horizontal bars report the factor loadings (correlation) of each gait parameter onto PC1 and PC2 (%, explained variance). The color indicates the strength of the correlation between a given parameter and the PC. B, In this example, the PC analysis was applied on all the gait cycles of a healthy subject and a subject with SCI (AIS-D). Each gait cycle was represented in the new "denoised" space created by PC1 and PC2. Each color-coded dot corresponds to a single gait cycle, while the circles indicate the average value for each condition. The PC score corresponds to the position of the gait cycle along each PC axis. The bar plots report the mean scores of gait cycles for each leg of both subjects. This analysis allowed the identification of the features captured on each axis: PC1 segregated gait cycles of the healthy subject from those of the SCI subject, PC2 distinguished the asymmetry between the left and right side of the SCI subject. The locomotor performance was quantified as the Euclidian distance between gait cycles of the two subjects in the PC1-2 space. C, The computed parameters that strongly correlated with a given PC (|loading factors| > 0.5) were extracted and regrouped into functional clusters, named for clarity. The name of each parameter is indicated in Appendix A. D, Bar plots reporting the mean values of some parameters from each of the functional clusters, highlighted in yellow. ***p < 0.001, two-way ANOVA with Tukey-Kramer post hoc tests. Data are means ± s.e.m. Adapted from the supplementary figure S3 of our article presented in Chapter 2 [85].

Graphical User Interface

All the gait parameters discussed above are computed in a unique software implemented in Matlab®. Through its graphical user interface, the raw data can be easily loaded, processed and visualized in various plotting modes. This elaborated graphical user interface, represented in Figure 1.7, is a useful tool for diagnosis and high-level characterization of motor disorders. As a matter of fact, it has been extensively used to evaluate the gait behavior of cohorts, such as the 28 subjects with stroke or spinal cord injury who tested the robotic postural assistance (see Chapter 2), the 35 subjects suffering from Parkinson's disease who were recorded for a study analyzing in details the effect of L-Dopa on human gait (paper in preparation), about 50 subjects suffering from multiple sclerosis, or the subjects with a chronic SCI enrolled in the feasibility study STIMO (see Chapter 3).

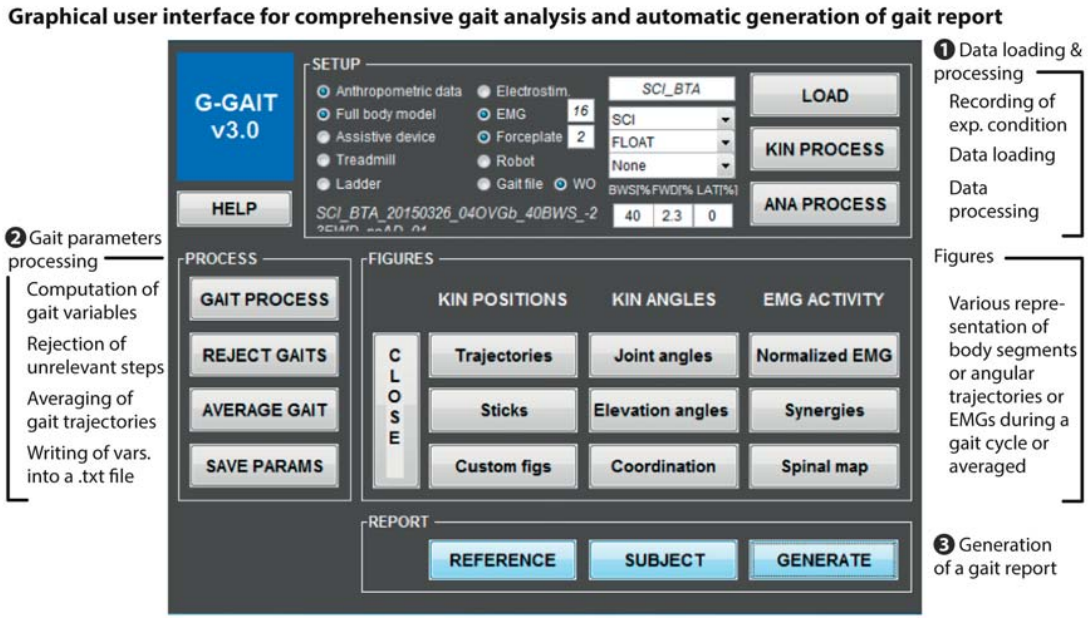

Figure 1.7 – Toolbox for quantitative gait analysis. Graphical user interface for data processing (step 1), computation of gait parameters (step 2), display of kinematic, electromyographic and kinetic graphs (optional) and automatic generation of the gait report (step 3).

Automatic Gait Report Generation

An additional step in the development of this software, facilitating its application in clinical routine, was the automatic creation of a report directly generated from the graphical user interface. Once the raw data are collected, the same user interface allows processing the data, visualizing them, computing more than a hundred of gait parameters, and generating a gait report summarizing the locomotor state of the recorded individual. The automatically-generated gait report can be as well directly delivered to the clinician to appreciate the gait characteristics of his patient as used by scientists to compare to a reference database or to monitor changes due to a therapy or a new condition (Figure 1.8 and Appendix B).

Since learning how to handle a user interface is more intuitive and efficient than learning to code and the corresponding methods of analysis, this version is suitable for a direct use by clinicians who wish to quickly obtain a complete gait report of their patients. Several automatic gait reports have been successfully run on subjects' data coming from two hospitals: Centre Hospitalier Universitaire de Bordeaux (CHU Bordeaux, France) and Centre Hospitalier Universitaire Vaudois (CHUV, Switzerland).

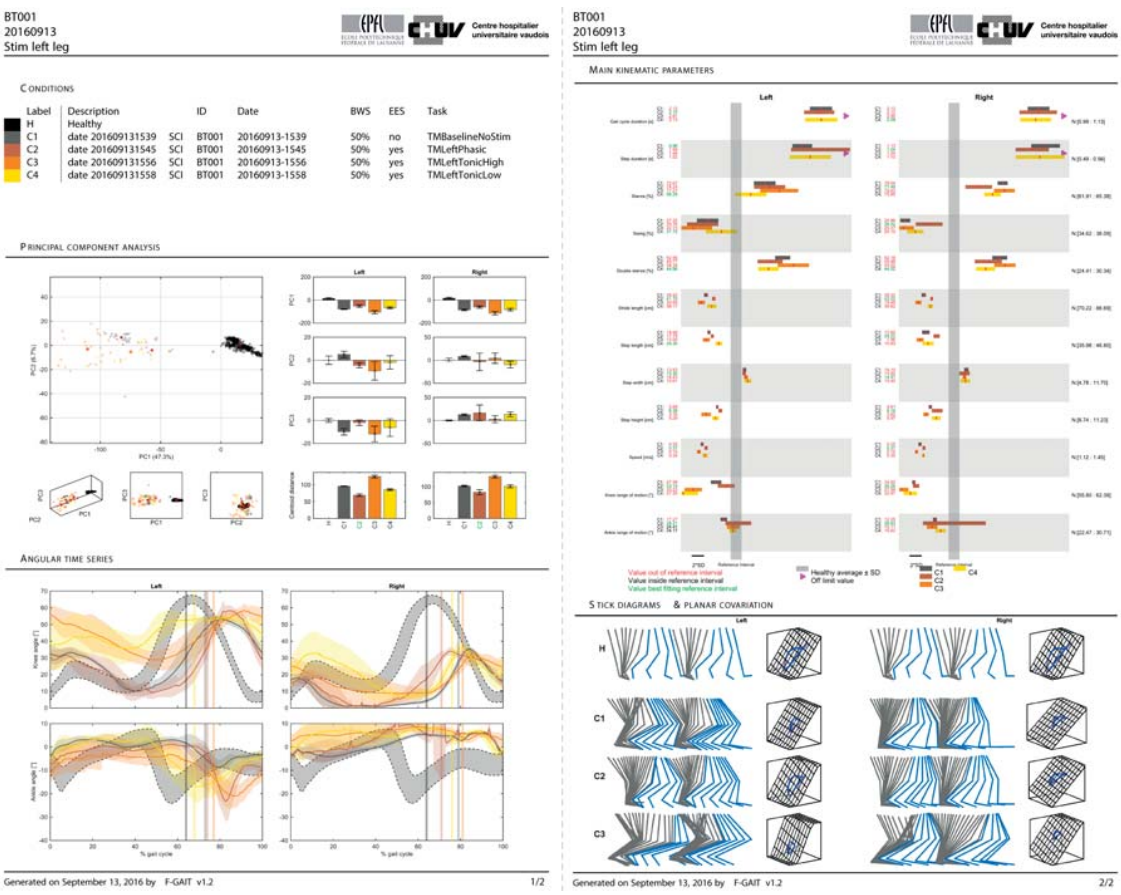

Figure 1.8 – **Quantitative gait analysis.** Light version of an automatically-generated gait report (the complete version is in Appendix B). In this case, a participant with a spinal cord injury walked with a 50% body weight support and with different program of epidural electrical stimulation (for more details on the intervention, see Chapter 3).

Discussion

This work established a solid backbone for the subsequent work carried out during my thesis, and also for future work related to the wide field of gait behavior with healthy or neuro-motor impaired humans. The presented toolbox for comprehensive gait analysis has been widely used to investigate the effect of a treatment on various human population in a precise and quantitative manner. Currently, we are using it on a cohort of 35 individuals with the Parkinson's disease. In a first step, we would determine whether a correlation between the clinical score of each individual and a locomotor score derived from the gait parameters computed by the developed software exists. Then, we would highlight how a treatment (L-Dopa) affects the gait behavior of these individuals and how it is related to his/her rigidity or tremor dominance. In parallel, the automatic gait report delivered by the same software were communicated to the individual's medical doctor, who took benefit from it to compare the gait behavior of their patients with and without treatment in a quantitative way.

The automatic gait reports were equally used to compare the different configurations of epidural electrical stimulation delivered to the spinal cord injured subjects enrolled in our feasibility study (see Chapter 3). These reports enabled to determine the stimulation protocol that produced the closest gait to the healthy one, before we had collected enough data and experience to implement a more sophisticated algorithm that pre-determined the best configurations for the next subjects. Furthermore, the reports allowed the participant to better grasp what were the effect of the stimulation on their gait behavior, may it be for different conditions tested on the same day or the same condition tested at different timepoints.

For the study described in Chapter 2, we took advantage from this work to analyze the effect of a robotic device on the gait behavior of individuals attached to the device via a trunk harness. It allowed us to rapidly access to numerous gait parameters and easily determine which parameters were affected by the device, depending on the neuro-motor disorder of the tested individual. The full ensemble of automatic gait reports for each individual in each situation they experienced with or without the robotic device had permitted to deliver a complete overview of our work, and had been well appreciated by the peer-reviewers who revised the paper (accessible as a database in the supplementary materials) as an effort towards data transparency.

Based on these different studies and experience, this presented toolbox had provided evidence about its effectiveness and suitability in the field of gait analysis. For

each study, a comprehensive gait analysis that took into account the full body including the trunk motion and inter-limb coordination was crucial to get a biomechanical signature as exhaustive as possible since the therapies we are developing apprehend the body neuro-biomechanics as a whole. Medical doctors from Bordeaux hospital, CHUV (centre hospitalier universitaire vaudois) and the medical rehabilitation and reintegration center of Sion (clinique romande de réadaptation SuvaCare, SUVA) had expressed their strong interest in it. In an outreach effort, the next main and logical step before spreading it to the medical corps would necessitate to create a cross-platform version of the here-developed software that wouldn't rely on Matlab® license anymore, thus allowing the distribution of an executable to generate the comprehensive automatic gait report outside the laboratory environment and accessing the clinical field.

2. Targeted Robotic Postural Assistance

To re-master the delicate interplay between body mechanics and gravitational forces, neurologically impaired individuals must exploit residual neural circuits to regain strength, precision and balance. Robotic devices to assist postural balance of individuals act as an adjustable link between individual's intrinsic abilities and external environment and its constraints (Figure 2.1). I believe that a fine tuning of the robotic assistance based on patient-specific residual abilities is crucial to re-learn walking. In this work, we developed the concept of multidirectional gravity-assist. We first assessed how the robotic device affects the gait behavior of healthy subjects for different amount of body weight support. We then determined how to adjust the robotic assistance, in upward and forward directions, based on patient's residual capacities, and we implemented an algorithm to guide physiotherapists in the settings of robotic assistance. We tested the multidirectional gravity-assist on a cohort of neurologically impaired subjects and provided a large-body of evidence highlighting the potential of the targeted postural assistance to augment gait recovery after neurological disorders.

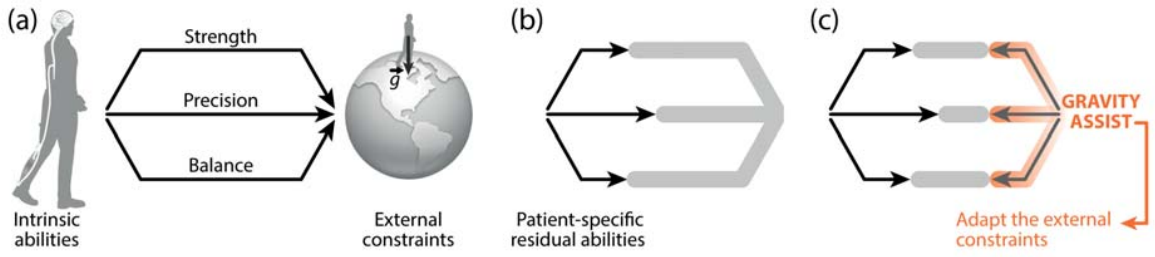

Figure 2.1 – A targeted robotic postural assistance to adapt external constraints to patient-specific residual abilities. A combination of strength, precision and balance are necessary to walk in the gravitational environment of the Earth (a). Neurological deficits induce a gap between these intrinsic motor control abilities and the external constraints, which prevents independent walking (b). The gravity-assist aims at reducing this gap by adapting the external constraints to patient-specific residual motor control abilities (c).

The content of this chapter is adapted from the article J.-B. Mignardot*, C.G. Le Goff*, R. van den Brand* et al., ***A multidirectional gravity-assist algorithm that enhances locomotor control in patients with stroke or spinal cord injury***, published in Science Translational Medicine, Volume 9, July 2017 (DOI: 10.1126/scitranslmed.aah3621), post-print version reprinted with permission from AAAS.

Personal contributions: overall study design, collection and analysis of the data, tracking of kinematic data, implementation of the software for data processing and generation of patients' gait report, algorithm design and implementation, figures preparation, and manuscript writing.

A multidirectional gravity-assist algorithm that enhances locomotor control in patients with stroke or spinal cord injury

Jean-Baptiste Mignardot[1,2*], ***Camille G. Le Goff[1,2*]***, Rubia van den Brand[1,2*], Marco Capogrosso[1,2], Nicolas Fumeaux[1], Heike Vallery[3], Selin Anil[1], Jessica Lanini[4], Isabelle Fodor[5], Gregoire Eberle[5], Auke Ijspeert[4], Brigitte Schurch[6], Armin Curt[7], Stefano Carda[2,5], Jocelyne Bloch[2,8,#], Joachim von Zitzewitz[1,#], Gregoire Courtine[1,8,#,$]

[1] Center for Neuroprosthetics and Brain Mind Institute, School of Life Sciences, Swiss Federal Institute of Technology Lausanne (EPFL), Lausanne, CH. [2] Clinical Neuroscience, University Hospital of Vaud (CHUV), Lausanne, CH. [3] Faculty of Mechanical, Maritime and Materials Engineering, Delft University of Technology, Delft, NL. [4] School of Engineering, EPFL, Lausanne, CH. [5] Neurorehabilitation, CHUV, Lausanne, CH. [6] Neuro-urology, CHUV, Lausanne, CH. [7] Spinal Cord Injury Center, Balgrist University Hospital, Zurich, CH. [8] Neurosurgery, CHUV, Lausanne, CH.

*, #, These authors contributed equally to this work.

$, Corresponding author.

Abstract

Gait recovery after neurological disorders requires remastering the interplay between body mechanics and gravitational forces. Despite the importance of gravity-dependent gait interactions and active participation for promoting this learning, these essential components of gait rehabilitation have received comparatively little attention. To address these issues, we developed an adaptive algorithm that personalizes multidirectional forces applied to the trunk based on patient-specific motor deficits. Implementation of this algorithm in a robotic interface reestablished gait dynamics during highly participative locomotion within a large and safe environment. This multidirectional gravity-assist enabled natural walking in non-ambulatory individuals with spinal cord injury or stroke and enhanced skilled locomotor control in the less-impaired subjects. A 1-hour training session with multidirectional gravity-assist improved locomotor performance tested without robotic assistance immediately after training, whereas walking the same distance on a treadmill did not ameliorate gait. These results highlight the importance of precise trunk support to deliver gait rehabilitation protocols and establish a practical framework to apply these concepts in clinical routine.

Introduction

Terrestrial locomotion is inherently contingent on gravity [86]. Although gravity challenges equilibrium at each step, the gravitational forces acting upon body mechanics enable the generation of ground reaction forces (GRFs) that propel the body forward [87, 88]. The bipedal posture of humans exacerbates the beneficial impact of gravity on gait dynamics [88, 89, 90, 91, 92]. The elevated center of mass (CoM) allows the human body to vault up and over the stance leg analogous to an inverted pendulum [91], whereas the contralateral leg performs a near-ballistic oscillation [93].

The apparent simplicity of the inverted pendulum-like gait behavior conceals sophisticated neurological control mechanisms [94, 95], which require several years of neural development to become mature [96]. However, locomotor impairments resulting from neurological insults such as spinal cord injury (SCI) and stroke remind us of the instability of human gait and the complexity of its neural control. Neurologically impaired individuals must exploit residual neural circuits to regain strength, precision, and balance to remaster the delicate interplay between body mechanics and gravitational forces.

Partial body weight supported gait therapy is the most common medical practice to facilitate this process [97, 98]. Robotic engineering has developed various types of body weight support systems. The most common solutions include passive springs, counterweight mechanisms, or force-controlled apparatus that deliver upward trunk support during stepping on a treadmill. These approaches suffer from several drawbacks. First, treadmill belt motion dictates the locomotor pace, imposing challenging conditions for neurologically impaired individuals who exhibit variable gait patterns [99]. Second, treadmill-restricted environments markedly differ from the rich repertoire of natural locomotor activities underlying daily living. Task-specific rehabilitation is essential to maximize gait recovery [100, 101]. Third, vertically restricted trunk support creates undesired forces that impede gait execution [102, 103, 104]. Fourth, overground rehabilitation triggers more active participation than treadmill-restricted training, which is critical for steering neural circuit reorganization after neurological disorders [47].

We previously developed robotic systems for mice [105] and rats [67] that addressed these issues. These suspension devices integrate soft actuation mechanisms that allow the application of multidirectional forces to the trunk while the rodents are progressing freely within a large workspace. These robot systems enabled skilled locomotion in rodents with SCI or stroke [67, 106, 107] and maximized activity-depen-

dent neural circuit reorganization during rehabilitation [47,106]. To establish a similar gait rehabilitation platform for humans, we used a robotic system that allows fine adjustment of forces applied to the trunk along the three Cartesian directions [68]. The quadrupedal posture of rodents minimizes the mechanical impact of trunk support on dynamic balance. However, the application of forces to the trunk in the bipedal posture of humans is likely to exert additional and specific constraints. We found that a vertically restricted trunk support profoundly alters gait dynamics. The addition of well-calibrated forward forces alleviated these effects. Therefore, we developed an adaptive multidirectional gravity-assist (MGA) algorithm that determines upward and forward forces applied to the trunk to reestablish gravity-dependent gait interactions while providing a support tailored to patient-specific needs.

This MGA enabled natural walking in nonambulatory individuals with SCI or stroke and enhanced skilled locomotion in less-impaired subjects. After a 1-hour gait training session with MGA, individuals with SCI exhibited improved locomotor performance without robotic assistance. These combined results stress the importance of applying precise assistive trunk support during gait rehabilitation.

Materials and Methods

Study Design

Our goal was to develop an evidenced-based algorithm that configures multidirectional forces applied to the trunk in order to establish a natural environment enabling each individual with neurological deficits to perform locomotion in natural conditions. For this purpose, we implemented 8 experimental protocols that were approved by the local ethical committee of the Canton de Vaud (Switzerland, n°141/14). The evaluations were conducted at the University Hospital of Vaud (CHUV), Lausanne, Switzerland.

Protocol 1: Evaluation of the neurorobotic platform during locomotion along curvilinear and straight paths in 8 healthy individuals.

Protocol 2: Impact of upward and forward forces applied to the trunk on the kinematics, kinetics and muscle activity during standing and walking. Evaluations in 5 healthy individuals.

Protocol 3: Development of the algorithm that automatically configures upward forces. Recordings were performed during standing and walking over varying upward forces in 9 subjects with SCI or stroke.

Protocol 4: Development of a decision map that automatically adjusts forward force corrections. Computational simulations were completed with recordings of 22 subjects with SCI or stroke during locomotion.

Protocol 5: Validation of the MGA algorithm developed in Protocol 3 and 4. Six subjects with SCI or stroke were recorded during walking with MGA and small variations of upward and forward forces.

Protocol 6: Ability of the MGA to improve locomotor performance during walking. 15 subjects with SCI and 12 subjects with stroke were recorded during locomotion with MGA. Locomotor performance was compared to 13 healthy individuals.

Protocol 7: Five subjects with SCI performed two one-hour training session: (i) overground with MGA; (ii) on a treadmill with upward support only. Locomotor performance was measured before and after training without robotic assistance.

Protocol 8: Thirteen subjects with SCI or stroke performed skilled locomotion along the irregularly spaced rungs of a horizontal ladder and along a curved path projected on the floor with and without MGA. A virtual ladder was projected on the floor in the condition without robot. The subjects were also tested during walking while receiving a sudden or sustained lateral perturbation.

All measurements were obtained using objective readouts with high-precision equipment. Blinding during data acquisition and analysis was not possible due to obvious differences between conditions with and without robot. All the recorded gait cycles were included in the analyses. No statistical outliners were excluded.

Participants

Twenty-six subjects with SCI or stroke and 13 healthy individuals took part in the study. Written informed consent was obtained for each participant. The protocols conformed to the latest revision of the Declaration of Helsinki. All the subjects were followed by a physician from the neurorehabilitation department (S.C.). Prior to their enrollment, their medical history was collected together with standard neurological evaluations. For subjects with stroke, motor scores were measured using the Motricity Index [108] while the severity was evaluated using the Functional Independence Measure (FIM) [109]. AIS and WISCI-II scores were collected in subjects with SCI. The main characteristics of the subjects are summarized in Table 2.1.

Spinal Cord Injury (SCI)

Subject ID	AIS grade	Age (Years)	Gender (M/F)	Weight (kg)	Time after injury (months)	Lesion level	Origin of the injury
SCI_HCU	D	37	M	82	182	C8	Traumatic (sport)
SCI_CFR	D	64	F	50	180	T8/T10	Peridura anaesthesia issue
SCI_DMZ	C	27	M	63	36	C7/D1	Traumatic (sport)
SCI_GBA	D	38	M	82	264	T5	Spondylodiscitis
SCI_FIM	D	62	F	55	156	D10	Peridura anaesthesia issue
SCI_BTA	D	53	M	86	21	T6	Ischemia (scuba diving)
SCI_LST	D	30	M	75	22	C4	Ischemia (scuba diving)
SCI_MRC	D	62	F	68	12	T1	Herniated disc
SCI_KGY	D	40	M	68	248	T6	Spondylodiscitis
SCI_POR	D	58	M	90	39	C7	Traumatic (sport)
SCI_EDE	C	59	M	76	14	D11	Herniated disc
SCI_BME	C	62	F	54	16	T10	Ischemia
SCI_TFA	C	24	M	85	18	T7	Traumatic (car accident)

Stroke (STK)

Subject id	Motor score	Age (Years)	Gender (M/F)	Weight (kg)	Time after stroke (months)	Severity index	Origin of the stroke
STK_CZI	54	66	F	66	235	103	Ischemia
STK_FDJ	200	39	M	99	14	116	Ischemia
STK_GTO	64	53	F	62	10	95	Haemorrage
STK_JEI	84	43	M	53	12	96	Ischemia
STK_LCS	152	32	M	64	10	107	Haemorrage
STK_PMA	140	64	M	88	60	110	Ischemia
STK_RSC	152	68	M	78	12	68	Haemorrage
STK_TMO	20	62	F	49	8	41	Haemorrage
STK_SBE	152	36	F	96	20	126	Ischemia
STK_CPE	152	52	F	69	50	116	Haemorrage
STK_CFO	165	36	M	77	108	126	Ischemia
STK_CAR	25	62	M	64	8	32	Ischemia
STK_JPA	144	58	M	90	120	118	Ischemia

Table 2.1 – Characteristics of the subjects.

Neurorobotic Platform

Commercially available technologies were integrated within a neurorobotic platform that combines (i) a physiological recording unit monitoring kinematics, kinetics and muscle activity signals, (ii) a robotic body-weight support system (The Float, Lutz engineering, Switzerland) [67] and (iii) a control processing unit. All three units were interconnected via an Ethernet network using a real-time EtherCat bus, as previously described for the system developed in rodents [105].

Kinematic, Kinetic, and Electromyographic Recordings

Kinematic recordings were obtained using a 3D motion capture system (Vicon, United Kingdom) featuring fourteen Bonita10 cameras and two Bonita720c DV cameras. Two force plates (9260AA6, Kistler, Switzerland) were positioned within the ground in the middle of the workspace to monitor ground reaction forces and center of foot pressure displacements. Electromyographic activity was monitored using a 16-chan-

nel wireless recording system (Myon 320, Myon AG, Switzerland).

Trunk, head and bilateral leg and arm kinematics were recorded using 34 markers positioned overlying anatomical landmarks defined by the full-body Plug-In-Gait model developed by Vicon. The 14 cameras covered a 12 x 4 x 2.5 m workspace. The movement of assistive devices was monitored using reflective markers. Video recordings were obtained at 100 Hz. 3D position of the markers was reconstructed offline using Vicon Nexus software. The body was modeled as an interconnected chain of rigid segments. Anthropometric data (body height, body weight, widths of the joints) were added to the full-body Plug-In-Gait model to determine the positions of joint centers, and calculate the elevation and joint angles of the lower limbs. The ground reaction vector and antero-posterior and medio-lateral torques were acquired using two force plates integrated in the floor. Bipolar surface electrodes (1 cm diameter, electrode separation of 1 cm) were placed over the following leg muscles to record electromyographic activity: soleus, medial and lateral gastrocnemius, tibialis anterior, semitendinosus, biceps femoris, vastus lateralis and rectus femoris. During standing and walking, kinetic and electromyographic signals were sampled at 1 kHz, amplified, synchronized on-line with kinematic data, and stored for off-line analysis. Electromyographic signals were filtered offline (band-pass 10-450 Hz).

Multidirectional Robotic Body-Weight Support System

We previously developed a multidirectional robotic interface for rats that provides adjustable trunk support in each of the Cartesian directions and in rotation about the vertical axis [67]. To develop a similar body-weight support system for humans, we exploited cable robot technology [68]. We designed an overhead body-weight support system that precisely controls the forces applied to the trunk in each of the Cartesian directions. The technical features of the robot have been described previously [68]. Briefly, two parallel rails are arranged horizontally on the ceiling. The rails are located at 3.5 m from the ground and cover a footprint of 11.5 m by 2.5 m. Each rail guides two interconnected deflection units, each composed of a ball-borne cart carrying an inclinable pulley. The resulting four pulleys guide four cables into the workspace, towards a common point above the user, termed the node. Motorized winches actuating these cables are positioned at the extremities of the rails. Four elastic elements consisting of spiral steel springs each with a parallel rubber cord inside connect the cables to stainless steel rings at the node. The arrangement allows the four cables to virtually intersect in one point. An inertial measurement unit (IMU) combining accelerometers, gyroscopes and a magnetometer are located in

the node. Winch positions are measured by encoders on the motor shafts, while the length of the elastic elements is monitored using wire potentiometers. These sensors provide redundant information allowing to calculate the position of the node and resultant force vector on the subject through optimization. Control algorithms have been detailed previously [68]. Communication procedures are implemented in Matlab using an EtherCat network operating at 1 kHz [110].

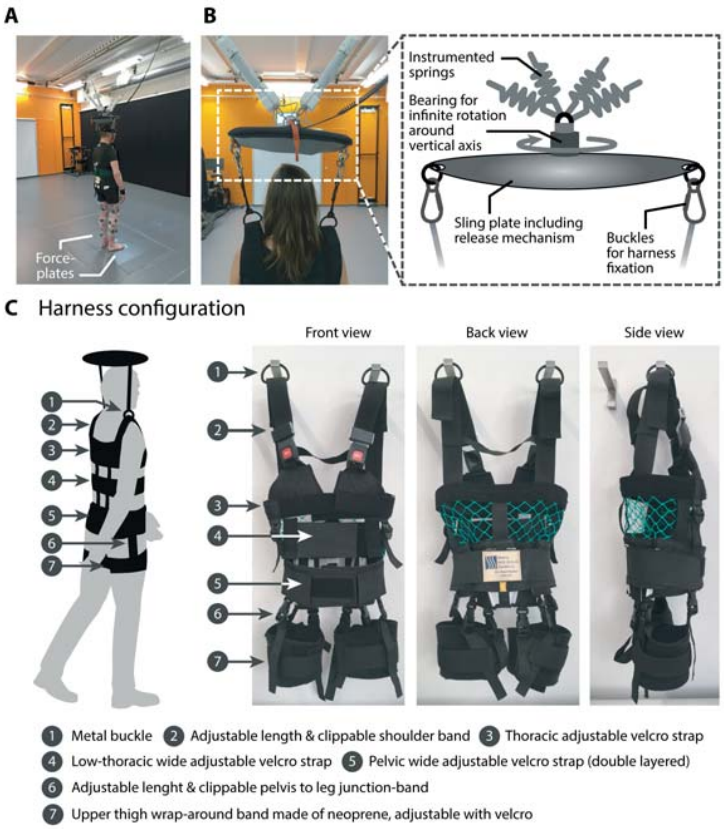

Figure 2.2 – Attachment to the robotic support system. **A**, Global view of a subject attached to the robotic support system during standing with various body weight support, as described in Figure 2.9A. **B**, Attachment of the suspension module to the harness, including an inset detailing the various elements of this module. **C**, Design and configuration of the harness.

The subjects were attached to the robot using a commercially available harness (Maine Anti-Gravity Systems, Inc., USA). The two shoulder straps of the harness are attached to the two outer ends of a plate by means of buckles (Figure 2.2). The plate itself is pivot-mounted to the lower end of the node. The plate can rotate infinitely, allowing the subject to take arbitrary turns. The robot enabled subjects to walk freely within a 20 m 2 workspace (10 m length by 2 m width by 2.6 m height). The robot is capable of supporting a body weight of 100 kg (1000N), with a maximal upward support of 900N and a maximal forward support of $\pm$ 50N in the lateral and longitudinal directions. A fall detector and smooth counteraction mechanism guaranteed patient safety in case of a fall (Figure 2.5).

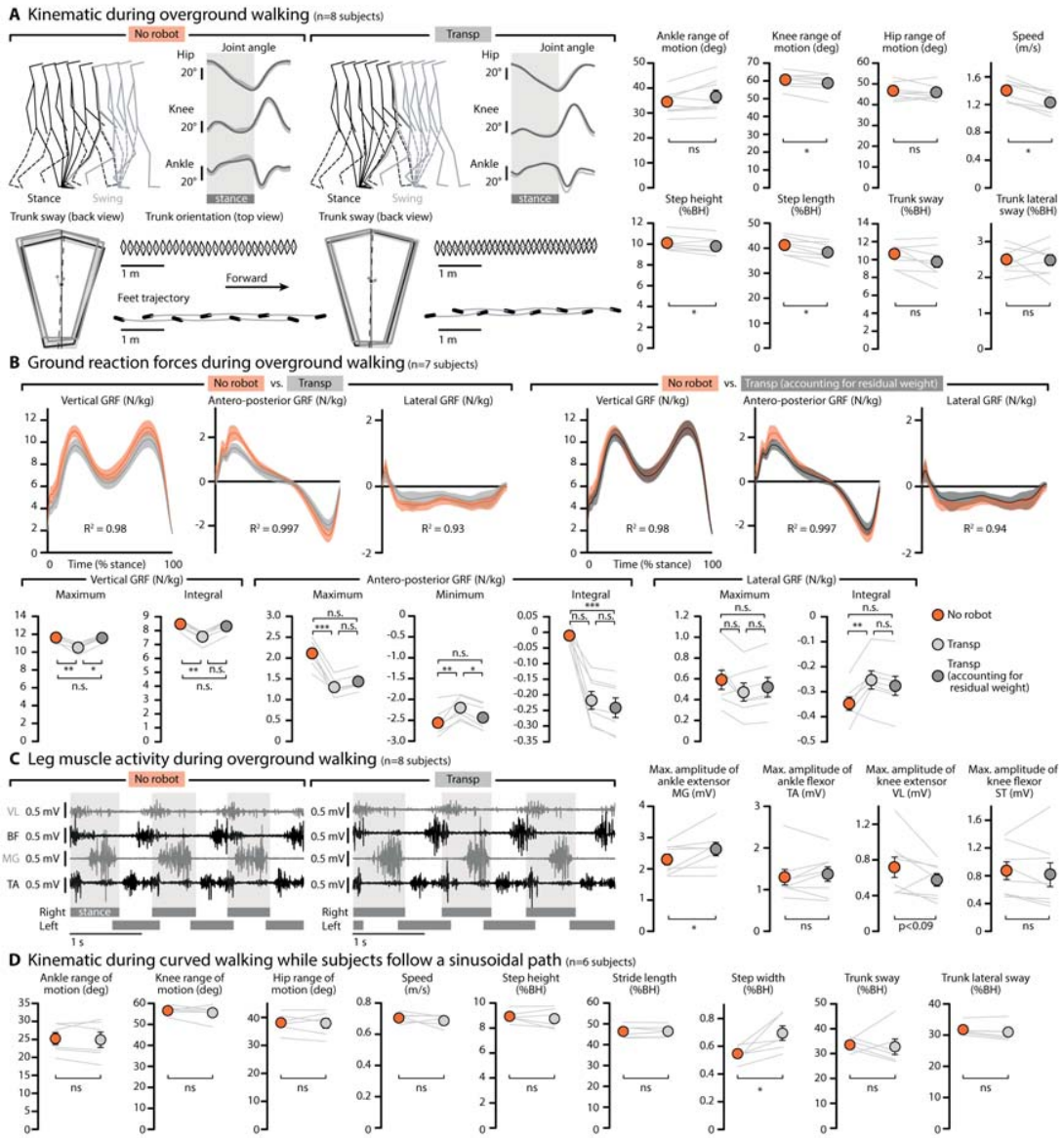

Figure 2.3 – **Transparent mode of the robotic support system.** Healthy subjects were asked to walk straight-ahead without robot and with the robot configured in transparent mode (upward force of 40N). **A**, Stick diagram decomposition, average joint trajectories, trunk position and feet trajectories are shown for both conditions. The plots report the mean values of classic gait parameters for each subject in each condition. **B**, Ground reaction force (GRF) during locomotion in each condition. The profile of GRFs are normalized to the body weight of the subject (left) or the residual body weight (right), i.e. taking into account the 40N removed from the subject's body weight to maintain the tension in the cables. The vertical component of the GRFs was decreased for the condition with robot compared to without robot (left side), as expected based on the application of a 40N upward force. When taking into account this upward force, however, the vertical component of the GRF became similar to the profile measured without robot. An offset remained observed in the peak amplitude of the anteroposterior component of the GRFs. The plots report the quantification of the GRFs in each direction. **C**, EMG activity of ankle (tibialis anterior, TA; medial gastrocnemius MG) and knee (biceps femoris, BF; vastus lateralis, VL) muscles in each condition, including plots reporting the max amplitude of these muscles. **D**, Healthy subjects were asked to walk along a sinusoidal path projected on the floor without and with robot configured in transparent mode. The plots report the mean values of classic gait parameters for each subject in both conditions. *p < 0.05, **p < 0.01, ***p < 0.001, n.s. non-significant, Wilcoxon signed-rank tests. Data are means per subject.

Data Acquisition and Analysis

Procedures to record kinematics, kinetics, and muscle activity were detailed previously. For locomotion, 140 parameters were computed automatically from kinematic and muscle activity recordings (Table 2.2) according to published methods [65, 67, 111, 112]. Clinical reports were generated automatically for each set of trials (database S1[1]). For standing, 15 classic parameters were calculated (Table 2.2). Locomotor performance was evaluated using a PC analysis [65, 67, 112], which is summarized in Figure 2.4 and described below.

Principal Component Analysis

PC analysis was applied to parameters computed from recordings obtained during quiet standing and locomotion. The various steps and interpretation of this analysis are detailed in Figure 2.4 and described in the following paragraph. PC analyses were applied using the correlation matrix [65, 67, 112]. Three types of datasets were examined with a PC analysis. For quiet standing, the PC analysis was applied on a set of 15 kinematic, kinetic and electromyographic parameters computed on 40 time-windows lasting 1 second for each experimental condition per subject. The analysis was applied for each subject independently. For locomotion, the PC analysis was applied to all the computed kinematic parameters from all individual gait cycles from all the subjects simultaneously, or on all the computed kinematic and muscle activity parameters for each subject independently. Gait cycles and postural time-windows were visualized in the new synthetic space defined by the two first PCs. The locomotor performance was measured as the Euclidian distance between the data points in PC1-PC2 space and the mean position of data points obtained in healthy individuals [65, 67, 112]. The relevant parameters to account for differences between experimental conditions or subjects were extracted based on the factor loadings (correlation) of individual parameters onto each PC.

Representation and processing of kinematic and muscle activity recordings

First, a typical representations is derived from kinematic and muscle activity recordings are shown for a healthy individual and a subject with a SCI who needed crutches in order to walk (Figure 2.4). Kinematics are depicted with a stick diagram decompo-

[1] Not included in the thesis

#	Details	Figures
	Spatiotemporal parameters	
1	gait cycle duration [s]	
2	step duration [s]	
3	stance duration [%GC]	
4	swing duration [%GC]	
5	drag duration [%GC]	
6	drag duration [%swing]	
7	single stance duration [%GC]	
8	double stance duration [%GC]	
9	step length [%BH]	
10	stride length [%BH]	
11	step width [%BH]	
12	stride speed [m/s]	
13	stride length at CoM [%BH]	
14	stride speed at CoM [m/s]	
15	length of foot trajectory [%BH]	
16	length of CoM trajectory [%BH]	
17	step height [%BH]	
18	lateral movement during swing [%BH]	
19	maximal hip vertical amplitude during gait cycle [%BH]	
	Joint angles	
20	minimal hip flexion/extension angle [deg]	
21	maximal hip flexion/extension angle [deg]	
22	amplitude of hip flexion/extension angle [deg]	
23	minimal knee flexion/extension angle [deg]	
24	maximal knee flexion/extension angle [deg]	
25	amplitude of knee flexion/extension angle [deg]	
26	minimal ankle flexion/extension angle [deg]	
27	maximal ankle flexion/extension angle [deg]	
28	amplitude of ankle flexion/extension angle [deg]	
	Elevation angles	
29	minimal femur elevation angle [deg]	
30	maximal femur elevation angle [deg]	
31	amplitude of femur elevation angle [deg]	
32	minimal tibia elevation angle [deg]	
33	maximal tibia elevation angle [deg]	
34	amplitude of tibia elevation angle [deg]	
35	minimal foot elevation angle [deg]	
36	maximal foot elevation angle [deg]	
37	amplitude of foot elevation angle [deg]	
38	minimal leg elevation angle [deg]	
39	maximal leg elevation angle [deg]	
40	amplitude of leg elevation angle [deg]	
41	minimal arm elevation angle [deg]	
42	maximal arm elevation angle [deg]	
43	amplitude of arm elevation angle [deg]	
	Angular velocity	
44	maximal speed of hip flexion/extension angle [deg/s]	
45	maximal speed of knee flexion/extension angle [deg/s]	
46	maximal speed of ankle flexion/extension angle [deg/s]	
47	maximal speed of femur elevation angle [deg/s]	
48	maximal speed of tibia elevation angle [deg/s]	
49	maximal speed of foot elevation angle [deg/s]	
50	maximal speed of leg elevation angle [deg/s]	
51	maximal speed of arm elevation angle [deg/s]	
	Intra and Interlimb coordination (frequency domain)	
52	difference of phase between femur and tibia elevation angles [deg]	
53	difference of phase between femur and foot elevation angles [deg]	
54	difference of phase between tibia and foot elevation angles [deg]	
55	difference of phase between hip and knee joint angles [deg]	
56	difference of phase between hip and ankle joint angles [deg]	
57	difference of phase between knee and ankle joint angles [deg]	
58	difference of phase between ipsi- and contra-arm angles [deg]	
59	difference of phase between ipsi- and contra-leg angles [deg]	
60	difference of phase between ipsi-arm and ipsi-leg angles [deg]	
61	difference of phase between ipsi-arm and contra-leg angles [deg]	
	Intra and Interlimb coordination (time domain)	
62	shift between femur and tibia elevation angles to obtain maximal correlation [%GC]	
63	shift between femur and foot elevation angles to obtain maximal correlation [%GC]	
64	shift between tibia and foot elevation angles to obtain maximal correlation [%GC]	
65	shift between hip and knee joint angles to obtain maximal correlation [%GC]	
66	shift between hip and ankle joint angles to obtain maximal correlation [%GC]	
67	shift between knee and ankle joint angles to obtain maximal correlation [%GC]	
68	maximal correlation between femur and tibia elevation angles	
69	maximal correlation between femur and foot elevation angles	
70	maximal correlation between tibia and foot elevation angles	
71	maximal correlation between hip and knee joint angles	
72	maximal correlation between hip and ankle joint angles	
73	maximal correlation between knee and ankle joint angles	
74	shift between arms elevation angles to obtain maximal correlation [%GC]	
75	shift between legs elevation angles to obtain maximal correlation [%GC]	
76	shift between femur elevation angles to obtain maximal correlation [%GC]	
77	shift between tibia elevation angles to obtain maximal correlation [%GC]	
78	shift between foot elevation angles to obtain maximal correlation [%GC]	
79	shift between hip joint angles to obtain maximal correlation [%GC]	
80	shift between knee joint angles to obtain maximal correlation [%GC]	
81	shift between ankle joint angles to obtain maximal correlation [%GC]	
82	maximal correlation between arms elevation angles	
83	maximal correlation between legs elevation angles	
84	maximal correlation between femur elevation angles	
85	maximal correlation between tibia elevation angles	
86	maximal correlation between foot elevation angles	
87	maximal correlation between hip joint angles	
88	maximal correlation between knee joint angles	
89	maximal correlation between ankle joint angles	
90	shift between ipsi- and contra-arm elevation angles for maximal correlation [%GC]	
91	shift between ipsi- and contra-leg elevation angles for maximal correlation [%GC]	
92	shift between ipsi-arm and ipsi-leg elevation angles for maximal correlation [%GC]	
93	shift between ipsi-arm and contra-leg elevation angles for maximal correlation [%GC]	
94	maximal correlation between ipsi- and contra-arm elevation angles	
95	maximal correlation between ipsi- and contra-leg elevation angles	
96	maximal correlation between ipsi-arm and ipsi-leg elevation angles	
97	maximal correlation between ipsi-arm and contra-leg elevation angles	

#	Details	Figures
	Planar covariation of leg elevation angles	
98	path length (PC1 variance; PCA applied on foot, tibia and femur elevation angles) [%]	
99	path width (PC2 variance; PCA applied on foot, tibia and femur elevation angles) [%]	
100	planarity factor (percent of variance accounted for by the two first PCs) [%]	
101	spatial orientation (angle between thigh axis and PC3 direction) [deg]	
102	spatial orientation (angle between shank axis and PC3 direction) [deg]	
103	spatial orientation (angle between foot axis and PC3 direction) [deg]	
	Trunk stability	
104	distance travelled by trunk barycenter in frontal plane [%BH]	
105	amplitude of trunk barycenter on lateral axis [%BH]	
106	amplitude of trunk barycenter on vertical axis [%BH]	
107	distance travelled by trunk barycenter in frontal plane [%BH]	
108	amplitude of trunk barycenter on lateral axis [%BH]	
109	amplitude of trunk barycenter on vertical axis [%BH]	
110	mean of trunk roll angle during double stance [deg]	
111	maximal absolute roll angle during single stance [deg]	
112	amplitude of roll angle during single stance [deg]	
113	maximal absolute roll angle during swing [deg]	
114	amplitude of roll angle during swing [deg]	
	Feet trajectory	
115	maximal distance between both feet [%BH]	
116	maximal distance of foot from center line during swing [%BH]	
117	mean angle of foot during stance [deg]	
118	maximal distance between both feet in body reference frame [%BH]	
119	maximal distance of foot from center line during swing in body reference frame [%BH]	
120	mean angle of foot during stance in body reference frame [deg]	
	EMG params	
121	burst duration of ankle extensor [%GC]	
122	burst duration of ankle flexor [%GC]	
123	onset of ankle extensor burst [%GC]	
124	onset of ankle flexor burst [%GC]	
125	end of ankle extensor burst [%GC]	
126	end of ankle flexor burst [%GC]	
127	root mean square of ankle extensor burst [mV]	
128	root mean square of ankle flexor burst [mV]	
129	maximal amplitude of ankle extensor burst [mV*100]	
130	maximal amplitude of ankle flexor burst [mV*100]	
131	burst duration of knee extensor [%GC]	
132	burst duration of knee flexor [%GC]	
133	onset of knee extensor burst [%GC]	
134	onset of knee flexor burst [%GC]	
135	end of knee extensor burst [%GC]	
136	end of knee flexor burst [%GC]	
137	root mean square of knee extensor burst [mV]	
138	root mean square of knee flexor burst [mV]	
139	maximal amplitude of knee extensor burst [mV*100]	
140	maximal amplitude of knee flexor burst [mV*100]	

#	Details	Figures
	Standing parameters for PCA to determine optimal upward force	
1	rms over a time window of 1s between CoM 3D position and mean CoM 3D position [cm]	
2	mean over a time window of 1s of the left tibia elevation angle [deg]	
3	mean over a time window of 1s of the left femur elevation angle [deg]	
4	mean over a time window of 1s of the right tibia elevation angle [deg]	
5	mean over a time window of 1s of the right femur elevation angle [deg]	
6	mean over a time window of 1s of the angle between gravity axis and segment from middle of heels to C7 [deg]	
7	mean over a time window of 1s of AP position of CoP [% heel to ankle AP distance]	
8	mean over a time window of 1s of ML position of CoP [% ML distance between ankles]	
9	mean over a time window of 1s of AP velocity of CoP [cm/s]	
10	mean over a time window of 1s of ML velocity of CoP [cm/s]	
11	mean over a time window of 1s of CoP to CoM distance [cm]	
12	mean over a time window of 1s of left soleus envelop [% maximal value accross all trials of the subject]	
13	mean over a time window of 1s of right soleus envelop [% maximal value accross all trials of the subject]	
14	rms over a time window of 1s of left tibialis anterior envelop [% maximal value accross all trials of the subject]	
15	rms over a time window of 1s of right tibialis anterior envelop [% maximal value accross all trials of the subject]	
	Standing parameters for Artificial Neuron Network to determine optimal upward force	
A	mean of 10 consecutive standing param#1 [cm]	
B	standard deviation of 10 consecutive standing param#1 [cm]	
C	mean of 10 consecutive standing param#6 [deg]	
D	standard deviation of 10 consecutive sum of standing param#2 and #4 [deg]	
E	standard deviation of 10 consecutive sum of standing param#3 and #5 [deg]	
F	mean of 10 consecutive standing param#7 [% heel to ankle AP distance]	
G	standard deviation of 10 consecutive standing param#7 [% heel to ankle AP distance]	
H	mean of 10 consecutive standing param#8 [% ML distance between ankles]	
I	standard deviation of 10 consecutive standing param#8 [% ML distance between ankles]	
J	standard deviation of 10 consecutive standing param#9 [cm/s]	
K	standard deviation of 10 consecutive standing param#10 [cm/s]	
L	mean of 10 consecutive standing param#11 [cm]	

Abbreviations	
%BH	in percent of body height
%GC	in percent of gait cycle
L	left
R	right
CoM	center of mass
CoP	center of pressure
AP	antero-posterior
ML	medio-lateral

Table 2.2 – List of parameters computed during walking and standing.

sition of the head, trunk and legs during the stance and swing phases of a complete gait cycle. Changes in hip, knee and ankle of the right and left legs are averaged over 10 gait cycles for each leg. A 3D plot shows the successive gait loops obtained by plotting the thigh, shank and foot elevation angles (oscillations with respect to the direction of gravity) against each other. The gait loops lie close to a plane of co-

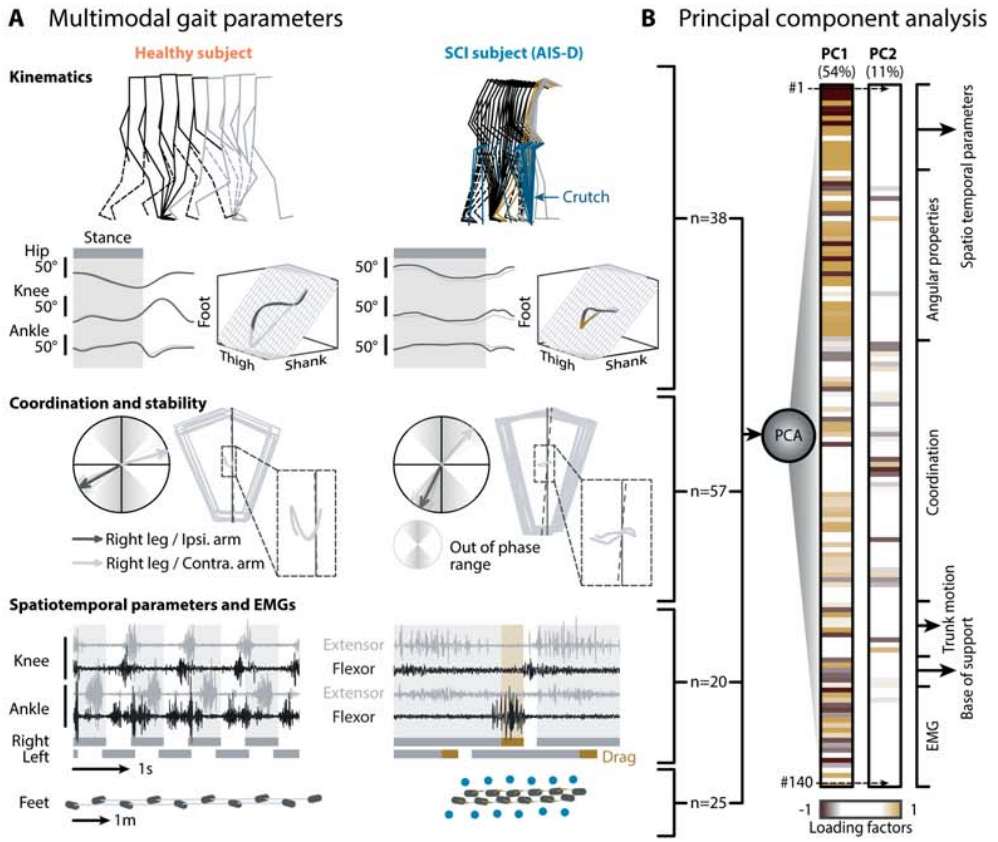
A Multimodal gait parameters
Healthy subject
SCI subject (AIS-D)
Kinematics
Crutch
Stance
Hip 50°
Knee 50°
Ankle 50°
Foot
Thigh
Shank
Coordination and stability
Right leg / Ipsi. arm
Right leg / Contra. arm
Out of phase range
Spatiotemporal parameters and EMGs
Knee
Ankle
Right
Left
1s
Feet
1m
Extensor
Flexor
Drag
B Principal component analysis
PC1 (54%)
PC2 (11%)
#1
#140
n=38
n=57
n=20
n=25
PCA
Spatio temporal parameters
Angular properties
Coordination
Trunk motion
Base of support
EMG
-1
1
Loading factors
C Visualisation of gait performance on PC1-2 space
PC1 (explained variance : 54.2%)
Pathological alteration, p < 0.001
PC2 (10.6%)
Left / right asymetry, p < 0.001
Healthy subject
Left
Right
SCI subject (AIS-D)
Left
Right
PC1 score (a.u.)
PC2 score (a.u.)
Locomotor performance
(PC1-2 score, a.u.)
+/- sem
Healthy
D Functional clustering
PC1
Spatiotemporal
Leg muscle activity
Base of support
PC1
Joint angle
Joint angle speed
PC2
Interlimb Coordination
Intralimb coordination
Trunk motion
E Selection of relevant parameters
PC1
Stride length (% body height)
Double stance (% gait cycle)
Ankle extensor burst duration (% gait cycle)
Whole leg angle range of motion (deg)
PC2
Leg coordination index (% gait cycle)
Trunk sway (deg)

Figure 2.4 – **Representation and processing of kinematic and muscle activity recordings. A**, From top to bottom. Kinematics: stick diagram decomposition (rate, 120ms) of the head, trunk and legs during the stance (dark) and swing (light) phases of a gait cycle. The filled and dashed lines differentiate the right and left legs, respectively. Changes in hip, knee and ankle of the right and left legs averaged over 10 gait cycles. Covariation of the thigh, shank and foot elevation angles. Coordination and stability: polar plots showing the coordination between the oscillations of the legs and arms during walking. The successive positions of the trunk (rate, 120 ms) are shown together with the trajectory of the center of mass (CoM) of the trunk. Spatiotemporal parameters and muscle activity: raw electromyographic signals of extensor (light) and flexor (dark) muscles of the knee and ankle during a series of steps. The horizontal bars indicate the stance phases of the legs. The brown bars indicate the occurrence of dragging during the transition from stance to swing. The positions of the feet on the floor are displayed together with the continuous trajectories of the feet in the horizontal (floor) plane. The blue dots indicate the locations of the crutches on the floor. The number of computed parameters is indicated for each type of recording modality. **B**, The vertical bars report the factor loadings (correlation) of each parameter onto PC1 and PC2 (%, explained variance). The color indicates the strength of the correlation between a given parameter and the PC. **C**, Each gait cycle is represented in the PC1 and PC2 space. Each color-coded dot corresponds to a single gait cycle, while the circles indicate the average value for each condition. The PC score corresponds to the position of the gait cycle along each PC axis. The bar plots report the mean scores of gait cycles for each leg. The locomotor performance is quantified as the Euclidian distance between gait cycles of neurologically impaired subjects and those of healthy individuals in the PC1 and PC2 space. The mean values (horizontal bar) $\pm$ s.e.m (thickness) measured during locomotion in healthy subject is represented in orange. **D**, Functional clusters. The name of each numbered parameter is indicated in Table 2.2. **E**, Bar plots reporting the mean values of representative parameters for each of the functional clusters, highlighted in yellow. ***$p < 0.001$, Two-way ANOVA with Tukey-Kramer post hoc tests. Data are means $\pm$ s.e.m.

variation that captures the strength and properties of inter-segmental coordination patterns. Polar plots show the coordination between the oscillations of the legs and arms during walking. The successive positions of the trunk are shown together with the trajectory of the center of mass of the trunk. Raw muscle activity is displayed along stance and swing phases. The positions of the feet on the floor are displayed together with the continuous trajectories of the feet in the horizontal (floor) plane, with the locations of the crutches on the floor. The number of computed parameters is indicated for each type of recording modality. The list of 140 computed parameters is detailed in Table 2.2. Then, to quantify locomotor performance and identify the most relevant parameters to explain differences between subjects or experimental conditions, a principal component (PC) analysis is applied to all the computed parameters. The factor loadings (correlation) of each parameter onto PC1 and PC2 (%, explained variance) are reported with a color code that indicates the strength of the correlation between a given parameter and the PC. In this example (Figure 2.4), the PC analysis was applied on all the gait cycles of the healthy individual and the subject with a SCI. Consecutively, each gait cycle is represented in the new "denoised" space created by PC1 and PC2. Each color-coded dot corresponds to a single gait cycle, while the circles indicate the average value for each condition. The PC score corresponds to the position of the gait cycle along each PC axis. The bar plots report the mean scores of gait cycles for each leg of the healthy individual and the subject with SCI. This analysis allows the identification of the features captured on each

axis. For example, PC1 segregated gait cycles of the healthy individual from those of the subject with SCI. PC2 distinguished the different deficits of the left and right side of the subject with SCI. Throughout the study, we quantified the locomotor performance as the Euclidian distance between gait cycles of neurologically impaired subjects and those of healthy individuals in the PC space defined by PC1 and PC2. The mean values (horizontal bar) $\pm$ s.e.m (thickness) measured during locomotion in healthy subject is represented in orange for reference. After this processing, the computed parameters that strongly correlate with a given PC ($|\text{loading factors}| > 0.5$) are extracted and regrouped into functional clusters that we name for clarity. The name of each numbered parameter is indicated in Table 2.2.

Statistical Analysis

All data are reported as mean values $\pm$ SEM, unless specified otherwise. The non-parametric Mann-Whitney U-test, or the Wilcoxon signed-rank test, was used to compare two unpaired, resp. paired, conditions. Kruskal-Wallis test was used to compare subject's gait cycles in several conditions. Two-ways ANOVA or its non-parametric equivalent, Friedman test, were used to compare subjects and conditions (Anderson-Darling test was used to evaluate normal distribution). Post-hoc comparisons were performed using the Tukey-Kramer test when appropriate. Statistical tests are specified in the legends of figures.

Extended Experimental Protocols

Protocol 1: Properties of the neurorobotic platform

Healthy subjects were recorded during locomotion without and with robot along a straight (8 subjects) or curvilinear path (6 subjects) projected on the floor using the augmented reality system. They were asked to walk naturally at their own selected pace. They wore the harness during both conditions. The robot was configured in transparent mode, which corresponds to the minimal upward force (40N) necessary to maintain cable tension. For each condition, 10 gait cycles were extracted from the middle of the recorded trials (i.e. excluding gait initiation and termination) and analyzed.

Protocol 2: Impact of upward and forward forces on posture and gait

Five subjects were first recorded during quiet standing while attached to the robotic interface. They were asked to stand quietly with eyes open. Each foot was positioned on its own force plate with a standardized location and orientation [113]. The distance between the medial side of the heels was set at 8.4 cm and the external rotation angle of the feet was kept at 9 degree with respect to the sagittal plane. The subjects were instructed to center and stabilize their center of foot pressure that was projected on the floor in real-time through the augmented reality system. This visual biofeedback was removed during recordings. The subjects were then asked to stare at a visual reference mark projected on the floor 3 m straight ahead in front of them. Each trial lasted 20 seconds. Two trials were collected for each upward and forward force.

The same subjects were then evaluated during locomotion across a broad range of upward and forward forces. The subjects were asked to walk naturally at their own selected pace. For each condition, a total of 10 steady-state gait cycles was recorded and analyzed.

Finally, five additional subjects were recorded during locomotion on a treadmill in transparent mode, with 60% of upward force, and with a combination of 60% of upward force and 2% of forward force. The speed of the treadmill belt was kept constant across conditions.

Protocol 3: Design of gravity-assist algorithm: personalization of upward force

Nine subjects with a SCI or a stroke were tested during quiet standing over the maximum possible range of upward forces under the same conditions as explained in Protocol 2. For each upward force, two trials were collected that each lasted 20 s and were separated by 1 min. Each trial was then divided into a set of 20 windows of 1 s over which 15 kinematic, kinetic and electromyographic parameters were computed (Table 2.2). A PC analysis was applied on these variables to determine the optimal upward force for each subject.

We then used this dataset and results to build an artificial neural network that calculated the necessary correction of upward force to provide each subject with optimal upward force. The artificial neural network integrated the kinematic and kinetic parameters (n = 12, 10 seconds of recording, see Table 2.2). We tested 13 learning rules and 11 structures with different numbers of neurons in the hidden layer. We ran-

domly and iteratively extracted 20% of the data from the training set in order to perform a cross-validation of the artificial neural network configuration. This process led to the selection of a one-layer feedforward model with log-sigmoid hidden neurons and linear output neurons showing the lowest mean squared error (Neural Network Toolbox from Matlab). The selected model combined 9 neurons and learned rules through the Levenberg-Marquardt algorithm. We then fed the selected model with a test dataset in order to validate the properties of the artificial neuronal network.

Protocol 4: Design of gravity-assist algorithm: personalization of forward force

To guide and initialize the forward force correction, we conducted computational simulations using a simple bipedal spring-mass model adapted from [114], which is the simplest model displaying human-walking behaviors such as a vertical oscillation of the center of mass and a double stance. The model is composed of a point mass m and two weightless segments attached to this mass, which represent the legs. A linear spring element of stiffness k is inserted in the leg model in order to enable deformations similar to a spring-loaded inverted pendulum [114]. The main difference compared to the model in [114] is the addition of a damper element with constant d in series with the spring in each leg segment that is necessary to counteract the effect of the forward and upward forces added at the level of the center of mass. The angle of attack of the leg at the end of swing is an open parameter defined as α. During the swing phase, the length l of the leg equals the resting length l_0. Consequently, the occurrence of impact is deduced from geometrical calculations. The end of the stance phase is defined at the moment when the leg extended beyond l_0. Two legs can be in contact with the ground simultaneously representing the double support phase typical of walking gaits. Forward and upward forces (F_y and F_z, respectively) were added at the level of the center of mass in order to emulate the robotic assistance.

$$\vec{F}_{tot} = -(||\vec{u}|| - l_0)k\frac{\vec{u}}{||\vec{u}||} - mg\vec{e_z} - d\frac{\dot{\vec{u}} \cdot \vec{u}}{||\vec{u}||^2}\vec{u} + F_y\vec{e_y}$$

$$\vec{u} = [y, z]^T$$

, with F_{tot} being the total force applied on the mass, y and z being the position of the mass (in forward and upward direction respectively), g being the acceleration due to gravity, and e_y and e_z being directional vectors.

The mass and the resting length of the leg l_0 in the model were fixed to 80 kg and 1 m, respectively, for all simulations. A reference stable walking behavior of the model

has been obtained by selecting values of α, k and the energy of the system E from the parameters domain analyzed in [109] (α = 69 deg, k = 13'500 N/m, E = 816 J and d = 0 N·s/m). From this reference behavior, we obtained the reference step length s_0, the reference walking speed v_0 and the reference amplitude Δz_0 of vertical oscillations of the center of mass. For each pair of upward-forward force values (from 10% to 60% by step of 10% for the upward force and from 0 to 10% by step of 0.5% for the forward force; in percent of model mass), we performed simulation with several combinations of open parameter values α, d, and k (values were chosen in a range around the reference values). For each set of the three open parameters, we measured the step length s_2, the walking speed v_2 and the amplitude Δz_2 of vertical oscillations of the center of mass. The set of the three open parameters that minimized the distance to the reference behavior (distance given by the cost function here-below) was selected for each particular upward force and the associated forward force was designated as the optimal forward force for that particular upward force value.

$$R = 1 - \frac{1}{3}\left(\frac{|s_2 - s_0|}{|s_1 - s_0|} + \frac{|v_2 - v_0|}{|v_1 - v_0|} + \frac{|\Delta z_2 - \Delta z_0|}{|\Delta z_1 - \Delta z_0|}\right)$$

, where s_1, v_1 and Δz_1 are the step length, walking speed and vertical oscillation of the center of mass (respectively) for the condition of the same upward force applied for s_2, v_2 and Δz_2 but without forward force, which enables to normalize the s, v and Δz values.

We then recorded a total of 22 subjects with a SCI or a stroke. The subjects were recorded during locomotion with the upward force predicted by the artificial neural network algorithm, and a range of forward forces of maximum $\pm$ 10% of body weight. The subjects were asked to walk at their own, comfortable pace. For each condition, the subjects performed 3 or 4 trials during which they walked straight ahead over a distance of approximately 10 m. We assessed the locomotor performance using a PCA gathering all the conditions collected for a single participant. For each participant, the forward force that enabled the highest locomotor performance was considered as the optimal forward force for the applied upward force.

The gait parameters were then represented in a three-dimensional space whereby the first dimension was the amount of upward force, the second dimension was the walking speed v normalized by leg length l (Froude number: $v^2/(g \cdot l)$), and the third dimension was the amount of forward force. We then fitted a polynomial function to the data obtained from simulations and from the patients, to predict optimal forward force from upward force and Froude number. For this, we tested 25 two-dimensional polynomial functions with degrees ranging from 1 to 5, including cross-terms. For

each polynomial, 75% of the data were randomly selected. A polynomial function was fitted to this dataset. The accuracy was evaluated using a 500-fold cross-validation and root mean square error (RMSE) on the 25% remaining data. The selected polynomial function was applied on the entire dataset to generate a final decision map that indicated the necessary forward force correction based on the selected upward force and walking speed of the subject.

Protocol 5: Validation of the gravity-assist algorithm to enable locomotion in individuals with SCI or stroke

Six subjects with a SCI or stroke were recorded during quiet standing with the optimal upward force calculated by the artificial neural networks. Two trials lasting 20 s each were recorded. Recordings were then performed with the addition and subtraction of an upward force corresponding to 10% of the bodyweight, resulting in 3 upward force conditions. Two trials were acquired per condition. The decision map was used to define the forward force correction for these three upward forces, and the subjects were then recorded during locomotion with these configurations. The subjects were asked to walk at their own, comfortable pace. For each condition, the subjects performed 3 or 4 trials during which they walk straight ahead over a distance of approximately 10 m. The two first steps (gait initiation) and the two last steps (gait termination) were rejected from the analysis.

Protocol 6: The gravity-assist improves locomotor performance in individuals with SCI and stroke

Twenty-six subjects with a SCI or stroke were recorded during quiet standing in order to configure the gravity-assist. Ambulatory subjects were then asked to walk in the straight direction at their own, comfortable pace using their preferred assistive device (without robot). All the subjects were then recorded during locomotion with gravity-assist. A total of 15.9 ± 0.85 gait cycles were analyzed for each subject and condition.

Protocol 7: The gravity-assist improved locomotor performance after a one-hour gait training session

Five subjects with SCI participated in two training sessions, separated by one week (Figure 2.13A). During the first session (60 min), subjects walked overground with

gravity-assist. During the second session (week 2), they were asked to walk the same distance on a treadmill with the same upward force, but without forward force corrections. Immediately before and after each training session, the subjects were recorded during overground locomotion without gravity-assist at their own selected pace. They were allowed to use their preferred assistive device. During each training session, subjects were allowed to rest when necessary.

Protocol 8: The gravity-assist enables subjects with SCI or stroke to perform skilled postural and locomotor paradigms

Irregular horizontal ladder (Figure 2.14A): Subjects who exhibited sufficient locomotor performance for this task were tested to evaluate skilled locomotion. They were asked to walk along a horizontal ladder consisting of a succession of ten irregularly spaced rungs (10 cm width) with gaps of 0, 10, 20 or 30 cm. The total length of the ladder was 270 cm. The ladder was located 15 cm above the ground. Without the gravity-assist, the vast majority of the subjects could not perform the task. In order to obtain a baseline, these subjects were asked to walk along the same ladder layout that was projected on the floor by means of the augmented reality system as shown.

Curved path (Figure 2.14B): An augmented reality system projected a curvilinear path on the floor. The subjects with SCI or stroke who were able to walk without assistive device under gravity-assist were asked to walk along the projected path.

Lateral perturbation (Figure 2.14C): To evaluate the ability of subjects to maintain dynamic balance, a sudden or sustained lateral force was applied to the trunk while subjects were walking in the straight-ahead direction. Two types of lateral perturbation were tested in subjects with SCI (n = 3) or stroke (n = 1). First, a 50 N lateral force was applied leftward or rightward over a 500 ms window. Second, a constant 50 N force was applied leftward prior to gait initiation and was kept constant during the first steps. Suddenly, a 50 N force was applied rightward. The transition occurred within a 500 ms window. The rightward force was maintained constant until the end of the trial.

Results

Properties of the Neurorobotic Platform

We used a cable robot [68] that provides a safe environment, preventing falls while allowing control of forces applied to the trunk through a dedicated harness (Figure 2.2) along the three Cartesian directions during locomotion in a large workspace (Figure 2.5A). We integrated the robotic interface within a platform [105], allowing real-time acquisition of forces applied to the trunk, whole-body kinematics, ground reaction forces and muscle activity (Figure 2.5B).

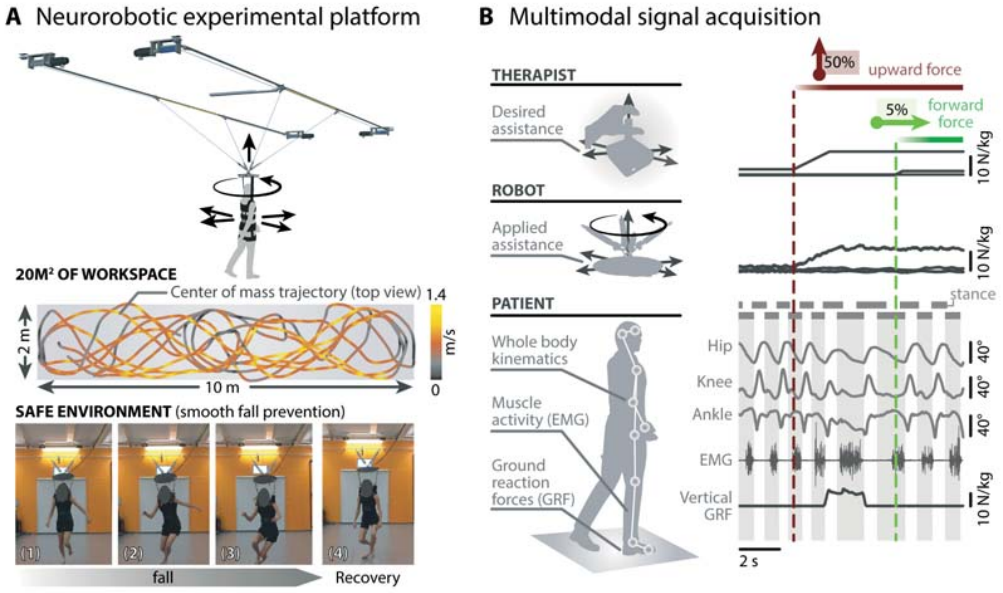

Figure 2.5 – Technological framework of the multidirectional gravity-assist. A, Schematic and photograph of the robotic support system, including the directions of the actuated and passive (rotation) degrees of freedom. The spatial trajectory and instantaneous speed of the CoM are shown during locomotion within the entire workspace. Photographs (1 to 4) illustrating recovery from a fall. **B**, Kinematics, EMG activity and GRFs are recorded concomitantly. A gait sequence is shown during which an upward force followed by an increasing forward force are applied to a healthy subject during walking. From top to bottom: desired forces, measured forces, left and right stance durations, leg joint angles, EMG activity, vertical GRFs, and timing of applied forces.

To evaluate the absence of detrimental interactions between the robotic system and locomotor performance, we recorded leg kinematics, muscle activity and kinetics during walking without and with robot in 8 healthy individuals. The robot delivered a 40 N upward force, which corresponds to the minimal upward force necessary to maintain tension in the cables (transparent mode). The majority of computed gait parameters did not differ between both conditions (Figure 2.3A). However, the upward force (40 N) did lead to a small decrease in the amplitude of vertical and

anteroposterior components of ground reaction forces (Figure 2.3B). These kinetic alterations were associated with a decrease in speed (Figure 2.3A) and an increase in the activity of ankle extensor muscles (medial gastrocnemius; Figure 2.3C).

When applying forces with the robot, the resulting interaction force components displayed variabilities due to imprecision in the force controller, dynamic friction and inertia [68]. However, the variability remained confined within 4.2 $\pm$ 1.7 N for forward forces, 3.5 $\pm$ 1.8 N for lateral forces, and 6.2 $\pm$ 1.2 N for upward forces (net force: 6.4 $\pm$ 1.3 N). As expected, inaccuracies increased during locomotion along a sinusoidal path (n = 6 subjects), but even in these challenging conditions, the alterations of gait patterns remained minimal (Figure 2.3D). These combined results indicate that the robotic attachment exerted minimal interference with the production of gait.

Impact of Upward and Forward Forces on Posture and Gait

We next evaluated the effects of forces applied to the trunk during standing and walking in healthy individuals. We first studied the impact of upward forces during standing. The upright human body can be modeled as an inverted pendulum (Figure 2.6A). Due to the natural forward tilt of the body (β), the center of mass (CoM) projects in front of the rotational axis (ankle) of the pendulum. Consequently, the mean antero-posterior position of the center of plantar pressure (CoP) was located at 25 $\pm$ 1% of the base of support length (n = 5 subjects). This biomechanical configuration allowed the maintenance of balance through the tonic activation of anti-gravity muscles acting at the ankle (Figure 2.6A) (26).

The application of upward forces (40 to 500 N) induced a backward tilt, which shifted the CoP position towards the heels (Figure 2.6B). Subjects displayed increased postural sways, paralleled by considerable changes in ankle muscle activity patterns (Figure 2.6A). We found that a forward force compensated for the detrimental impacts of upward force. Forward forces restored the position and dynamics of the CoP, which reestablished appropriate ankle muscle activity (Figure 2.6A,B).

We then evaluated the occurrence of similar interactions between upward and forward forces during locomotion. To capture the effects of force interactions, we calculated a comprehensive number of parameters (n = 120, table 2.2) that we subjected to a principal component (PC) analysis (Figure 2.4) (22, 27). Upward forces alone led to a gradual alteration of gait features and muscle activity (Figure 2.6B,C,D and Figure 2.7A,B). We detected negative correlations between upward forces and

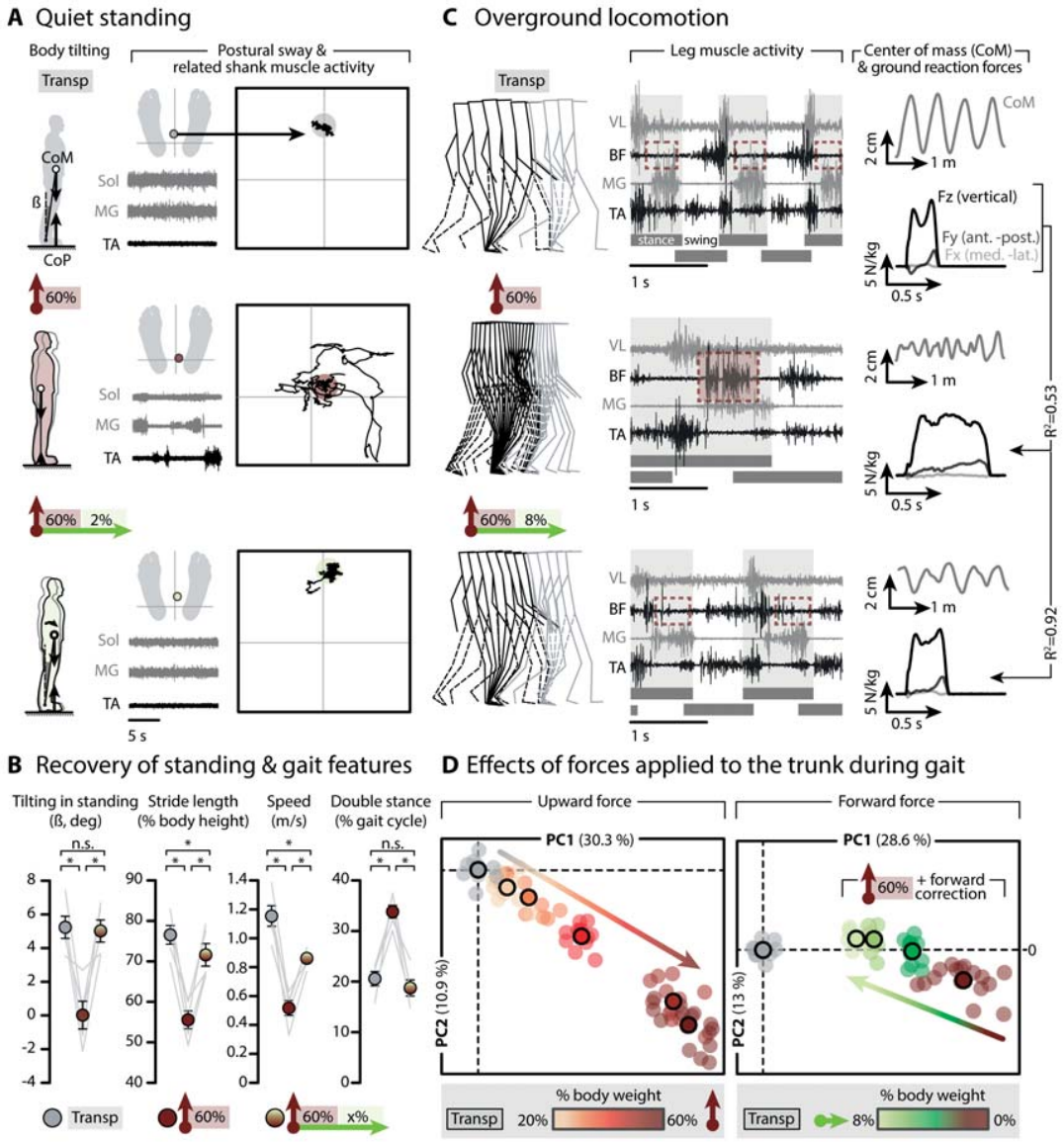

Figure 2.6 – Interaction between upward and forward forces during standing and walking. A, Schematic of the body, including the CoM, the postural orientation (β), and the center of foot pressure (CoP). The mean position of the CoP with respect to the feet is shown during standing with transparent (Transp) support, upward force only, and both upward and forward forces. A concomitant sequence of EMG activity from ankle extensor (soleus, Sol; medial gastrocnemius, MG) and ankle flexor muscles (tibialis anterior, TA) is displayed. The plot represents the continuous and mean (colored circle) positions of the CoP for each condition. The X-axis refers to the axis passing through the malleoli, whereas the Y-axis corresponds to the midline between the feet. B, Plots reporting the mean values (± s.e.m.) of during standing, and gait parameters under the conditions shown in (A) and (C), *p < 0.05, n.s. non-significant, Wilcoxon signed-rank tests, n = 5 healthy subjects. C, Stick diagram decomposition (rate, 120 ms) of head, trunk and leg movements during stance (dark, shading) and swing (light, unshaded). The stick diagram decomposition of trunk and leg movements are shown for sides. The filled and dashed lines differentiate the right and left legs, respectively. The EMG activity of extensor and flexor muscles acting at the ankle and knee (vastus lateralis, VL; biceps femoris, BF) is displayed, together with the CoM trajectory in the sagittal plane and GRFs. D, Gait kinematics of one subject shown in the space created by PC1 and PC2 (%, explained variance). Each color-coded dot corresponds to a single gait cycle, whereas the black circles indicate the average value for each condition.

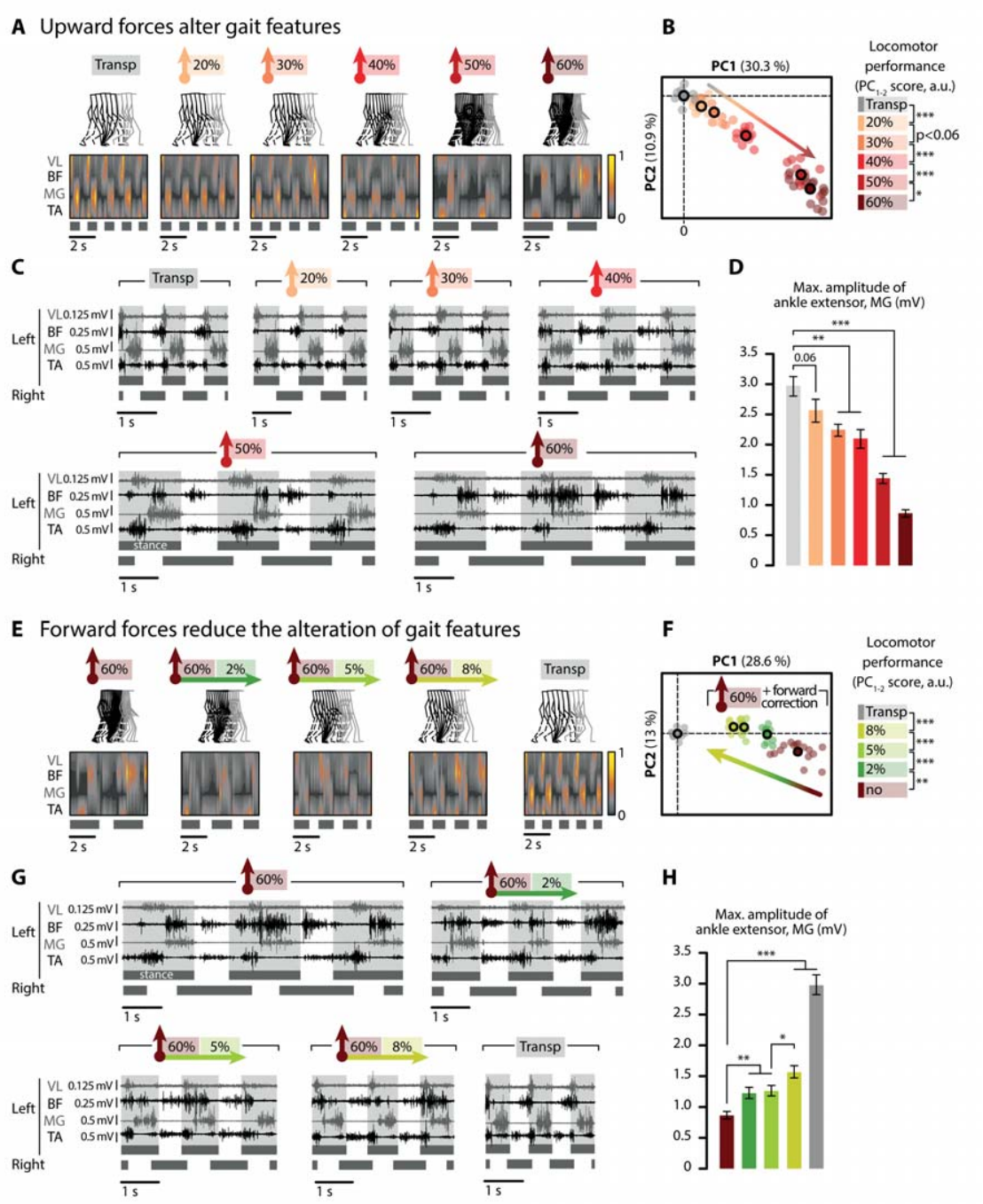
A Upward forces alter gait features
Transp
20%
30%
40%
50%
60%
VL
BF
MG
TA
2 s
B
PC1 (30.3 %)
PC2 (10.9 %)
Locomotor performance
(PC1-2 score, a.u.)
p<0.06
C
Left
Right
VL 0.125 mV
BF 0.25 mV
MG 0.5 mV
TA 0.5 mV
stance
1 s
D
Max. amplitude of ankle extensor, MG (mV)
0.06
E Forward forces reduce the alteration of gait features
60% 2%
60% 5%
60% 8%
F
PC1 (28.6 %)
PC2 (13 %)
60% + forward correction
8%
5%
2%
no
G
H
Max. amplitude of ankle extensor, MG (mV)

Figure 2.7 – **Impact of upward and forward forces on body kinematics and muscle activity.** **A**, Representative stick diagram decomposition of whole body movement during an entire gait cycle of the right leg during locomotion without robot, and with a range of increasing upward forces, as indicated by the color-coded boxes with an upward arrow. A sequence of EMG activity recorded from flexor and extensor muscles of the knee and ankle is represented as a heat map, showing the activity of these muscles averaged over multiple steps (n = 10). The EMG signal is normalized to the maximum level of activity recorded across conditions for each muscle. The grey boxes at the bottom indicate the duration of the right stance phase. The duration of the sequence is maintained constant across conditions, allowing to rapidly appreciate the graded impact of upward forces on the timing of gait events. **B**, A PCA was applied on the 140 gait parameters computed for each gait cycle, shown by each dot. The outlined circles indicate the mean of the gait cycles under a specific condition. **C**, Raw EMG signals corresponding to the conditions shown in (A). **D**, Bar plots showing the mean activity of ankle extensor muscles (anti-gravity muscle) for each condition of upward force. (E-H) The same representations and analyses are shown when adding a range of increasing forward forces during locomotion while the upward force was maintained constant at 60% of the bodyweight. The amount of forward force is indicated in the color-coded boxes with the arrow pointing in the direction of walking, which also corresponds to the direction of the applied forward forces. ***p < 0.001, **p < 0.01, *p < 0.05, Mann-Whitney U-tests. Data are means ± s.e.m.

the alteration of key gait features such as the stride length (R^2 = 0.78), speed (R^2 = 0.91), and anti-gravity muscle activity (Figure 2.7C,D). Large upward forces required an abnormal activation of knee flexor muscles during stance to pull the body forward, concomitant to a threefold drop in the activation of anti-gravity muscles (Figure 2.6C and Figure 2.7A,C).

The application of increasing forward forces mediated a gradual recovery of the stride length, speed, double stance duration and anti-gravity muscle activity (Figure 2.6B,C,D, Figure 2.7E-H). Forward forces improved the oscillations of the CoM and the profile of ground reaction forces (Figure 2.6C). Analysis of the interactions between upward and forward forces during walking on a treadmill confirmed these observations (Figure 2.8A). These results highlight critical interactions between upward and forward forces on posture and gait with body weight support, stressing the importance of developing evidence-based procedures to configure these forces based on patient-specific needs.

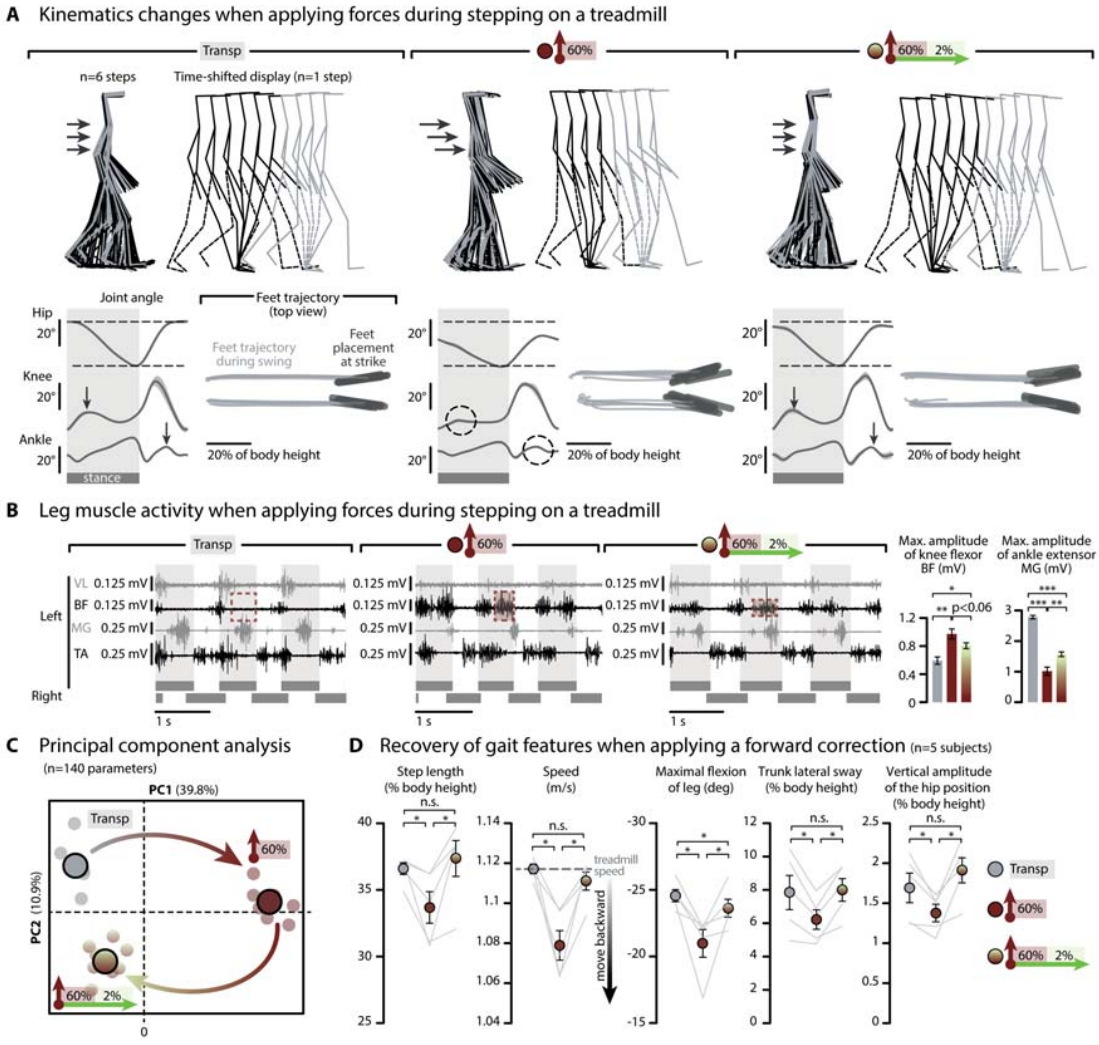

Figure 2.8 – Interaction between upward and forward forces during locomotion on a treadmill. A, Stick diagram decomposition (rate, 120 ms) of head, trunk and leg movements during stance (dark) and swing (light). The filled and dashed lines differentiate the right and left legs, respectively. A representative example is shown for locomotion in transparent mode, with vertically restricted support, and with an optimal combination of upward and forehead force recorded in a healthy subject. Contrary to overground locomotion, the walking speed is maintained constant across conditions. The stick diagrams on the left of each panel have been aligned on the barycenter of the pelvis to emphasize the change in trunk posture. The average changes in the joint angles (average ± SD) over a gait cycle are shown together with the projection of the trajectories of the feet onto the floor during a succession of steps (n = 6). The arrows and dotted circles emphasize the important alterations of key gravity-dependent kinematic features during vertically-restricted support. B, Concomitant sequence of EMG activity from ankle and knee muscles of the left leg over three successive steps. The brown box highlights the abnormal activation of leg muscles. C, Gait kinematics is shown in the space created by PC1 and PC2 (%, explained variance). Conventions are the same as in Figure 2. D, Bar plots reporting the mean values of gait parameters for each experimental condition. ***p < 0.001, **p < 0.01, *p < 0.05, Mann-Whitney U-tests. Data are means ± s.e.m.

Gravity-Assist: Personalization of Upward Force

Individuals with motor deficits require personalized upward forces to compensate for their specific impairments. Currently, therapists select this support from empirical observations. Here, we aimed at developing an algorithm that configures upward forces based on objective measurements.

Nine subjects with SCI or stroke were asked to stand with robotic assistance (Table 2.1). To determine the optimal upward force, we recorded kinematics, kinetics and muscle activity over a range of upward forces (from 15% to 70% of bodyweight, depending on the capacity of each subject, Figure 2.9A). We applied a PC analysis on the computed parameters (n = 15, Table 2.2) recorded in each subject and healthy individual (n = 5). The optimal upward force was defined as the condition minimizing the distance to healthy individuals (Figure 2.9B).

This method requires extensive recordings that are unpractical in clinical practice. To automate this procedure, we applied a supervised machine learning using an artificial neural network that predicted optimal upward forces for each subject based on easily collected kinematic and kinetic variables (n = 12, Table 2.2). The artificial neural network aimed at minimizing errors in the predicted corrections of upward forces (Δ, % of bodyweight). Performances were tested on independent datasets (32 trials, n = 3 subjects). The errors in the predicted corrections never exceeded 5% of the experimentally measured optimal upward force (Figure 2.9C).

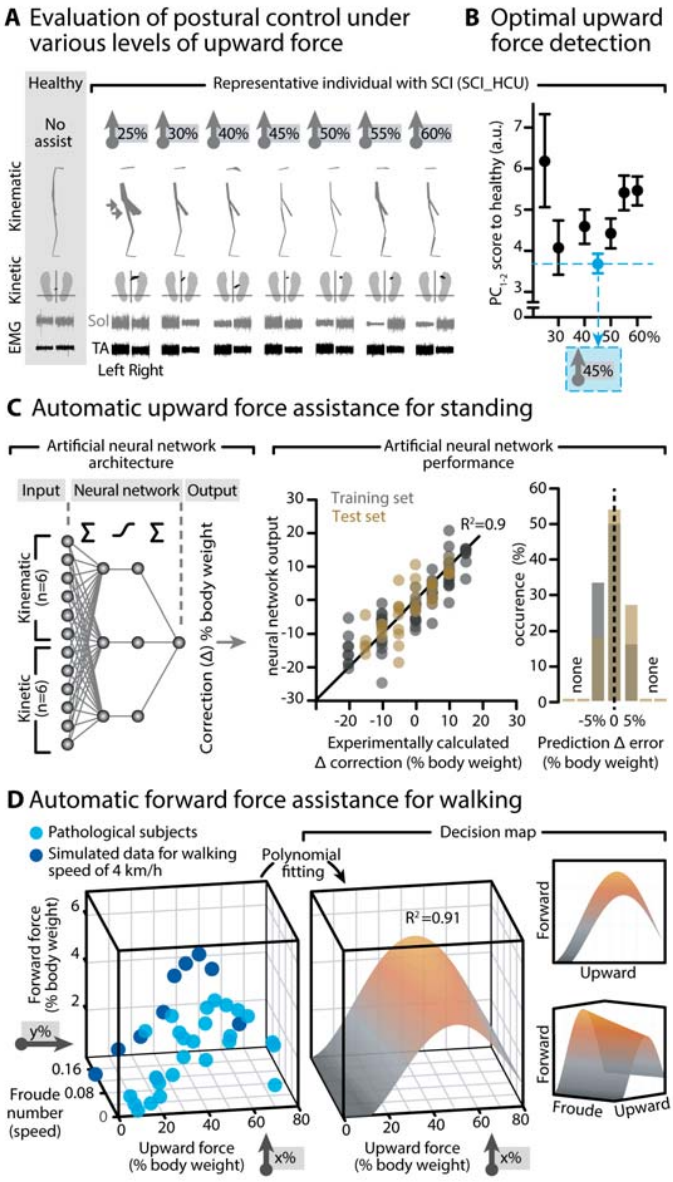

Figure 2.9 – Design of the MGA algorithm. A, Stick diagram decomposition of whole-body movements, continuous CoP trajectory, and EMG activity of ankle muscles during standing with upward forces ranging from 25 to 60% of bodyweight support (5% increments) for a non-ambulatory individual with a SCI. B, Plot showing the relationship between the upward force and the Euclidian distance between the data of the participant shown in (A) and healthy subjects in the space defined by PC1 and PC2 (PC analysis performed on 15 parameters). The minimal distance (blue dot) was defined as the optimal upward force. C, The measured variables were fed into an artificial neural network that calculated the correction of bodyweight support (Δ, upward force in % of bodyweight) to facilitate gait. The plot shows the relationship between the experimentally determined correction and the prediction of the neural network. Each dot corresponds to a given condition of upward force for a subject with SCI or stroke who contributed to the training or test data set. The histogram plot reports the occurrence rate of errors in the prediction of the corrections calculated by the artificial neural network. D, 3D plots reporting the relationships between the upward force, the optimal forward force, and the speed. Each data point corresponds to values measured in the simulations and in subjects with SCI or stroke. To include data from subjects with varying biometry, the speed is represented as the Froude number, which takes into account the length of the leg to normalize the speed. A polynomial function was fitted through both simulated and experimental data points.

Gravity-Assist: Personalization of Forward Force

We next sought to calibrate the forward force during walking for each upward force and patient-specific needs. To guide this process, we performed simulations using a damped, spring-loaded inverted pendulum model. This simulation captures the main features of human locomotion (Materials & Methods). As observed experimentally, upward forces reduced the walking speed, stride length, and CoM oscillations. Simulations searched the optimal configuration to normalize the speed, stride length and CoM oscillations towards values obtained without any external force. We obtained an inverted, U-shape curve defining the forward force correction at a given speed (Figure 2.9D).

We exploited these results to guide the experimental identification of forward force corrections. Individuals with neurological deficits exhibit optimal performance at a preferred speed. Since forward force corrections were linked to the speed, we created a map integrating the preferred speed in the configuration of the MGA. Twenty-two subjects with SCI or stroke walked with optimal upward force and a narrow range of forward forces centered around the values derived from simulations. Optimal locomotor performances were calculated from the PC analysis (Figure 2.4). To calculate optimal upward and forward forces for each speed, we fitted an optimal polynomial function to the data. We obtained an inverted, U-shaped map (Figure 2.9D). We used this decision map to configure the MGA in the subsequent experiments.

Gravity-Assist: Validation

We next evaluated the performance of the MGA algorithm to establish optimal upward and forward forces during locomotion. We tested the algorithm in 6 individuals with SCI or stroke (Table 2.1) using a framework that can easily be implemented in clinical routine (Figure 2.10A). Subjects were first recorded during standing with optimal upward force, and with the addition or subtraction of an upward force corresponding to 10% of their bodyweight. The optimal force was determined with PC analysis. For each condition of upward forces, kinematic and kinetic recordings were independently provided to the artificial neural network, which calculated upward force corrections to establish the optimal condition for each subject. For example, Figure 2.10B illustrates kinematic and kinetic recordings during walking for one of the subjects included in the testing dataset of the artificial neural network. This subject

was not capable of standing or walking independently (SCI-BME, ASIA Impairment Scale C, Table 2.1). The artificial neural network yielded the same predictions of optimal upward force, regardless of the initial upward force (among the three tested force values). We used this correction and the preferred walking speed to configure the forward force using the decision map (Figure 2.9D).

The MGA enabled this subject to progress overground with coordinated, weight-bearing locomotor movements (Figure 2.10B). Improved dynamics of the CoM revealed the partial restoration of gravity-dependent gait interactions (Figure 2.10C). A 10% increase or decrease in the amount of upward force drastically altered gait features, almost preventing this subject from progressing forward (Figure 2.10B).

We measure the performance of the MGA algorithm using a PC analysis applied on all the kinematic parameters (n = 120, Table 2.2, Figure 2.4A,B). Locomotor performance was quantified as the distance between each subject and healthy individuals in the space defined by PC1 and PC2 (Figure 2.4C). This analysis showed that the MGA algorithm yielded appropriate configurations of upward and forward forces in all of the tested subjects (Figure 2.10C; $P < 0.001$, repeated measures two-ways ANOVA). The importance of the precision in the MGA configuration increased with the severity of gait deficits, as quantified with PC scores (Figure 2.10D; $R^2 = 0.88$, $P < 0.01$). The pronounced modulation of individual gait parameters confirmed the importance of the MGA configuration to facilitate locomotion (Figure 2.10E). These results illustrate the critical importance of personalizing upward and forward forces to enable locomotion in neurologically impaired subjects, and validate the capacity of the MGA algorithm to configure these forces based on patient-specific needs.

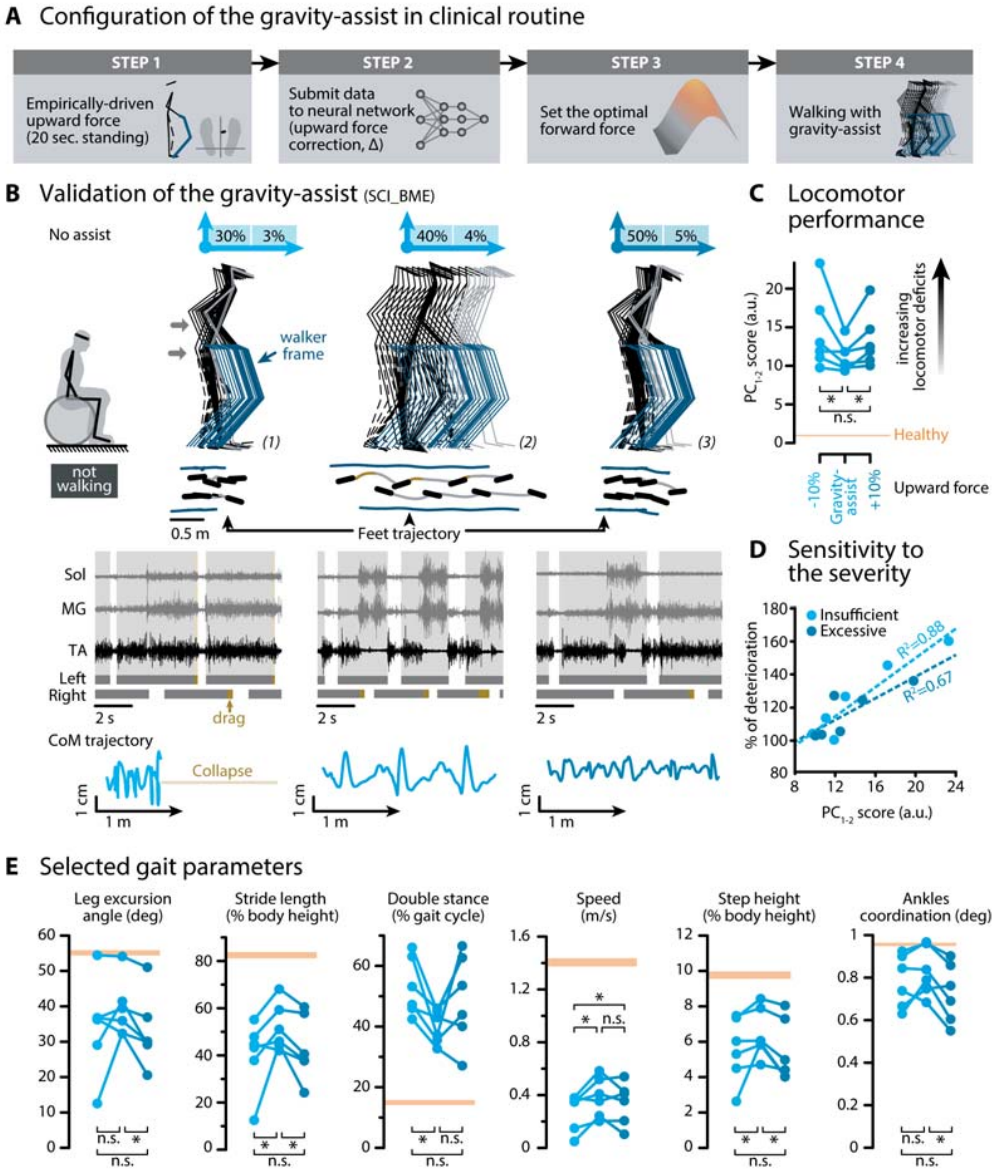

Figure 2.10 – Validation of MGA algorithm in individuals with SCI or stroke. A, Steps for configuring of the MGA. B, Stick diagram decomposition of whole body movements (and walker, blue) for a non-ambulatory subject with SCI walking with 3 ranks of upward force and associated forward force. The position of the feet during stance and their trajectories during swing is indicated (grey) together with the trajectory of the wheels of the walker (blue). A representative sequence of EMG activity recorded from ankle muscles is reported for each condition, together with the stance duration of each leg (grey bar). Foot dragging is indicated in brown. The CoM trajectory is displayed at the bottom in blue. C, Locomotor performance was quantified as the Euclidian distance between gait cycles of each subject in three different conditions of upward assistance versus healthy individuals in the PC space (see Figure 2.4). Middle blue refers to the gravity-assist condition. Light blue and dark blue correspond to a 10% decrease or increase in the amount of upward force, respectively. *$p < 0.05$, n.s. non-significant, Friedman test with Tukey-Kramer post hoc tests. D, Impact of sub-optimal force configurations based on locomotor performance. E, Plots reporting the mean values of selected gait parameters under the three conditions of upward force. The mean values (horizontal orange bar) ± s.e.m. (thickness) measured during locomotion in healthy subjects is represented. *$p < 0.05$, n.s. non-significant, Wilcoxon signed-rank tests. Data are means per subject, n = 6 pathological subjects.

Gravity-Assist: Improvement of Locomotor Performance after SCI and Stroke

We next tested the capacity of the MGA to enable or enhance locomotor performance in two cohorts of individuals with varying severities of SCI (n = 15) and stroke (n = 12). Locomotor performance ranged from non-ambulatory individuals who could not stand nor walk independently, to individuals with mild motor impairments who could walk without assistive device (Table 2.1).

With the exception of non-ambulatory individuals, all of the subjects were first recorded during locomotion without the robot using the assistive device that they used in their daily life. All the subjects were then evaluated during locomotion with MGA, both with and without assistive device when possible. To quantify locomotor performance, kinematic variables (n = 120, Table 2.2) recorded in healthy individuals (n = 13) and in all of the subjects with SCI or stroke were subjected to separate PC analyses. These quantifications revealed that the MGA enabled walking in non-ambulatory subjects with kinematic features similar to ambulatory subjects, both after SCI (Figure 2.11) and stroke (Figure 2.12). Each subject showed specific responses, which are documented in the Database S1[2] that shows individual gait analyses for the 26 individuals with SCI or stroke.

To identify the specific gait features improved by the MGA, we extracted the parameters that highly correlated with PC1 and PC2 (factor loadings, |value| > 0.5) and regrouped them into functional clusters corresponding to basic gait features. We first conducted this analysis for individuals with SCI (Figure 2.11A). We found that PC1 quantified improvements of leg kinematics, whereas PC2 captured changes in postural control. The improvements depended on the initial locomotor performance (R^2 = 0.64, P < 0.005). For example, the MGA enabled subjects who could not stand independently to walk overground with or without assistive device (3/3 subjects, Figure 2.11B,C top row). Subjects who were only able to locomote with crutches or a walker progressed without assistive device (4/10 subjects), and exhibited improved spatiotemporal gait features (Figure 2.11B,C middle rows). Subjects who were able to walk without assistive device exhibited increased postural stability (Figure 2.11B,C bottom row).

[2]Not included in the thesis

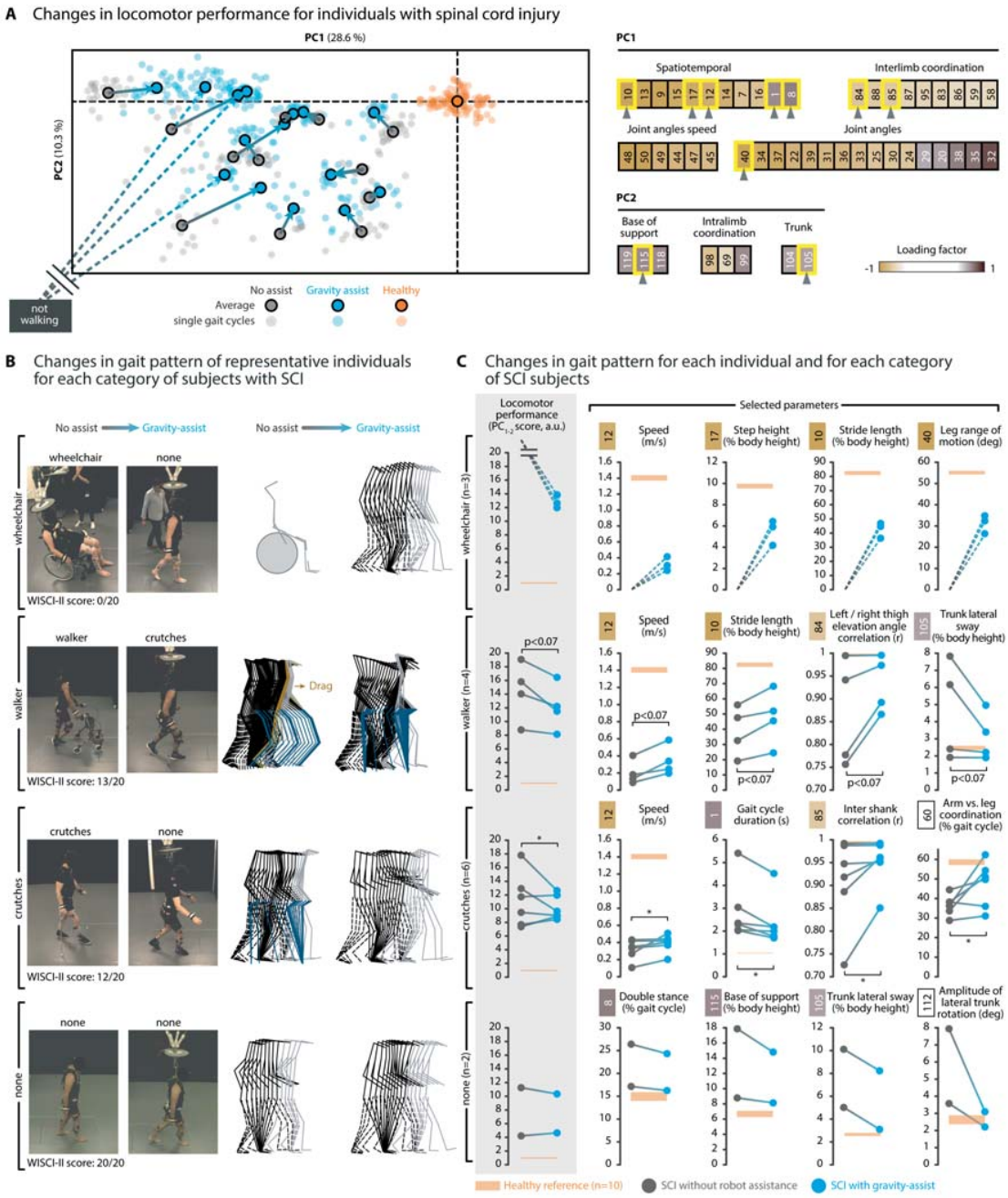

Figure 2.11 – Performance of the MGA to enable or enhance locomotor control after SCI. A, Subjects with SCI walked overground without and with MGA using the least assistive device possible. To quantify locomotor performance and identify the most relevant parameters, a PCA based method has been applied as described in Figure 2.4. On the right, the computed parameters that strongly correlated with a given PC (|loading factors| > 0.5) were regrouped into functional clusters. Numbers refer to Table 2.2. B, Subjects were segregated into four categories: non-ambulatory (wheelchair), walker, crutches, none. Photographs and stick diagram decomposition of whole body movements (and assistive device) are shown for each category and condition. C, Plots reporting the mean values of locomotor performance and classic gait parameters for each subject during locomotion without and with MGA. The horizontal orange bars report the mean values ± s.e.m. (thickness) measured during locomotion in healthy subjects. *p < 0.05, Wilcoxon signed-rank tests, n = 15 subjects with SCI.

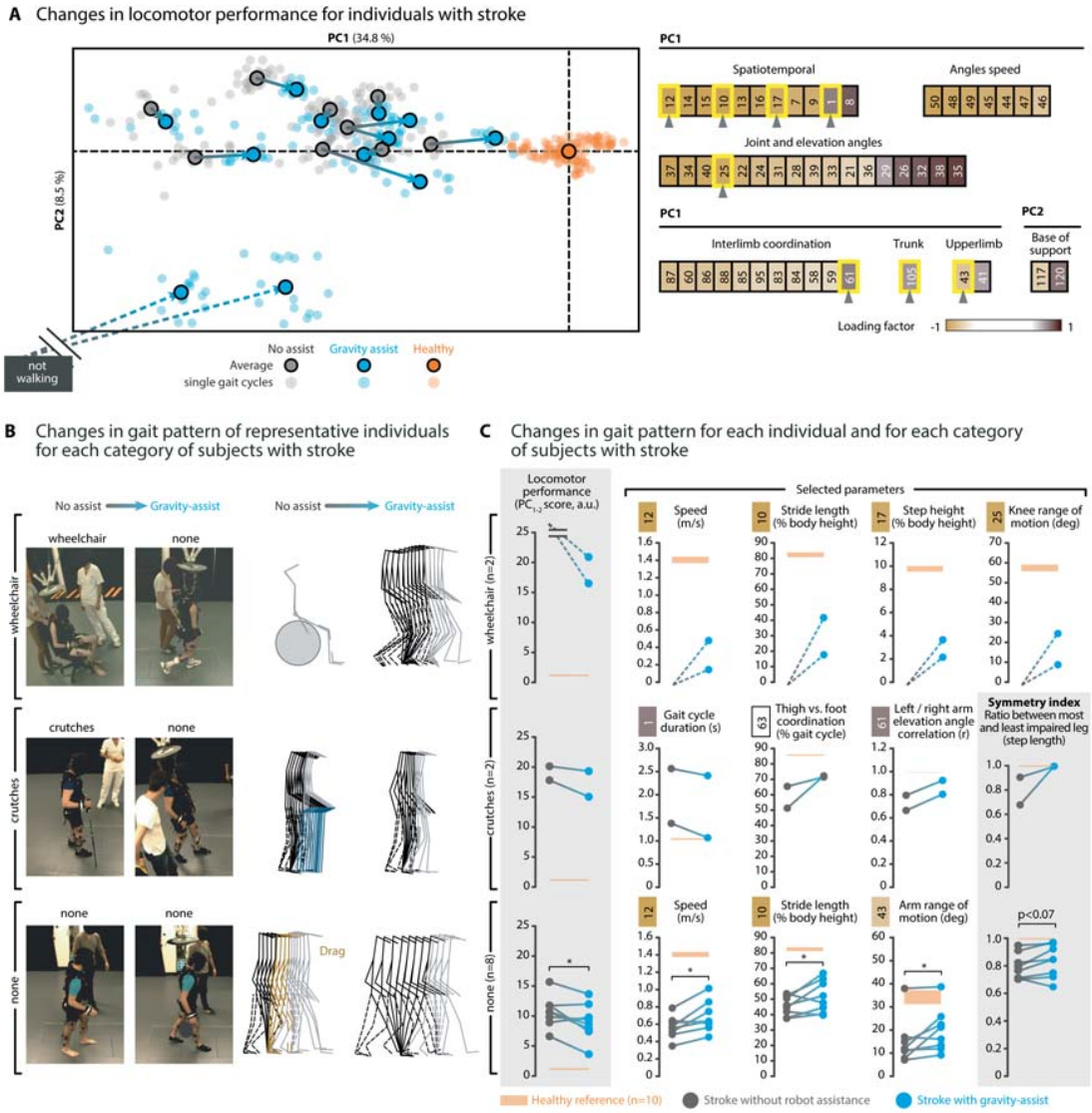

Figure 2.12 – Performance of the MGA to enable or enhance locomotor control after stroke. A, Subjects with stroke walked overground without and with MGA using the least assistive device possible. To quantify locomotor performance and identify the most relevant parameters, a PCA based method has been applied as described in Figure 2.4. On the right, the computed parameters that strongly correlated with a given PC (|loading factors| > 0.5) were regrouped into functional clusters. Numbers refer to Table 2.2. B, Subjects were segregated into three categories: non-ambulatory (wheelchair), crutches, none. Photographs and stick diagram decomposition of whole body movements (and assistive device) are shown for each category and condition. C,. Plots reporting the mean values of locomotor performance and classic gait parameters for each subject during locomotion without and with MGA. Additionally, a symmetry index reports the relative symmetry between left and right step lengths for each subject. The mean values (horizontal orange bar) ± s.e.m. (thickness) measured during locomotion in healthy subjects is represented. *p < 0.05, Wilcoxon signed-rank tests, n = 12 subjects with stroke.

Individuals with stroke exhibited similar or even superior amelioration of locomotor performance (Figure 2.12). The PC analysis (Figure 2.12A) showed that individuals who could only walk with crutches exhibited improved intra-limb coordination (Figure 2.12B,C middle row). Individuals who walked without assistive device showed improvements of basic gait parameters such as the stride length and walking speed, as well as enhanced arm movements and improved gait symmetry (Figure 2.12B,C bottom row). Together, these results show that the MGA enabled or enhanced locomotor control in individuals with severe to moderate gait deficits due to SCI or stroke.

Gravity-Assist: Improvement of Locomotor Performance after a one-hour Training Session

We then sought to demonstrate the ability of the overground gait training environment with MGA to improve locomotor performance. We enrolled five subjects with a chronic SCI who were capable of walking overground, but only with an assistive device (Table 2.1). They participated in two training sessions, separated by one week (Figure 2.13A). During the first session (60 min), subjects walked overground with MGA. During the second training session (week 2), they were asked to walk the same distance on a treadmill. Immediately before and after each training session, the subjects were recorded during overground locomotion without MGA at their own selected pace using their preferred assistive device.

With the exception of the least affected subject, the training session with MGA mediated a significant increase ($P < 0.001$ for 4 out of 5 subjects) in locomotor performance in all the participants. For example, the increase in gait speed and decrease in double stance duration enabled by the MGA throughout training persisted during overground locomotion without MGA (Figure 2.13B, left). However, evaluations conducted one week later revealed that these improvements did not persist (Figure 2.13B). In contrast, overground locomotor performance remained unchanged or even deteriorated after treadmill-restricted step training (Figure 2.13C). Basic gait features such as the speed and double stance duration improved during training, but the values returned to baseline when the subjects walked overground with their assistive device after training (Figure 2.13B). These results show that a one-hour gait training session facilitated by the MGA improved locomotor performance immediately after training.

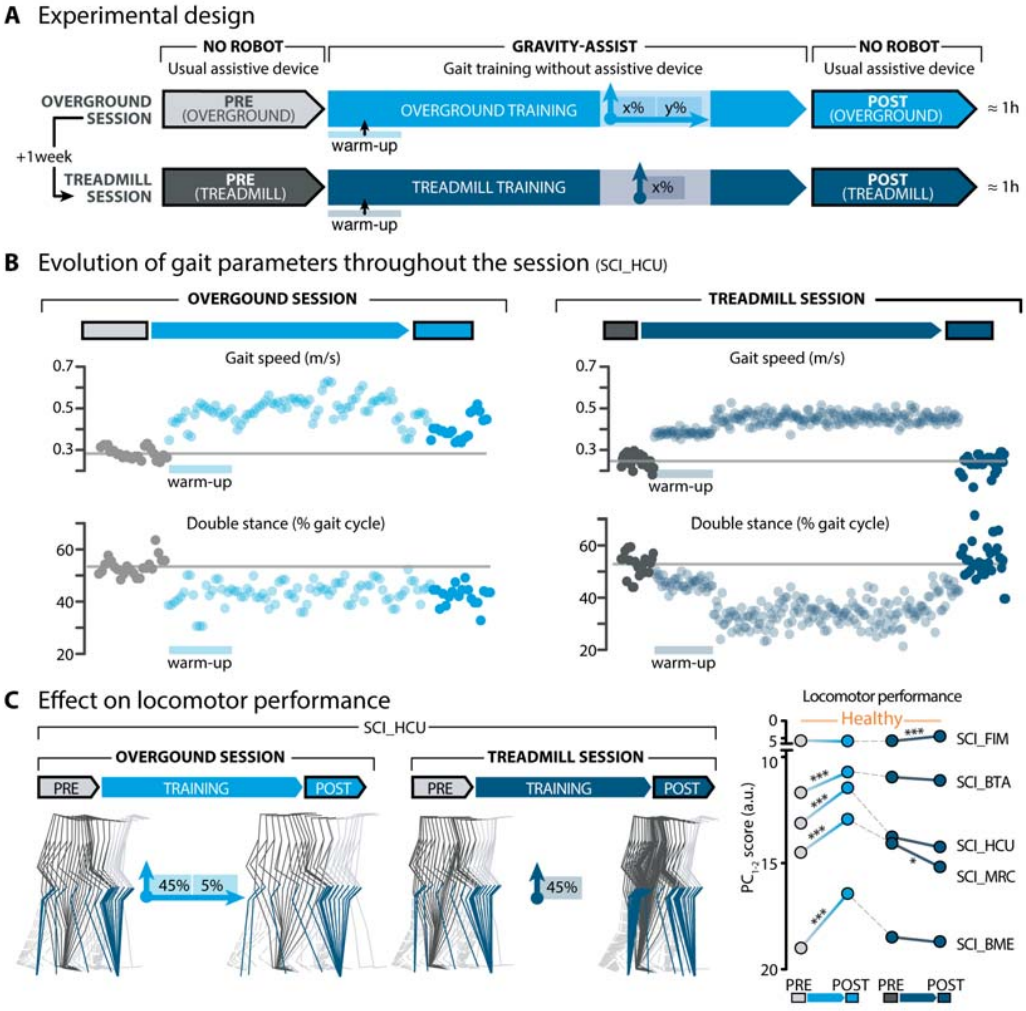

Figure 2.13 – Gait training session overground with MGA or on a treadmill with upward support. A, Experimental design of the one-hour training sessions. B, Plots reporting gait speed and double stance duration for each successive gait cycle of subject SCI-HCU over the course of the entire session. The color coding refers to the experimental design detailed in (A). C, Stick diagram decomposition of whole-body movements recorded overground without robotic assistance. The blue stick represents the crutch. The plot reports the locomotor performance of n = 5 subjects with SCI before and after training with MGA (light blue), as well as one week later (before and after training restricted to a treadmill, dark blue). Locomotor performance was evaluated using the PCA based method described in Figure 2.4. The horizontal orange bars report the mean values ± s.e.m. (thickness) measured during locomotion in healthy subjects. ***p < 0.001, *p < 0.05, Mann-Whitney U tests. Data are means per subject.

Gravity-Assist: Training of Skilled Locomotion and Dynamic Balance

Task-specific training plays a critical role in determining the outcome of gait rehabilitation [101]. We thus tested the ability of the MGA to enable tasks underlying activities of daily living. We first tested skilled foot placements along the rungs of a horizontal ladder placed 15 cm above the ground in subjects with SCI or stroke who displayed sufficient locomotor performance for this task (n = 13). Without the MGA, these subjects considered this task too challenging or too risky. The MGA allowed all the tested subjects to climb up the staircase and progress with accurate foot placement onto the rungs of the ladder (Figure 2.14A).

The multidirectional actuation of the MGA also allowed the subjects to practice their steering abilities, dynamic balance and upper/lower limb coordination during natural walking. For instance, they could walk safely along a curvilinear path projected onto the floor without assistive device (Figure 2.14B). Finally, we studied the ability to train dynamic balance. We designed perturbations consisting of laterally oriented forces that were applied to the trunk suddenly or continuously during walking. As expected, the perturbations altered the trajectory, position and posture of the trunk (Figure 2.14C). These perturbations thus allow training and evaluation of dynamic balance in a safe environment. Together, these results illustrate the ability of the MGA to enable activities of daily living that require skilled and finely balanced movements, thus providing the opportunity to expand task-specific training in neurologically impaired individuals.

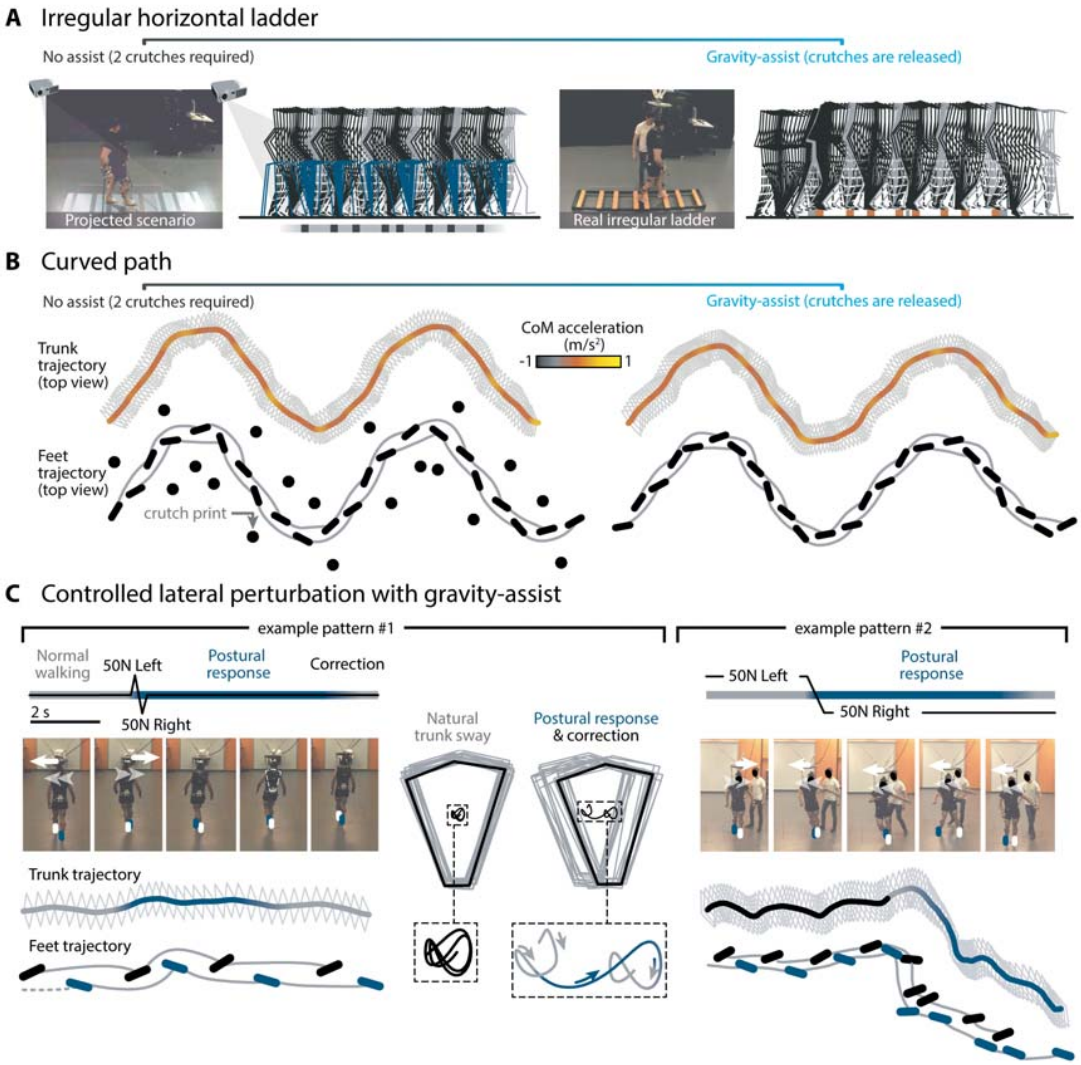

Figure 2.14 – The MGA allows training of skilled locomotor and postural activities. A, Photograph and stick diagram decomposition showing a subject with SCI who could position his feet onto the irregularly spaced rungs of a ladder projected onto the floor during locomotion assisted with two crutches. The subject could not walk over the actual ladder in this condition. The MGA enabled the subject to climb up the first staircase and progress onto the actual ladder without assistive device. B, Successive positions of the trunk in the coronal plane while a subject with SCI was asked to progress along a curvilinear path projected onto the floor, both without and with MGA. The CoM trajectory and acceleration are also displayed, together with the position of the feet (dashes) during stance and their trajectory during swing. The dot indicates the positions of the crutches onto the floor without MGA. C, Photograph sequences showing the behavior of a subject with SCI during the application of postural perturbations during walking. The perturbation is schematized above each sequence. Left: sudden leftward and then rightward forces. Right: sustained leftward and then rightward forces. The impact of these perturbations on the position, posture and trajectory of the trunk and feet are shown.

Discussion

We developed an algorithm that configures upward and forward support forces applied to the trunk to restore gait dynamics despite the application of a body weight support during standing and walking. The MGA establishes a safe and natural rehabilitation environment wherein individuals with neurological deficits can perform basic and skilled locomotor activities that would not be possible without robotic assistance. This environment allows task-specific training in optimal conditions. The immediate and short-term ameliorations of gait performance during locomotion with MGA illustrate the potential of this environment to augment motor recovery.

Partial body weight supported gait therapy is a common medical practice to improve recovery after neurological disorders [97, 98]. This condition allows the repetition of locomotor movements that would not be possible without assistance. Currently, therapists configure the amount of support empirically based on visual observations. As observed in rodents [67, 106], we found that the clinical phenotype of each neurologically impaired subject determined the precise amount of upward support required to facilitate gait execution. In the most affected subjects, even minimal changes in support conditions strongly affected locomotor performance.

Current body weight support systems generally deliver assistance restricted to the upward direction [103]. Yet, we found that the application of upward forces induced a backward shift in body orientation, which considerably destabilized the control of standing and walking. The addition of well-calibrated forward forces was critical to restore the postural orientation, and thus alleviate the undesirable impact of upward forces on gait and balance. Importantly, the detrimental effects of a vertically restricted body weight support were similar on a treadmill.

These results confirmed previous findings that high amounts of body weight support lead to abnormal patterns of leg muscle activity, which would be detrimental for relearning to walk [104]. This observation led to the recommendation to limit the amount of body weight support to 30 or 40% [104, 115]. This guideline has been consistently applied in clinical studies [116, 117, 118]. However, our results indicate that this recommendation arises from an improper configuration of the trunk support. These findings may partly explain why locomotor training on a treadmill with body weight support was not shown to be superior to progressive exercise at home managed by a physical therapist after SCI [31] or stroke [119]. Together, these observations reveal that the prevailing design and utilization of clinical body weight support systems are suboptimal for the rehabilitation of posture and gait.

On the contrary, the MGA established a rehabilitation environment that is mechanically and physiologically optimized for patient-specific needs. The external constraints can be adapted to the residual motor control abilities of each patient within each session and throughout a rehabilitation program. The resulting facilitation of gait execution was unexpected. Subjects with SCI or stroke immediately exhibited improved locomotor performance, which translated into the ability to walk overground for non-ambulatory individuals who had sufficient residual control over leg movements. For the less affected individuals, the MGA allowed skilled locomotor activities that were not possible without robotic assistance. This result is important since task-specific training determines the outcome of gait rehabilitation after neurological disorders [101].

The MGA restored kinematic and kinetic patterns that resembled natural gait dynamics. Despite the application of upward force, both healthy and neurologically impaired subjects regained the profiles of ground reaction forces that are specific to human walking. We surmise that these gravity-dependent gait interactions are critical for learning and relearning to walk. For example, evidence suggests that gravity-dependent gait interactions during the first unsupported steps in toddlers act as a functional trigger for gait maturation [75, 120].

The short-term improvements of locomotor performance following a one-hour training session corroborated this hypothesis. The practice of natural walking with the MGA enabled the subjects to become confident in their residual motor abilities and to re-learn the interactions between their body mechanics and gravitational forces. Hence, this type of robotic assistance in a safe yet natural environment represents an ecological approach to gait rehabilitation [121]. Similar learning did not occur on a treadmill. Moreover, the MGA enabled the practice of skilled locomotion, steering and balance in natural conditions. We suggest that training neurologically impaired individuals in these activities of daily living, which can only be practiced naturally with MGA, may lead to enhanced recovery [101]. Such task-specific training may facilitate the transition into community ambulation.

These results need to be confirmed in a larger number of subjects and through a long period of rehabilitation. Indeed, the one-hour training session was insufficient to mediate lasting locomotor improvements. Here, we provided a clinically relevant framework to implement such rehabilitation programs across multiple activities of daily living for subjects with various types and severities of neurological deficits.

The significant role of gravity-dependent gait interactions in enabling or enhancing motor control after neurological disorders stresses the importance of optimizing the hardware and software underlying the MGA algorithm. In the present scenario, the forces applied to the trunk remained constant throughout gait execution. Moreover, the MGA only targeted upward and forward oscillations. However, the dynamics of human gait require precisely timed trunk movements in multiple directions [89, 102, 120, 122]. For example, the cyclic mediolateral movements of the trunk play a pivotal function in balance regulation during locomotion. We thus predict that the application of time-varying forces, tailored to specific phases of the gait cycle in each of the relevant Cartesian directions as well as torques will further improve the interactions between body mechanics and gravitational forces and thus the facilitation of gait execution. Predicting this dynamic MGA from simulations would require a more advanced biomechanical model to emulate the multidirectional interactions between body dynamics and gravitational forces. This type of assistance also relies on a number of hardware and software innovations to expand the spectrum of locations where forces and moments can be applied, and to develop control policies for adjusting these loads based on real-time movement feedback. Here, we introduced a neurorobotic platform that combines important features to implement dynamic trunk assistance.

Additional improvements may play an important role in optimizing the performance and usability of the robotic platform, in particular for dynamic assistance. For instance, the force controller introduced variability in the interaction forces that may be optimized with more precise sensors and improved robot mechanics. Furthermore, smart design of the trunk harness may reduce the displacement of the body center of mass by moving the force application to the pelvis [123]. These hardware and software improvements combined with real-time force adaptation may greatly improve locomotor performance in injured individuals.

Evidence suggests that gait rehabilitation should be conducted overground [64], across activities of daily living [101, 124], with optimized support conditions [64, 125, 126], enabling systems [18, 19, 30, 125, 127], unconstrained arm movements [128, 129], and active participation [18, 130], but these concepts remain fragmented. Here we introduced a neurorobotic platform that crystallizes these views into a unified framework to augment gait recovery after neurological disorders.

Conclusion & Perspectives

The manuscript reproduced in this chapter represents an extensive work gathering an ensemble of studies around the core concept of a multidirectional gravity-assist. For the first time, we demonstrated that the application of a force to the trunk against the direction of gravity induced a backward shift of the center of mass, which significantly altered gravity-dependent interactions during standing and walking. Surprisingly, this detrimental effect of body-weight support systems had never been investigated before from the best of our knowledge, but led to the recommendation to limit the body weight support to an arbitrary maximum of 30 to 40% [104, 115, 116, 117, 118]. Consequently, individuals who required a higher body weight support were excluded from body weight supported training programs. In addition, the Cochrane database of systematic reviews[3] has reported insufficient evidence from randomized clinical trials to conclude that body weight supported training is better than other locomotor training after spinal cord injury or stroke [116, 117], which conclusion may have been drawn from an improper configuration of the trunk support. Here, we evidenced that the whole range of body weight support is adequate for training, provided that the appropriate additional forces are delivered to reestablish the gravity-dependent gait interactions. We developed an algorithm to guide the physiotherapist to expertly adjust the multidirectional forces applied to the trunk by our robotic platform. We used high-resolution recordings and comprehensive analyses to validate the algorithm in 27 individuals with various severities of spinal cord injury and stroke.

Albeit we provide the technological tools and conceptual framework to personalize this assistance based on objective measures easily collected in clinical settings, the algorithm, in itself, may fail to determine the required multidirectional forces in other clinical and rehabilitation centers, without being adapted to their own robotic devices. However, the core concept – the multidirectional gravity-assist, personalized to the individual's residual capacities – remains critical to restore the gravity-dependent gait interactions necessary to relearn standing and walking. Indeed, we showed that the multidirectional gravity-assist instantly enabled non-ambulatory individuals to walk overground, or even to perform skilled locomotion.

This groundbreaking work underlines an unknown aspect of robot-assisted gait training and will affect the commonly-accepted way to carry out gait rehabilitation

[3]Cochrane database of systematic reviews synthesize high-quality, independent evidence as a resource for systematic reviews used for healthcare decision-making.

therapies. Based on this work, a new robotic support system, RYSEN® [131], has been engineered together with the Swiss company GTX medical, the Dutch company Motek medical, the Dutch technological university TU Delft and the Swiss rehabilitation hospital CRR SUVA in Sion (SUVA), within a collaborative Eurostars project. One of its prototype has been installed in the SUVA, where it has been tested before commercialization (Figure 2.15). In November 2018, theFLOAT® has been replaced by the commercial version of RYSEN® in the gait rehabilitation room of CHUV (Lausanne University Hospital, where we conduct our clinical studies).

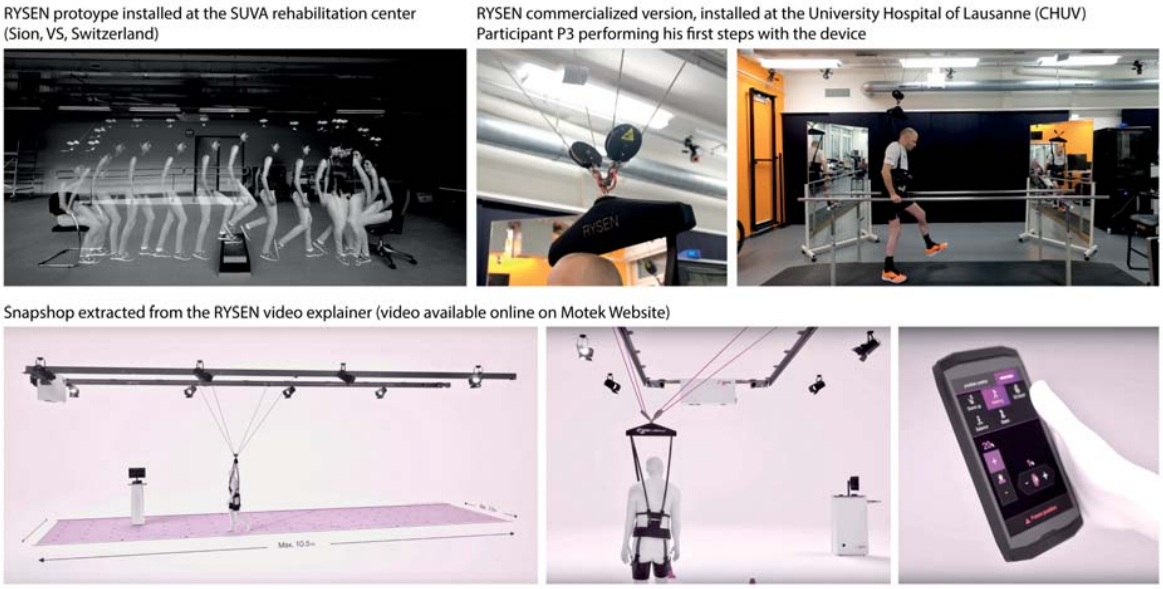

Figure 2.15 – RYSEN®. The new robotic support system by Motek medical.

3. Targeted Neuroprosthesis to Restore Walking

The multidirectional gravity-assist, described in Chapter 2, opened an exciting and realistic pathway in the development of an effective neuro-rehabilitation for people with a spinal cord injury (SCI) in combination with epidural electrical stimulation (EES). We hypothesized that the synergistic effect of robot-assisted overground training with electrical stimulation delivered on the dormant spinal cord region could trigger plasticity, enabling individuals to regain control over their paralyzed legs.

Few years ago, we proved in the rodent model that spatiotemporal neuromodulation therapies improved gait quality, weight-bearing capacity, endurance and skilled locomotion in the rodent model [65]. My contribution to this article had highlighted the temporal activation profiles of muscle synergies and how the spatiotemporal stimulations allowed mimicking the complex activation pattern of the leg motoneurons at the level of the spinal segments during a gait cycle. This work was based on the rostrocaudal architecture of the spinal cord, along which the leg motoneurons are arranged into pools that are muscle-specific [132, 133, 134], suggesting that different sites of EES would elicit distinct patterns of motor responses in lower limb muscles. Consistent with the rostrocaudal anatomical gradient of flexor and extensor motor pools, we observed a facilitation of flexion with lumbar EES, whereas sacral EES primarily facilitated extension, both during standing and stepping. Moreover, the combination of two [19], and, even more efficiently, three [48] sites of EES promoted clear synergistic facilitation of stepping which was evident in the increased consistency of hindlimb kinematics and enhanced weight bearing capacities [14]. To further enhance the efficacy of EES to facilitate locomotion in rodents with SCI, our laboratory worked in collaboration with Prof. Lacour group to design novel flexible multi-electrode arrays that afford delivery of complex stimulation patterns over multiple lumbosacral locations simultaneously. We found that laterally located electrodes facilitate hindlimb movements on the ipsilateral side, and that there is a gradi-

ent along the rostrocaudal extent of the spinal cord whereby rostral electrodes facilitate flexion whereas caudal electrodes primarily promote extension. Consequently, we developed advanced stimulation paradigms that exploited this new knowledge and showed that stimulation applied to rostral electrodes during swing, and caudal electrodes during stance, alternatively on the left and right sides of the spinal cord, promoted markedly improved stepping patterns compared to continuous stimulation of the same electrodes [65].

The translation of this approach – namely real-time spatiotemporal EES – to a non-human primate model of partial spinal cord injury has been successfully achieved [72]. We showed that real-time spatiotemporal EES of the lumbar and sacral spinal region during swing and stance respectively enabled the restoration of walking in the two primates. The delivery of EES was crucial to enable the motor control of the, otherwise paralyzed, lower limbs. Subsequently, we brought our technology – a wireless and fully implanted stimulation technology that can modulate the activity of the spinal cord system in closed-loop with a latency as short as 100 ms – into the STIMO clinical study on humans. In this study, eight participants with chronic SCI are implanted with an electrode array, and are then trained for five months of intensive neuro-rehabilitation with a robotic-assistance for treadmill and overground walking. At the moment I write this text, the study is still running. I relate here the first results obtained on the clinical, neurophysiological and neuro-biomechanical evolution of three participants.

The content of this chapter is adapted from the article F.B. Wagner*, J.B. Mignardot*, C.G. Le Goff-Mignardot* et al., ***Targeted neurotechnologies to restore walking in humans with spinal cord injury***, in Nature, October 2018 (DOI: 10.1038/s41586-018-0649-2), post-print version reprinted with permission of Springer Nature.

Personal contributions: first author contribution equally shared with J.-B. Mignardot and F. Wagner; reviewing of the study protocol, participation to the human research ethics application and to other regulatory works (e.g., preparation and testing of the electronic case report form with the contract research organization of CHUV), implementation and operation of the technological framework for all recordings of kinematics, electromyography and kinetics, data collection of all experiments carried out, participation and/or supervision of neurorehabilitation sessions, management of all recorded data, data processing and analysis, software implementation for all kinematic analysis, software implementation for analysis of maximal voluntary contractions, figures generation and editing, and manuscript editing.

Targeted neurotechnologies restore walking in humans with spinal cord injury

Fabien B. Wagner[1,2*], Jean-Baptiste Mignardot[1,2*], ***Camille G. Le Goff-Mignardot***[1,2*], Robin Demesmaeker[1,2,#], Salif Komi[1,2,#], Marco Capogrosso[3,#], Andreas Rowald[1,2], Ismael Seanez[1,2], Miroslav Caban[4,5], Elvira Pirondini[1,2,6], Molywan Vat[7], Laura A. McCracken[1,2], Roman Heimgartner[1,2], Isabelle Fodor[2], Anne Watrin[4], Perrine Seguin[1,2], Edoardo Paoles[4], Katrien Van Den Keybus[2], Gregoire Eberle[2], Brigitte Schurch[2], Etienne Pralong[2], Fabio Becce[8], John Prior[9], Nicholas Buse[10], Rik Buschman[10], Esra Neufeld[11], Niels Kuster[11,12], Stefano Carda[2], Joachim von Zitzewitz[4], Vincent Delattre[4], Tim Denison[10], Hendrik Lambert[4], Karen Minassian[1,2,&], Jocelyne Bloch[2,7,&] and Gregoire Courtine[1,2,7,&,$]

[1] Center for Neuroprosthetics and Brain Mind Institute, School of Life Sciences, Swiss Federal Institute of Technology Lausanne (EPFL), Lausanne, CH. [2] Clinical Neuroscience, University Hospital of Vaud (CHUV), Lausanne, CH. [3] Faculty of biology, University of Fribourg, Fribourg, CH. [4] GTX medical, Lausanne, CH. [5] Institute for Bioengineering, Swiss Federal Institute of Technology Lausanne (EPFL), Lausanne, CH. [6] Department of Radiology and Medical Informatics, University of Geneva, Geneva, CH. [7] Department of Neurosurgery, University Hospital of Vaud (CHUV), Lausanne, CH. [8] Department of Diagnostic and Interventional Radiology, University Hospital of Vaud (CHUV), Lausanne, CH. [9] Department of Nuclear Medicine and Molecular Imaging, University Hospital of Vaud (CHUV), Lausanne, CH. [10] Medtronic, Minneapolis, USA. [11] Foundation for Research on Information Technologies in Society (IT'IS), Zurich, CH. [12] Department for Information Technology and Electrical Engineering, Swiss Federal Institute of Technology (ETHZ), Zurich, CH.

*,#,&, These authors contributed equally to this work.

$, Corresponding author.

Abstract

Spinal cord injury leads to severe locomotor deficits or even complete leg paralysis. Here we introduce targeted spinal cord stimulation neurotechnologies that enabled voluntary control of walking in individuals who had sustained a spinal cord injury more than four years ago and presented with permanent motor deficits or complete paralysis despite extensive rehabilitation. Using an implanted pulse generator with real-time triggering capabilities, we delivered trains of spatially selective stimulation to the lumbosacral spinal cord with timing that coincided with the intended movement. Within one week, this spatiotemporal stimulation had re-established adaptive control of paralysed muscles during overground walking. Locomotor performance

improved during rehabilitation. After a few months, participants regained voluntary control over previously paralysed muscles without stimulation and could walk or cycle in ecological settings during spatiotemporal stimulation. These results establish a technological framework for improving neurological recovery and supporting the activities of daily living after spinal cord injury.

Introduction

Spinal cord injury (SCI) disrupts communication within the nervous system, leading to the loss of essential neurological functions. At present, activity-based therapies are the only medical practices that can be used to enhance recovery [135, 136, 137, 138]. The volitional production of active movements during training promotes reorganization of neuronal pathways and thereby augments recovery [139, 140]. However, the most affected patients, who fail to produce active movements voluntarily, experience minimal benefits from these therapies [136].

This situation has prompted the development of multifaceted neurotechnologies [141] such as lower limb exoskeletons, bodyweight support systems, functional electrical stimulation of muscles, and spinal cord neuromodulation therapies, all of which share the same goal: to enable patients to sustain active movements during training to enhance the reorganization of neuronal pathways [142]. Three decades of clinical research using these neurotechnologies suggested that epidural electrical stimulation (EES) of the spinal cord may be pivotal to achieve this goal [70, 71, 118]. EES not only enables the brain to exploit spared but functionally silent descending pathways in order to produce movements of paralysed limbs [22, 143], but also improves the ability of the spinal cord to translate task-specific sensory information into the muscle activity that underlies standing and walking [22, 144, 145, 146, 147].

To harness the therapeutic potential of EES, we studied its underlying mechanisms. We found that EES activates motor neurons by recruiting proprioceptive circuits within the posterior roots of the spinal cord [52, 53, 148, 149]. This understanding translated into EES protocols that target individual posterior roots to access the motor neuron pools located in the spinal cord segment innervated by each root [65]. To engage motor neurons at the appropriate time, spatially selective EES trains are delivered with timing that coincides with the intended movement. Compared to empirical stimulation protocols, spatiotemporal EES enhances the potency of leg movements, which enabled weight-bearing locomotion in animal models of leg paraly-

sis [65, 72, 112]. When combined with overground locomotor training enabled by a gravity-assist device [67], this stimulation promotes extensive reorganization of residual neural pathways that improves locomotion with and even without stimulation [47, 65, 69].

Here, we report the development of targeted neurotechnologies for delivering spatiotemporal EES during overground locomotor training with a gravity-assist device in humans [85]. We hypothesized that spatiotemporal EES would immediately enable voluntary locomotion despite chronic paralysis, and that the ability to sustain active movements during training would promote meaningful functional improvements with and even without stimulation.

Materials & Methods

Clinical Study and Participants

Study Design and Objectives

All experiments were carried out as part of the ongoing clinical feasibility study STIMO (Stimulation Movement Overground), which investigates the effects of spatiotemporal EES combined with weight-supported overground locomotor training on the recovery of motor function after SCI. This study was approved by the Swiss ethical authorities (Swissethics protocol number 04/2014 ProjectID: PB_2016-00886, Swissmedic protocol 2016-MD-0002) and was conducted in accordance with the Declaration of Helsinki. All participants signed a written informed consent prior to their participation. More information at clinicaltrials.gov (NCT02936453).

All surgical and experimental procedures were performed at the Lausanne University Hospital (CHUV). The timeline of the study is reported in Figure 3.7b. Briefly, the study involved assessments before surgery, the surgical implantation of the neurostimulation system, a one-month period during which EES protocols were configured, and a five-month rehabilitation period with physiotherapists taking place four to five times per week for one to three hours (Figure 3.16a), including monthly assessments.

The rehabilitation program was personalised to the participants' improvements. Each session was typically segmented into three parts: (i) conventional physiotherapy (30 min), (ii) locomotor training with gravity-assist and EES (60 to 90 minutes), (iii) Recovery (stretching, massage). The physiotherapy sessions included muscle stretching and/or muscle strengthening, volitional control of movement and standing.

Based on improvements observed in P1 and P2, an optional three-year study extension was submitted and approved by the ethical authorities to allow the use of EES without body weight support outside the laboratory environment. This amendment included 9 sessions of training with gravity-assist, 3 times per week, which was performed by P3 only. There was no serious adverse event during the course of the study.

Study Participants

Three individuals who had suffered a traumatic cervical SCI participated in the study. Their neurological status was evaluated according to the International Standards for Neurological Classification of Spinal Cord Injury [150], and is reported in Table 3.1. At enrolment, participant P1 was 28 years old and was classified with a C7 lesion that occurred six years earlier during a gymnastics accident. His left leg was completely paralysed while his right leg retained some residual functions (lower limb motor scores left: 0/25, right: 14/25). He could ambulate with a walker with no braces and no physical assistance over ten meters (WISCI score: 13). Participant P2 was 35 years old and was classified with a C4 lesion that occurred six years earlier during a bicycle accident. His impairments were bilateral, with some residual functions in both legs (left: 12/25, right: 13/25). He could ambulate with a walker, braces and physical assistance of one person over ten meters (WISCI score: 6). Participant P3 was 47 years old, classified with a C7 lesion that occurred four years earlier during a bicycle accident. He presented bilateral flaccid leg paralysis, with motor scores of 0 on all key leg muscles. He did not have any spasticity in his legs and could neither stand nor ambulate at all (WISCI score: 0).

Participant	P1	P2	P3
Gender	m	m	m
Age (yo)	28	35	47
Years after SCI	6	6	4
WISCI II score	13	6	0
AIS	C	D	C*
Neurological level of injury	C7	C4	C7
Upper extremity motor score Total (max. 50)	46	31	45
Lower extremity motor score Total (max. 50)	14	25	0
Lower extremity motor score L2 (hip flexors) (right-left)	2 - 0	2 - 2	0 - 0
Lower extremity motor score L3 (knee extensors) (right-left)	2 - 0	4 - 4	0 - 0
Lower extremity motor score L4 (ankle flexors) (right-left)	4 - 0	2 - 1	0 - 0
Lower extremity motor score L5 (long toe extensors) (right-left)	4 - 0	1 - 1	0 - 0
Lower extremity motor score S1 (ankle extensors) (right-left)	2 - 0	4 - 4	0 - 0
Light touch sensory score Total	75	65	55
Light touch, dermatomes L1-S2 subscore (right-left)	7 - 7	5 - 8	1 - 4
Pin prick sensory score Total	33	65	28
Pin prick, dermatomes L1-S2 subscore (right-left)	0 - 0	4 - 8	0 - 0

Table 3.1 – Neurological status of the three participants. Subjects' neurological status according to the International Standards for Neurological Classification of Spinal Cord Injury at study entry. *Reason for AIS C classification in spite of motor scores of 0 throughout all lower extremity key muscles is the presence of voluntary anal contraction.

Surgical Implantation

Investigational Device

Participants were implanted in the posterior epidural space with a 16-electrode paddle array (Figure 3.1 Step 1-2) clinically approved for the treatment of chronic pain (Specify™ 5-6-5 surgical lead for participants P1 and P2, Specify® SureScan® MRI 5-6-5 for participant P3; Medtronic plc, Fridley, MN, USA). This paddle array was connected to an IPG (Medtronic Activa™ RC) standardly used for Deep-Brain Stimulation. These combined elements and associated firmware constitute an investigational device that was tested as part of this clinical study.

Pre-Surgical Planning

Pre-operative MRI allowed the identification of the conus medullaris (Figure 3.1 Step 1). Average spinal cord anatomical dimensions [151, 152] were then used to estimate the position of the targeted spinal cord segments (L1-S2) with respect to the vertebrae.

Laminectomy and Paddle Array Insertion

The insertion level was identified under fluoroscopy. An approximately 5 cm midline skin incision was performed, the fascia opened and the muscles retracted bilaterally. Excision of the midline ligamentous structures and L1/L2 flavectomy enabled the insertion of the paddle array that was placed over the midline of the exposed dura and advanced rostrally to the target location (Figure 3.1 Step 3).

Electrophysiological Monitoring

Electrophysiological testing was conducted using the NIM Eclipse® monitoring and stimulation system (Medtronic Xomed Inc, Jacksonville, FL, USA) to optimise the medial and segmental position of the paddle array. EES was delivered at increasing amplitude (0.5 Hz) to elicit muscle responses that were recorded with subdermal (Neuroline Twisted Pair Subdermal, 12 x 0.4 mm, Ambu A/S, Ballerup, Denmark) or intramuscular needle electrodes (Ultra Sharp, 44 mm/27 g, Chalgren Enterprises, Inc.

Gilroy, CA, USA), as explained in Figure 3.1b. The final location of the paddle array overlaid lumbar and upper sacral segments in participant P1 and P3. Due to his height (192 cm), the paddle array was too short in P2, which imposed the selection of a position targeting the weak hip flexor muscles rather than ankle extensor muscles (Figure 3.1 Step 4-5).

Pulse Generator Implantation

The implantable pulse generator (IPG) was inserted into a subcutaneous pocket in the abdomen. An extension cable was then tunnelled from one opening to the other and connected to the IPG.

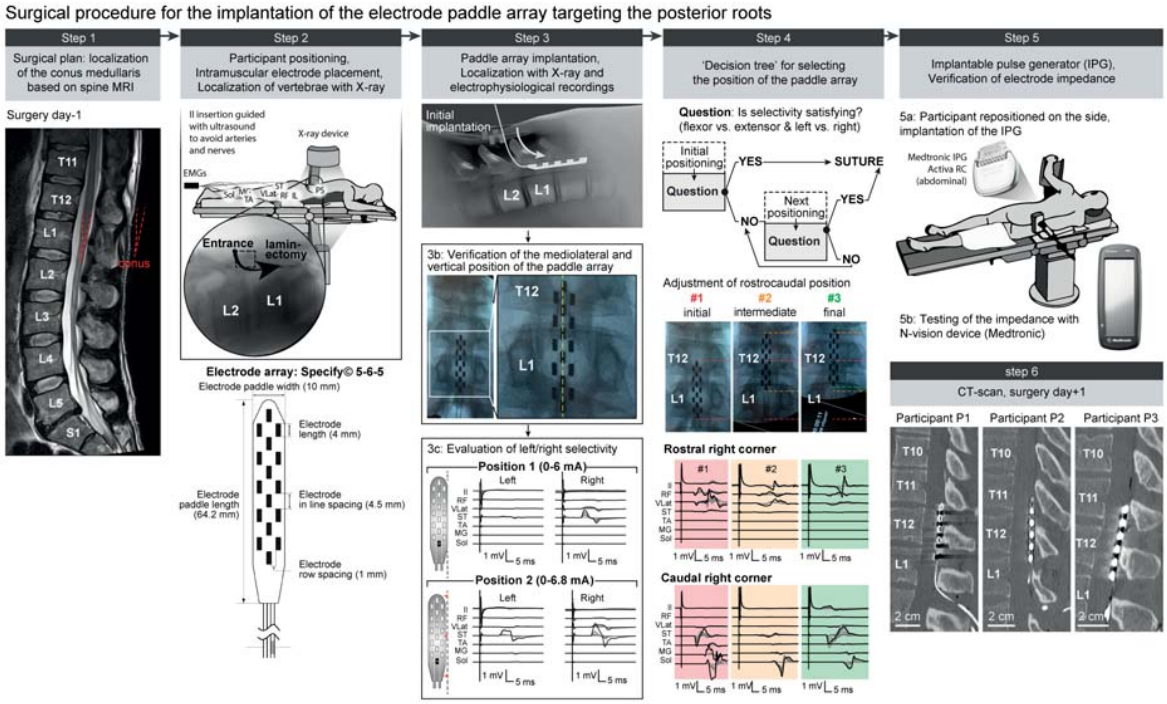

Figure 3.1 – Surgical procedure. Step 1: high-resolution MRI for pre-surgical planning. The entry point into the epidural space is based on the position of the conus. Step 2: placement of subdermal and intramuscular needle EMG electrodes for key leg muscles and paraspinal (PS) muscles. A subdermal needle is inserted over the sacrum and used as a return electrode for stimulation. Bottom, schematic of the 16-electrode paddle array. Step 3: surgical openings based on pre-surgical planning, typically between the L1 and L2 vertebrae, which are identified through intraoperative X-ray. The mediolateral positions of the paddle array are evaluated with X-ray and recordings of EMG responses following single pulses of EES delivered to the most rostral or most caudal midline electrodes. Step 4: the rostrocaudal position of the paddle array is optimised using EMG responses to single-pulse EES delivered to the electrodes located at each corner of the paddle array. The aim is to obtain strong ipsilateral responses in hip flexors with the most rostral electrodes and strong ipsilateral responses in ankle extensors with the most caudal electrodes. Step 5: implantable pulse generator (IPG) placed within the abdomen. Once connected to the paddle array, the impedance of the electrodes is evaluated to verify that all the components are properly connected. Step 6: post-surgical CT scan showing the location of the paddle array with respect to the vertebrae in each participant.

Personalised Computational Model

Personalization

We personalised computational models to simulate the spread of electric potential and currents generated by single pulses of EES. The model is composed of an anatomically accurate volume conductor model including the human spinal cord that is coupled to a geometrically realistic biophysical model of human primary afferents. First, we elaborated an average human spinal cord model comprising white and grey matter compartments combining information from the Paxinos human atlas and anatomical measurements of segments lengths and widths taken from 15 human cadaveric spinal cords. Second, for each participant we adapted the length of the white and grey matter compartments to patient-specific data extracted at the L1 vertebral level from pre-operative T2-weighted MRI images. The cerebrospinal fluid (CSF) dimensions were also segmented out of the pre-operative MRI-images.

Anatomically realistic vertebral bones and discs were generated and fitted to post-operative CT-data for each patient and the epidural fat was initialised to fit the inner borders of the bone. Finally, the whole spinal model was placed in a saline conductor to represent the human body [53]. Isotropic dielectric coefficients for each compartment were taken from previous studies [153]. We then estimated the precise position of each electrode by segmentation of post-implantation CT-data and registered it to the vertebral bone.

The model was discretised and Maxwell's equations were solved under quasi-static conditions with the Finite Element Method to determine an accurate representation of electric potentials and currents generated by single pulses of EES in each subject. Monopolar pulses were modelled as Dirichlet-boundary conditions of 1 V at the active electrode site with a duration of 500 μs. Dirichlet-boundary conditions of 0 V were initialised at the outermost boundaries of the model or at contacts selected as anodes in case of multipolar configurations. The models were all implemented in Sim4Life v3.4 (ZMT Zurich MedTech AG).

We used NEURON [154] in Sim4Life to model 50 myelinated Group-I afferent fibres per posterior root as a log-norm function with a mean fibre diameter of 16 μm and a standard deviation of 4 μm. An anatomically accurate trajectory of the afferent fibres was initialised and fitted around their entry and exit point determined by the anatomical parameters extracted from MRI and CT-data. A Sweeney model was used to describe the equation of the active membrane at the nodes of Ranvier and

at the passive internodal segments. The electrical compartments were automatically initialised in Sim4Life. The resting potential was set to -80 mV. Recruitment of group-Ia afferents was evaluated by linearly scaling the extracellular voltage applied at each fibre's compartment until an action potential was generated.

Posterior Root Selectivity Index for Simulations

For a given electrode configuration and EES amplitude, computational simulations yielded the percentage of fibres activated in each posterior root. We derived a root selectivity index $SI_{computational}\left(r_i, I\right)$ for each root r_i and each stimulation amplitude I:

$$SI_{computational}\left(r_i, I\right) = \frac{A_{r_i}\left(I\right)}{1 + \Sigma_{other\ ipsilateral\ roots} A_{r_j}\left(I\right)} \cdot f + \left(\frac{A_{r_i}\left(I\right) - A_{r_{contralateral(i)}}\left(I\right)}{A_{r_i}\left(I\right) + A_{r_{contralateral(i)}}\left(I\right)} \right)$$

where $A_{r_i}\left(I\right)$ represents the percentage of fibers activated in root r_i, $r_{contralateral(i)}$ is the root contralateral to root r_i, and $f_+\left(x\right) = \begin{cases} x & \text{if } x > 0 \\ 0 & \text{if } x \leqslant 0 \end{cases}$.

The first term of this selectivity index represents the rostro-caudal ipsilateral root selectivity, while the second term indicates the medio-lateral selectivity and penalises configurations that activate the root contralateral to the targeted one. If the contralateral root is more activated than the targeted root, the selectivity index is equal to 0. If only the targeted root is recruited, the selectivity equals 1. This selectivity index was calculated for a range of stimulation amplitudes (number of recruited afferent fibres) and the maximum was taken to characterise the overall selectivity of each electrode configuration.

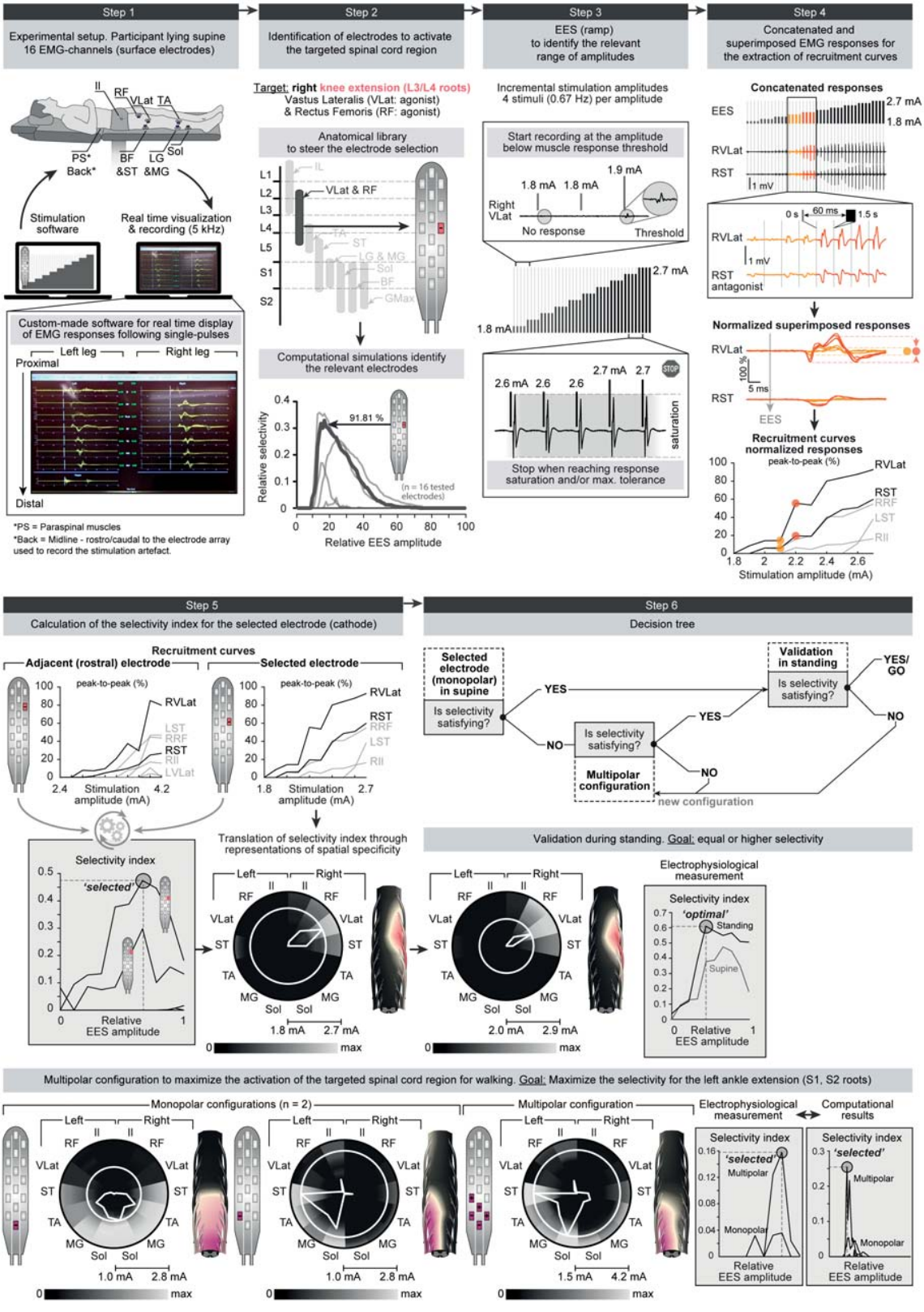
Step 1
Experimental setup. Participant lying supine 16 EMG-channels (surface electrodes)
Step 2
Identification of electrodes to activate the targeted spinal cord region
Step 3
EES (ramp) to identify the relevant range of amplitudes
Step 4
Concatenated and superimposed EMG responses for the extraction of recruitment curves
Target: right knee extension (L3/L4 roots)
Vastus Lateralis (VLat: agonist)
& Rectus Femoris (RF: agonist)
Incremental stimulation amplitudes
4 stimuli (0.67 Hz) per amplitude
Concatenated responses
Anatomical library to steer the electrode selection
Start recording at the amplitude below muscle response threshold
Normalized superimposed responses
Custom-made software for real time display of EMG responses following single-pulses
Computational simulations identify the relevant electrodes
Stop when reaching response saturation and/or max. tolerance
Recruitment curves normalized responses
*PS = Paraspinal muscles
*Back = Midline - rostro/caudal to the electrode array used to record the stimulation artefact.
Step 5
Calculation of the selectivity index for the selected electrode (cathode)
Step 6
Decision tree
Recruitment curves
Translation of selectivity index through representations of spatial specificity
Validation during standing. Goal: equal or higher selectivity
Multipolar configuration to maximize the activation of the targeted spinal cord region for walking. Goal: Maximize the selectivity for the left ankle extension (S1, S2 roots)
Monopolar configurations (n = 2)
Multipolar configuration
Electrophysiological measurement
Computational results

Figure 3.2 – Identification of electrode configurations to target selected posterior roots. Step 1: single-pulse EES and EMG recording setup. Step 2: motor neuron pools are located in specific segments, which provides information on the relative recruitment of each posterior root with EES. For example, electrodes targeting the L3 or L4 posterior roots will elicit the strongest EMG responses in the knee extensors. A personalised computational model of EES allows the performance of simulations that evaluate the relative activation of a given posterior root with a given electrode over the entire amplitude range. Each curve corresponds to an electrode. The highlighted curve corresponds to the electrode selected after steps 3-5. Step 3: single pulses of EES are delivered through the subset of electrodes identified by simulations. The EMG responses are recorded over a broad range of EES amplitudes. Step 4: the EMG responses are concatenated and averaged across n = 4 repetitions for each EMG amplitude, and the peak-to-peak amplitude of the average responses is calculated to elaborate a recruitment curve for each recorded leg muscle (black traces: targeted muscles). Step 5: the circular plots display the normalised EMG responses (greyscale) when delivering single-pulse EES at increasing amplitudes (radial axis), where the white circle highlights the optimal EES amplitude and the polygon quantifies the relative muscular selectivity at this amplitude. The motor neuron activation maps are shown for the optimal amplitudes. Step 6: decision tree to validate or optimise electrode configurations. The selected electrode is tested during standing as the position of the spinal cord with respect to the paddle array can change between supine and standing. In this example, the selectivity improves during standing. When the selectivity is deemed insufficient, the current is steered towards the targeted posterior roots using multipolar configurations. The example shows the increased selectivity of a multipolar configuration with two cathodes surrounded by three anodes, compared to the two corresponding monopolar configurations. These results were verified experimentally and with computer simulations.

Single-Pulse EES

Single-pulse EES was used to identify electrode configurations recruiting the targeted posterior roots (L1, L3, L4, S1). This identification was based on the recruitment order of lower-limb muscles with specific segmental innervations in response to single pulses of EES (300 μs pulse width) repeated every 1.5 s with increasing amplitudes.

Participants were lying relaxed in supine position on an examination table (Figure 3.2 Step 1). EMG activity was recorded bilaterally from the iliopsoas (Il), rectus femoris (RF), vastus lateralis (VLat), semitendinosus (ST), tibialis anterior (TA), medial gastrocnemius (MG), and soleus (Sol) muscles with wireless bipolar surface electrodes (Myon 320, Myon AG, Schwarzenberg, CH). Each electrode pair was placed centrally over the muscle with a longitudinal alignment and an inter-electrode distance of 3 cm. Abrasive paste (Nuprep, Weaver and Company, Aurora, CO) was used for skin preparation to reduce electrode-skin resistance and improve EMG signal quality. Stimulation artefacts required to display stimulus-triggered EMG activity were picked up by an additional pair of surface-EMG electrodes placed over the spine at the thoracolumbar junction. EMG signals were amplified with a gain of 500 and band-pass filtered between 20 and 450 Hz. Continuous EMG signals were sampled at 5 kHz and saved to a desktop computer. Stimulus-triggered EMGs were visualised in real-time as superimposed traces for each muscle within a 50-ms time window following each stimulus.

Recordings were performed with graded stimulation amplitudes in order to compute recruitment curves, which indicate the degree of recruitment of each muscle as the stimulation amplitude is increased (Figure 3.2 Step 3). Specific electrode sites were tested according to the segmental organisation of lower limb muscle innervation [134] and predictions from computer simulations (Figure 3.2 Step 2). Each selected electrode was stimulated in monopolar configuration as the cathode, with the case of the implantable pulse generator set as the anode. First, low-amplitude stimulation was applied to identify the lowest response threshold across all recorded muscles. Then, EES amplitude was increased manually to identify the amplitudes at which the responses reached a plateau, limited to levels that did not cause discomfort to the participant. Finally, single-pulse EES at amplitudes ranging from response threshold to saturation was performed automatically, with four repetitions at each EES amplitude, and recorded EMG responses were used to compute recruitment curves (Figure 3.2 Step 4) and a functional selectivity index (see Posterior root selectivity index for simulations; Figure 3.2 Step 5).

This procedure was repeated to identify eight sites targeting the left and right L1 (hip flexion), L3 (knee extension), L4 (ankle flexion) and S1 (ankle extension) posterior roots. If the selectivity was not satisfactory, EES was refined with multipolar electrode configurations, using additional anodes and cathodes to steer the electrical field towards the targeted posterior roots. Finally, the optimal electrode configurations for each targeted posterior root were validated during standing with body weight support (Figure 3.2 Step 6).

Evaluation of Single-Joint Torque Production

Assessment of Voluntary Force Production

Maximum torques produced at the knee, ankle and hip in flexion and extension were measured using the Humac Norm Cybex dynamometer system (Computer Sports Medicine Inc., Stoughton, MA). For measuring maximum isometric knee flexion and extension, the participant was seated in upright position, the knee placed in line with the dynamometer axis of rotation, and the lever arm pad of the system secured to the lower leg just above the ankle. Hip, knee, and ankle assumed angles of 90°, respectively. For ankle flexion and extension, the participant was seated reclined, with an angle of 120°between the trunk and the thigh of the leg under examination. The thigh was secured to a stabilisation arm provided by the system, and the ankle was strapped to the foot platform attachment, with the joint aligned with the dynamometer axis of rotation. Knee and ankle were at angles of 90°. Hip flexion and extension were assessed in supine position, with the distal thigh strapped to the measuring lever arm, and hip and knee at 90°of flexion. For each single-joint task, the participants were asked to produce a progressive contraction from rest to maximum strength with real-time visual torque biofeedback, with three repetitions and at least a 1-minute resting period between each attempt. If spasticity was induced during the attempted task, the trial was repeated. The torques developed were measured at a sample frequency of 5 kHz, and in parallel, EMG was acquired from the main agonists and antagonists of the respective movement attempt, sampled at 5 kHz. This assessment was carried out at all the main and monthly intermediate time points, with identical settings of the dynamometer system for each participant.

Impact of EES on Voluntary Force Production

A similar setup was used to study the interactions between targeted EES and voluntary attempts of single-joint movements. EES was applied with parameters optimised to facilitate hip flexion, hip extension, knee extension or ankle extension. Electrode configurations derived from single-pulse experiments were used to target the posterior roots projections to the spinal cord regions containing motoneurons associated with the intended movement. EES amplitude and frequency were adjusted manually. If necessary, EES was refined using multipolar electrode configurations. EES was applied with a delay following the onset of the voluntary motor task for a duration of a few seconds and was stopped 1-2 seconds after the participant had stopped the voluntary movement. This procedure was repeated three times for each of the studied tasks. The torques produced were assessed by dynamometry in the standardised positions as described above, except for the hip flexion which was assessed in prone position, with the hip at 10°of extension and the knee fully extended.

Technological Framework

Gait Analysis and Rehabilitation Environment

For assisting treadmill and overground locomotion, we used an overhead support system based on cable robot technology (FLOAT, Lutz Medical Engineering GmbH, Rudlingen, CH) that allows the application of forces to the trunk through a dedicated harness (Maine Anti-Gravity Systems, Inc. Portland, ME) in each of the Cartesian directions [85]. The robotic interface was integrated within a gait analysis platform, which allowed acquisition of EMG activity, ground reaction forces and whole-body kinematics in real-time (Figure 3.3 Step 1). EMG activity during walking was acquired bilaterally at 1 kHz using the 16-channel wireless Myon system, with bipolar surface electrodes placed over the iliopsoas (Il), rectus femoris (RF), vastus lateralis (VLat), semitendinosus (ST), biceps femoris (BF), tibialis anterior (TA), medial gastrocnemius (MG), and soleus (Sol) muscles. Kinematic recordings were obtained at a 100-Hz sampling rate using a 3D motion capture system (Vicon Motion Systems, Oxford, UK), consisting of 14 infrared cameras that covered a 12 x 4 x 2.5 m workspace. Head, trunk, and bilateral upper and lower extremity kinematics were captured by these infrared cameras and 34 small infrared-reflective markers (16 mm, Prophysics AG, Schaffhauserstrasse 121, Kloten, CH) positioned over standardised anatomical landmarks. Two force plates (9260AA6, Kistler, Winterthur, CH) were installed in

the middle of the workspace to monitor ground reaction forces. We also captured chronophotographic images of participants using a high-definition camera (FUJIFILM X-T2, 5 images/s, ISO 6400, shutter speed 1/250 sec) and overlaid successive images offline for illustrative purposes.

Real-Time Gait Event Detection

To perform real-time gait event detection, we placed large infrared-reflective markers (46 mm, Prophysics AG, Schaffhauserstrasse 121, Kloten, CH) on the main joints of the leg (greater trochanter, lateral femoral condyle and lateral malleolus) and an extra marker on the left arm to differentiate body sides. We developed a custom C++ based control software to detect gait events in real time based on kinematic information from the motion capture system and to send EES triggering commands to the neurostimulation system (Figure 3.3 Step 2). This control software streamed the real-time 3D-positions of all the large kinematic markers detected. The labelling of these markers was then performed in the control software itself, based on their vertical position and additional geometrical constraints. Then, the control software computed the trajectory of the foot with respect to the hip and the barycentre of this trajectory over the last few steps. An overlay of past trajectories and the current barycentre were displayed as feedback for the user. The vector between the current point on the foot trajectory and the barycentre was used to define an angular variable evolving monotonically throughout the gait cycle. A set of user-defined thresholds were applied on this angular variable to define the occurrence of desired gait events, such as foot off, foot strike, mid-swing or mid-stance. These events were used as triggers to start or stop specific spinal cord stimulation protocols.

Neurostimulation System

EES was delivered with an IPG (Medtronic Activa™ RC) that enabled monopolar and multipolar stimulation at constant current or constant voltage through one or a subset of the 16 electrodes of the paddle array or the case of the IPG (anode) (Figure 3.3 Step 4). The IPG was modified from its clinical version with an investigational firmware that enabled real-time communication with a software running on an external computer (NEUWalk Research Programmer Application NRPA, Medtronic). The NRPA acted as a relay between EES triggering commands sent by the control software described in the previous section and the IPG. It communicated wirelessly with the IPG through the following communication chain: the NRPA sent commands via

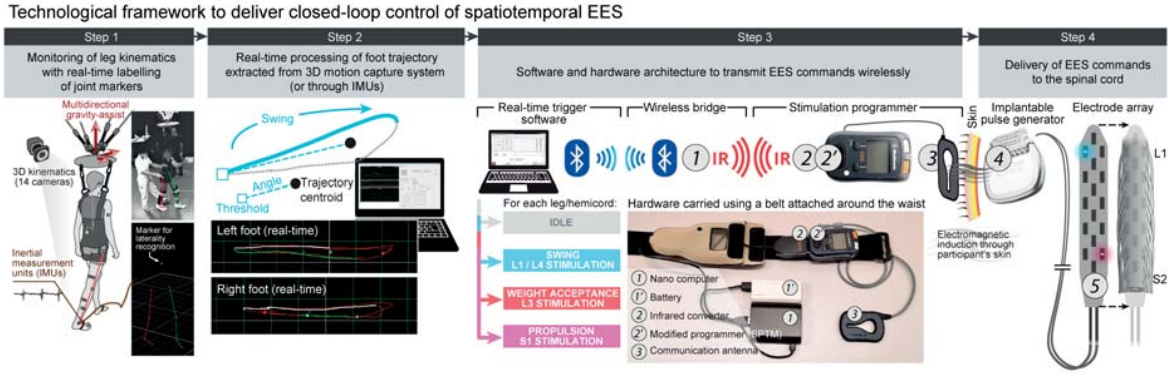

Figure 3.3 – Technological framework. Step 1: participants wear reflective markers that are monitored using infrared cameras. An algorithm assigns the markers to the joints in real-time. Step 2: the spatiotemporal trajectory of the foot around a calculated centre of rotation (centroid, updated every 3 s) is converted into angular coordinates that trigger and terminate EES protocols when a user-defined threshold is crossed. Step 3: EES commands are transmitted to the IPG via Bluetooth (1) to a module that converts them into infrared signals (2), which are then transferred to the stimulation programmer device (2'). Step 4: the stimulation programmer transmits EES commands into the IPG (4) via induction telemetry, using an antenna (3) taped to the skin and aligned to the IPG. EES is delivered through the paddle array (5).

a virtual COM port corresponding to a Bluetooth adapter, a custom wireless bridge consisting of a nano computer (Raspberry Pi) received this command and forwarded it to a virtual COM port corresponding to a USB adapter, a USB to infrared adapter (ACTiSYS Corporation, Fremont, CA, USA) transformed this command into infrared signals that were then read by a modified Medtronic patient's programmer (Sensing Programmer Telemetry Module SPTM, Medtronic), which finally transmitted the command to the patient's IPG by electromagnetic induction through the skin (Figure 3.3 Step 3). This constituted our overall investigational system: motion capture system, control software, NRPA relay software, wireless bridge, SPTM and IPG with modified firmware connected to the 16-electrode paddle array. This system allowed real-time triggering of stimulations with a median latency of 110 ms (99th percentile, 135 ms).

Configuration of Targeted EES

After approximately ten days of rest following the surgery, participants started a one-month period during which we configured EES protocols to enable single-joint movements and walking.

Single-Joint Movements

We delivered EES with electrode configuration targeting the posterior roots projecting to the spinal cord regions containing the motoneuron pools associated with the intended movement. Electrode configurations were selected using the selectivity index calculated from single-pulse EES experiments and optimised with multipolar configurations when necessary (Figure 3.2).

Continuous EES during Overground Walking

Continuous EES was delivered using a variety of locations that covered the broad range of protocols employed in previous studies [22, 143, 145, 146], both on a treadmill and overground. We report the results from the most efficient protocols for each participant. In general, these protocols involved the widespread activation of the spinal cord through the recruitment of the L1 and S1 roots or L1 and L4 roots on both sides simultaneously. EES pulses were interleaved with a 2 ms interval to avoid superposition of the electric fields generated by each configuration. EES amplitude and frequency were optimised visually.

Spatiotemporal EES during Walking

These EES protocols were guided by the spatiotemporal maps of motoneuron activation reconstructed from EMG activity of healthy individuals during walking [155, 156] (see Data processing). These spatiotemporal maps revealed that walking involved the successive activation of three hotspots restricted to specific spinal cord regions. EES protocols targeting the posterior roots projecting to these hotspots were selected from the selectivity index that was calculated during single-pulse EES experiments. The configuration, amplitude and frequency of EES were optimised during standing and refined during walking (Figure 3.5). The onset and duration of each

EES protocol was optimised using the procedures described in Figure 3.4. EES train durations could be pre-determined or terminated by a gait event (e.g. mid-swing).

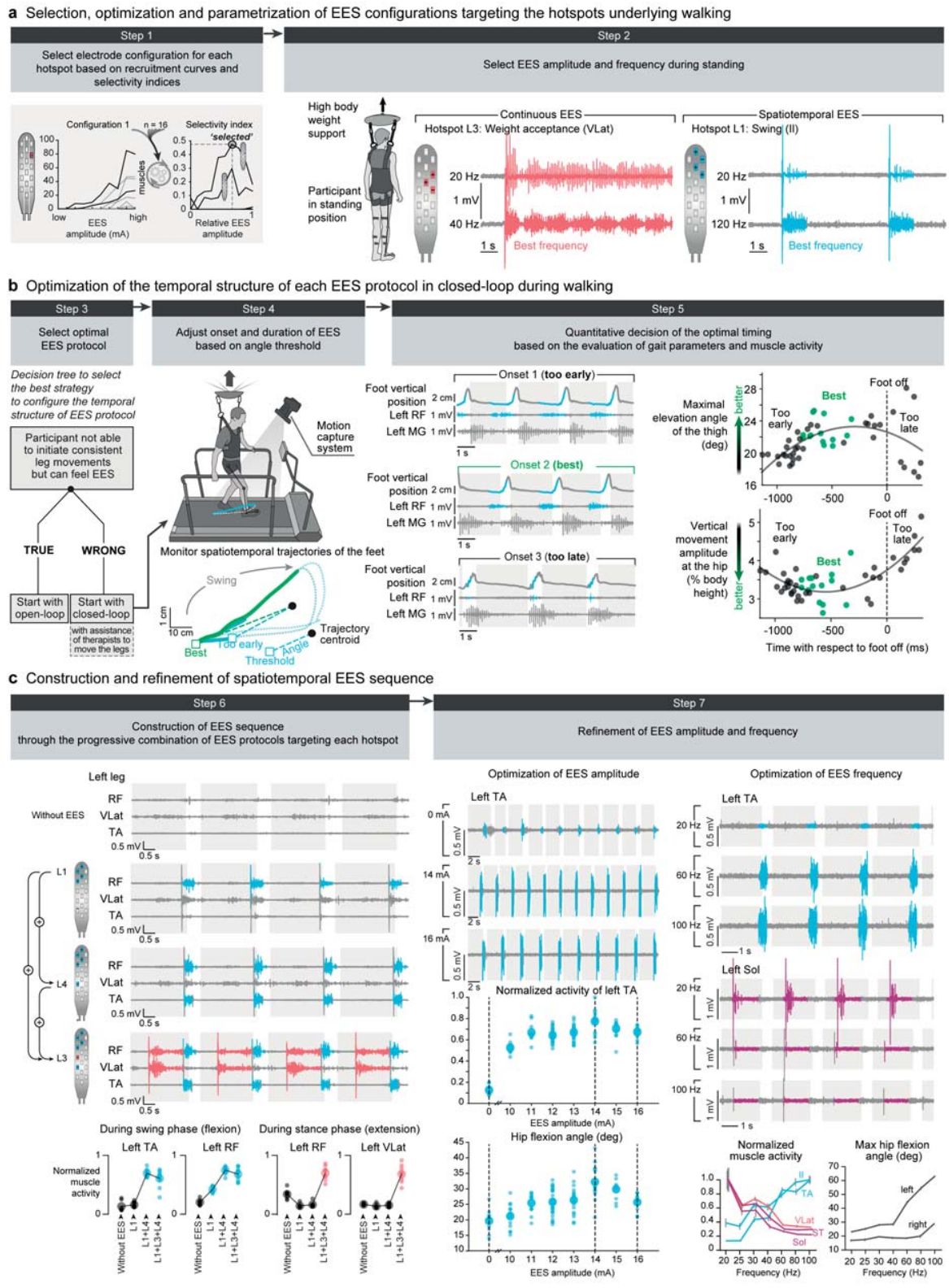

Figure 3.4 – **Configuration of spatiotemporal EES to enable walking. a**, Spatial configuration. Step 1: select electrode configurations from single-pulse experiments to target the three hotspots underlying the production of walking in healthy individuals (weight acceptance: L3; propulsion: S1; swing: L1/L4). Step 2: optimise EES amplitude and frequency while delivering EES during standing. Multipolar configurations can be used to refine selectivity of EES protocols. Example shows continuous EES targeting the right L3 posterior root to facilitate right knee extension during standing, and trains (500 ms) of EES targeting the right L1 posterior root stimulation to facilitate hip flexion. Two EES frequencies are shown (P3). **b**, Temporal configuration. Step 3: decision tree to select the best strategy to configure the temporal structure of EES protocols. If the participant is able to initiate leg movements consistently, use closed-loop EES based on real-time processing of foot trajectory. If the participant is not able to initiate consistent leg movements but can feel when EES is applied, use open-loop EES. If the participant is not able to generate movement and cannot feel EES, use closed-loop EES combined with physiotherapist assistance to move the legs. Step 4: real-time monitoring of the spatiotemporal trajectory of the feet. The trajectory is modelled as a foot rotating in space around the centroid of the movement (updated every 3 s). Angular thresholds determine the onset and end of EES protocols. Step 5: example showing the effect of three different angular thresholds on the onset of EES and resulting kinematics and EMG activity, including the quantification of kinematics for each step and condition that enables selecting the optimal onset of EES trains (P1). The same approach is used to optimise the duration of each train. **c**, Resulting EMG patterns. Step 6: example of the progressive addition of EES protocols targeting specific hotspots. Plots show the quantification of EMG activity for the displayed muscles (n = 7, 9 gait cycles for no EES and for every stimulation condition, P2). Step 7: EES amplitudes and frequencies are adjusted to avoid detrimental interactions between the different EES protocols and thus obtain the desired kinematic and EMG activity. Plots report the modulation of EMG activity and kinematics with increases in EES amplitude and frequency (mean ± s.e.m.; amplitude data: n = 10, 12, 12, 30, 19, 12, 11, 10 gait cycles for amplitudes in increasing order, P2; frequency data: n = 20, 15, 16, 17, 15, 16, 15 gait cycles for frequencies in increasing order, P3).

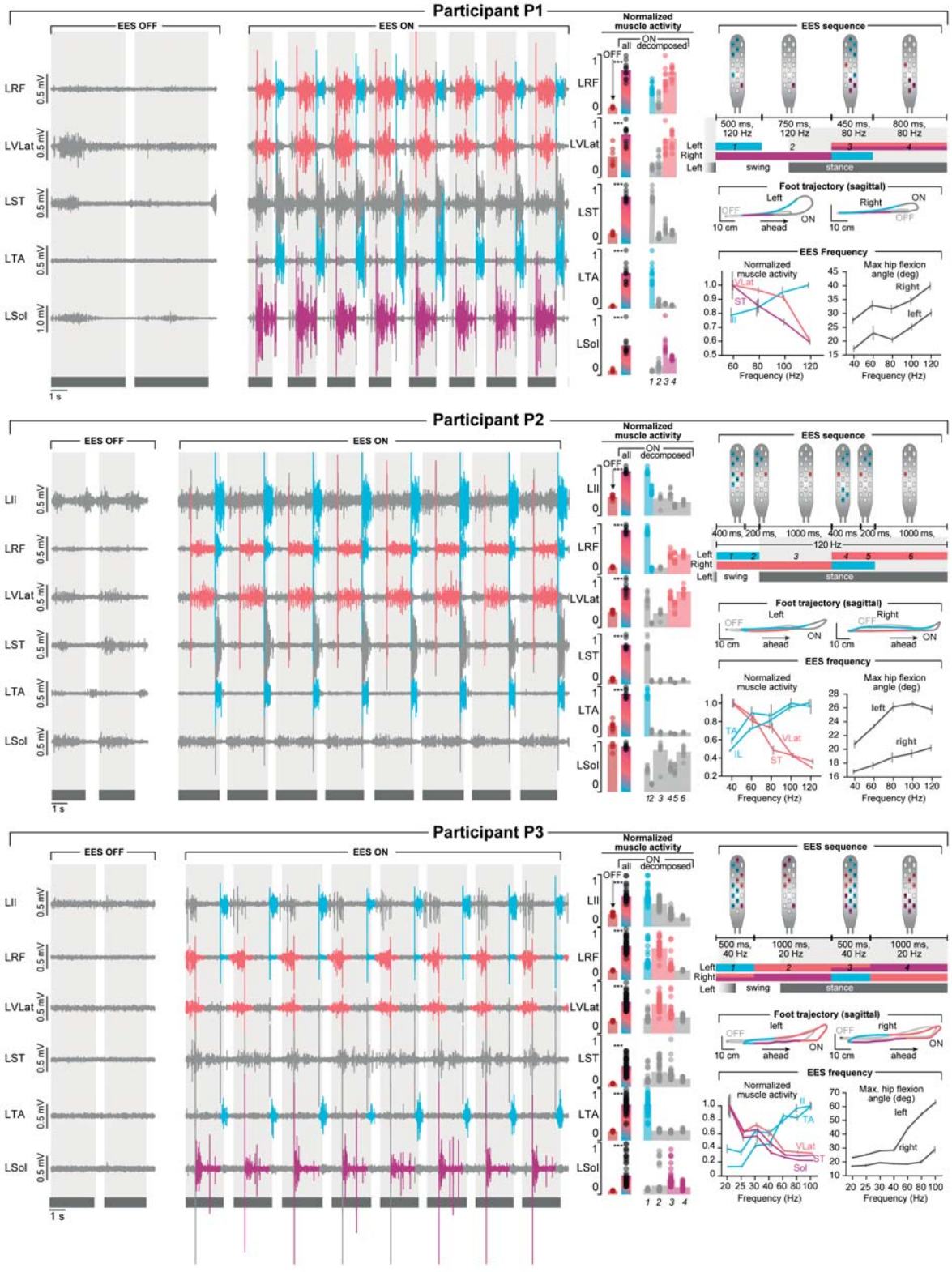
Participant P1
EES OFF
EES ON
LRF
LVLat
LST
LTA
LSol
0.5 mV
1.0 mV
1 s
Normalized muscle activity
all
ON decomposed
OFF
1 2 3 4
EES sequence
500 ms, 120 Hz
750 ms, 120 Hz
450 ms, 80 Hz
800 ms, 80 Hz
Left
Right
swing
stance
Foot trajectory (sagittal)
10 cm
ahead
EES Frequency
Normalized muscle activity
Max hip flexion angle (deg)
Frequency (Hz)
Participant P2
LIl
400 ms, 200 ms, 1000 ms, 400 ms 200 ms, 1000 ms,
120 Hz
1 2 3 4 5 6
EES frequency
Participant P3
500 ms, 40 Hz
1000 ms, 20 Hz
500 ms, 40 Hz
1000 ms, 20 Hz

Figure 3.5 – **Targeted modulation of muscle activity during walking.** Each panel reports the same representative data and quantification for one participant. Left, EMG activity of leg muscles during walking on a treadmill without EES (EES OFF) and with spatiotemporal EES (EES ON) while applying 50%, 45% and 70% body weight support for participants P1, P2 and P3, respectively. Stance and swing phases are indicated by grey and white backgrounds, respectively. The personalised spatiotemporal EES sequence (open loop) is schematised at the top right. The colours of each EES protocol refer to the targeted hotspots: weight acceptance (salmon), propulsion (magenta) and swing (cyan). These colours are used in the EMG traces to indicate the temporal window over which each targeted EES protocol is active. The bar plots report the amplitude of muscle activity without EES and with spatiotemporal EES, for which the quantification was performed over the entire burst of EMG activity and during each temporal window with targeted EES. The temporal windows are labelled with a number that refers to the spatiotemporal EES sequence. These results show the pronounced increase in the EMG activity of the targeted muscles (P1, n = 7, 11; P2, n = 9, 9; P3, n = 10, 57 gait cycles without EES and with EES). The average spatiotemporal trajectories of both feet with respect to the hip in the sagittal plane are shown for walking without EES and with spatiotemporal EES. The presence of targeted EES is indicated with the same colour code. Plots at bottom right show the relationships between EES frequency and the modulation of the EMG activity of flexor (blue) and extensor (magenta or salmon) muscles and maximum amplitude of hip movements during walking (mean ± s.e.m.; P1: n = 14, 17, 15, 19 gait cycles for increasing frequencies; P2: n = 13, 16, 10, 17, 12 gait cycles for increasing frequencies; P3: n = 20, 15, 16, 17, 15, 16, 15 gait cycles for increasing frequencies). ***P < 0.001. Student's t-test.

EEG Recordings

Subjects were asked to produce an isometric torque at the right knee without and with targeted EES (Figure 3.11). The subjects seated on the Humac Norm Cybex dynamometer with the knee flexed at 90°and were instructed to follow a sequence displayed on a screen in front of them: movement preparation (auditory cue), GO cue around 2 s after movement preparation, movement execution (about 3 seconds). During trials with EES, 2 s after the initiation of the movement the stimulation was switched on for about 5 s. EEG data were continuously acquired using 64 channels in standard 10-20 configuration (ANT neuro) at a sampling rate of 1024 Hz.

Clinical Evaluations

International Standards for Neurological Classification of Spinal Cord Injury

Each participant's neurological status was assessed before surgery and after 5 months of rehabilitation based on the International Standards for Neurological Classification of Spinal Cord Injury, a comprehensive clinician-administered neurological examination of residual sensory and motor function quantifying SCI severity [6].

WISCI II Score

Functional walking ability was assessed by the WISCI II score [157], which evaluates the amount of physical assistance, assistive devices or braces required to walk overground for ten meters.

Muscle Mass and Quality

Muscle mass and quality were quantified using CT images obtained at abdominal (L3 vertebra) and mid-thigh (25 cm above femorotibial joint space) levels, assessed before surgery and after rehabilitation. Muscle segmentations were performed semi-automatedly using ImageJ and specific HU thresholds [158] (-29 to 150 HU) (Figure 3.18a). Muscle quality was assessed using CT attenuation numbers, which reflect lipid content in skeleton muscle [159].

10-Meter Walk Test

Walking speed was assessed by a timed 10-meter walk test without body weight support. Participants were instructed to walk with the preferred assistive device as fast as they could. Participants P1 and P2 performed the test with a standard 4-wheel walker. This test was also performed with spatiotemporal EES after rehabilitation and during follow-up after obtaining the authorisation to use spatiotemporal EES without body weight support. Participant P3 performed the test only after rehabilitation using a 4-wheel walker with armrests, spatiotemporal EES, and the presence of the body weight support for safety.

6-Minute Walk Test

Endurance was assessed by the distance covered overground within 6 minutes with the preferred assistive device. Participants P1 and P2 performed this test in the same conditions as the 10-meter walk test. Participant P3 was unable to perform this test.

Study Extension and Technologies for Home Use

Technological Framework

The home-based system consists of a tablet (Surface Pro 4, Microsoft) containing personalised EES programs, each associated with a specific training activity. Custom software was developed in C# to allow switching between EES protocols and loading them onto the IPG. A Graphical User Interface (GUI) allows the participant to change the amplitudes of EES protocols, and to start or stop an activity from the tablet or using a commercially available smartwatch (Fossil Q Marshal, Fossil Group, Inc., USA) connected to the tablet via bluetooth. Participants can either tap on the smartwatch screen or use a voice controller implemented using a keyword detection system (Snowboy Hotword Detection, non-commercial license, KITT.AI, Baidu, Inc., China) built on artificial neural networks.

Participants could select activities with EES delivered in open-loop or closed-loop. The controller of closed-loop EES used a pair of inertial measurement units (IMUs, NGIMU, FW v.1.5 HW v1.6, x-io Technologies Limited, UK) connected to the tablet via WiFi, streaming data at 90 Hz.

Closed-Loop Walking

During closed-loop walking, the pitch angle of IMUs placed on the feet or tibia enabled gait event detection based on a Kalman filter combining the accelerations and angular velocities of IMU signals:
Noisy measurement from accelerometers: $\theta_{measured} = atan2\left(A_y, Ax\right)$
Kalman observation model: $\theta_{measured} = H \cdot \begin{pmatrix} \theta_{real} \\ \dot{\theta} \end{pmatrix} + \omega_1$

with $H = \begin{pmatrix} 1 & 0 \end{pmatrix}$

Kalman state-transition model: $\begin{pmatrix} \theta_{real} \\ \dot{\theta} \end{pmatrix}_{i+1} = A \cdot \begin{pmatrix} \theta_{real} \\ \dot{\theta} \end{pmatrix}_{i} + \omega_2$

with $A = \begin{pmatrix} 1 & 1/f_s \\ 0 & 1 \end{pmatrix}$

where A_x and A_y represent the accelerations measured by the accelerometers in the plane of movement, $\dot{\theta}$ represents the angular velocity measured by the gyroscope around the axis of the joint (ankle or knee), $\theta_{measured}$ is an approximation of the pitch angle assuming that the IMU is static and that only gravity contributed to the accel-

erations, $atan2$ is the four-quadrant inverse tangent, θ_{real} is the real pitch angle that estimated by the Kalman filter, and ω_1 and ω_2 are Gaussian noises. Gait events are detected when the pitch angle crosses a pre-defined threshold personalised for each participant.

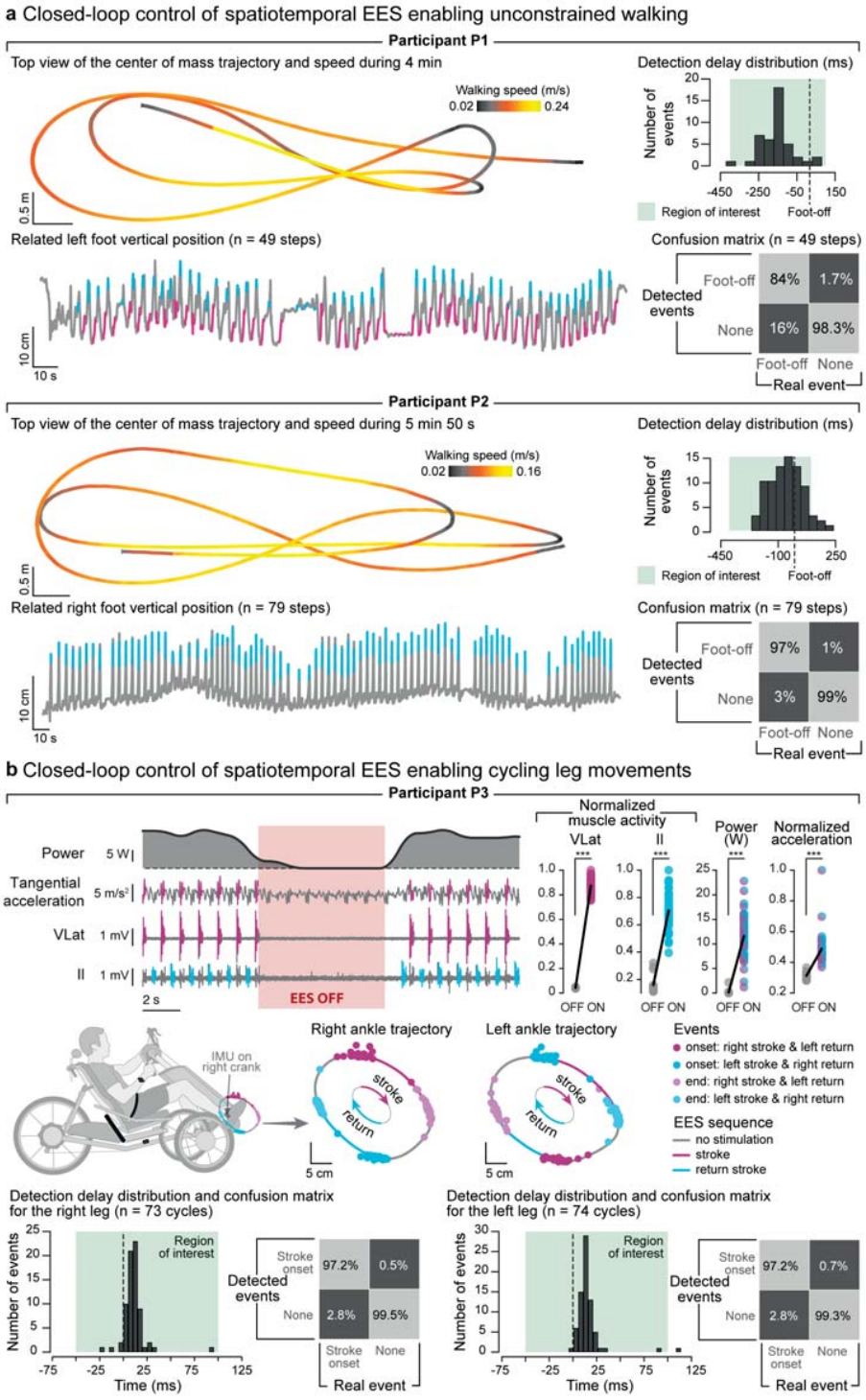

Figure 3.6 – **Performance of closed-loop spatiotemporal EES to enable walking and cycling outside the laboratory.** **a**, P1 and P2 were asked to walk freely overground with a walker (no body weight support) for 6 min. The concomitant vertical displacements of the foot show the consistency of EES triggering events despite variable foot kinematics and voluntary breaks. The trajectory of the centre of mass is shown from a top view to illustrate the ability to steer locomotion along any desired path. EES protocols took into account the deficits of each participant (cyan, EES targeting hip flexion; magenta, EES targeting knee and ankle extension). Histograms indicate the number of detected foot-off events for the represented leg as a function of the latency with respect to real foot-off events. The confusion matrix associated with these detections is represented below, as a percentage of the real events that were correctly or incorrectly classified. Detections were considered valid if they occurred between 400 ms before and 100 ms after real foot-off events, as highlighted in green on histograms (P1, n = 49 gait cycles; P2, n = 79 gait cycles). **b**, Closed-loop spatiotemporal EES was delivered in P3 using an electric trike powered by hand and foot pedals. Traces show EMG activities of the targeted hip flexor and knee extensor muscles on one leg together with the tangential acceleration of the pedal and power generated at the foot pedal. Plots report the quantification of flexor and extensor EMG activities, peak tangential accelerations and generated power without and with EES. Successive ankle trajectories during cycling are shown together with the timing of EES protocols targeting the hip flexor and knee extensor muscles. The histograms and confusion matrices report the performance of the controller following the same conventions as in **a**, except that the correct detection window was restricted to 50 ms before and 100 ms after the desired crank position (P3, n = 73 pedalling cycles). ***P < 0.001. Student's t-test.

Closed-Loop Biking

Gait event detection was based on one IMU placed on the crank and another IMU attached on the frame of the trike. These IMUs were used to measure the angle of the crank and the current slope on non-levelled terrains, respectively. Detections were based on the above described Kalman filter that first estimated the measured angle from the accelerometers:

$$\theta_{measured} = atan2\left(A_y, A_x - r \cdot \dot{\theta}^2\right)$$

Communication delays with the IPG could result in variability in EES timing as the angular velocity is varied. To avoid this issue, we estimated the angular velocity $\dot{\theta}$ over the last cycle and thresholded the crank angle at $\theta_{threshold} - \dot{\theta} \cdot \tau_{communication}$, where $\theta_{threshold}$ is the desired angular threshold and $\tau_{communication}$ is the communication delay (about 110 ms).

EES protocols promoted knee extension when the crank reached 90°(top) together with hip flexion of the contralateral leg. This system was mounted on a tricycle specially conceived for patients with motor impairments, combining foot and hand pedals and electrically-powered assistance (Trike, GBY SA, Vuisternens-en-Ogoz, CH).

Data Processing

Recruitment Curves during Single-Pulse EES

EMG signals were band-passed filtered between 10 and 450 Hz (4th-order Butterworth filter). EES onset was determined using semi-automatic methods based on stimulation artefact recordings. The evoked responses were extracted and superimposed to isolate the monosynaptic components based on visual inspection by an experienced neurophysiologist. The temporal window of these responses started 10 to 20 ms after EES onset and lasted 40 to 50 ms, depending on the muscle and participant. For each EES amplitude, the responses were quantified as the peak-to-peak amplitude to generate recruitment curves that we displayed in circular plots. Muscles are distributed at different angular positions, while the radial axis corresponds to EES amplitude (Figure 3.8d, Figure 3.2 and Figure 3.9). A greyscale shading reports the normalised EMG activity. The white circle highlights the EES amplitude that corresponds to the highest selectivity index. The polygon describes the muscle selectivity at the optimal EES amplitude: the edges of the polygon represent the normalised EMG activity on the radial axis for a particular muscle, scaled so that the polygon fills the circle.

Selectivity Index

We targeted the posterior roots projecting to L1, L3, L4 and S1 segments to modulate motoneurons associated with hip flexion, knee extension, ankle flexion and ankle extension. To identify the relevant electrodes, we computed a selectivity index $SI_{experimental}\left(g_i, I\right)$ for each targeted muscle group g_i and EES amplitude I. This selectivity index contains two terms, one indicating the selectivity on the targeted side, and one indicating the mediolateral selectivity for the targeted side s_i:

$$SI_{experimental}\left(g_i, I\right) = SI_{targeted\,muscles}\left(g_i, I\right) \cdot SI_{left\,vs\,right}\left(s_i, I\right)$$

$$\begin{cases} SI_{targeted\,muscles}\left(g_i, I\right) = \dfrac{\Sigma_{muscles\,in\,g_i}\omega_{i,j} \cdot log\left(1 + A_j\left(I\right)\right)}{log\left(2\right)} \\ SI_{left\,vs\,right}\left(s_i, I\right) = f_+\left(\dfrac{max_{ipsilateral(s_i)}\left(A_j\left(I\right)\right) - max_{contralateral(s_i)}\left(A_j\left(I\right)\right)}{max_{ipsilateral(s_i)}\left(A_j\left(I\right)\right) + max_{contralateral(s_i)}\left(A_j\left(I\right)\right)}\right) \\ f_+\left(x\right) = \begin{cases} x & \text{if } x > 0 \\ 0 & \text{if } x \leqslant 0 \end{cases} \end{cases}$$

where $A_j\,(I)$ represents the normalised EMG activity of muscle j in response to EES amplitude I. $\omega_{i,j}$ is a weight associated with muscle j for the targeted muscle group g_i. For each targeted muscle group, weights of agonists (respectively antagonists) are positive (respectively negative), and the sum of weights over agonists (respectively antagonists) is equal to 1 (respectively -1). These weights were chosen empirically to capture the respective contributions of each muscle in the targeted muscle group (see Table 3.2).

	Il	RF	VLat	ST	TA	MG	Sol
Hip flexion (L1)	0.8	0.2	-	-1	-	-	-
Knee extension (L3)	-0.5	0.2	0.8	-0.5	-	-	-
Ankle flexion (L4)	-	-	-	-	1	-0.2	-0.8
Ankle extension (S1)	-	-	-	-	-1	0.2	0.8

Table 3.2 – Muscle contributions.

Torque and EMG Activity during Voluntary Contractions

The recorded torque was low-pass filtered below 5 Hz and EMG activities were band-pass filtered between 10 and 450 Hz (4^{th}-order Butterworth filter). The root mean square (RMS) of the EMG activity was calculated with a 500-ms centred running window. During maximum voluntary contractions without EES, the torque produced was quantified as the average within a 500-ms time window centred at the peak torque. EMG activities were quantified as their RMS value at the peak torque. During maximum voluntary contractions with EES, the task was divided into four time periods: onset of voluntary contribution, EES onset, end of voluntary contribution, EES end. Because the sudden onset of EES created a transient peak in the torque and EMG activities, we further split the analysis between the transient (EES onset to 1.1 s) and sustained effects after EES onset (Figure 3.10).

EMG Activity during Walking

EMG activities were processed according to the SENIAM (Surface Electromyography for the Non-Invasive Assessment of Muscles) standards for EMG recordings. All displayed EMG activities during walking were band-pass filtered between 10 and 450 Hz (4^{th}-order Butterworth filter). A moving average of the rectified EMG signal within a centred 250-ms time window was used to generate normalised EMG envelopes for quantification. With EES, the sudden EES onset created transient peaks of EMG

activity that did not translate into sustained muscle contractions but nevertheless contributed to the computation of EMG envelopes. To avoid this issue, we systematically clipped EMG responses within a time window of 50 ms around the onset of EES trains.

Calculation of Motoneuron Activation Maps

Motoneuron pools innervating hip flexors (Il, RF), knee extensors (VLat, RF), ankle flexors (TA) and ankle extensors (MG, Sol) are spatially distributed along the rostrocaudal axis of the lumbosacral spinal cord [160]. We modelled the activation of motoneuron pools in each spinal segment S_i as a linear combination of the normalised EMG activities of leg muscles M_j:

$$S_i = \frac{\Sigma_{muscles} W_{i,j} \cdot M_j}{\Sigma_{muscles} W_{i,j}}$$

If all muscles reach their maximum activity, the activation of each spinal segment is equal to 1. The coefficients $W_{i,j}$ represent how much each muscle reflects the underlying activity of a spinal segment [155]. As an approximation, we took for $W_{i,j}$ the ratio of motoneurons innervating the muscle j and present in the spinal segment i, with respect to all motoneurons innervating the muscle j. These coefficients were derived from anatomical studies [134] (see Table 3.3).

	Il	RF	VLat	ST	TA	MG	Sol
L1	0.4	0	0	0	0	0	0
L2	0.4	0.12	0.12	0	0	0	0
L3	0.2	0.19	0.19	0	0	0	0
L4	0	0.19	0.19	0.12	0	0.77	0
L5	0	0	0	0.4	0.23	0.23	0.09
S1	0	0	0	0.4	0.77	0	0.45
S2	0	0	0	0.08	0	0	0.45

Table 3.3 – Coefficients $W_{i,j}$.

Motoneuron activation maps derived from single-pulse EES experiments were calculated from the peak-to-peak responses, while motoneuron activation maps during functional tasks were computed with the instantaneous or average value of EMG envelopes. Motoneuron activation maps were interpolated and superimposed onto a 3D illustration of the human spinal cord.

Extraction of Hotspots underlying Walking

Three hotspots were extracted from the spatiotemporal maps of motoneuron activation underlying walking of healthy individuals. Hotspots were extracted from the iso-potential lines at 45, 55, 65 and 75 % of the maximum activation in the maps [65]. The correlations between each targeted hotspot and EES-induced EMG activity were calculated based on the average motoneuron activation maps of each hotspot and those obtained from the EMG activity induced by a 500 ms train of EES during standing.

Processing of EEG Signals

Raw EEG signals were filtered (1-40 Hz, zero-phase IIR filters), down-sampled at 128 Hz, and re-referenced to a common average. Eye blink and eye movements artefacts were removed by Independent Component Analysis. EES evoked activity was computed by averaging EEG signals from -0.6 to 1 s after stimulation artefact. During volitional movements, epochs were extracted from -1.5 to 1 s after GO cue and from -500 to 500 ms after movement termination, defined as the torque reaching 2 % of the local maximum value. Time frequency spectra were calculated using sliding Hamming windows of 200 ms with time steps of 32 ms. Power spectra were normalised to the average values of the corresponding frequency bin. Beta (17-30Hz) power spectra over leg sensorimotor area (Cz) was calculated during event related resynchronization (ERS), defined 0 to 500 ms after movement.

Statistics

All quantifications show the mean and standard error of the mean of the represented variables, in addition to all individual data. Comparisons between two conditions were performed using a Student's t-test. Comparisons involving more than two categories were performed using a 1-way ANOVA, followed post hoc by Tukey's Honest Significance Difference tests. *, **, *** indicate a p-value smaller than 0.05, 0.01, 0.001 respectively. Significant differences for EEG data were obtained by randomly permuting single trial beta ERS values of the two conditions. The number of permutations was determined to reach $\alpha = 0.05$.

Results

Targeted Neurotechnologies and Surgery

We developed a wireless environment that allows real-time control over independently adjusted EES trains to the spinal cord during overground walking (Figure 3.7a). A gravity-assist applied multidirectional forces to the trunk to provide personalised bodyweight support in a safe workspace [85]. A recording platform allowed real-time processing of whole-body kinematics, ground reaction forces and electromyographic (EMG) activity of leg muscles. To deliver stimulation, we upgraded an implantable pulse generator commonly used for deep brain stimulation with wireless communication modules [72] that enabled real-time control over EES parameters (Figure 3.1). EES sequences could be pre-programmed in an open loop or triggered in a closed loop on the basis of external signals [65, 112]. The lumbosacral posterior roots were targeted using a 16-electrode paddle array designed for pain therapy.

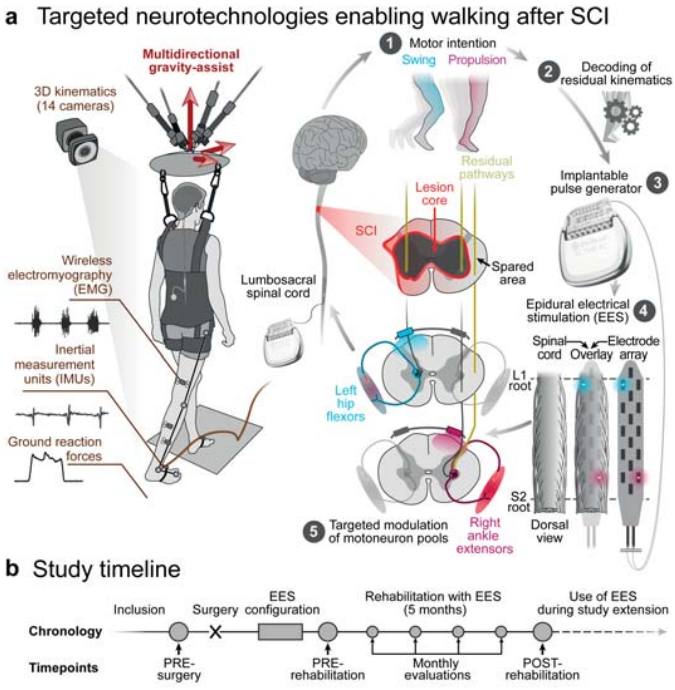

Figure 3.7 – Technology and study design. **a**, Targeted neurotechnologies enable walking after SCI. Multidirectional assistance of trunk movements during overground locomotion while 3D kinematics, ground reaction forces and EMG activity are recorded wirelessly. An implantable pulse generator connected to a 16-electrode paddle array was used to target the posterior roots projecting to specific motor neuron pools, illustrated for hip flexors and ankle extensors. Real-time processing of residual kinematics ensures that targeted EES coincides with movement intent. **b**, Study timeline.

We enrolled three males with a chronic cervical SCI who displayed severe lower limb deficits or complete paralysis that prevented them from walking overground (Table 3.1).

To target the posterior roots that project to motor neuron pools that innervate leg muscles (Figure 3.8a), we developed a surgical protocol consisting of pre-operative imaging combined with intraoperative electrophysiology and radiology that guided the precise placement of the paddle array (Figure 3.7b).

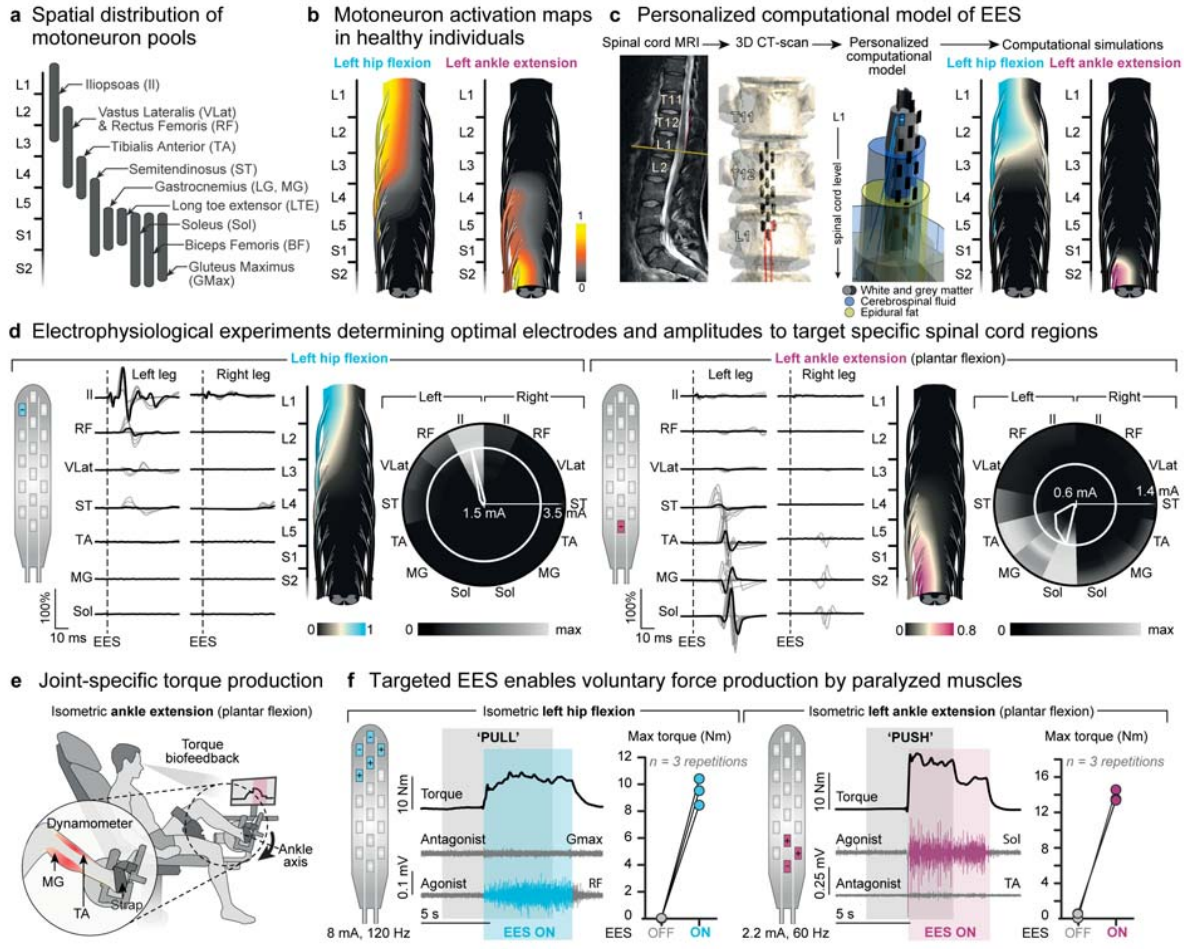

Figure 3.8 – **Configuration of targeted EES.** **a**, Distribution of motor neuron pools within the spinal cord [134]. **b**, Map of motor neuron activation underlying isometric torque production in a healthy subject (consistent across three repetitions and subjects). **c**, Personalised computational model of EES. Simulated map of motor neuron activation following EES targeting the L1 and S2 posterior roots. **d**, EMG responses when delivering single-pulse EES at increasing amplitudes (grey traces). Motoneuron activation maps correspond to optimal amplitudes (black traces). Circular plots report EMG amplitude (in grey scale) at increasing amplitudes (radial axis). White circles show optimal amplitudes; polygons quantify selectivity at this amplitude. **e**, Instrumented chair used to measure single-joint torques. **f**, Isometric torque and EMG activity while delivering targeted EES, including quantification (n = 3 repetitions, P1).

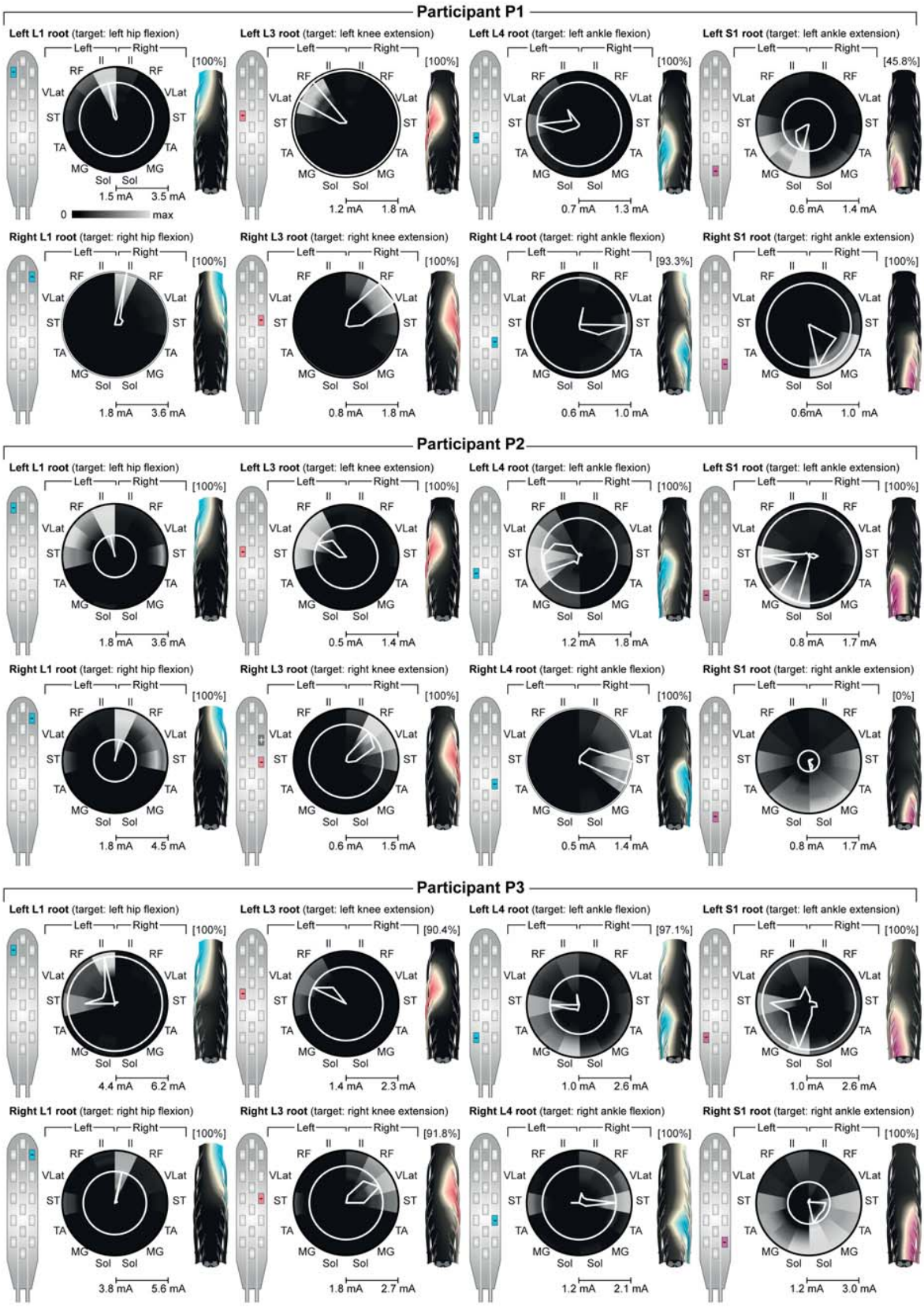
Participant P1
Left L1 root (target: left hip flexion)
Left L3 root (target: left knee extension)
Left L4 root (target: left ankle flexion)
Left S1 root (target: left ankle extension)
Right L1 root (target: right hip flexion)
Right L3 root (target: right knee extension)
Right L4 root (target: right ankle flexion)
Right S1 root (target: right ankle extension)
Participant P2
Left L1 root (target: left hip flexion)
Left L3 root (target: left knee extension)
Left L4 root (target: left ankle flexion)
Left S1 root (target: left ankle extension)
Right L1 root (target: right hip flexion)
Right L3 root (target: right knee extension)
Right L4 root (target: right ankle flexion)
Right S1 root (target: right ankle extension)
Participant P3
Left L1 root (target: left hip flexion)
Left L3 root (target: left knee extension)
Left L4 root (target: left ankle flexion)
Left S1 root (target: left ankle extension)
Right L1 root (target: right hip flexion)
Right L3 root (target: right knee extension)
Right L4 root (target: right ankle flexion)
Right S1 root (target: right ankle extension)
Left
Right
RF
VLat
ST
TA
MG
Sol
0
max

Figure 3.9 – Spatial selectivity of targeted electrode configurations. Monopolar configurations (shown on paddle array schematics) experimentally selected to target the left and right posterior roots associated with hip flexion (L1), knee extension (L3), ankle flexion (L4) and ankle extension (S1) for the three participants. The circular plots and motor neuron activation maps use the same conventions as in Figure 3.8 and Figure 3.2 (median of n = 4 pulses). The normalised selectivity index is reported above each motor neuron activation map. This index represents the percentage of posterior root selectivity for the electrode configuration selected experimentally, with respect to the maximum posterior root selectivity that can be achieved among all monopolar configurations (all selectivity indices obtained from computational simulations). Note that in P2, the electrode selected experimentally to target the right S1 root was located on the midline and resulted in bilateral activation within computational simulations, which resulted in a normalised selectivity index of zero.

EES enables Control of Paralysed Muscles

We aimed to identify electrode configurations that target the posterior roots that project to spinal cord regions that contain motor neurons involved in mobilising the hip, knee and ankle joints.

We compiled an atlas of motor neuron activation maps underlying flexion or extension of each joint in healthy individuals. We projected the EMG activity from leg muscles onto the expected anatomical locations of the associated motor neuron pools [155, 156]. We obtained consistent motor neuron activation maps. For example, hip flexion involved the activation of upper lumbar segments, whereas ankle extension activated motor neuron pools restricted to upper sacral segments (Figure 3.8b). To identify electrodes that could target the posterior roots that project to the spinal cord regions associated with these motor neuron activation maps, we performed simulations using hybrid computational models of EES [53]. Each model was personalised using magnetic resonance imaging (MRI) and computerised tomography (CT) scans. Simulations estimated the relative recruitment of each posterior root by each electrode of the array (Figure 3.8c).

These simulations guided the identification of optimal electrode configurations. While participants laid supine, we delivered monopolar pulses of EES at increasing intensities through the electrodes that had the highest probabilities of activating the targeted posterior roots (Figure 3.2). Projection of muscle response amplitudes into circular plots described the spatial selectivity of each electrode, which we quantified with an algorithm (Figure 3.8c). If the selectivity was insufficient, we steered the electrical field with multipolar electrode configurations (Figure 3.2). For all participants, computer simulations and electrophysiological experiments confirmed high correlations between the identified electrode configurations and the recruitment of the posterior roots that project to each of the targeted spinal cord regions involved in mobilising hip, knee and ankle joints (Figure 3.9).

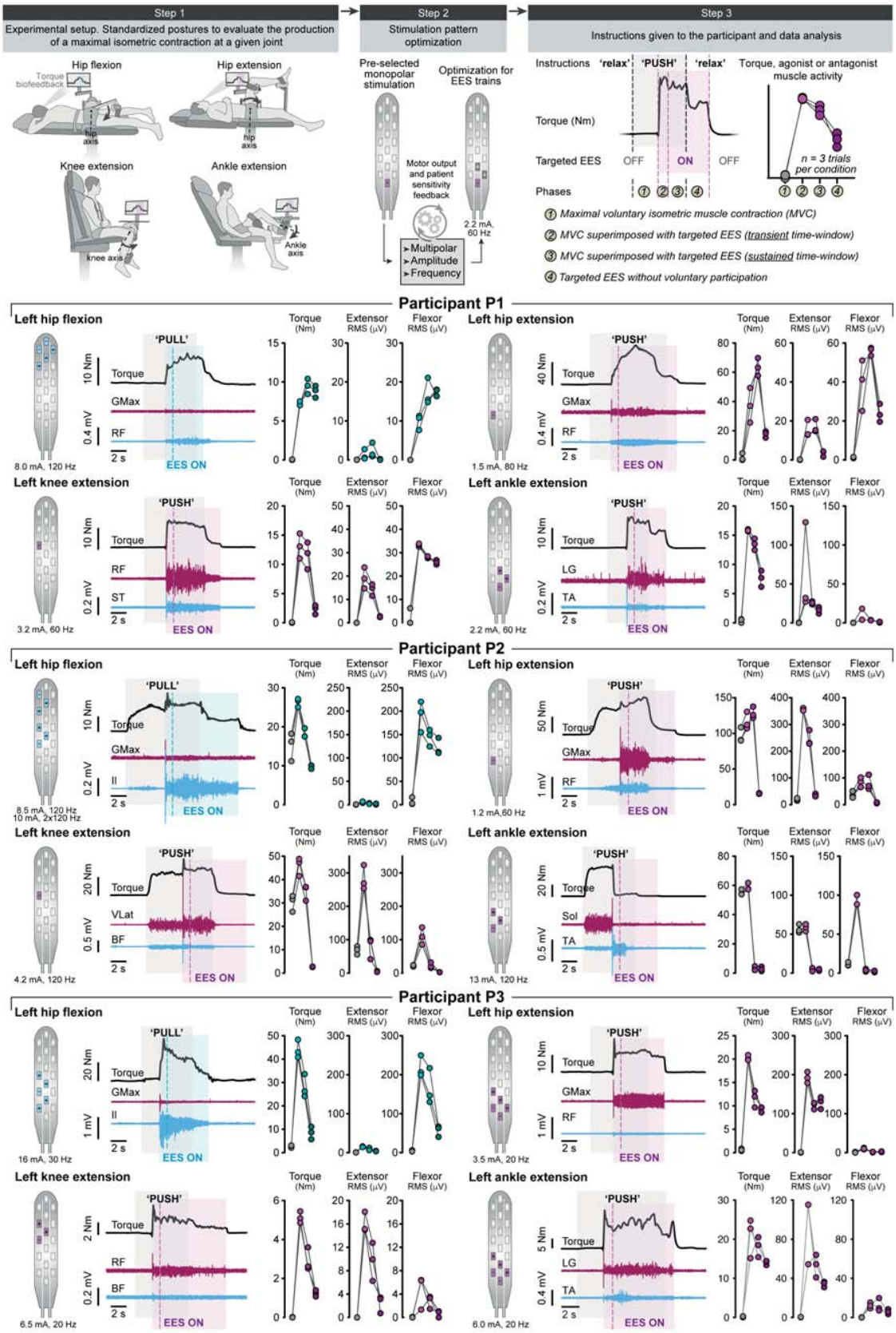
Step 1
Experimental setup. Standardized postures to evaluate the production of a maximal isometric contraction at a given joint
Step 2
Stimulation pattern optimization
Step 3
Instructions given to the participant and data analysis
Hip flexion
Hip extension
Knee extension
Ankle extension
Torque biofeedback
hip axis
knee axis
Ankle axis
Pre-selected monopolar stimulation
Optimization for EES trains
Motor output and patient sensitivity feedback
2.2 mA, 60 Hz
Multipolar
Amplitude
Frequency
Instructions 'relax' 'PUSH' 'relax'
Torque, agonist or antagonist muscle activity
Torque (Nm)
Targeted EES OFF ON OFF
Phases
n = 3 trials per condition
1 Maximal voluntary isometric muscle contraction (MVC)
2 MVC superimposed with targeted EES (transient time-window)
3 MVC superimposed with targeted EES (sustained time-window)
4 Targeted EES without voluntary participation
Participant P1
Left hip flexion
'PULL'
Torque
GMax
RF
8.0 mA, 120 Hz
EES ON
Torque (Nm)
Extensor RMS (μV)
Flexor RMS (μV)
Left hip extension
'PUSH'
1.5 mA, 80 Hz
Left knee extension
ST
3.2 mA, 60 Hz
Left ankle extension
LG
TA
2.2 mA, 60 Hz
Participant P2
II
8.5 mA, 120 Hz
10 mA, 2x120 Hz
1.2 mA,60 Hz
VLat
BF
4.2 mA, 120 Hz
Sol
13 mA, 120 Hz
Participant P3
16 mA, 30 Hz
3.5 mA, 20 Hz
6.5 mA, 20 Hz
6.0 mA, 20 Hz

Figure 3.10 – **Single-joint movements enabled by targeted EES.** Step 1: participants are placed in standardised positions to allow assessment of voluntary torque production at a single joint (isometric contractions) without and with targeted EES. Step 2: EES protocols elaborated from single-pulse experiments (Figures 3.2 and 3.9) are optimised for each task using multipolar configurations and adjustments of EES amplitude and frequency. Step 3: sequence of each trial. Participants were asked to produce a maximal voluntary contribution, but failed in most cases, as evidenced by the absence of EMG activity during this period. While they continued trying to activate the targeted muscle, EES was switched on. After a few seconds, participants were instructed to stop their voluntary contribution. After a short delay, EES was switched off. For each sequence, the produced torque and EMG activity of the key agonist and antagonist muscles acting at the targeted joint were calculated over the four indicated phases of the trial. Plots report the measured torques and EMG activity during the various phase of the trial for the left legs of all participants for the four tested joints (cyan, flexor; magenta, extensor), together with EES parameters and electrode configurations. All measurements were performed before rehabilitation, except for hip extension in P1 and P2 (not tested before), and ankle extension in P3 (no capacity before), which were carried out after rehabilitation. Targeted EES enabled or augmented the specific recruitment of the targeted muscle, which resulted in the production of the desired torque at the targeted joint, except for ankle extension of P2. Plots show quantification of the EMG activity and torque for n = 3 trials per condition. Note that hip flexion can be enabled or augmented with EES targeting L1 and/or L4 posterior roots (heteronymous facilitation of flexor motor neuron pools).

We next tested whether spatially selective EES could facilitate force production from the targeted muscles. While seated, participants were asked to produce an isometric force restricted to a single joint. Participant P1 failed to produce hip flexion and ankle extension torques with his paralysed leg (Figure 3.8e, f). EES immediately enabled voluntary activation of the targeted muscles to produce the desired torque. These observations were repeated for all targeted joints and participants (Figure 3.10).

Without any voluntary contribution, EES induced minimal muscle contraction (Figure 3.10). At the amplitudes used, EES augmented the excitability of the targeted motor neurons, which enabled residual but functionally silent descending inputs to activate muscles.

EES modulates Cortical Activity

These results opened the possibility that the recruitment of proprioceptive pathways with EES modulates cortical excitability, which may facilitate movement [161].

To study this hypothesis, we recorded electro-encephalo-graphic (EEG) activity when participants attempted to produce knee extension torques without and with EES (Figure 3.11a). EES triggered a robust response in the sensorimotor cortex (latency: 90-140 ms, Figure 3.11b), probably resulting from the recruitment of proprioceptive afferents.

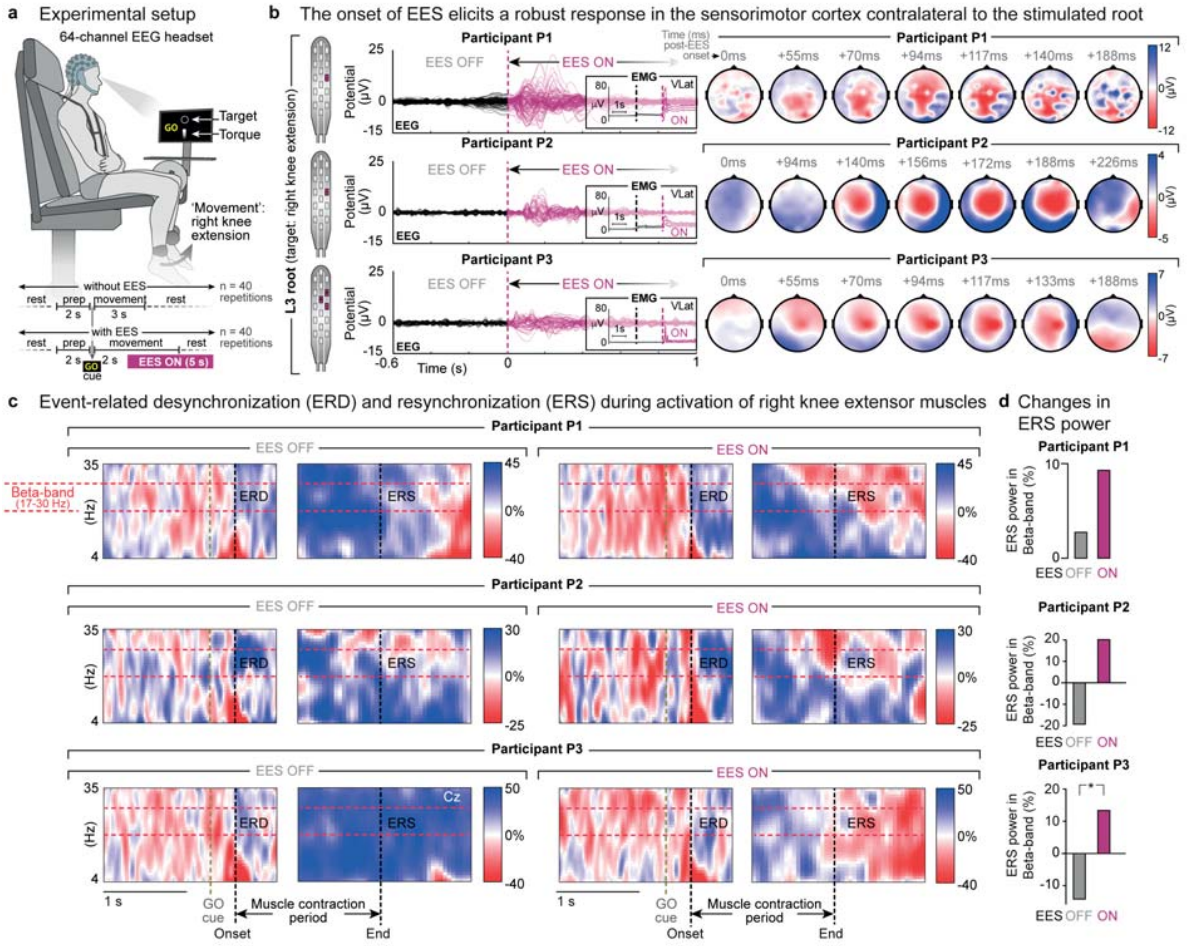

Figure 3.11 – Modulation of EEG activity during volitional contraction of leg muscles without and with EES. **a**, Recordings of EEG activity while participants were asked to produce an isometric torque at the knee joint without and with continuous EES targeting motor neuron pools innervating knee extensors, as shown in b. **b**, Superimposed EEG responses and temporal changes in the topography of average activity over the cortical surface after the onset of EES, as indicated above each map. The onset was calculated from the onset of EMG responses in the targeted VLat muscle (insets). The stimulation elicited a robust event-related response over the left sensorimotor cortex with a latency of 90 ± 40 ms for P1 and P3, and of 170 ± 40 ms for P2 (full range of the peaks and middle of this range indicated). **c**, Average normalised time-frequency plots (n = 40 trials) showing ERD and ERS over the Cz electrode (central top electrode) for each individual during the voluntary activation of knee extensor muscles without and with EES. Schematic drawings (left) indicate the motor scores of the tested legs, including the targeted muscles (*), at the time of study enrolment. Both legs were tested in P1 owing to his asymmetric deficits. **d**, Normalised average power (mean ± s.e.m.) of the β-band over the Cz electrode during ERS from 0 to 500 ms after termination of contraction without and with continuous EES (n = 40 repetitions for each condition). ***P < 0.00, permutation tests, see Materials & Methods.

Attempts to activate knee extensor muscles triggered event-related desynchronization (ERD) of the contralateral sensorimotor cortex in β-band frequencies, both without and with EES. This cortical activity has been linked to movement execution, and is followed by event-related resynchronisation (ERS) after movement termination. Previous studies showed that the amplitude of ERS decreases in proportion to severity of SCI [162]. Voluntary activation of paralysed muscles during EES led to

an increase in ERS amplitude (Figure 3.11c-d). These results suggest that EES enhances cortical excitability, promoting more natural dynamics during movement execution [161].

Spatiotemporal EES enables Walking

Walking involves reproducible sequences of muscle activation (Figure 3.12a). The underlying motor neuron activation maps involve a succession of hotspots for which the migration reflects body mechanics [155], ensuring weight acceptance, propulsion and swing (Figure 3.12b).

Targeted EES effectively activated the regions embedding these hotspots (Figure 3.12c). To configure EES sequences (Figure 3.12d-e), we fine-tuned the timing of each spatially selective stimulation train using a closed- loop controller that triggered EES on the basis of foot trajectory [65, 112]. We adjusted the onset and duration of each train to approach the motor neuron activation maps of healthy individuals (Figure 3.4). Relatively small changes in the timing of each train altered performance (Figure 3.4b). Once optimised, EES could be delivered in an open loop: participants regulated the timing of their movements to pre-programmed EES sequences, which improved gait consistency (Figure 3.4c).

To tune muscle activity, we adjusted EES amplitudes and frequencies (Figure 3.4). As observed in animal models [65,112], we found a monotonic relationship between EES frequency and flexor muscle activity (Figure 3.12f), such that increasing frequency proportionally enhanced flexion (Figure 3.4d). Unexpectedly, extensor motor neuron pools responded inversely. Proprioceptive afferents elicit strong monosynaptic responses in extensor motor neurons, whereas these afferents primarily engage flexor motor neurons through polysynaptic circuits [163]. In humans, monosynaptic projections are highly sensitive to low-frequency depression [164], which may explain the decrease in extensor motor neuron activation with increasing frequency.

Within five days, this procedure led to EES sequences (Figure 3.12d, e) that enabled robust EMG activity in otherwise quiescent muscles during stepping on a treadmill (Figure 3.5).

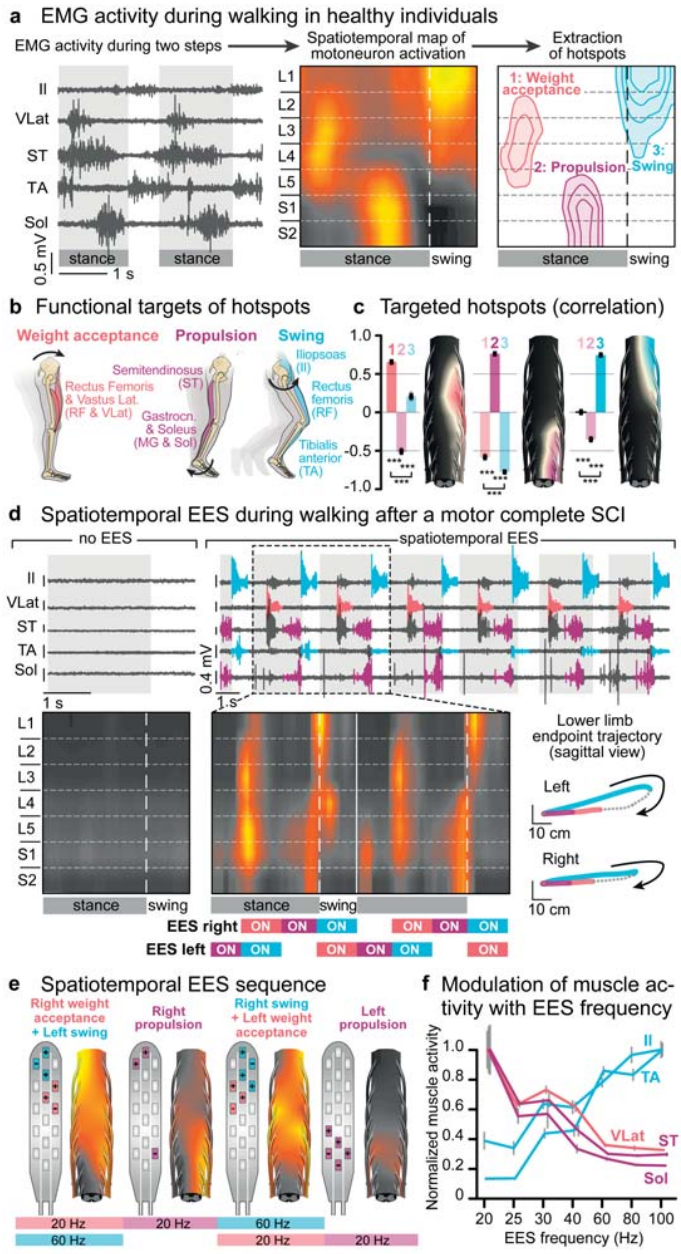

Figure 3.12 – Configuration of spatiotemporal EES for walking. **a**, EMG activity during walking in healthy individuals. Spatiotemporal map of motor neuron activation highlights hotspots (mean, n = 12 gait cycles). Equipotential lines represent 45-75% activation. **b**, Functional target of each hotspot. **c**, Map of motor neuron activation following 500-ms bursts of targeted EES during standing. Bar plots show Pearson's correlations for each hotspot (mean ± s.e.m., n = 12 bursts, ***P < 0.001; one-way ANOVA, post hoc Tukey's HSD). **d**, EMG activity and map of motor neuron activation during EES or without EES after a motor complete SCI while stepping on a treadmill with support and assistance (P3). EES timing is indicated along foot trajectories (bottom right; n = 73 steps) and below motor neuron activation maps. **e**, Spatiotemporal EES sequence for data shown in d. **f**, Mean (± s.e.m.) modulation of EMG amplitude in flexor and extensor muscles during walking with increasing EES frequencies (n = 17 ± 3 gait cycles; P3).

Participants were then asked to walk overground using the gravity-assist and spatiotemporal EES. The stimulation enabled all participants to walk voluntarily until the stimulation was stopped. They could resume locomotion as soon as the stimulation was reintroduced (Figure 3.13a and Figure 3.14a).

We next investigated participants' ability to adjust leg movements. First, we asked them to produce exaggerated step elevations without changing EES parameters. All participants were able to enhance their step elevation three-to-fivefold compared to regular steps (Figure 3.13b and Figure 3.14b). Second, we asked them to adjust their stride to varying speeds. Not only were the participants able to adjust their

stride length, but they also could stop locomotor movements despite the treadmill belt motion and ongoing stimulation (Figure 3.14b, e).

Finally, we asked participants to walk on a treadmill for one hour. All participants sustained more than 1,200 steps, covering distances as long as 1.0 km without showing muscle exhaustion or gait impairments (Figure 3.13c and Figure 3.14c).

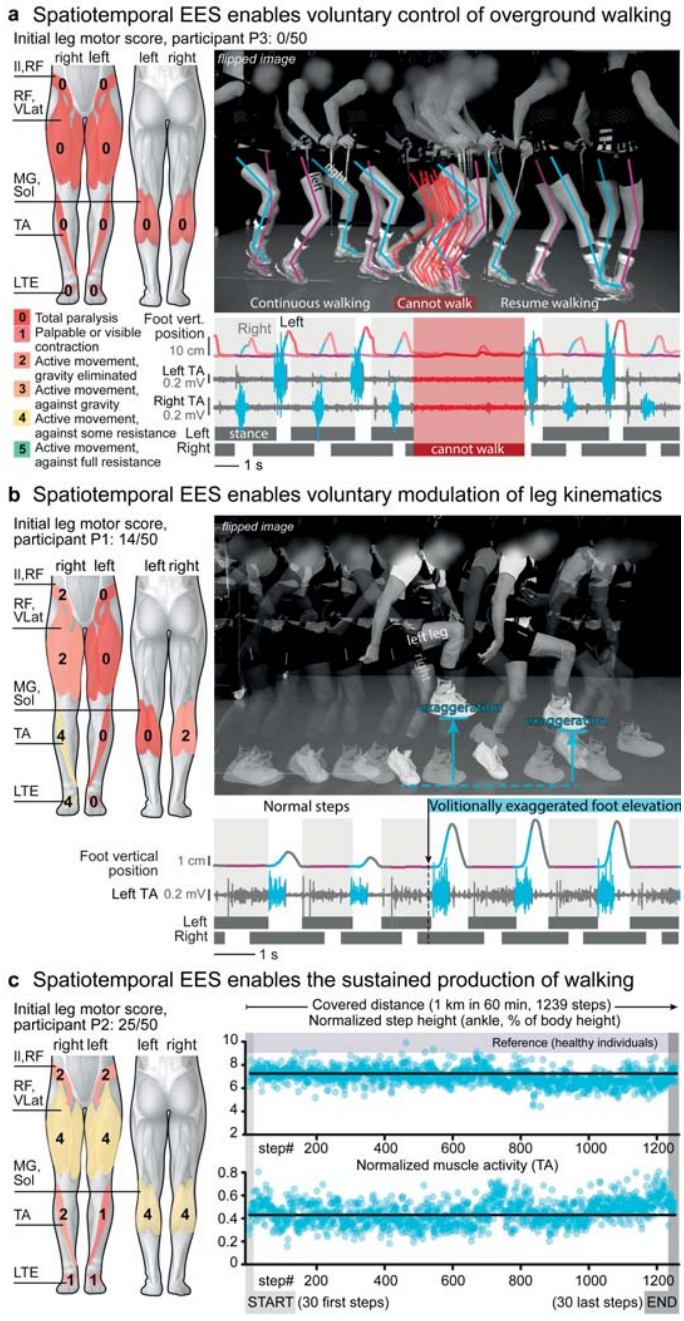

Figure 3.13 – Voluntary control of adaptive and sustained locomotion. **a**, Chronophotography, TA EMG activity and foot vertical position during overground walking with gravity-assist and sticks while EES is switched on, then off, then on. **b**, Overground walking when participants were requested to perform steps with normal heights and then exaggerated step elevations. **c**, Consecutive values of step height and EMG activity over 60 min of walking with EES (P1: 1.2 km; P2, P3: 1 km). Quantifications for all participants are in Figure 3.14a-c.

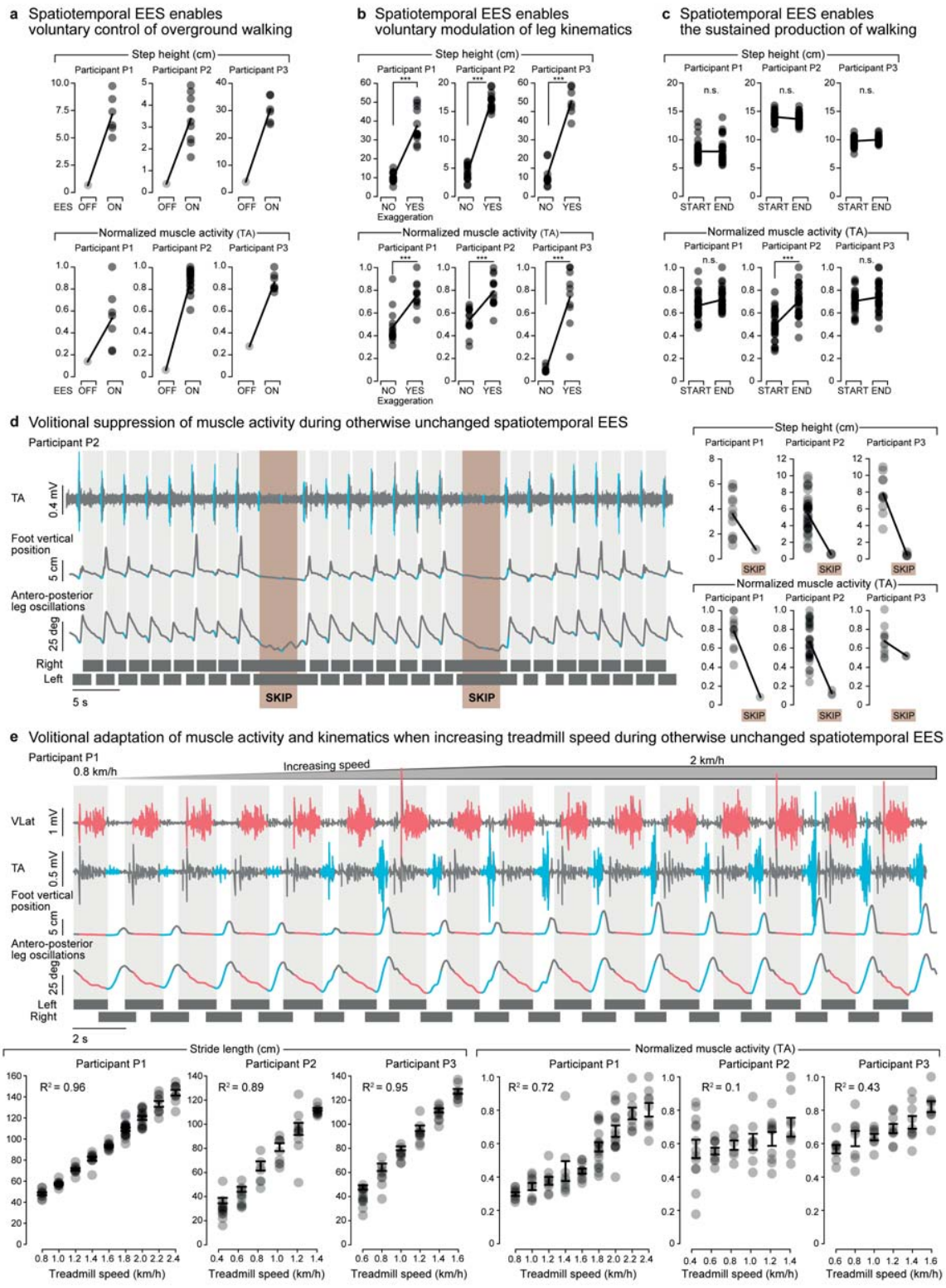
a Spatiotemporal EES enables voluntary control of overground walking
b Spatiotemporal EES enables voluntary modulation of leg kinematics
c Spatiotemporal EES enables the sustained production of walking
Step height (cm)
Participant P1
Participant P2
Participant P3
EES OFF ON
OFF ON
Normalized muscle activity (TA)
NO YES
Exaggeration
n.s.
***
START END
d Volitional suppression of muscle activity during otherwise unchanged spatiotemporal EES
Participant P2
TA
0.4 mV
Foot vertical position
5 cm
Antero-posterior leg oscillations
25 deg
Right
Left
5 s
SKIP
e Volitional adaptation of muscle activity and kinematics when increasing treadmill speed during otherwise unchanged spatiotemporal EES
Participant P1
0.8 km/h
Increasing speed
2 km/h
VLat
1 mV
0.5 mV
2 s
Stride length (cm)
Normalized muscle activity (TA)
R² = 0.96
R² = 0.89
R² = 0.95
R² = 0.72
R² = 0.1
R² = 0.43
Treadmill speed (km/h)

Figure 3.14 – **Volitional adaptations of walking during otherwise unchanged spatiotemporal EES.** **a-c**, Quantifications of experiments shown in Figure 3.13a-c for each participant. **a**, Step height and TA EMG activity with and without EES during overground walking (P1, n = 7; P2, n = 16; P3, n = 7 gait cycles during EES ON). **b**, Step height and TA EMG activity during normal steps and when participants were requested to perform exaggerated step elevations during overground walking (P1, n = 15, 11; P2, n = 31, 23; P3, n = 14, 10 normal and exaggerated gait cycles). **c**, Step height and TA EMG activity during the first and last 30 steps extracted from a sequence of 1 h of locomotion on a treadmill (n = 30 gait cycles for all conditions). ***P < 0.001; n.s., non-significant; Student's t-test. **d**, EMG activity of representative leg muscles, vertical displacements of the foot and anteroposterior oscillations of the leg (virtual limb joining the hip to the foot) while P2 was walking continuously on the treadmill with spatiotemporal EES (open loop). The participant was asked to suppress the effects of EES and stand during one cycle of open-loop spatiotemporal EES sequence, highlighted in brown (SKIP), whereas he actively contributed to the production of movement the rest of the time. Plots report the quantification of step height and TA EMG activity during walking and when skipping steps for each participant (P1, n = 13, 1 skipped cycles; P2, n = 36, 3; P3, n = 11, 2 normal and skipped gait cycles). **e**, EMG activity of two representative muscles, vertical displacements of the foot and anteroposterior oscillations of the leg while P1 was walking on the treadmill and the speed of the belt increased progressively from 0.8 to 2 km/h. Plots show relationships between treadmill speed and mean stride length and TA EMG activity in all participants (P1: n = 9, 9, 9, 9, 10, 18, 15, 9, 9; P2: n = 13, 10, 7, 8, 10, 9; P3: n = 8, 8, 10, 9, 9, 8 gait cycles for increasing speeds; ± s.e.m.). The range of tested speeds was adapted to the walking ability of each participant.

These results show that spatiotemporal EES not only enabled completely or partially paralysed individuals to walk overground, but also allowed them to adjust leg movements to stand and walk over a range of speeds for durations as long as one hour.

Continuous EES is poorly Effective

Recent studies have shown that continuous EES enabled overground walking after nearly one year of intense training [22, 145]. As spatiotemporal EES enabled locomotion within one week, we evaluated whether continuous EES could achieve similar efficacy.

We delivered widespread stimulation targeting the posterior roots associated with flexor motor neuron pools, as previously recommended [145]. However, we did not further optimise the stimulation. Continuous EES enhanced muscle activity, but was poorly effective in facilitating locomotion overground. All participants reported a loss of limb position awareness combined with co-activation across muscles (Figure 3.15). These detrimental outcomes are due to the cancellation of proprioceptive information during continuous EES [165].

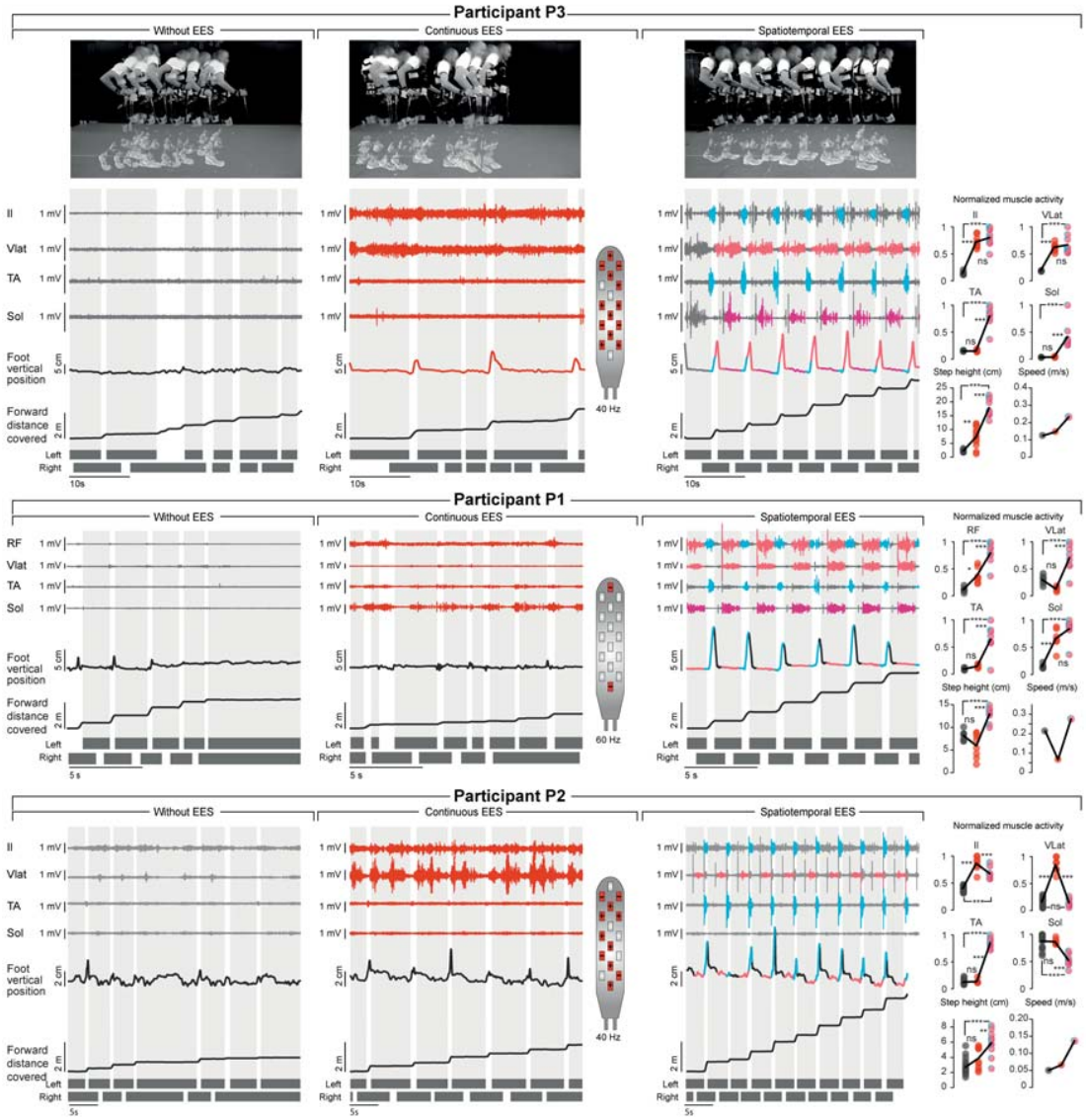

Figure 3.15 – Comparison between continuous and spatiotemporal EES during overground walking. Each panel represents one participant who is attempting to walk overground with gravity-assist without EES, with continuous EES and with spatiotemporal EES. EMG activity of representative leg muscles, vertical position of the foot and distance covered by the foot in the forward direction are displayed for each experimental condition. Continuous EES is applied throughout the trial (red). For P2 and P3, we optimised EES protocols that targeted the posterior roots on both sides, whereas EES was applied over the most rostral and most caudal midline electrodes for P1, as shown next to each plot. Spatiotemporal EES is represented using the same colour scheme as in Figure 3.12 and Figure 3.5. The plots report quantification of EMG activity, step height and mean speed (based on distance covered) for the three experimental conditions (P1, n = 6, 7, 8 gait cycles; P2, n = 17, 7, 9 gait cycles; P3, n = 6, 10, 9 gait cycles for no, continuous and spatiotemporal EES). ***P < 0.001; **P < 0.01; n.s., non-significant. One-way ANOVA, post hoc Tukey's HSD.

Rehabilitation improves Walking with EES

Participants followed a rehabilitation program four to five times per week for five months (Figure 3.7b), focused on walking on a treadmill and overground; this was complemented with muscle strengthening and standing, each of which was enabled by task-specific EES (Figure 3.16a).

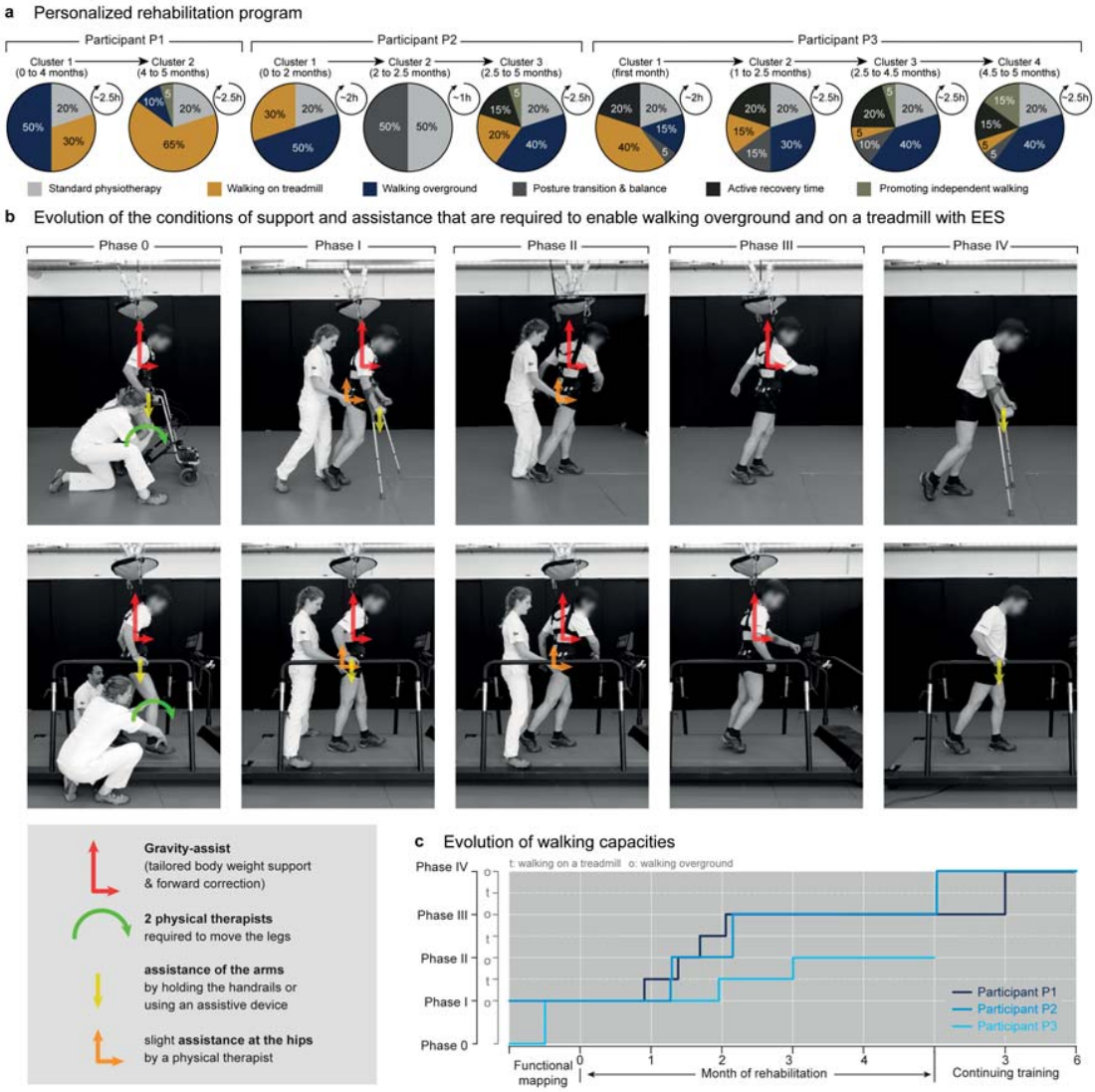

Figure 3.16 – Rehabilitation program and evolution of walking capacity. **a**, Rehabilitation programs were continuously personalised on the basis of the current motor performance of participants. Walking capacities evolved in phases (b). For this reason, the relative percentage of training in the various tasks has been divided into clusters, which correspond to the evolution of walking capacities. To facilitate the sustained production of reproducible locomotor movements (Figure 3.4c), EES was delivered in open-loop mode during gait rehabilitation. **b**, Walking capacities evolved through stereotypical phases that are illustrated in the snapshots. **c**, Plots showing the progression of the three participants along the phases of recovery during the rehabilitation program, and during the subsequent 6 months for P1 and P2. P3 had just completed the rehabilitation program at the time of submission of this study.

With spatiotemporal EES, all participants improved their walking capacities following a reproducible chronology (Figure 3.16b): non-ambulatory participants initially required crutches and the gravity-assist to walk overground. After one to three months, they could walk hands-free when provided with hip support in the gravity-assist. Eventually, P1 and P2 regained independent walking while 35% of their bodyweight was supported against gravity. P3 needed a walker to progress overground with EES.

Neurological Recovery without EES

Improvements were not limited to walking with EES. Rehabilitation promoted neurological recovery that translated into improvements without EES.

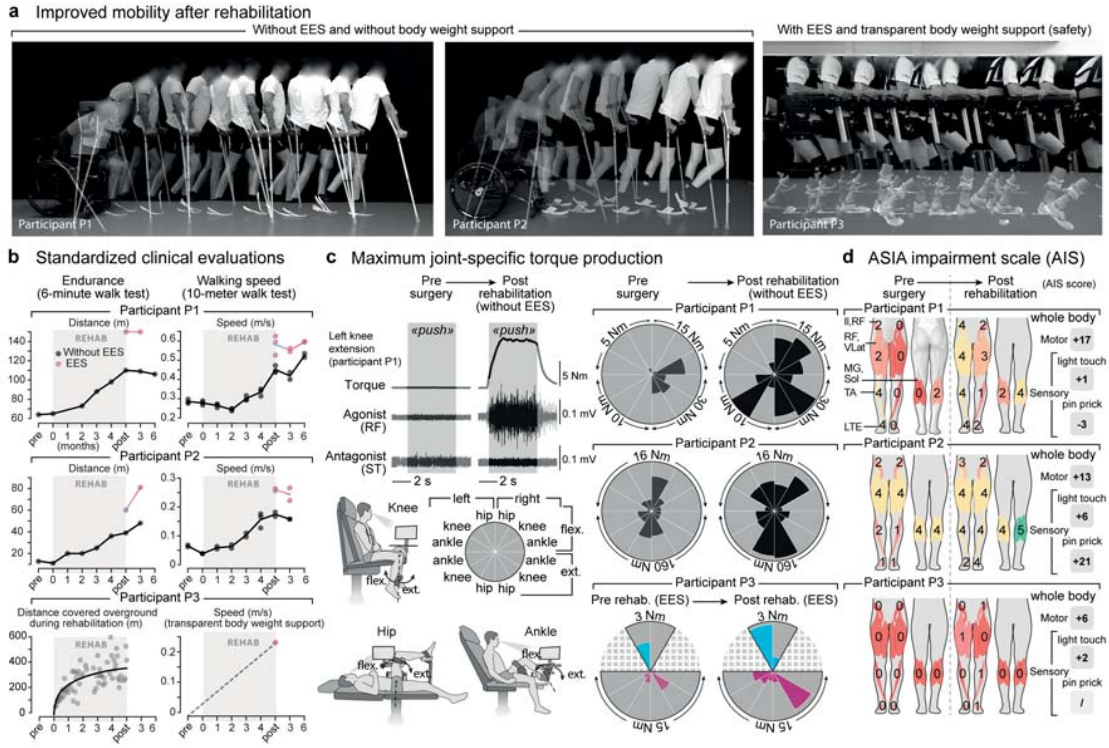

Figure 3.17 – **Rehabilitation mediates neurological recovery.** **a**, Chronophotography shows P1 and P2 transiting from sitting to walking with crutches without EES; P3 progresses overground with a walker and EES. **b**, Plots reporting changes in 6-min and 10-m walk tests for P1 and P2. Tests were performed without gravity-assist, following clinical guidance. For P3 plots report changes in walking distance during rehabilitation and walking speed with EES (with transparent body weight support). **c**, Evaluations of isometric torque production for each joint, quantified before surgery and after rehabilitation without EES for P1 and P2, and with EES for P3. **d**, Changes in lower limb motor and sensory scores after rehabilitation. Changes in motor and sensory scores on abbreviated injury scale (AIS) for all levels below injury are summarised (see Table 3.1).

P1 and P2 could transit from sitting to standing and walking independently with crutches (Fig. 5a). P1 could even walk without an assistive device for several steps (Figure 3.17a). Consequently, P1 and P2 increased their WISCI (walking index for spinal cord injury) scores from 13 to 16 and 6 to 13, respectively. They displayed substantial improvements in clinical evaluations such as ten-metre and six-minute walking tests without EES (Figure 3.17b). Several months after completing the rehabilitation program, both participants, who continued practicing once or twice per week with EES, maintained or further improved their performance.

Participants also recovered voluntary leg movements without EES. For example, P1 and P3 could sustain a full extension of their previously paralysed legs against gravity (P3, lying only; Figure 3.16c). Quantified measurements revealed that P1 and P2 improved their ability to produce a torque at each joint of both legs (Figure 3.17c). This recovery translated into an increase of 16 and 11 points in lower extremity motor scores, respectively (Figure 3.17d). Both participants had previously followed extensive conventional rehabilitation without showing neurological recovery. The lower extremity motor score increased by 4 points in participant P3, but without EES this recovery was insufficient to produce measurable forces when seated. However, force production improved during EES (Figure 3.17c). He showed a considerable increase in mass and quality of thigh and trunk muscles (Figure 3.18). P1, P2 and P3 also showed improvements in upper limb motor scores of 1, 2 and 2 points, respectively.

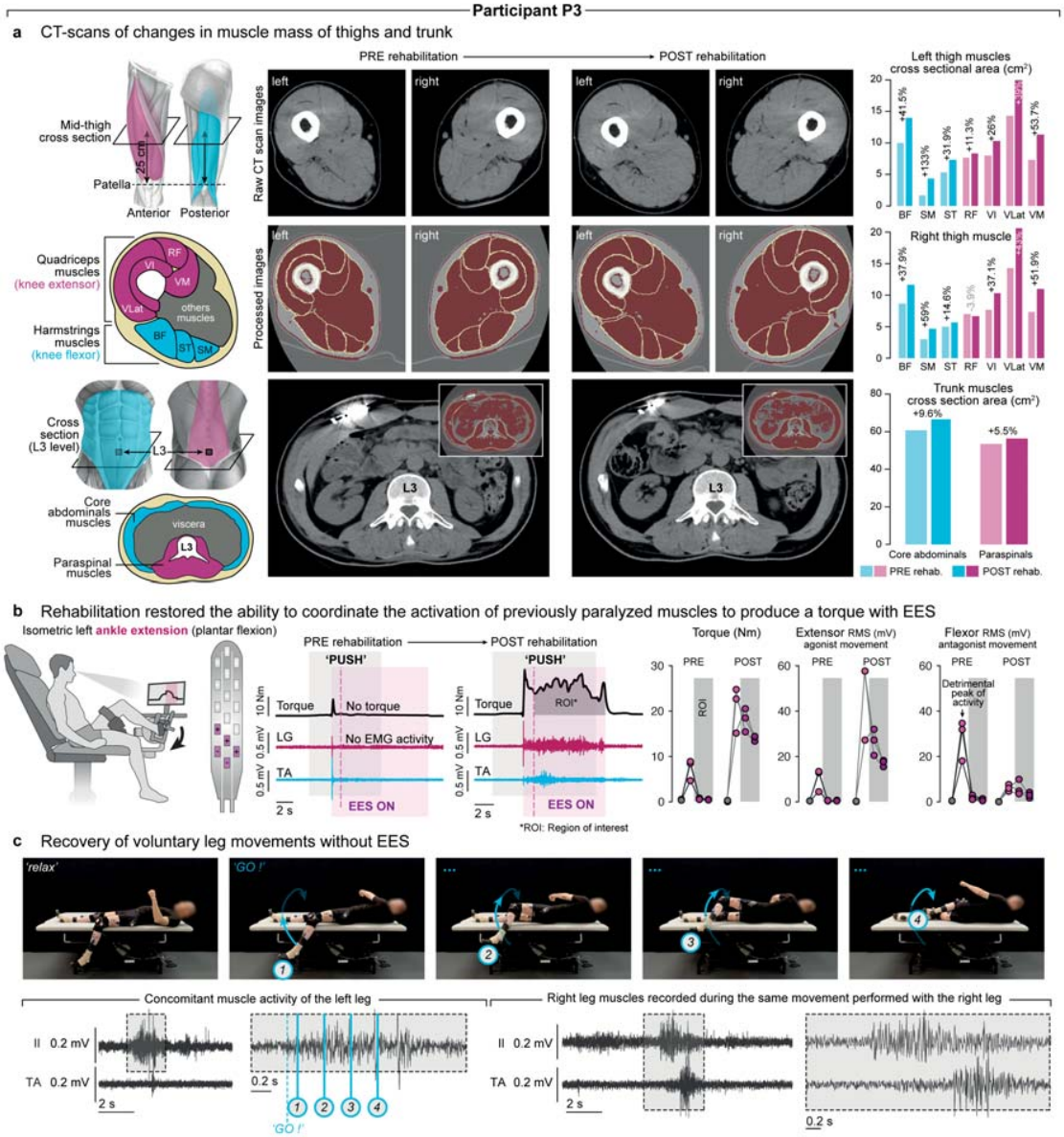

Figure 3.18 – Changes in muscle mass and quality, and recovery of voluntary movements with and without EES in participant P3. **a**, Skeletal muscle mass and quality were assessed at the pre- and post-rehabilitation time points using X-ray attenuation from CT images obtained at the abdomen (L3 vertebra) and mid-thigh (25 cm above femorotibial joint space). Muscle mass was determined by measuring the cross-sectional areas (CSAs) of muscle tissues, while muscle quality was reflected by CT attenuation numbers (in Hounsfield units, HU) within the CSAs. Muscle segmentations were performed semi-automatically using ImageJ and muscle-specific HU thresholds (-29 to 150 HU). Plots report the substantial changes in muscle mass at mid-thigh, for both flexor and extensor muscles, and of trunk muscles. Muscle quality was also improved at both levels: total mid-thigh, left: 52.9 to 56.1 HU, right: 51.9 to 56.7 HU; total L3, 45.9 to 48.3 HU. This increase in CT attenuation numbers between the baseline CT scan and the follow-up imaging reflected the decrease in muscle fibre lipid content at the mid-thigh and abdomen. These evaluations were part of a protocol amendment obtained when enrolling P3. **b**, Assessment of voluntary torque production at the ankle (extension) with targeted EES before and after rehabilitation. Conventions are as in Figure 3.10. **c**, Snapshots showing voluntary extension of the left leg against the direction of gravity together with the concomitant sequence of EMG activity in the extensor and flexor muscles of this leg. The zoomed window shows the relationship between the movement and the EMG activity, indicated with the numbers. P3 presented flaccid paralysis, and had thus no control over leg muscles before the surgery.

Support of Activities in the Community

All three participants learned to take advantage of spatiotemporal EES to execute functional leg movements, suggesting that practical stimulation technologies could support activities of daily living. For this purpose, we engineered an integrated solution based on a tablet to enable the configuration of task-specific EES sequences that are switched on and off with a personalised voice-controlled watch (Figure 3.19a). To adapt stimulation sequences to movement intents, we conceived adaptive algorithms that trigger EES trains in closed-loop based on real-time acquisition of signals from wearable inertial measurement units.

Figure 3.19 – Spatiotemporal EES in ecological settings. **a**, Tablet featuring a mobile App allows participants to select EES sequences, delivered in open loop or closed loop based on inertial measurement units (IMUs) located on both feet or attached onto the cranks and frame of a trike. **b**, Walking and cycling activities in ecological settings are enabled by spatiotemporal EES.

The robustness of trigger-event detections allowed the participants to transit from sitting to standing and walking freely in ecological settings (Figure 3.19b and Figure 3.6a). A stimulation program specific for cycling permitted rides with an adapted trike powered with the arms and legs (Figure 3.6b).

Discussion

We developed targeted EES neurotechnologies that immediately restored voluntary control of walking in individuals with severe or complete paralysis. The electrode configurations targeted proprioceptive circuits through the recruitment of selected posterior roots [52, 53, 148, 166]. This strategy was pivotal to enable the immediate control of walking despite chronic paralysis. This framework guided the rapid personalization of spatiotemporal EES sequences that continuously coincided with intended movements. Consequently, EES augmented the excitability of motor neuron pools that were concomitantly engaged by the natural flow of sensory information and residual supraspinal commands. This spatiotemporal convergence enabled more robust and natural control of leg movements compared to empirical stimulation paradigms such as continuous EES [22, 145, 167].

We hypothesize that this spatiotemporal convergence is responsible for the neurological recovery observed in all participants without EES. We showed that mice lacking proprioceptive circuits exhibit defective rearrangement of descending pathways after SCI, which abolishes recovery [168]. Conversely, we propose that the spatiotemporal contingence between residual supraspinal commands and proprioceptive circuit activations with EES may increase the strength and number of terminals from spared descending projections through bidirectional spike-timing-dependent plasticity [169, 170]. Electrophysiological studies have documented such plasticity in humans with SCI [171, 172]. This interpretation is consistent with the pronounced reorganization of cortico-reticulo-spinal circuits observed in rodents when EES enables gait training despite paralysis [47, 69]. As we observed in humans, rodents regained cortical control of leg movements that persisted without EES [69] when rehabilitation commenced early after SCI. We thus anticipate that this therapy will be even more efficacious early after SCI in humans, when the potential for plasticity is elevated and the neuromuscular system has not yet undergone the atrophy that follows chronic paralysis [160]. Moreover, improvements in muscle mass and other physiological functions [173, 174] suggest that EES may help to counteract these deteriorations.

Clinical trials starting early after SCI will require a stratification of participants who may benefit from the therapy, combined with statistical models that predict their potential for recovery [175]. Here, we validated our neurotechnologies in a few individuals. This proof-of-concept stresses the urgency of developing neurotechnologies that not only harness targeted EES to enable movement, but also provide the usability features to support rehabilitation in clinical settings and use in the community.

Conclusion & Perspectives

Over the past decade, our laboratory has developed a neuroprosthesis and therapeutic approach to restore locomotion in spinal cord injured animals and translated the technology and therapy to humans. In combination with an overground, robot-assisted, intensive 5-months rehabilitation program, leg motor control was improved in three individuals with severe SCI. The reported results provide a proof of concept that the therapeutic effects observed in animal models of SCI may translate into a viable intervention to improve quality of life of individuals with chronic paraplegia.

On the month preceding the publication of our article [84], two closely-related articles came out. One, in Nature Medicine [71], described the evolution in locomotor performance of a single participant with a chronic, complete SCI (AIS-A). The participant has been implanted with the same electrode array that we used in our study. During 43 weeks, he followed a dynamic task-specific training in the presence of continuous EES. This intervention resulted in the ability to perform overground walking with a walker, the assistance of a physiotherapist at the hips for balance control and continuous EES. In parallel, he was able to stand with EES and with one hand on a bar for slight balance correction. Gill and colleagues claimed that dynamic approach of standing and stepping during each training session with EES enabled the partial recovery of both tasks, contrarily to what Rejc et al. reported [176].

The second article, in The New England Journal of Medicine from Angeli and colleagues [70], described the outcome of a clinical study on four individuals with a chronic, complete SCI. The two first participants had a T4 SCI level and they had no sensation below T4 (AIS-A). The third participant had a C5 SCI level while the fourth had a T1 SCI level; they both reported some degree of spared sensation (AIS-B). After the surgical implantation of the same electrode array, muscle activity was recorded to select the electrode combinations for standing and stepping. Then, for 24 to 85 weeks, the participants received an intensive training with continuous EES; the electrode configurations were adjusted if needed. The training session gathered stepping on a treadmill, overground standing and overground walking if stepping skills on a treadmill was previously reached. The four participants achieved independent standing and sitting in the presence of electrical stimulations. The two who were graded as AIS-B were able to perform intentional, overground walking in the presence of EES and assistive devices. One of them increased by 1 point his motor score on the right leg and his grade went from AIS-B to C.

These two studies corroborated the crucial need of EES during training to enable the production of leg movements and improve locomotor performance, as we also claimed. Indeed, they both started with a period of intensive training (22 weeks of locomotor training in the first study [71], 8 to 9 weeks with 5 days of 2 hours of leg mobilization on a treadmill with trainers and body weight support in the second study [70]) before implantation of the electrode array, which resulted in no improvement in leg motor control, or locomotion ability. Dr. Harkema's research group reported no change in the neurologic level, in the sensation below the SCI level, or in voluntary movements following the intense locomotor training [70]. While the combination of intensive locomotor training with EES has shown improvement in motor control in these two studies and ours. Further investigations have to be done to understand the exact mechanisms involved in this interaction effect of EES on the spinal system.

Interestingly, participants with complete SCI are able to intentionally act on muscles targeted by EES. Angeli et al. indeed reported that two of their participants (AIS-B) were stepping only when they wanted to do so during EES, and the muscles activity could be modulated by intention [70]. The participant from Gill and colleagues could stand with the stepping-enabling EES program instead of stepping depending on his will [71]. We confirmed this supraspinal modulation of muscles activity for each of our participants. Subsequently, despite a clinical diagnosis of complete loss of motor function after SCI, descending neural connections across the lesion seems to remain present. Such spared connections are sub-functional (i.e. not strong enough to produce a motor output), however they can modulate the excitability of the spinal regions below the lesion that are "pre"-activated by EES (EES likely re-activates the dormant spinal circuits below the lesion). This observation strongly favors a rehabilitation that combines EES-enabled locomotion training and patient's strong involvement in the execution of the locomotor tasks.

The EES programs differ between the studies described here and ours. Both Angeli et al. and Gill et al. applied continuous EES [70, 71]; the active electrode configuration, the frequency and the amplitude are kept constant during a whole gait cycle. Gill et al. discovered that two interleaved active electrode configurations enable bilateral control of leg functions via independent adjustment of voltage intensities within each electrode configuration; while with a single configuration that combined both active electrode configurations, the voltage intensity enabling the control of one leg was sub-optimal for the contralateral leg [71]. We deliver targeted spatio-temporal EES, to selectively activate the adequate group of muscles at the adequate timing for the different phases of a gait cycle.

To better characterized the effect of continuous and targeted spatio-temporal stimulations, we conducted several studies in silico and in vivo, both in rats and humans [165]. We concluded that, depending on the amplitude and frequency parameters, EES interferes with proprioceptive feedback in humans. This interference decreases or cancels the perception of leg position, and affects the normal modulation of spinal circuits in response to leg movements. Spatio-temporal stimulation may diminish this effect and allow descending plasticity. In the study we published, we tuned the targeted EES to coincide as much as possible with the supra-spinal inputs, in the attempt to promote plasticity. We hypothesize that this stimulation approach, which tried to mimic the natural spinal activation, is responsible for the neurological recovery we have measured in our patients. Indeed, one of our participant (AIS-C) had a zero motor score on both legs, and another one had a zero motor score on his left leg (AIS-C), which reflected their total incapacity in controlling their legs. They both recovered some motor control over previously paralyzed muscles after the training period, and one was evaluated AIS-D at the end of the rehabilitation program. Their motor scores increased by 6 points, resp. by 17 points following the 5-months rehabilitation. Our last participant increased by 13 points his motor score.

However, at this time, the direct comparison of the neurological recovery after a rehabilitation with continuous EES [70, 71] vs. with targeted EES [84] is hard to address since the protocols of the studies differ from each other, thereby introducing confounding factors. For example, the initial degree of severity of the patients (AIS-A and B vs. AIS-C), the rehabilitation protocols (different trained tasks, amount of body weight support, etc.), the optimization procedure to define the electrode configuration for EES, or the amount and the duration of training sessions vary between studies. Accordingly, to determine to which extend targeted EES enhanced the recovery of motor control compared to continuous EES, a next step could be to conduct the same rehabilitation protocol on participants with a severe chronic SCI, where targeted EES would be delivered during locomotion training on one subgroup of participants and continuous EES on the second subgroup. Alternatively, a hybrid approach, where targeted EES might be superimposed on continuous EES, could be envisaged as an interesting stimulation strategy. We could indeed conceive to deliver background continuous EES at a low (sub-motor-threshold) amplitude to lower the motoneuron response threshold to supraspinal inputs and simultaneously deliver targeted EES where and when the supraspinal inputs still cannot trigger the expected muscle response, during locomotion rehabilitation.

Overall, these two studies and ours have clearly shown that epidural electrical stimulation permits the recovery of voluntary movements of paralyzed legs in chronic patients with a degree of SCI severity ranging from AIS-C to A. While standard rehabilitation has proven to be unsuccessful with these chronic patients, EES-enabled locomotion training efficiently improved motor functions after several weeks.

Yet, despite the improvement obtained after the several months of rehabilitation in the course of the study, the participants were still benefiting from EES to execute motor tasks: long-term recovery may probably be achieved only with a really long-term training. Similar to sportspeople, individuals with SCI have to follow a long-term training plan to maintain or improve their residual capacities and motor control. Hence, to offer our participants the possibility to make durable the fruitful training they achieved in the hospital environment, we designed and provided an integrated solution based on a voice-controlled smartwatch and a tablet. With this novel technology, the participants could select the targeted EES corresponding to a training program such as standing, sit-to-stand transitioning, walking or even biking, directly in the community.

As a last point, when an intensive training with EES might be too exhaustive at the neurological level for individuals with severe SCI, a supply in specific neurotransmitters, such as serotonin, could potentially help. An intensive locomotion training enabled by EES may indeed rapidly deplete the stock of these neurotransmitters, as EES strongly activates the spinal circuits. Monoamines are synthesized in the brain before being transported to the spinal cord; the lesion partially disrupts this descending flow. To alleviate the depletion of serotonin, or other monoamines, in the spinal cord below the lesion, exogenous serotonin, its precursor or agonists could be delivered [46]. Actually, based on several years of research in the laboratory of Prof. Courtine, we have strong evidence on the animal models [47] that the therapy would benefit from intrathecal infusion of a cocktail of monoamines, combined with the targeted spinal cord neurotechnologies. Furthermore, the ongoing progression of our understanding on the mechanisms that followed a spinal cord injury and took place during the neuro-rehabilitation may offer new routes to a viable intervention improving the neurological recovery after a spinal cord injury.

Integration & Perspectives

Nowadays, people with a chronic paraplegia have no viable therapeutic intervention to recover their motor functions. Over the past decades, our laboratory led by Prof. Courtine has worked on a therapy combining a neuroprosthesis and an intensive rehabilitation program aiming at the recovery of locomotor functions in individuals with SCI. I have actively participated to this team effort to permit the successful proceedings of a first study on humans with the therapy developed on animal models. In this translational research program, I developed, evaluated and used the tools to comprehensively characterize the gait behavior of our participants in order to evaluate how our therapy affects their gait in the short- and long-term. This work can be generalized, and have been generalized, to evaluate other kind of motor disorders, such as individuals with a stroke, or suffering from the Parkinson's disease. In parallel, my work on the robotic postural assistance for overground walking and standing enabled a deeper understanding of the interactions between the robotic device and the subject attached to it, and its effect on the gait. Based on these findings, I designed and implemented an algorithm that defines the best support parameter customized to each individual's residual capacities. The work on the toolbox and on the robotic device brought two main stones to the edification of the clinical study. My analyses of the gait behavior of the three participants enrolled in this study enabled to emphasize the immediate effect of the neuroprosthesis, their ability to adapt their gait to task-specific requirements, the evolution of their motor control over the leg muscles and the long-term effect of the therapy on their kinematics. These three participants with a chronic SCI who have undergone our therapy are now pursuing their progression in the community. From these results, I believe that a therapy combining targeted epidural electrical stimulations to an intensive training may answer the actual needs of the SCI population wishing to improve their locomotor function. Here, we brought a proof of concept of this novel clinical application. Finally, I consider as crucial the development of ecological technologies, such as the integrated system based on a smart watch for our participants, which enables an uninterrupted training outside dedicated rehabilitation centers but directly in the community.

In an effort to bring this therapy to the paraplegic population, the next step is a multi-centric clinical study, where the therapy will be proposed to a wider population with SCI. For training of overground walking, the Rysen® – the new robotic trunk assistance, now on the market – will be a valuable help. This study should start in the coming years. Still, for the proper completion of the multi-centric study, some challenges remain. We found limitations in the implanted hardware, such as the size of the electrode array. Indeed, the current electrode array is not long enough to cover the full region of the spinal cord containing the leg motoneurons. A new electrode array has been designed to fulfill this requirement and to achieve a higher spatial selectivity of the motoneuron pools. Another challenge is raised by the increased number of actors and less specialized engineers who will drive the sessions aiming at configuring the stimulation program for each individual enrolled in the multi-centric study. This challenge is currently tackled by a team of engineers and researchers who are developing a software simplifying the configuration steps, automatizing the procedure that determines the optimal program customized to the specific needs of each individual. A last point to consider will be to work and train individuals from the "average" population. Indeed, the recruited individuals in our feasibility study shared common features such as their curiosity about the developed technologies, their deep understanding of their own body and the effect of the stimulation on their nervous system, and their strong motivation to push themselves in order to obtain the best possible results. Overall, their durable implication in the feasibility study helped our investigational work; they were psychologically prepared for an intensive period of training. Thankfully, these pioneers helped us to refine our technology, to simplify the procedures, and determine the evaluations that we should keep or remove for the multi-centric study.

Bibliography

[1] W. H. Organization and I. S. C. Society, eds., *International perspectives on spinal cord injury*. Geneva, Switzerland: World Health Organization, 2013. OCLC: ocn871342223.

[2] J. D. Chamberlain, O. Deriaz, M. Hund-Georgiadis, S. Meier, A. Scheel-Sailer, M. Schubert, G. Stucki, and M. W. Brinkhof, "Epidemiology and contemporary risk profile of traumatic spinal cord injury in Switzerland," *Injury Epidemiology*, vol. 2, Dec. 2015.

[3] L. H. Sekhon and M. G. Fehlings, "Epidemiology, demographics, and pathophysiology of acute spinal cord injury," *Spine*, vol. 26, no. 24S, pp. S2–S12, 2001.

[4] R. A. Cripps, B. B. Lee, P. Wing, E. Weerts, J. Mackay, and D. Brown, "A global map for traumatic spinal cord injury epidemiology: towards a living data repository for injury prevention," *Spinal cord*, vol. 49, no. 4, p. 493, 2011.

[5] "Spinal Cord Injury: Facts and Figures at a Glance," 2017.

[6] S. C. Kirshblum, S. P. Burns, F. Biering-Sorensen, W. Donovan, D. E. Graves, A. Jha, M. Johansen, L. Jones, A. Krassioukov, M. Mulcahey, M. Schmidt-Read, and W. Waring, "International standards for neurological classification of spinal cord injury (Revised 2011)," *The Journal of Spinal Cord Medicine*, vol. 34, pp. 535–546, Nov. 2011.

[7] J. W. Fawcett, A. Curt, J. D. Steeves, W. P. Coleman, M. H. Tuszynski, D. Lammertse, P. F. Bartlett, A. R. Blight, V. Dietz, and J. Ditunno, "Guidelines for the conduct of clinical trials for spinal cord injury as developed by the ICCP panel: spontaneous recovery after spinal cord injury and statistical power needed for therapeutic clinical trials," *Spinal cord*, vol. 45, no. 3, p. 190, 2007.

[8] C. Winslow, R. K. Bode, D. Felton, D. Chen, and P. R. Meyer, "Impact of respiratory complications on length of stay and hospital costs in acute cervical spine injury," *Chest*, vol. 121, no. 5, pp. 1548–1554, 2002.

[9] A. Ackery, C. Tator, and A. Krassioukov, "A global perspective on spinal cord injury epidemiology," *Journal of neurotrauma*, vol. 21, no. 10, pp. 1355–1370, 2004.

[10] R. van den Brand, J.-B. Mignardot, J. von Zitzewitz, C. Le Goff, N. Fumeaux, F. Wagner, M. Capogrosso, E. Martin Moraud, S. Micera, B. Schurch, A. Curt,

S. Carda, J. Bloch, and G. Courtine, "Neuroprosthetic technologies to augment the impact of neurorehabilitation after spinal cord injury," *Annals of Physical and Rehabilitation Medicine*, vol. 58, pp. 232–237, Sept. 2015.

[11] L. Filli and M. E. Schwab, "The rocky road to translation in spinal cord repair," *Annals of Neurology*, vol. 72, pp. 491–501, Oct. 2012.

[12] K. D. Anderson, J. D. Guest, W. D. Dietrich, M. Bartlett Bunge, R. Curiel, M. Dididze, B. A. Green, A. Khan, D. D. Pearse, E. Saraf-Lavi, E. Widerström-Noga, P. Wood, and A. D. Levi, "Safety of Autologous Human Schwann Cell Transplantation in Subacute Thoracic Spinal Cord Injury," *Journal of Neurotrauma*, vol. 34, pp. 2950–2963, Nov. 2017.

[13] H. S. Satti, A. Waheed, P. Ahmed, K. Ahmed, Z. Akram, T. Aziz, T. M. Satti, N. Shahbaz, M. A. Khan, and S. A. Malik, "Autologous mesenchymal stromal cell transplantation for spinal cord injury: A Phase I pilot study," *Cytotherapy*, vol. 18, pp. 518–522, Apr. 2016.

[14] P. Musienko, J. Heutschi, L. Friedli, R. v. den Brand, and G. Courtine, "Multisystem neurorehabilitative strategies to restore motor functions following severe spinal cord injury," *Experimental Neurology*, vol. 235, pp. 100–109, May 2012.

[15] M. A. Anderson, T. M. O'Shea, J. E. Burda, Y. Ao, S. L. Barlatey, A. M. Bernstein, J. H. Kim, N. D. James, A. Rogers, B. Kato, A. L. Wollenberg, R. Kawaguchi, G. Coppola, C. Wang, T. J. Deming, Z. He, G. Courtine, and M. V. Sofroniew, "Required growth facilitators propel axon regeneration across complete spinal cord injury," *Nature*, vol. 561, pp. 396–400, Sept. 2018.

[16] M. B. Orr and J. C. Gensel, "Spinal Cord Injury Scarring and Inflammation: Therapies Targeting Glial and Inflammatory Responses," *Neurotherapeutics*, vol. 15, pp. 541–553, July 2018.

[17] A. Raspa, E. Bolla, C. Cuscona, and F. Gelain, "Feasible stabilization of chondroitinase abc enables reduced astrogliosis in a chronic model of spinal cord injury," *CNS Neuroscience & Therapeutics*, May 2018.

[18] V. R. Edgerton and R. R. Roy, "Robotic training and spinal cord plasticity," *Brain Research Bulletin*, vol. 78, pp. 4–12, Jan. 2009.

[19] G. Courtine, Y. Gerasimenko, R. van den Brand, A. Yew, P. Musienko, H. Zhong, B. Song, Y. Ao, R. M. Ichiyama, I. Lavrov, R. R. Roy, M. V. Sofroniew, and V. R. Edgerton, "Transformation of nonfunctional spinal circuits into functional states after the loss of brain input," *Nature Neuroscience*, vol. 12, pp. 1333–1342, Oct. 2009.

[20] R. M. Gorodnichev, E. N. Machueva, E. A. Pivovarova, D. V. Semenov, S. M. Ivanov, A. A. Savokhin, R. Edgerton, and I. P. Gerasimenko, "[Novel method for activation of the locomotor circuitry in human]," *Fiziologiia Cheloveka*, vol. 36, pp. 95–103, Dec. 2010.

[21] N. AuYong and D. C. Lu, "Neuromodulation of the Lumbar Spinal Locomotor Circuit," *Neurosurgery Clinics of North America*, vol. 25, pp. 15–23, Jan. 2014.

[22] C. A. Angeli, V. R. Edgerton, Y. P. Gerasimenko, and S. J. Harkema, "Altering spinal cord excitability enables voluntary movements after chronic complete paralysis in humans," *Brain: A Journal of Neurology*, vol. 137, pp. 1394–1409, May 2014.

[23] M. E. Schwab, "Increasing plasticity and functional recovery of the lesioned spinal cord," *Progress in Brain Research*, vol. 137, pp. 351–359, 2002.

[24] F. M. Bareyre, M. Kerschensteiner, O. Raineteau, T. C. Mettenleiter, O. Weinmann, and M. E. Schwab, "The injured spinal cord spontaneously forms a new intraspinal circuit in adult rats," *Nature Neuroscience*, vol. 7, pp. 269–277, Mar. 2004.

[25] G. Courtine, B. Song, R. R. Roy, H. Zhong, J. E. Herrmann, Y. Ao, J. Qi, V. R. Edgerton, and M. V. Sofroniew, "Recovery of supraspinal control of stepping via indirect propriospinal relay connections after spinal cord injury," *Nature Medicine*, vol. 14, pp. 69–74, Jan. 2008.

[26] K. C. Cowley, E. Zaporozhets, and B. J. Schmidt, "Propriospinal neurons are sufficient for bulbospinal transmission of the locomotor command signal in the neonatal rat spinal cord: Propriospinal neurons are sufficient for activation of locomotion," *The Journal of Physiology*, vol. 586, pp. 1623–1635, Mar. 2008.

[27] O. Raineteau, "Plastic responses to spinal cord injury," *Behavioural Brain Research*, vol. 192, pp. 114–123, Sept. 2008.

[28] E. S. Rosenzweig, G. Courtine, D. L. Jindrich, J. H. Brock, A. R. Ferguson, S. C. Strand, Y. S. Nout, R. R. Roy, D. M. Miller, M. S. Beattie, L. A. Havton, J. C. Bresnahan, V. R. Edgerton, and M. H. Tuszynski, "Extensive spontaneous plasticity of corticospinal projections after primate spinal cord injury," *Nature Neuroscience*, vol. 13, pp. 1505–1510, Dec. 2010.

[29] M.-L. Beaud, E. Rouiller, J. Bloch, A. Mir, M. Schwab, T. Wannier, and E. Schmidlin, "Invasion of lesion territory by regenerating fibers after spinal cord injury in adult macaque monkeys," *Neuroscience*, vol. 227, pp. 271–282, Dec. 2012.

[30] S. Harkema, Y. Gerasimenko, J. Hodes, J. Burdick, C. Angeli, Y. Chen, C. Ferreira, A. Willhite, E. Rejc, R. G. Grossman, and V. R. Edgerton, "Effect of epidural stimulation of the lumbosacral spinal cord on voluntary movement, standing, and assisted stepping after motor complete paraplegia: a case study," *Lancet (London, England)*, vol. 377, pp. 1938–1947, June 2011.

[31] B. Dobkin, H. Barbeau, D. Deforge, J. Ditunno, R. Elashoff, D. Apple, M. Basso, A. Behrman, S. Harkema, M. Saulino, M. Scott, and Spinal Cord Injury Locomotor Trial Group, "The evolution of walking-related outcomes over the first 12

weeks of rehabilitation for incomplete traumatic spinal cord injury: the multicenter randomized Spinal Cord Injury Locomotor Trial," *Neurorehabilitation and Neural Repair*, vol. 21, pp. 25–35, Feb. 2007.

[32] L. Schnell and M. E. Schwab, "Axonal regeneration in the rat spinal cord produced by an antibody against myelin-associated neurite growth inhibitors," *Nature*, vol. 343, pp. 269–272, Jan. 1990.

[33] E. J. Bradbury, L. D. F. Moon, R. J. Popat, V. R. King, G. S. Bennett, P. N. Patel, J. W. Fawcett, and S. B. McMahon, "Chondroitinase ABC promotes functional recovery after spinal cord injury," *Nature*, vol. 416, pp. 636–640, Apr. 2002.

[34] M. L. Starkey, K. Bartus, A. W. Barritt, and E. J. Bradbury, "Chondroitinase ABC promotes compensatory sprouting of the intact corticospinal tract and recovery of forelimb function following unilateral pyramidotomy in adult mice," *The European Journal of Neuroscience*, vol. 36, pp. 3665–3678, Dec. 2012.

[35] V. K. Mushahwar and K. W. Horch, "Selective activation of muscle groups in the feline hindlimb through electrical microstimulation of the ventral lumbo-sacral spinal cord," *IEEE transactions on rehabilitation engineering: a publication of the IEEE Engineering in Medicine and Biology Society*, vol. 8, pp. 11–21, Mar. 2000.

[36] V. K. Mushahwar, P. L. Jacobs, R. A. Normann, R. J. Triolo, and N. Kleitman, "New functional electrical stimulation approaches to standing and walking," *Journal of Neural Engineering*, vol. 4, pp. S181–197, Sept. 2007.

[37] D. Barthélemy, H. Leblond, and S. Rossignol, "Characteristics and Mechanisms of Locomotion Induced by Intraspinal Microstimulation and Dorsal Root Stimulation in Spinal Cats," *Journal of Neurophysiology*, vol. 97, pp. 1986–2000, Mar. 2007.

[38] P. E. Musienko, I. N. Bogacheva, and I. P. Gerasimenko, "[Significance of peripheral feedback in stepping movement generation under epideral spinal cord stimulation]," *Rossiiskii Fiziologicheskii Zhurnal Imeni I.M. Sechenova*, vol. 91, pp. 1407–1420, Dec. 2005.

[39] I. Lavrov, C. J. Dy, A. J. Fong, Y. Gerasimenko, G. Courtine, H. Zhong, R. R. Roy, and V. R. Edgerton, "Epidural stimulation induced modulation of spinal locomotor networks in adult spinal rats," *The Journal of Neuroscience: The Official Journal of the Society for Neuroscience*, vol. 28, pp. 6022–6029, June 2008.

[40] I. Lavrov, G. Courtine, C. J. Dy, R. van den Brand, A. J. Fong, Y. Gerasimenko, H. Zhong, R. R. Roy, and V. R. Edgerton, "Facilitation of stepping with epidural stimulation in spinal rats: role of sensory input," *The Journal of Neuroscience: The Official Journal of the Society for Neuroscience*, vol. 28, pp. 7774–7780, July 2008.

[41] P. E. Musienko, P. V. Zelenin, G. N. Orlovsky, and T. G. Deliagina, "Facilitation of postural limb reflexes with epidural stimulation in spinal rabbits," *Journal of Neurophysiology*, vol. 103, pp. 1080–1092, Feb. 2010.

[42] S. Rossignol, N. Giroux, C. Chau, J. Marcoux, E. Brustein, and T. A. Reader, "Pharmacological aids to locomotor training after spinal injury in the cat," *The Journal of Physiology*, vol. 533, pp. 65–74, May 2001.

[43] E. S. Landry, N. P. Lapointe, C. Rouillard, D. Levesque, P. B. Hedlund, and P. A. Guertin, "Contribution of spinal 5-HT1a and 5-HT7 receptors to locomotor-like movement induced by 8-OH-DPAT in spinal cord-transected mice," *The European Journal of Neuroscience*, vol. 24, pp. 535–546, July 2006.

[44] Y. P. Gerasimenko, R. M. Ichiyama, I. A. Lavrov, G. Courtine, L. Cai, H. Zhong, R. R. Roy, and V. R. Edgerton, "Epidural spinal cord stimulation plus quipazine administration enable stepping in complete spinal adult rats," *Journal of Neurophysiology*, vol. 98, pp. 2525–2536, Nov. 2007.

[45] N. P. Lapointe and P. A. Guertin, "Synergistic effects of D1/5 and 5-HT1a/7 receptor agonists on locomotor movement induction in complete spinal cord-transected mice," *Journal of Neurophysiology*, vol. 100, pp. 160–168, July 2008.

[46] P. Musienko, R. van den Brand, O. Märzendorfer, R. R. Roy, Y. Gerasimenko, V. R. Edgerton, and G. Courtine, "Controlling specific locomotor behaviors through multidimensional monoaminergic modulation of spinal circuitries," *The Journal of Neuroscience: The Official Journal of the Society for Neuroscience*, vol. 31, pp. 9264–9278, June 2011.

[47] R. van den Brand, J. Heutschi, Q. Barraud, J. DiGiovanna, K. Bartholdi, M. Huerlimann, L. Friedli, I. Vollenweider, E. M. Moraud, S. Duis, N. Dominici, S. Micera, P. Musienko, and G. Courtine, "Restoring voluntary control of locomotion after paralyzing spinal cord injury," *Science (New York, N.Y.)*, vol. 336, pp. 1182–1185, June 2012.

[48] P. Musienko, R. van den Brand, O. Maerzendorfer, A. Larmagnac, and G. Courtine, "Combinatory electrical and pharmacological neuroprosthetic interfaces to regain motor function after spinal cord injury," *IEEE transactions on biomedical engineering*, vol. 56, pp. 2707–2711, Nov. 2009.

[49] P. E. Musienko, I. N. Bogacheva, and Y. P. Gerasimenko, "Significance of peripheral feedback in the generation of stepping movements during epidural stimulation of the spinal cord," *Neuroscience and Behavioral Physiology*, vol. 37, pp. 181–190, Feb. 2007.

[50] Y. P. Gerasimenko, I. A. Lavrov, G. Courtine, R. M. Ichiyama, C. J. Dy, H. Zhong, R. R. Roy, and V. R. Edgerton, "Spinal cord reflexes induced by epidural spinal cord stimulation in normal awake rats," *Journal of Neuroscience Methods*, vol. 157, pp. 253–263, Oct. 2006.

[51] J. Holsheimer, "Computer modelling of spinal cord stimulation and its contribution to therapeutic efficacy," *Spinal Cord*, vol. 36, pp. 531–540, Aug. 1998.

[52] F. Rattay, K. Minassian, and M. R. Dimitrijevic, "Epidural electrical stimulation of posterior structures of the human lumbosacral cord: 2. quantitative analysis by computer modeling," *Spinal Cord*, vol. 38, pp. 473–489, Aug. 2000.

[53] M. Capogrosso, N. Wenger, S. Raspopovic, P. Musienko, J. Beauparlant, L. Bassi Luciani, G. Courtine, and S. Micera, "A Computational Model for Epidural Electrical Stimulation of Spinal Sensorimotor Circuits," *Journal of Neuroscience*, vol. 33, pp. 19326–19340, Dec. 2013.

[54] R. G. Lovely, R. J. Gregor, R. R. Roy, and V. R. Edgerton, "Effects of training on the recovery of full-weight-bearing stepping in the adult spinal cat," *Experimental Neurology*, vol. 92, pp. 421–435, May 1986.

[55] H. Barbeau and S. Rossignol, "Recovery of locomotion after chronic spinalization in the adult cat," *Brain Research*, vol. 412, pp. 84–95, May 1987.

[56] A. Wernig and S. Müller, "Laufband locomotion with body weight support improved walking in persons with severe spinal cord injuries," *Paraplegia*, vol. 30, pp. 229–238, Apr. 1992.

[57] A. Wernig, S. Müller, A. Nanassy, and E. Cagol, "Laufband therapy based on 'rules of spinal locomotion' is effective in spinal cord injured persons," *The European Journal of Neuroscience*, vol. 7, pp. 823–829, Apr. 1995.

[58] V. Dietz and G. Colombo, "Recovery from spinal cord injury–underlying mechanisms and efficacy of rehabilitation," *Acta Neurochirurgica. Supplement*, vol. 89, pp. 95–100, 2004.

[59] A. L. Behrman and S. J. Harkema, "Physical Rehabilitation as an Agent for Recovery After Spinal Cord Injury," *Physical Medicine and Rehabilitation Clinics of North America*, vol. 18, pp. 183–202, May 2007.

[60] R. D. De Leon, J. A. Hodgson, R. R. Roy, and V. R. Edgerton, "Full Weight-Bearing Hindlimb Standing Following Stand Training in the Adult Spinal Cat," *Journal of Neurophysiology*, vol. 80, pp. 83–91, July 1998.

[61] R. D. de Leon, J. A. Hodgson, R. R. Roy, and V. R. Edgerton, "Locomotor Capacity Attributable to Step Training Versus Spontaneous Recovery After Spinalization in Adult Cats," *Journal of Neurophysiology*, vol. 79, pp. 1329–1340, Mar. 1998.

[62] N. J. K. Tillakaratne, R. D. de Leon, T. X. Hoang, R. R. Roy, V. R. Edgerton, and A. J. Tobin, "Use-dependent modulation of inhibitory capacity in the feline lumbar spinal cord," *The Journal of Neuroscience: The Official Journal of the Society for Neuroscience*, vol. 22, pp. 3130–3143, Apr. 2002.

[63] S. J. Harkema, "Plasticity of interneuronal networks of the functionally isolated human spinal cord," *Brain Research Reviews*, vol. 57, pp. 255–264, Jan. 2008.

[64] M. Wessels, C. Lucas, I. Eriks, and S. de Groot, "Body weight-supported gait training for restoration of walking in people with an incomplete spinal cord injury: a systematic review," *Journal of Rehabilitation Medicine*, vol. 42, pp. 513–519, June 2010.

[65] N. Wenger, E. M. Moraud, J. Gandar, P. Musienko, M. Capogrosso, L. Baud, C. G. Le Goff, Q. Barraud, N. Pavlova, N. Dominici, I. R. Minev, L. Asboth, A. Hirsch, S. Duis, J. Kreider, A. Mortera, O. Haverbeck, S. Kraus, F. Schmitz, J. DiGiovanna, R. van den Brand, J. Bloch, P. Detemple, S. P. Lacour, E. Bézard, S. Micera, and G. Courtine, "Spatiotemporal neuromodulation therapies engaging muscle synergies improve motor control after spinal cord injury," *Nature Medicine*, vol. 22, pp. 138–145, Feb. 2016.

[66] J. DiGiovanna, N. Dominici, L. Friedli, J. Rigosa, S. Duis, J. Kreider, J. Beauparlant, R. van den Brand, M. Schieppati, S. Micera, and G. Courtine, "Engagement of the Rat Hindlimb Motor Cortex across Natural Locomotor Behaviors," *The Journal of Neuroscience*, vol. 36, pp. 10440–10455, Oct. 2016.

[67] N. Dominici, U. Keller, H. Vallery, L. Friedli, R. van den Brand, M. L. Starkey, P. Musienko, R. Riener, and G. Courtine, "Versatile robotic interface to evaluate, enable and train locomotion and balance after neuromotor disorders," *Nature Medicine*, vol. 18, pp. 1142–1147, July 2012.

[68] H. Vallery, P. Lutz, J. von Zitzewitz, G. Rauter, M. Fritschi, C. Everarts, R. Ronsse, A. Curt, and M. Bolliger, "Multidirectional transparent support for overground gait training," *IEEE ... International Conference on Rehabilitation Robotics: [proceedings]*, vol. 2013, p. 6650512, June 2013.

[69] L. Asboth, L. Friedli, J. Beauparlant, C. Martinez-Gonzalez, S. Anil, E. Rey, L. Baud, G. Pidpruzhnykova, M. A. Anderson, P. Shkorbatova, L. Batti, S. Pagès, J. Kreider, B. L. Schneider, Q. Barraud, and G. Courtine, "Cortico-reticulo-spinal circuit reorganization enables functional recovery after severe spinal cord contusion," *Nature Neuroscience*, vol. 21, pp. 576–588, Apr. 2018.

[70] C. A. Angeli, M. Boakye, R. A. Morton, J. Vogt, K. Benton, Y. Chen, C. K. Ferreira, and S. J. Harkema, "Recovery of Over-Ground Walking after Chronic Motor Complete Spinal Cord Injury," *New England Journal of Medicine*, vol. 379, pp. 1244–1250, Sept. 2018.

[71] M. L. Gill, P. J. Grahn, J. S. Calvert, M. B. Linde, I. A. Lavrov, J. A. Strommen, L. A. Beck, D. G. Sayenko, M. G. Van Straaten, D. I. Drubach, D. D. Veith, A. R. Thoreson, C. Lopez, Y. P. Gerasimenko, V. R. Edgerton, K. H. Lee, and K. D. Zhao, "Neuromodulation of lumbosacral spinal networks enables independent stepping after complete paraplegia," *Nature Medicine*, Sept. 2018.

[72] M. Capogrosso, T. Milekovic, D. Borton, F. Wagner, E. M. Moraud, J.-B. Mignardot, N. Buse, J. Gandar, Q. Barraud, D. Xing, E. Rey, S. Duis, Y. Jianzhong, W. K. D. Ko, Q. Li, P. Detemple, T. Denison, S. Micera, E. Bezard, J. Bloch, and G. Courtine, "A brain-spine interface alleviating gait deficits after spinal cord injury in primates," *Nature*, vol. 539, no. 7628, pp. 284–288, 2016.

[73] G. Courtine, "Organisation neurale et contrôle adaptatif de la marche humaine," p. 233, 2003.

[74] N. A. Borghese, L. Bianchi, and F. Lacquaniti, "Kinematic determinants of human locomotion," *The Journal of Physiology*, vol. 494 (Pt 3), pp. 863–879, Aug. 1996.

[75] Y. P. Ivanenko, N. Dominici, and F. Lacquaniti, "Development of independent walking in toddlers," *Exercise and Sport Sciences Reviews*, vol. 35, pp. 67–73, Apr. 2007.

[76] G. Cheron, E. Bouillot, B. Dan, A. Bengoetxea, J. P. Draye, and F. Lacquaniti, "Development of a kinematic coordination pattern in toddler locomotion: planar covariation," *Experimental Brain Research*, vol. 137, pp. 455–466, Apr. 2001.

[77] G. Cheron, A. Bengoetxea, E. Bouillot, F. Lacquaniti, and B. Dan, "Early emergence of temporal co-ordination of lower limb segments elevation angles in human locomotion," *Neuroscience Letters*, vol. 308, pp. 123–127, Aug. 2001.

[78] R. Grasso, M. Zago, and F. Lacquaniti, "Interactions Between Posture and Locomotion: Motor Patterns in Humans Walking With Bent Posture Versus Erect Posture," *Journal of Neurophysiology*, vol. 83, pp. 288–300, Jan. 2000.

[79] V. Dietz, "Do human bipeds use quadrupedal coordination?," *Trends in Neurosciences*, vol. 25, pp. 462–467, Sept. 2002.

[80] J. L. Stephenson, A. Lamontagne, and S. J. De Serres, "The coordination of upper and lower limb movements during gait in healthy and stroke individuals," *Gait & Posture*, vol. 29, pp. 11–16, Jan. 2009.

[81] S. F. Donker and P. J. Beek, "Interlimb coordination in prosthetic walking: effects of asymmetry and walking velocity," *Acta Psychologica*, vol. 110, pp. 265–288, June 2002.

[82] M. Milosevic, K. M. V. McConville, and K. Masani, "Arm movement improves performance in clinical balance and mobility tests," *Gait & Posture*, vol. 33, pp. 507–509, Mar. 2011.

[83] Y. Ivanenko, R. Poppele, and F. Lacquaniti, "Distributed neural networks for controlling human locomotion," *Brain Research Bulletin*, vol. 78, pp. 13–21, Jan. 2009.

[84] F. B. Wagner, J.-B. Mignardot, C. G. Le Goff-Mignardot, R. Demesmaeker, S. Komi, M. Capogrosso, A. Rowald, I. Seáñez, M. Caban, E. Pirondini, M. Vat, L. A. McCracken, R. Heimgartner, I. Fodor, A. Watrin, P. Seguin, E. Paoles, K. Van Den Keybus, G. Eberle, B. Schurch, E. Pralong, F. Becce, J. Prior, N. Buse, R. Buschman, E. Neufeld, N. Kuster, S. Carda, J. von Zitzewitz, V. Delattre, T. Denison, H. Lambert, K. Minassian, J. Bloch, and G. Courtine, "Targeted neurotechnology restores walking in humans with spinal cord injury," *Nature*, vol. 563, pp. 65–71, Nov. 2018.

[85] J.-B. Mignardot, C. G. Le Goff, R. van den Brand, M. Capogrosso, N. Fumeaux, H. Vallery, S. Anil, J. Lanini, I. Fodor, G. Eberle, A. Ijspeert, B. Schurch, A. Curt,

S. Carda, J. Bloch, J. von Zitzewitz, and G. Courtine, "A multidirectional gravity-assist algorithm that enhances locomotor control in patients with stroke or spinal cord injury," *Science Translational Medicine*, vol. 9, no. 399, 2017.

[86] G. A. Cavagna, P. A. Willems, and N. C. Heglund, "Walking on Mars," *Nature*, vol. 393, p. 636, June 1998.

[87] A. A. Biewener, "Biomechanics of mammalian terrestrial locomotion," *Science (New York, N.Y.)*, vol. 250, pp. 1097–1103, Nov. 1990.

[88] M. H. Dickinson, C. T. Farley, R. J. Full, M. A. Koehl, R. Kram, and S. Lehman, "How animals move: an integrative view," *Science (New York, N.Y.)*, vol. 288, pp. 100–106, Apr. 2000.

[89] N. E. Thompson, B. Demes, M. C. O'Neill, N. B. Holowka, and S. G. Larson, "Surprising trunk rotational capabilities in chimpanzees and implications for bipedal walking proficiency in early hominins," *Nature Communications*, vol. 6, p. 8416, Oct. 2015.

[90] G. A. Cavagna, N. C. Heglund, and C. R. Taylor, "Mechanical work in terrestrial locomotion: two basic mechanisms for minimizing energy expenditure," *The American Journal of Physiology*, vol. 233, pp. R243–261, Nov. 1977.

[91] R. M. Alexander, "Optimization and gaits in the locomotion of vertebrates," *Physiological Reviews*, vol. 69, pp. 1199–1227, Oct. 1989.

[92] A. D. Kuo, J. M. Donelan, and A. Ruina, "Energetic consequences of walking like an inverted pendulum: step-to-step transitions," *Exercise and Sport Sciences Reviews*, vol. 33, pp. 88–97, Apr. 2005.

[93] R. W. Selles, J. B. Bussmann, R. C. Wagenaar, and H. J. Stam, "Comparing predictive validity of four ballistic swing phase models of human walking," *Journal of Biomechanics*, vol. 34, pp. 1171–1177, Sept. 2001.

[94] F. Lacquaniti, Y. P. Ivanenko, and M. Zago, "Development of human locomotion," *Current Opinion in Neurobiology*, vol. 22, pp. 822–828, Oct. 2012.

[95] C. Capaday, "The special nature of human walking and its neural control," *Trends in Neurosciences*, vol. 25, pp. 370–376, July 2002.

[96] D. Sutherland, R. Olshen, E. Biden, and M. Wyatt, *The Development of Mature Walking*. Cambridge University Press, 1988. Google-Books-ID: wqB5aRFxeJMC.

[97] S. Harkema, A. Behrman, and H. Barbeau, "Evidence-based therapy for recovery of function after spinal cord injury," *Handbook of Clinical Neurology*, vol. 109, pp. 259–274, 2012.

[98] P. Sale, M. Franceschini, A. Waldner, and S. Hesse, "Use of the robot assisted gait therapy in rehabilitation of patients with stroke and spinal cord injury," *European Journal of Physical and Rehabilitation Medicine*, vol. 48, pp. 111–121, Mar. 2012.

[99] L. Awai, M. Bolliger, A. R. Ferguson, G. Courtine, and A. Curt, "Influence of Spinal Cord Integrity on Gait Control in Human Spinal Cord Injury," *Neurorehabilitation and Neural Repair*, vol. 30, no. 6, pp. 562–572, 2016.

[100] G. Hornby, D. Campbell, D. Zemon, and J. Kahn, "Clinical and Quantitative Evaluation of Robotic-Assisted Treadmill Walking to Retrain Ambulation After Spinal Cord Injury," *Topics in Spinal Cord Injury Rehabilitation*, vol. 11, pp. 1–17, Sept. 2005.

[101] D. D. Straube, C. L. Holleran, C. R. Kinnaird, A. L. Leddy, P. W. Hennessy, and T. G. Hornby, "Effects of dynamic stepping training on nonlocomotor tasks in individuals poststroke," *Physical Therapy*, vol. 94, pp. 921–933, July 2014.

[102] E. Swinnen, J.-P. Baeyens, S. Pintens, J. Van Nieuwenhoven, S. Ilsbroukx, R. Clijsen, R. Buyl, M. Goossens, R. Meeusen, and E. Kerckhofs, "Trunk muscle activity during walking in persons with multiple sclerosis: the influence of body weight support," *NeuroRehabilitation*, vol. 34, no. 2, pp. 323–335, 2014.

[103] A. Pennycott, H. Vallery, D. Wyss, M. Spindler, A. Dewarrat, and R. Riener, "A novel body weight support system extension: initial concept and simulation study," *IEEE ... International Conference on Rehabilitation Robotics: [proceedings]*, vol. 2013, p. 6650489, June 2013.

[104] L. Finch, H. Barbeau, and B. Arsenault, "Influence of body weight support on normal human gait: development of a gait retraining strategy," *Physical Therapy*, vol. 71, pp. 842–855; discussion 855–856, Nov. 1991.

[105] J. von Zitzewitz, L. Asboth, N. Fumeaux, A. Hasse, L. Baud, H. Vallery, and G. Courtine, "A neurorobotic platform for locomotor prosthetic development in rats and mice," *Journal of Neural Engineering*, vol. 13, p. 026007, Apr. 2016.

[106] W. K. Timoszyk, J. A. Nessler, C. Acosta, R. R. Roy, V. R. Edgerton, D. J. Reinkensmeyer, and R. de Leon, "Hindlimb loading determines stepping quantity and quality following spinal cord transection," *Brain Research*, vol. 1050, pp. 180–189, July 2005.

[107] W. Song and S. F. Giszter, "Adaptation to a cortex-controlled robot attached at the pelvis and engaged during locomotion in rats," *The Journal of Neuroscience: The Official Journal of the Society for Neuroscience*, vol. 31, pp. 3110–3128, Feb. 2011.

[108] G. Demeurisse, A. Capon, M. Verhas, and E. Attig, "Pathogenesis of aphasia in deep-seated lesions: likely role of cortical diaschisis," *European Neurology*, vol. 30, no. 2, pp. 67–74, 1990.

[109] R. A. Keith, C. V. Granger, B. B. Hamilton, and F. S. Sherwin, "The functional independence measure: a new tool for rehabilitation," *Advances in Clinical Rehabilitation*, vol. 1, pp. 6–18, 1987.

[110] J. von Zitzewitz, A. Morger, G. Rauter, L. Marchal-Crespo, F. Crivelli, D. Wyss, T. Bruckmann, and R. Riener, "A reconfigurable, tendon-based haptic interface

for research into human-environment interactions," *Robotica*, vol. 31, pp. 441–453, May 2013.

[111] L. Friedli, E. S. Rosenzweig, Q. Barraud, M. Schubert, N. Dominici, L. Awai, J. L. Nielson, P. Musienko, Y. Nout-Lomas, H. Zhong, S. Zdunowski, R. R. Roy, S. C. Strand, R. van den Brand, L. A. Havton, M. S. Beattie, J. C. Bresnahan, E. Bézard, J. Bloch, V. R. Edgerton, A. R. Ferguson, A. Curt, M. H. Tuszynski, and G. Courtine, "Pronounced species divergence in corticospinal tract reorganization and functional recovery after lateralized spinal cord injury favors primates," *Science Translational Medicine*, vol. 7, p. 302ra134, Aug. 2015.

[112] N. Wenger, E. M. Moraud, S. Raspopovic, M. Bonizzato, J. DiGiovanna, P. Musienko, M. Morari, S. Micera, and G. Courtine, "Closed-loop neuromodulation of spinal sensorimotor circuits controls refined locomotion after complete spinal cord injury," *Science Translational Medicine*, vol. 6, p. 255ra133, Sept. 2014.

[113] J.-B. Mignardot, O. Beauchet, C. Annweiler, C. Cornu, and T. Deschamps, "Postural sway, falls, and cognitive status: a cross-sectional study among older adults," *Journal of Alzheimer's disease: JAD*, vol. 41, no. 2, pp. 431–439, 2014.

[114] H. Geyer, A. Seyfarth, and R. Blickhan, "Compliant leg behaviour explains basic dynamics of walking and running," *Proceedings. Biological Sciences*, vol. 273, pp. 2861–2867, Nov. 2006.

[115] S. Hesse, M. Konrad, and D. Uhlenbrock, "Treadmill walking with partial body weight support versus floor walking in hemiparetic subjects," *Archives of Physical Medicine and Rehabilitation*, vol. 80, pp. 421–427, Apr. 1999.

[116] A. M. Moseley, A. Stark, I. D. Cameron, and A. Pollock, "Treadmill training and body weight support for walking after stroke," *The Cochrane Database of Systematic Reviews*, p. CD002840, Oct. 2005.

[117] J. Mehrholz, J. Kugler, and M. Pohl, "Locomotor training for walking after spinal cord injury," *The Cochrane Database of Systematic Reviews*, p. CD006676, Apr. 2008.

[118] E. C. Field-Fote and K. E. Roach, "Influence of a locomotor training approach on walking speed and distance in people with chronic spinal cord injury: a randomized clinical trial," *Physical Therapy*, vol. 91, pp. 48–60, Jan. 2011.

[119] P. W. Duncan, K. J. Sullivan, A. L. Behrman, S. P. Azen, S. S. Wu, S. E. Nadeau, B. H. Dobkin, D. K. Rose, J. K. Tilson, S. Cen, S. K. Hayden, and LEAPS Investigative Team, "Body-weight-supported treadmill rehabilitation after stroke," *The New England Journal of Medicine*, vol. 364, pp. 2026–2036, May 2011.

[120] Y. P. Ivanenko, N. Dominici, G. Cappellini, B. Dan, G. Cheron, and F. Lacquaniti, "Development of pendulum mechanism and kinematic coordination from the first unsupported steps in toddlers," *The Journal of Experimental Biology*, vol. 207, pp. 3797–3810, Oct. 2004.

[121] G. Courtine and J. Bloch, "Defining ecological strategies in neuroprosthetics," *Neuron*, vol. 86, pp. 29–33, Apr. 2015.

[122] A. Thorstensson, J. Nilsson, H. Carlson, and M. R. Zomlefer, "Trunk movements in human locomotion," *Acta Physiologica Scandinavica*, vol. 121, pp. 9–22, May 1984.

[123] T. Ijmker, H. Houdijk, C. J. C. Lamoth, P. J. Beek, and L. H. V. van der Woude, "Energy cost of balance control during walking decreases with external stabilizer stiffness independent of walking speed," *Journal of Biomechanics*, vol. 46, pp. 2109–2114, Sept. 2013.

[124] K. Musselman, K. Brunton, T. Lam, and J. Yang, "Spinal cord injury functional ambulation profile: a new measure of walking ability," *Neurorehabilitation and Neural Repair*, vol. 25, pp. 285–293, Apr. 2011.

[125] D. J. Reinkensmeyer, D. Aoyagi, J. L. Emken, J. A. Galvez, W. Ichinose, G. Kerdanyan, S. Maneekobkunwong, K. Minakata, J. A. Nessler, R. Weber, R. R. Roy, R. de Leon, J. E. Bobrow, S. J. Harkema, and V. R. Edgerton, "Tools for understanding and optimizing robotic gait training," *Journal of Rehabilitation Research and Development*, vol. 43, pp. 657–670, Sept. 2006.

[126] L. Ada, C. M. Dean, J. Vargas, and S. Ennis, "Mechanically assisted walking with body weight support results in more independent walking than assisted overground walking in non-ambulatory patients early after stroke: a systematic review," *Journal of Physiotherapy*, vol. 56, no. 3, pp. 153–161, 2010.

[127] G. Kwakkel, B. J. Kollen, and H. I. Krebs, "Effects of robot-assisted therapy on upper limb recovery after stroke: a systematic review," *Neurorehabilitation and Neural Repair*, vol. 22, pp. 111–121, Apr. 2008.

[128] P. K. Shah, G. Garcia-Alias, J. Choe, P. Gad, Y. Gerasimenko, N. Tillakaratne, H. Zhong, R. R. Roy, and V. R. Edgerton, "Use of quadrupedal step training to reengage spinal interneuronal networks and improve locomotor function after spinal cord injury," *Brain: A Journal of Neurology*, vol. 136, pp. 3362–3377, Nov. 2013.

[129] V. Dietz, "Quadrupedal coordination of bipedal gait: implications for movement disorders," *Journal of Neurology*, vol. 258, pp. 1406–1412, Aug. 2011.

[130] A. Duschau-Wicke, A. Caprez, and R. Riener, "Patient-cooperative control increases active participation of individuals with SCI during robot-aided gait training," *Journal of Neuroengineering and Rehabilitation*, vol. 7, p. 43, Sept. 2010.

[131] M. Plooij, U. Keller, B. Sterke, S. Komi, H. Vallery, and J. von Zitzewitz, "Design of RYSEN: An Intrinsically Safe and Low-Power Three-Dimensional Overground Body Weight Support," *IEEE Robotics and Automation Letters*, vol. 3, pp. 2253–2260, July 2018.

[132] E. Vrieseling and S. Arber, "Target-induced transcriptional control of dendritic patterning and connectivity in motor neurons by the ETS gene Pea3," *Cell*, vol. 127, pp. 1439–1452, Dec. 2006.

[133] C. M. Schirmer, J. L. Shils, J. E. Arle, G. R. Cosgrove, P. K. Dempsey, E. Tarlov, S. Kim, C. J. Martin, C. Feltz, M. Moul, and S. Magge, "Heuristic map of myotomal innervation in humans using direct intraoperative nerve root stimulation: Clinical article," *Journal of Neurosurgery: Spine*, vol. 15, pp. 64–70, July 2011.

[134] W. J. Sharrard, "THE SEGMENTAL INNERVATION OF THE LOWER LIMB MUSCLES IN MAN," *Annals of the Royal College of Surgeons of England*, vol. 35, pp. 106–122, Aug. 1964.

[135] E. C. Field-Fote, "Exciting recovery: augmenting practice with stimulation to optimize outcomes after spinal cord injury," *Progress in Brain Research*, vol. 218, pp. 103–126, 2015.

[136] A. L. Behrman, E. M. Ardolino, and S. J. Harkema, "Activity-Based Therapy: From Basic Science to Clinical Application for Recovery After Spinal Cord Injury," *Journal of neurologic physical therapy: JNPT*, vol. 41 Suppl 3 Supplement, IV STEP Special Issue, pp. S39–S45, July 2017.

[137] M. L. Jones, N. Evans, C. Tefertiller, D. Backus, M. Sweatman, K. Tansey, and S. Morrison, "Activity-based therapy for recovery of walking in individuals with chronic spinal cord injury: results from a randomized clinical trial," *Archives of Physical Medicine and Rehabilitation*, vol. 95, pp. 2239–2246.e2, Dec. 2014.

[138] E. C. Field-Fote, S. D. Lindley, and A. L. Sherman, "Locomotor training approaches for individuals with spinal cord injury: a preliminary report of walking-related outcomes," *Journal of neurologic physical therapy: JNPT*, vol. 29, pp. 127–137, Sept. 2005.

[139] V. R. Edgerton, G. Courtine, Y. P. Gerasimenko, I. Lavrov, R. M. Ichiyama, A. J. Fong, L. L. Cai, C. K. Otoshi, N. J. K. Tillakaratne, J. W. Burdick, and R. R. Roy, "Training locomotor networks," *Brain Research Reviews*, vol. 57, pp. 241–254, Jan. 2008.

[140] M.-P. Côté, M. Murray, and M. A. Lemay, "Rehabilitation Strategies after Spinal Cord Injury: Inquiry into the Mechanisms of Success and Failure," *Journal of Neurotrauma*, vol. 34, pp. 1841–1857, May 2017.

[141] D. Borton, S. Micera, J. d. R. Millán, and G. Courtine, "Personalized neuroprosthetics," *Science Translational Medicine*, vol. 5, p. 210rv2, Nov. 2013.

[142] R. R. Roy, S. J. Harkema, and V. R. Edgerton, "Basic concepts of activity-based interventions for improved recovery of motor function after spinal cord injury," *Archives of Physical Medicine and Rehabilitation*, vol. 93, pp. 1487–1497, Sept. 2012.

[143] G. Barolat, J. B. Myklebust, and W. Wenninger, "Enhancement of voluntary motor function following spinal cord stimulation–case study," *Applied Neurophysiology*, vol. 49, no. 6, pp. 307–314, 1986.

[144] S. M. Danner, U. S. Hofstoetter, B. Freundl, H. Binder, W. Mayr, F. Rattay, and K. Minassian, "Human spinal locomotor control is based on flexibly organized burst generators," *Brain: A Journal of Neurology*, vol. 138, pp. 577–588, Mar. 2015.

[145] P. J. Grahn, I. A. Lavrov, D. G. Sayenko, M. G. Van Straaten, M. L. Gill, J. A. Strommen, J. S. Calvert, D. I. Drubach, L. A. Beck, M. B. Linde, A. R. Thoreson, C. Lopez, A. A. Mendez, P. N. Gad, Y. P. Gerasimenko, V. R. Edgerton, K. D. Zhao, and K. H. Lee, "Enabling Task-Specific Volitional Motor Functions via Spinal Cord Neuromodulation in a Human With Paraplegia," *Mayo Clinic Proceedings*, vol. 92, pp. 544–554, Apr. 2017.

[146] M. R. Carhart, J. He, R. Herman, S. D'Luzansky, and W. T. Willis, "Epidural spinal-cord stimulation facilitates recovery of functional walking following incomplete spinal-cord injury," *IEEE transactions on neural systems and rehabilitation engineering: a publication of the IEEE Engineering in Medicine and Biology Society*, vol. 12, pp. 32–42, Mar. 2004.

[147] K. Minassian, B. Jilge, F. Rattay, M. M. Pinter, H. Binder, F. Gerstenbrand, and M. R. Dimitrijevic, "Stepping-like movements in humans with complete spinal cord injury induced by epidural stimulation of the lumbar cord: electromyographic study of compound muscle action potentials," *Spinal Cord*, vol. 42, pp. 401–416, July 2004.

[148] E. M. Moraud, J. von Zitzewitz, J. Miehlbradt, S. Wurth, E. Formento, J. DiGiovanna, M. Capogrosso, G. Courtine, and S. Micera, "Closed-loop control of trunk posture improves locomotion through the regulation of leg proprioceptive feedback after spinal cord injury," *Scientific Reports*, vol. 8, p. 76, Jan. 2018.

[149] Y. Gerasimenko, R. R. Roy, and V. R. Edgerton, "Epidural stimulation: comparison of the spinal circuits that generate and control locomotion in rats, cats and humans," *Experimental Neurology*, vol. 209, pp. 417–425, Feb. 2008.

[150] S. Kirshblum and W. Waring, "Updates for the International Standards for Neurological Classification of Spinal Cord Injury," *Physical Medicine and Rehabilitation Clinics of North America*, vol. 25, pp. 505–517, vii, Aug. 2014.

[151] K. Minassian, I. Persy, F. Rattay, M. M. Pinter, H. Kern, and M. R. Dimitrijevic, "Human lumbar cord circuitries can be activated by extrinsic tonic input to generate locomotor-like activity," *Human Movement Science*, vol. 26, pp. 275–295, Apr. 2007.

[152] S. Canbay, B. Gürer, M. Bozkurt, A. Comert, Y. Izci, and M. K. Başkaya, "Anatomical relationship and positions of the lumbar and sacral segments of the spinal cord according to the vertebral bodies and the spinal roots," *Clinical Anatomy (New York, N.Y.)*, vol. 27, pp. 227–233, Mar. 2014.

[153] B. Howell, S. P. Lad, and W. M. Grill, "Evaluation of intradural stimulation efficiency and selectivity in a computational model of spinal cord stimulation," *PloS One*, vol. 9, no. 12, p. e114938, 2014.

[154] M. L. Hines and N. T. Carnevale, "The NEURON simulation environment," *Neural Computation*, vol. 9, pp. 1179–1209, Aug. 1997.

[155] G. Cappellini, Y. P. Ivanenko, N. Dominici, R. E. Poppele, and F. Lacquaniti, "Migration of motor pool activity in the spinal cord reflects body mechanics in human locomotion," *Journal of Neurophysiology*, vol. 104, pp. 3064–3073, Dec. 2010.

[156] S. Yakovenko, V. Mushahwar, V. VanderHorst, G. Holstege, and A. Prochazka, "Spatiotemporal activation of lumbosacral motoneurons in the locomotor step cycle," *Journal of Neurophysiology*, vol. 87, pp. 1542–1553, Mar. 2002.

[157] P. L. Dittuno, J. F. Ditunno, and J. F. Dittuno, "Walking index for spinal cord injury (WISCI II): scale revision," *Spinal Cord*, vol. 39, pp. 654–656, Dec. 2001.

[158] B. H. Goodpaster, D. E. Kelley, F. L. Thaete, J. He, and R. Ross, "Skeletal muscle attenuation determined by computed tomography is associated with skeletal muscle lipid content," *Journal of Applied Physiology (Bethesda, Md.: 1985)*, vol. 89, pp. 104–110, July 2000.

[159] J. Aubrey, N. Esfandiari, V. E. Baracos, F. A. Buteau, J. Frenette, C. T. Putman, and V. C. Mazurak, "Measurement of skeletal muscle radiation attenuation and basis of its biological variation," *Acta Physiologica (Oxford, England)*, vol. 210, pp. 489–497, Mar. 2014.

[160] V. Dietz, "Behavior of spinal neurons deprived of supraspinal input," *Nature Reviews. Neurology*, vol. 6, pp. 167–174, Mar. 2010.

[161] H. Asanuma and R. Mackel, "Direct and indirect sensory input pathways to the motor cortex; its structure and function in relation to learning of motor skills," *The Japanese Journal of Physiology*, vol. 39, no. 1, pp. 1–19, 1989.

[162] K. Gourab and B. D. Schmit, "Changes in movement-related β-band EEG signals in human spinal cord injury," *Clinical Neurophysiology: Official Journal of the International Federation of Clinical Neurophysiology*, vol. 121, pp. 2017–2023, Dec. 2010.

[163] M. Schieppati, "The Hoffmann reflex: a means of assessing spinal reflex excitability and its descending control in man," *Progress in Neurobiology*, vol. 28, no. 4, pp. 345–376, 1987.

[164] S. Schindler-Ivens and R. K. Shields, "Low frequency depression of H-reflexes in humans with acute and chronic spinal-cord injury," *Experimental Brain Research*, vol. 133, pp. 233–241, July 2000.

[165] E. Formento, K. Minassian, F. Wagner, J. B. Mignardot, C. G. Le Goff-Mignardot, A. Rowald, J. Bloch, S. Micera, M. Capogrosso, and G. Courtine, "Electrical

spinal cord stimulation must preserve proprioception to enable locomotion in humans with spinal cord injury," *Nature Neuroscience*, vol. 21, pp. 1728–1741, Dec. 2018.

[166] E. M. Moraud, M. Capogrosso, E. Formento, N. Wenger, J. DiGiovanna, G. Courtine, and S. Micera, "Mechanisms Underlying the Neuromodulation of Spinal Circuits for Correcting Gait and Balance Deficits after Spinal Cord Injury," *Neuron*, vol. 89, pp. 814–828, Feb. 2016.

[167] Y. P. Gerasimenko, D. C. Lu, M. Modaber, S. Zdunowski, P. Gad, D. G. Sayenko, E. Morikawa, P. Haakana, A. R. Ferguson, R. R. Roy, and V. R. Edgerton, "Noninvasive Reactivation of Motor Descending Control after Paralysis," *Journal of Neurotrauma*, vol. 32, pp. 1968–1980, Dec. 2015.

[168] A. Takeoka, I. Vollenweider, G. Courtine, and S. Arber, "Muscle spindle feedback directs locomotor recovery and circuit reorganization after spinal cord injury," *Cell*, vol. 159, pp. 1626–1639, Dec. 2014.

[169] A. Holtmaat and K. Svoboda, "Experience-dependent structural synaptic plasticity in the mammalian brain," *Nature Reviews. Neuroscience*, vol. 10, pp. 647–658, Sept. 2009.

[170] Y. Nishimura, S. I. Perlmutter, R. W. Eaton, and E. E. Fetz, "Spike-timing-dependent plasticity in primate corticospinal connections induced during free behavior," *Neuron*, vol. 80, pp. 1301–1309, Dec. 2013.

[171] M. A. Perez, E. C. Field-Fote, and M. K. Floeter, "Patterned sensory stimulation induces plasticity in reciprocal ia inhibition in humans," *The Journal of Neuroscience: The Official Journal of the Society for Neuroscience*, vol. 23, pp. 2014–2018, Mar. 2003.

[172] M. A. Urbin, R. A. Ozdemir, T. Tazoe, and M. A. Perez, "Spike-timing-dependent plasticity in lower-limb motoneurons after human spinal cord injury," *Journal of Neurophysiology*, vol. 118, pp. 2171–2180, Oct. 2017.

[173] C. R. West, A. A. Phillips, J. W. Squair, A. M. Williams, M. Walter, T. Lam, and A. V. Krassioukov, "Association of Epidural Stimulation With Cardiovascular Function in an Individual With Spinal Cord Injury," *JAMA neurology*, vol. 75, pp. 630–632, May 2018.

[174] A. N. Herrity, C. S. Williams, C. A. Angeli, S. J. Harkema, and C. H. Hubscher, "Lumbosacral spinal cord epidural stimulation improves voiding function after human spinal cord injury," *Scientific Reports*, vol. 8, p. 8688, June 2018.

[175] J. J. van Middendorp, A. J. Hosman, A. R. T. Donders, M. H. Pouw, J. F. Ditunno, A. Curt, A. C. Geurts, and H. Van de Meent, "A clinical prediction rule for ambulation outcomes after traumatic spinal cord injury: a longitudinal cohort study," *The Lancet*, vol. 377, pp. 1004–1010, Mar. 2011.

[176] E. Rejc, C. A. Angeli, N. Bryant, and S. J. Harkema, "Effects of Stand and Step Training with Epidural Stimulation on Motor Function for Standing in Chronic

Complete Paraplegics," *Journal of Neurotrauma*, vol. 34, pp. 1787–1802, May 2017.

Publications & Contributions

Journal Publications

2018 – *Targeted neurotechnologies restore walking in humans with spinal cord injury*, F.B. Wagner*, J.-B. Mignardot*, **C.G. Le Goff-Mignardot***, R. Demesmaeker, S. Komi, M. Capogrosso, A. Rowald, I. Seanez, M. Caban, E. Pirondini, M. Vat, L. McCracken, R. Heimgartner, I. Fodor, A. Watrin, P. Seguin, E. Paoles, K. Van Den Keybus, G. Eberle, B. Schurch, E. Pralong, F. Becce, J. Prior, N. Buse, R. Buschman, E. Neufeld, N. Kuster, S. Carda, J. von Zitzewitz, V. Delattre, T. Denison, H. Lambert, K. Minassian°, J. Bloch°, G. Courtine°, Nature. * these authors contributed equally to this work, °co-senior author.

Contribution: 1st co-author.

2018 – *Electrical spinal cord stimulation must preserve proprioception to enable locomotion in humans with spinal cord injury*, E. Formento, K. Minassian, F. Wagner, J.-B. Mignardot, **C.G. Le Goff**, A. Rowald, J. Bloch, S. Micera°, M. Capogrosso°, G. Courtine°, Nature Neuroscience. °co-senior author.

Contribution: implementation and operation of the technological framework for the experiments with humans, manuscript editing.

2017 – *A multidirectional gravity-assist algorithm that enhances locomotor control in patients with stroke or spinal cord*, J.-B. Mignardot*, **C.G. Le Goff***, R. van den Brand*, M. Capogrosso, N. Fumeaux, H. Vallery, S. Anil, J. Lanini, I. Fodor, G. Eberle, A. Ijspeert, B. Schurch, A. Curt, S. Carda, J. Bloch°, J. von Zitzewitz°, G. Courtine°. Science Translational Medicine. * these authors contributed equally to this work, °co-senior author.

Contribution: 1st co-author.

2017 – *Interactive locomotion: Investigation and modeling of physically-paired humans while walking*, J. Lanini, A. Duburcq, H. Razavi, **C.G. Le Goff**, A.J. Ijspeert. PLoS ONE

Contribution: implementation and operation of the technological framework, methodology, resources and data curation for the experiments with humans.

2016 – *A decision model to predict the risk of the first fall onset*, T. Deschamps*, **C.G. Le Goff***, G. Berrut, C. Cornu, J.-B. Mignardot. Experimental Gerontology. * these authors contributed equally to this work.

Contribution: 1st co-author.

2016 – *Spatiotemporal neuromodulation therapies engaging muscle synergies improve motor control after spinal cord injury*, N. Wenger*, E. Martin Moraud*, J. Gandar*, P. Musienko, M. Capogrosso, L. Baud, **C.G. Le Goff**, Q. Barraud, N. Pavlova, N. Dominici, I.R. Minev, L. Asboth, A. Hirsch, S. Duis, J. Kreider, A. Mortera, O. Haverbeck, S. Kraus, F. Schmitz, J. DiGiovanna, R. van den Brand, J. Bloch, P. Detemple, S.P. Lacour, E. Bezard, S. Micera, G. Courtine. Nature Medicine. * these authors contributed equally to this work.

Contribution: functional data analysis, figures and manuscript preparation.

2015 – *Neuromuscular electrical stimulation leads to physiological gains enhancing postural balance in the pre-frail elderly*, J.-B. Mignardot, T. Deschamps, **C.G. Le Goff**, F.-X. Roumier, J. Duclay, A. Martin, M. Sixt, M. Pousson, C. Cornu. Physiological Reports.

Contribution: data analysis, figures and manuscript editing.

2015 – *Neuroprosthetic technologies to augment the impact of neurorehabilitation after spinal cord injury*, R. van den Brand, J.-B. Mignardot, J. von Zitzewitz, **C. Le Goff**, N. Fumeaux, F. Wagner, M. Capogrosso, E. Martin Moraud, S. Micera, B. Schurch, A. Curt, S. Carda, J. Bloch, G. Courtine. Annals of Physical and Rehabilitation Medicine.

Contribution: manuscript editing.

In preparation – (title and list of authors may change) *Comprehensive gait analysis in humans suffering from Parkinson's disease*, **C.G. Le Goff-Mignardot***, J.B. Mignardot*, Y. Thenaisie, F. Bourre, E. Martin Moraud, J. Bloch°, E. Bezard°, G. Courtine°. * these authors contributed equally to this work, °co-senior author.

Contribution: 1st co-author.

In re-writing process – *Encoding of leg movements across natural locomotor behaviors in the primate motor cortex*, D.A. Borton*, J. Laurens*, J. DiGiovana, **C.G. Le Goff**, S. Micera°, E. Bezard°, G. Courtine°. * these authors contributed equally to this work, °co-senior author.

Contribution: analysis of kinematic data on monkeys, design and implementation of the figure presenting kinematic analysis on monkeys and manuscript editing.

Conference Proceedings

2018 – *Spatiotemporal neuromodulation of the spinal cord combined with robot-assisted training in humans with spinal cord injury (STIMO): Long-term recovery of walking*, **C.G. Le Goff-Mignardot***, J.-B. Mignardot*, F.B. Wagner*, M. Capogrosso, S. Komi, R. Demesmaeker, I. Seanez, M. Vat, L. A. McCracken, M. Caban, A. Watrin, A. Rowald, K. van den Keybus, G. Eberle, B. Schurch, S Carda, E. Pralong, M. Bolliger, J. von Zitzewitz, M. Bakx, R. Buschman, N. Buse, V. Delattre, T. Denison, H. Lambert, A. Curt, K. Minassian°, J. Bloch°, G. Courtine°. Society for Neuroscience (SfN) 2018, 48th Annual Meeting. * these authors contributed equally to this work, °co-senior author.

2018 – *Spatiotemporal neuromodulation of the spinal cord combined with robot-assisted training in humans with spinal cord injury (STIMO): Immediate recovery of walking*, F.B. Wagner*, J.-B. Mignardot*, **C.G. Le Goff-Mignardot***, M. Capogrosso, S. Komi, R. Demesmaeker, I. Seanez, M. Vat, L. A. McCracken, M. Caban, A. Watrin, A. Rowald, K. van den Keybus, G. Eberle, B. Schurch, S Carda, E. Pralong, M. Bolliger, J. von Zitzewitz, M. Bakx, R. Buschman, N. Buse, V. Delattre, T. Denison, H. Lambert, A. Curt, K. Minassian°, J. Bloch°, G. Courtine°. Society for Neuroscience (SfN) 2018, 48th Annual Meeting. * these authors contributed equally to this work, °co-senior author.

2017 – *Spatiotemporal neuromodulation of the spinal cord combined with robot-assisted training in humans with spinal cord injury (STIMO): Technological and conceptual framework*, **C.G. Le Goff***, F.B. Wagner*, J.-B. Mignardot*, M. Capogrosso, I. Seanez-Gonzalez, M. Caban, R. Heimgartner, N. Fumeaux, F. Raschella, A. Watrin, M. Vat, M. Avanthay, I. Fodor, K. van den Keybus, G. Eberle, B. Schurch, S Carda, E. Pralong, M. Bolliger, J. von Zitzewitz, R. Buschman, N. Buse, V. Delattre, S. Micera, T. Denison, H. Lambert, A. Curt, K. Minassian°, J. Bloch°, G. Courtine°. Society for Neuroscience (SfN) 2017, 47th Annual Meeting. * these authors contributed equally to this work, °co-senior author.

2016 – *Gait rehabilitation enabled by epidural electrical stimulation of lumbar segments in a person with a chronic incomplete spinal cord injury*, **C.G. Le Goff***, J.-B. Mignardot*, R. Van Den Brand*, M. Capogrosso, I. Fodor, G. Eberle, B. Schurch, S. Carda, J. von Zitzewitz°, J. Bloch°, G. Courtine°. Society for Neuroscience (SfN) 2016, 46th Annual Meeting. * these authors contributed equally to this work, °co-senior author.

2016 – *Robotic platform maximizing gravity-dependent gait interactions to train standing and walking after neurological disorders*, J.-B. Mignardot*, **C.G. Le Goff***, R. Van Den Brand*, N. Fumeaux, S. Carda, J. von Zitzewitz°, J. Bloch°, G. Courtine°. Society for Neuroscience (SfN) 2016, 46th Annual Meeting. * these authors contributed equally to this work, °co-senior author.

2015 – *A brain spinal interface to alleviate lower limb deficits after neuromotor disorders*, M. Capogrosso, T. Milekovic, D. Borton, E. Martin Moraud, J. Gandar, F. Wagner, **C. Le Goff**, N. Buse, P. Detemple, T. Denison, J. Bloch, E. Bezard, S. Micera, G. Courtine. Society for Neuroscience (SfN) 2015, 45th Annual Meeting.

2014 – *Multidirectional robotic support enables gait rehabilitation under natural conditions in individuals with neuromotor disorders*, J.-B. Mignardot*, J. von Zitzewitz*, **C. Le Goff***, R. Van Den Brand*, J. Bloch, S. Carda, G. Courtine. Society for Neuroscience (SfN) 2014, 44th Annual Meeting. * these authors contributed equally to this work.

Patent

European patent application – *Apparatus comprising a support system for a user and its operation in a gravity-assist mode*, J. von Zitzewitz, J.-B. Mignardot, **C.G.M. Le Goff**, G. Courtine, H. Vallery, M. Plooij, N°16184544.

Camille Le Goff - Mignardot
Swiss & French citizenship
19 June 1990

Rue _____
CP_____
+41 _____
camille.legoff@alumni.epfl.ch

With a translational background at the edge of medicine and engineering, I'm a conscientious and efficient hard-working person, eager to participate to the team effort.

EDUCATION

2015 – 2019 **PhD candidate in Doctoral School of Neuroscience**, Center for Neuroprosthetic & Brain Mind Institute, EPFL (Swiss Federal Institute of Technology) & CHUV (University Hospital of Vaud)

- Prof. G. Courtine laboratory aims at deploying technologies and interventions to restore motor functions after spinal cord injury, working primarily on rodents. My PhD research work started with the design and implementation of the first clinical study conducted by Prof. Courtine, where I established an algorithm, now patented, for the personalization of a robotic trunk assistance to enable unconstraint locomotion. Then, I contributed to transfer and integrate into this innovative environment the technologies previously developed on animal models. In this neuroprosthetic environment, I investigated the ability of the translated neuro-rehabilitation to improve motor control in spinal cord injured individuals.

2011 – 2014 **Master of Science in Bioengineering in the School of Life Sciences and Technologies, Specialization in Neuroprosthetics**, EPFL, CH

- Master project: software development for comprehensive gait analysis of neuromotor-impaired populations – in Prof. Dr. G. Courtine laboratory.
- Specialization project: effect of an interoceptive signal on brain computer interface control – in Prof. Dr. J.R. Millàn laboratory.
- 2014, **EPFL Prize**: reward the best Master project in Neuroprosthetics.
- 2014, **EPFL Prize**: reward the best grade over the Master cycle.

2008 – 2011 **Bachelor of Science in Life Sciences and Technologies**, EPFL, CH

- 2009, **A. Tschumy Prize**: reward the best grade of the 1st year over >1'000 students.
- 2011, **EPFL Prize**: reward the second best grade over the 2nd and 3rd years.

PROFESSIONAL EXPERIENCE

2014 – 2015 Prof. Dr. Courtine Laboratory, Center for Neuroprosthetics and Brain Mind Institute of the Life Science School, EPFL

- **Research Assistant**, 9 months, full time: provide support to lab members for all aspects related to experimental recordings with animals and humans, data analyses, and development of graphical user interfaces in MATLAB.

2011 – 2013 H&LG Consultants sàrl (provision of technological and scientific services in the field of safety, security and surety)

- **Assistant to Research and Development Director**, two years, partial time (~20%): development of computational methods for integration in proprietary software, review and proofreading.

summer 2013 FEDEA School, a Swiss private school for children, teenagers and adults with autism

- **Assistant to Office Manager**, 4 weeks at 60%: preparation of staff planning and classes given to young children suffering from autism.

summer 2011 Debio Recherche Pharmaceutique S.A. (development and manufacturing of controlled-release drugs)

- Internship of 8-weeks, full time: Parametrical optimization of a biotechnological process; my job was to elaborate a method in order to optimize a biotechnological process, which involved the determination of critical parameters, the design and the application of an experimental plan to finally identify the operational optimum.

TRANSVERSAL SKILLS

Languages English (fluent), French (mother tongue).

Knowledge in Neurosciences, Human Physiology, Biomechanics, Cellular and Molecular Biology, Pharmacology, Biotechnologies, Informatics, Brain Computer Interfaces, Dynamical Systems Theory, Machine Learning, Data Analysis and Model Classification, Signal and Image Processing.

Good Clinical Practices (GCPs) for medical device clinical study (certificate up-to-date).

Computer skills Proficient in MATLAB, from data processing to development of user-friendly GUIs.
Adobe Illustrator for data valuation in presentations and high-impact journals.
Basic skills in C/C++/C#, Java, html, LaTex, Unity, ImageJ, TwinCat, TDT (Tucker-Davis Technologies), well-experienced to quickly start and progress in a new computer skill.

Teaching Class representative at the teaching commission (2010-2014).
Teaching assistant for physics classes (2012-2015).

Leisure time Outdoors sports in the mountains, on the rock, ice, snow, and trails.

SCIENTIFIC PRODUCTION

Patent European patent (publication number WO/2018/033591) – Apparatus comprising a support system for a user and its operation in a gravity-assist mode. J. von Zitzewitz, J.-B. Mignardot, C.G.M. Le Goff, G. Courtine, H. Vallery.

Articles in peer-reviewed journals (selection)

- *Targeted neurotechnologies restore walking in humans with spinal cord injury*, C.G. Le Goff-Mignardot*, F. Wagner*, J.-B. Mignardot*, R. Demesmaeker, S. Komi, M. Capogrosso, […], K. Minassian, J. Bloch, G. Courtine. ***Nature***, 2018.
- *Electrical spinal cord stimulation must preserve proprioception to enable locomotion in humans with spinal cord injury*, E. Formento*, M. Capogrosso*, K. Minassian K., F. Wagner F., J.-B. Mignardot, C.G. Le Goff, A. Rowald, J. Bloch, S. Micera, G. Courtine, ***Nature Neuroscience***, 2018.
- *A multidirectional gravity-assist algorithm that enhances locomotor control in patients with stroke or spinal cord*, C.G. Le Goff*, J.-B. Mignardot*, R. van den Brand*, M. Capogrosso, […], G. Courtine. ***Science Translational Medicine***, 2017.
- *A decision model to predict the risk of the first fall onset*, C.G. Le Goff*, T. Deschamps*, G. Berrut, C. Cornu, J.-B. Mignardot. ***Experimental Gerontology***, 2016.
- *Spatiotemporal neuromodulation therapies engaging muscle synergies improve motor control after spinal cord injury*, N. Wenger*, E. Martin Moraud*, J. Gandar*, P. Musienko, M. Capogrosso, L. Baud, C.G. Le Goff, […], J. Bloch, P. Detemple, S.P. Lacour, E. Bézard, S. Micera, G. Courtine. ***Nature Medicine***, 2016.
- *Neuromuscular electrical stimulation leads to physiological gains enhancing postural balance in the pre-frail elderly*, J.-B. Mignardot*, T. Deschamps, C.G. Le Goff, […], M. Pousson, C. Cornu. ***Physiological Reports***, 2015.

**these authors contributed equally.*

Appendix A

Gait parameters

	#	Code	Details	Comments (for users)
	A	ID	subject ID	
	B	File	filename	
	C	Cond1	condition 1 (neuromotor disorder status)	
	D	Cond2	condition 2 (task)	
	E	Cond3	condition 3 (assistive device)	
	F	Side	Leg side (L or R)	
	G	BWS	vertical assistance by FLOAT [%BW]	
	H	Forward F	forward assistance by FLOAT [%BW or kg]	Unit needs to be chosen depending on the case
	I	Lateral F	lateral assistance by FLOAT [%BW or kg]	Unit needs to be chosen depending on the case
	J	Cycle	cycle number	
Spatiotemporal parameters				
	1	D_Cycle	GC duration [s]	
	2	D_Step	step duration [s]	
	3	P_stance	stance duration [%GC]	
	4	P_swing	swing duration [%GC]	
	5	P_drag	drag duration [%GC]	
	6	P_drag in swing	drag duration [%swing]	
	7	P_single stance	single stance duration [%GC]	
	8	P_double stance	double stance duration [%GC]	
	9	L_Step length	step length [%BH]	AJC of foot
	10	L_Stride length	stride length [%BH]	AJC of both feet
	11	L_Step width	step width [%BH]	AJC of both feet
	12	V_Stride	stride speed [m/s]	
	13	L_Stride length (CoM)	stride length at CoM [%BH]	
	14	V_Stride (CoM)	stride speed at CoM [m/s]	
	15	L_Foot trajectory	length of foot trajectory [%BH]	
	16	L_CoM trajectory	length of CoM trajectory [%BH]	CoM trajectory during GC
	17	A_Step height	step height [%BH]	max amplitude of AJC on vertical axis
	18	A_Lateral movement	lateral movement during swing [%BH]	max amplitude of AJC on lateral axis
	19	A_Hip vertical movement	maximal hip vertical amplitude during GC [%BH]	
Joint angles				
	20	MIN_Hip Flex	minimal hip flexion/extension angle [deg]	minimal hip angle
	21	MAX_Hip Flex	maximal hip flexion/extension angle [deg]	maximal hip angle
	22	A_Hip Flex	amplitude of hip flexion/extension angle [deg]	max - min of hip angle
	23	MIN_Knee Flex	minimal knee flexion/extension angle [deg]	
	24	MAX_Knee Flex	maximal knee flexion/extension angle [deg]	
	25	A_Knee Flex	amplitude of knee flexion/extension angle [deg]	
	26	MIN_Ankle Flex	minimal ankle flexion/extension angle [deg]	
	27	MAX_Ankle Flex	maximal ankle flexion/extension angle [deg]	
	28	A_Ankle Flex	amplitude of ankle flexion/extension angle [deg]	
Elevation angles				
	29	MIN_Femur	minimal femur elevation angle [deg]	
	30	MAX_Femur	maximal femur elevation angle [deg]	
	31	A_Femur	amplitude of femur elevation angle [deg]	
	32	MIN_Tibia	minimal tibia elevation angle [deg]	
	33	MAX_Tibia	maximal tibia elevation angle [deg]	
	34	A_Tibia	amplitude of tibia elevation angle [deg]	
	35	MIN_Foot	minimal foot elevation angle [deg]	
	36	MAX_Foot	maximal foot elevation angle [deg]	
	37	A_Foot	amplitude of foot elevation angle [deg]	
	38	MIN_Leg	minimal leg elevation angle [deg]	
	39	MAX_Leg	maximal leg elevation angle [deg]	
	40	A_Leg	amplitude of leg elevation angle [deg]	
	41	MIN_Arm	minimal arm elevation angle [deg]	
	42	MAX_Arm	maximal arm elevation angle [deg]	
	43	A_Arm	amplitude of arm elevation angle [deg]	
Angular velocity				
	44	MAX_V_Hip Flex	maximal speed of hip flexion/extension angle [deg/s]	
	45	MAX_V_Knee Flex	maximal speed of knee flexion/extension angle [deg/s]	
	46	MAX_V_Ankle Flex	maximal speed of ankle flexion/extension angle [deg/s]	
	47	MAX_V_Femur	maximal speed of femur elevation angle [deg/s]	
	48	MAX_V_Tibia	maximal speed of tibia elevation angle [deg/s]	
	49	MAX_V_Foot	maximal speed of foot elevation angle [deg/s]	
	50	MAX_V_Leg	maximal speed of leg elevation angle [deg/s]	
	51	MAX_V_Arm	maximal speed of arm elevation angle [deg/s]	
Intra and Interlimb coordination (frequency domain)				
	52	FFTphase_FemurTibia	difference of phase between femur and tibia elevation angles [deg]	
	53	FFTphase_FemurFoot	difference of phase between femur and foot elevation angles [deg]	
	54	FFTphase_TibiaFoot	difference of phase between tibia and foot elevation angles [deg]	
	55	FFTphase_HipKnee	difference of phase between hip and knee joint angles [deg]	
	56	FFTphase_HipAnkle	difference of phase between hip and ankle joint angles [deg]	
	57	FFTphase_KneeAnkle	difference of phase between knee and ankle joint angles [deg]	(-180 <= phase lag <= 180)
	58	FFTphase_ArmIpsi ArmContra	difference of phase between ipsi- and contra-arm angles [deg]	
	59	FFTphase_LegIpsi LegContra	difference of phase between ipsi- and contra-leg angles [deg]	
	60	FFTphase_ArmIpsi LegIpsi	difference of phase between ipsi-arm and ipsi-leg angles [deg]	
	61	FFTphase_ArmIpsi LegContra	difference of phase between ipsi-arm and contra-leg angles [deg]	
Intra and Interlimb coordination (time domain)				
	62	Lag_FemurTibia	shift between femur and tibia elevation angles to obtain maximal correlation [%GC]	

63	Lag_FemurFoot	shift between femur and foot elevation angles to obtain maximal correlation [%GC]	
64	Lag_TibiaFoot	shift between tibia and foot elevation angles to obtain maximal correlation [%GC]	(-50% <= lag <= +50%)
65	Lag_HipKnee Flex	shift between hip and knee joint angles to obtain maximal correlation [%GC]	
66	Lag_HipAnkle Flex	shift between hip and ankle joint angles to obtain maximal correlation [%GC]	
67	Lag_KneeAnkle Flex	shift between knee and ankle joint angles to obtain maximal correlation [%GC]	
68	R_FemurTibia	maximal correlation between femur and tibia elevation angles	
69	R_FemurFoot	maximal correlation between femur and foot elevation angles	
70	R_TibiaFoot	maximal correlation between tibia and foot elevation angles	(-1 <= R <= 1)
71	R_HipKnee Flex	maximal correlation between hip and knee joint angles	
72	R_HipAnkle Flex	maximal correlation between hip and ankle joint angles	
73	R_KneeAnkle Flex	maximal correlation between knee and ankle joint angles	
74	Lag_Coord_Arm	shift between arms elevation angles to obtain maximal correlation [%GC]	
75	Lag_Coord_Leg	shift between legs elevation angles to obtain maximal correlation [%GC]	
76	Lag_Coord_Femur	shift between femur elevation angles to obtain maximal correlation [%GC]	
77	Lag_Coord_Tibia	shift between tibia elevation angles to obtain maximal correlation [%GC]	(-50% <= lag <= +50%)
78	Lag_Coord_Foot	shift between foot elevation angles to obtain maximal correlation [%GC]	
79	Lag_Coord_Hip Flex	shift between hip joint angles to obtain maximal correlation [%GC]	
80	Lag_Coord_Knee Flex	shift between knee joint angles to obtain maximal correlation [%GC]	
81	Lag_Coord_Ankle Flex	shift between ankle joint angles to obtain maximal correlation [%GC]	
82	R_Coord_Arm	maximal correlation between arms elevation angles	
83	R_Coord_Leg	maximal correlation between legs elevation angles	
84	R_Coord_Femur	maximal correlation between femur elevation angles	
85	R_Coord_Tibia	maximal correlation between tibia elevation angles	
86	R_Coord_Foot	maximal correlation between foot elevation angles	(-1 <= R <= 1)
87	R_Coord_Hip Flex	maximal correlation between hip joint angles	
88	R_Coord_Knee Flex	maximal correlation between knee joint angles	
89	R_Coord_Ankle Flex	maximal correlation between ankle joint angles	
90	Lag_ArmIpsi ArmContra	shift between ipsi- and contra-arm elevation angles to obtain maximal correlation [%GC]	
91	Lag_LegIpsi LegContra	shift between ipsi- and contra-leg elevation angles to obtain maximal correlation [%GC]	
92	Lag_ArmIpsi LegIpsi	shift between ipsi-arm and ipsi-leg elevation angles to obtain maximal correlation [%GC]	(-50% <= lag <= +50%)
93	Lag_ArmIpsi LegContra	shift between ipsi-arm and contra-leg elevation angles to obtain maximal correlation [%GC]	
94	R_ArmIpsi ArmContra	maximal correlation between ipsi- and contra-arm elevation angles	
95	R_LegIpsi LegContra	maximal correlation between ipsi- and contra-leg elevation angles	
96	R_ArmIpsi LegIpsi	maximal correlation between ipsi-arm and ipsi-leg elevation angles	(-1 <= R <= 1)
97	R_ArmIpsi LegContra	maximal correlation between ipsi-arm and contra-leg elevation angles	
Planar covariation of leg elevation angles			
98	PC_Path length	path length (PC1 variance) [%]	
99	PC_Path width	path width (PC2 variance) [%]	
100	PC_Planarity	planarity factor (percent of variance accounted for by the two first PCs) [%]	PCA applied on 3d space formed by foot, tibia and femur elevation angles (they covary in a plane during walking)
101	PC_Orientation - Thigh	spatial orientation (angle between thigh axis and PC3 direction) [deg]	
102	PC_Orientation - Shank	spatial orientation (angle between shank axis and PC3 direction) [deg]	
103	PC_Orientation - Foot	spatial orientation (angle between foot axis and PC3 direction) [deg]	
Trunk stability			
104	Trunk_BaryC_L_path	distance travelled by trunk barycenter in frontal plane [%BH]	
105	Trunk_BaryC_A_lateral	amplitude of trunk barycenter on lateral axis [%BH]	
106	Trunk_BaryC_A_vertical	amplitude of trunk barycenter on vertical axis [%BH]	
107	Trunk_BaryC_L_path (rot)	distance travelled by trunk barycenter in frontal plane [%BH]	
108	Trunk_BaryC_A_lateral (rot)	amplitude of trunk barycenter on lateral axis [%BH]	rotated in Body Reference Frame
109	Trunk_BaryC_A_vertical (rot)	amplitude of trunk barycenter on vertical axis [%BH]	
110	Trunk_Rollmean_2stance	mean of trunk roll angle during double stance [deg]	
111	Trunk_Rollmax_SingleStance	maximal absolute roll angle during single stance [deg]	
112	Trunk_Rollamp_SingleStance	amplitude of roll angle during single stance [deg]	roll angle = angle between trunk in frontal plane and gravity vector
113	Trunk_Rollmax_Swing	maximal absolute roll angle during swing [deg]	
114	Trunk_Rollamp_Swing	amplitude of roll angle during swing [deg]	
Feet trajectory and base of support			
115	Feet_A_BoS	maximal distance between both feet [%BH]	sum of maximal absolute distance between toe marker and CoM of both feet
116	Feet_A_Swing	maximal distance of foot from center line during swing [%BH]	foot position is given by AJC, center line by CoM
117	Feet_O_Stance	mean angle of foot during stance [deg]	angle between foot (Heel to Toe markers) and center line
118	Feet_A_BoS (rot)	maximal distance between both feet [%BH]	
119	Feet_A_Swing (rot)	maximal distance of foot from center line during swing [%BH]	scalar product with lateral axis
120	Feet_O_Stance (rot)	mean angle of foot during stance [deg]	
EMG params			
121	D_AnkleExtensor	burst duration of ankle extensor [%GC]	
122	D_AnkleFlexor	burst duration of ankle flexor [%GC]	
123	ONSET_AnkleExtensor	onset of ankle extensor burst [%GC]	
124	ONSET_AnkleFlexor	onset of ankle flexor burst [%GC]	
125	END_AnkleExtensor	end of ankle extensor burst [%GC]	
126	END_AnkleFlexor	end of ankle flexor burst [%GC]	
127	RMS_AnkleExtensor	root mean square of ankle extensor burst [mV]	not normalized
128	RMS_AnkleFlexor	root mean square of ankle flexor burst [mV]	not normalized
129	A_AnkleExtensor	maximal amplitude of ankle extensor burst [mV*100]	not normalized
130	A_AnkleFlexor	maximal amplitude of ankle flexor burst [mV*100]	not normalized
131	D_KneeExtensor	burst duration of knee extensor [%GC]	
132	D_KneeFlexor	burst duration of knee flexor [%GC]	
133	ONSET_KneeExtensor	onset of knee extensor burst [%GC]	
134	ONSET_KneeFlexor	onset of knee flexor burst [%GC]	
135	END_KneeExtensor	end of knee extensor burst [%GC]	
136	END_KneeFlexor	end of knee flexor burst [%GC]	
137	RMS_KneeExtensor	root mean square of knee extensor burst [mV]	not normalized
138	RMS_KneeFlexor	root mean square of knee flexor burst [mV]	not normalized
139	A_KneeExtensor	maximal amplitude of knee extensor burst [mV*100]	not normalized
140	A_KneeFlexor	maximal amplitude of knee flexor burst [mV*100]	not normalized

Appendix B

Gait report

CONDITIONS

Label	Description		ID	Date	BWS	EES	Task
H	Healthy						
C1	date 201609131539	SCI	BT001	20160913-1539	50%	no	TMBaselineNoStim
C2	date 201609131545	SCI	BT001	20160913-1545	50%	yes	TMLeftPhasic
C3	date 201609131556	SCI	BT001	20160913-1556	50%	yes	TMLeftTonicHigh
C4	date 201609131558	SCI	BT001	20160913-1558	50%	yes	TMLeftTonicLow

PRINCIPAL COMPONENT ANALYSIS

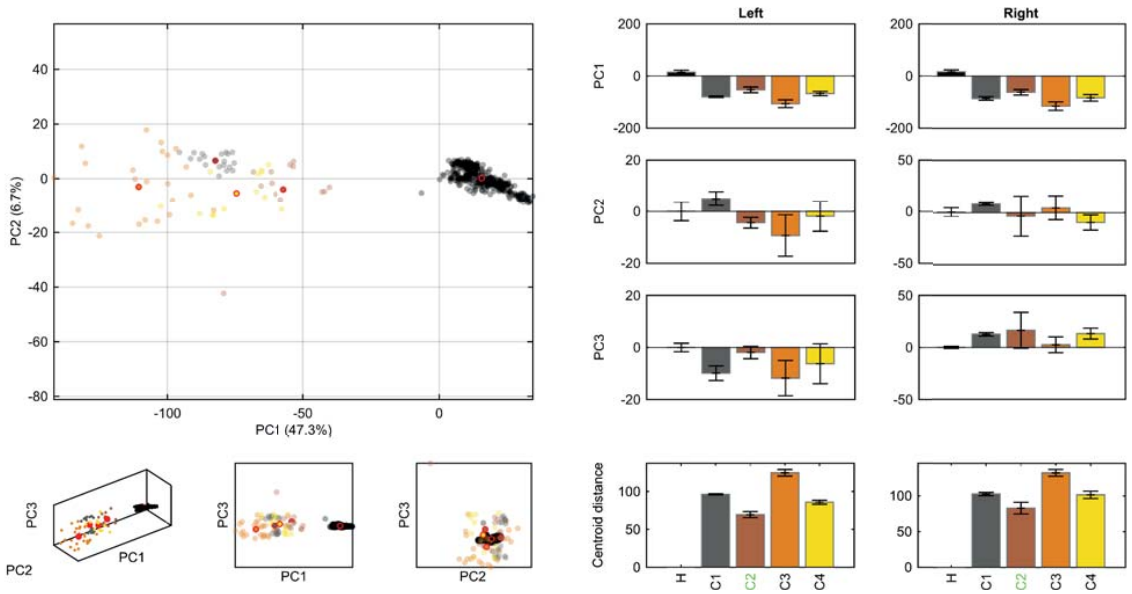

Main kinematic parameters

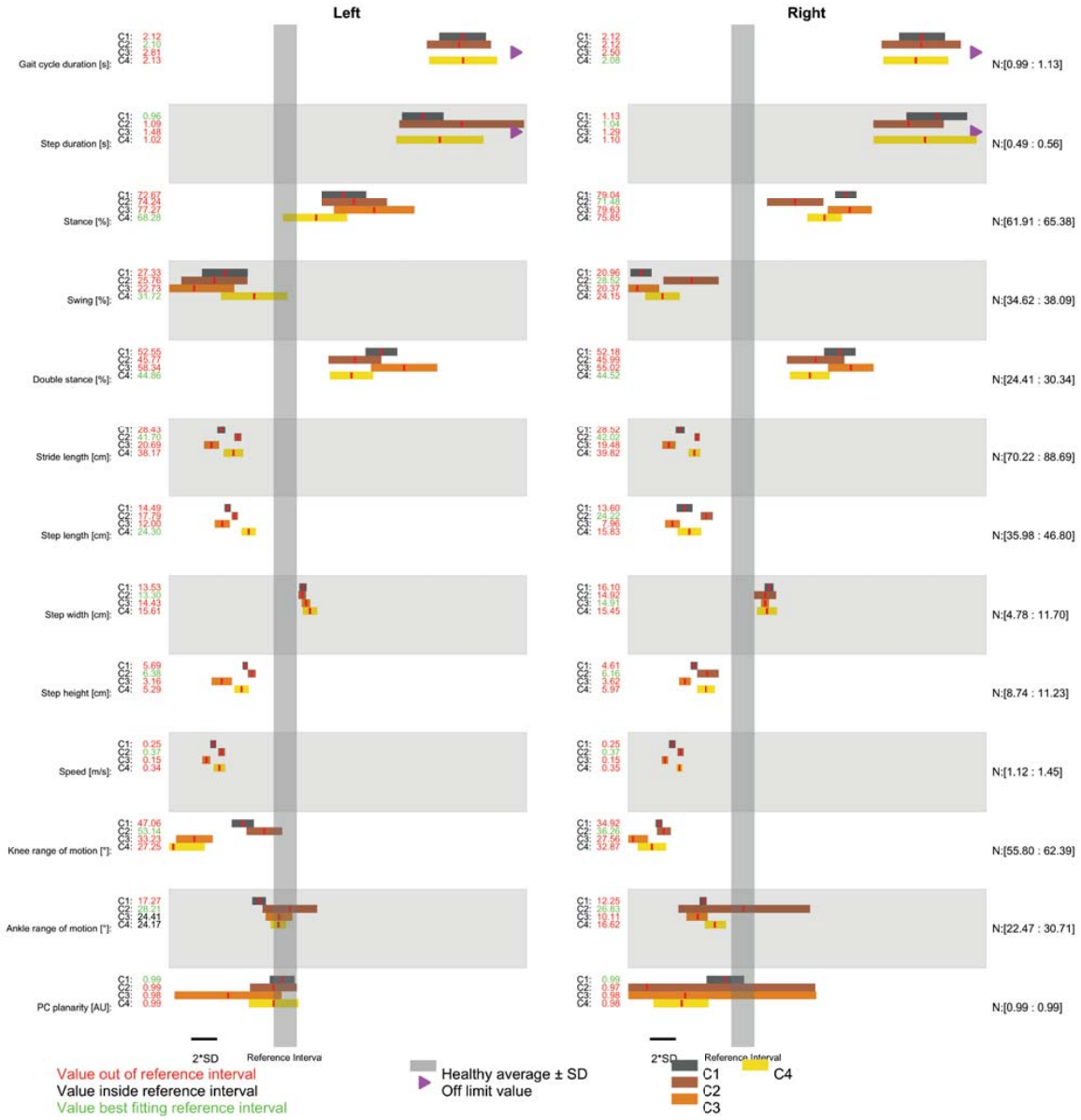

ANGULAR TIME SERIES

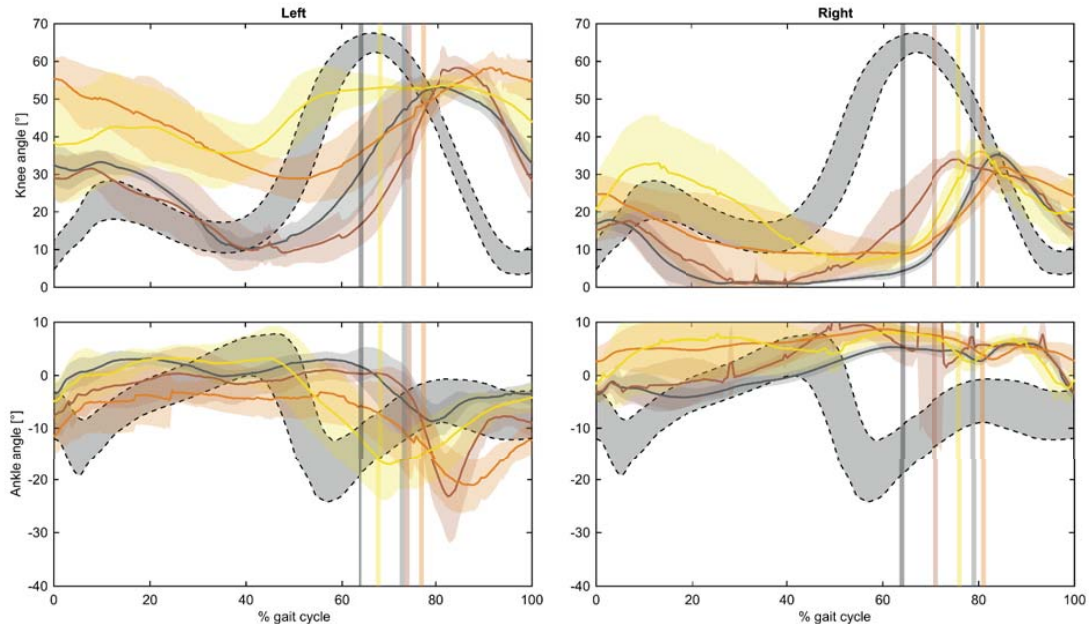

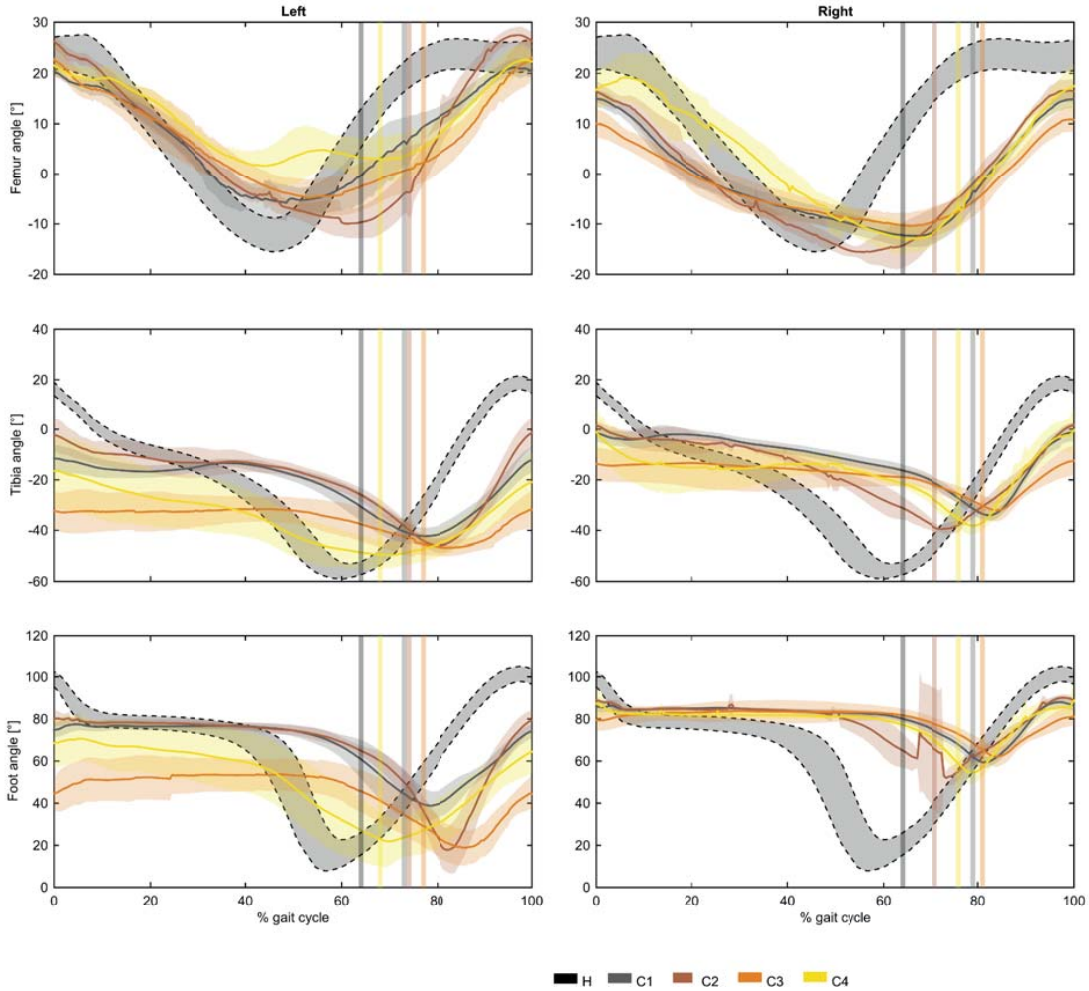

STICK DIAGRAMS & PLANAR COVARIATION

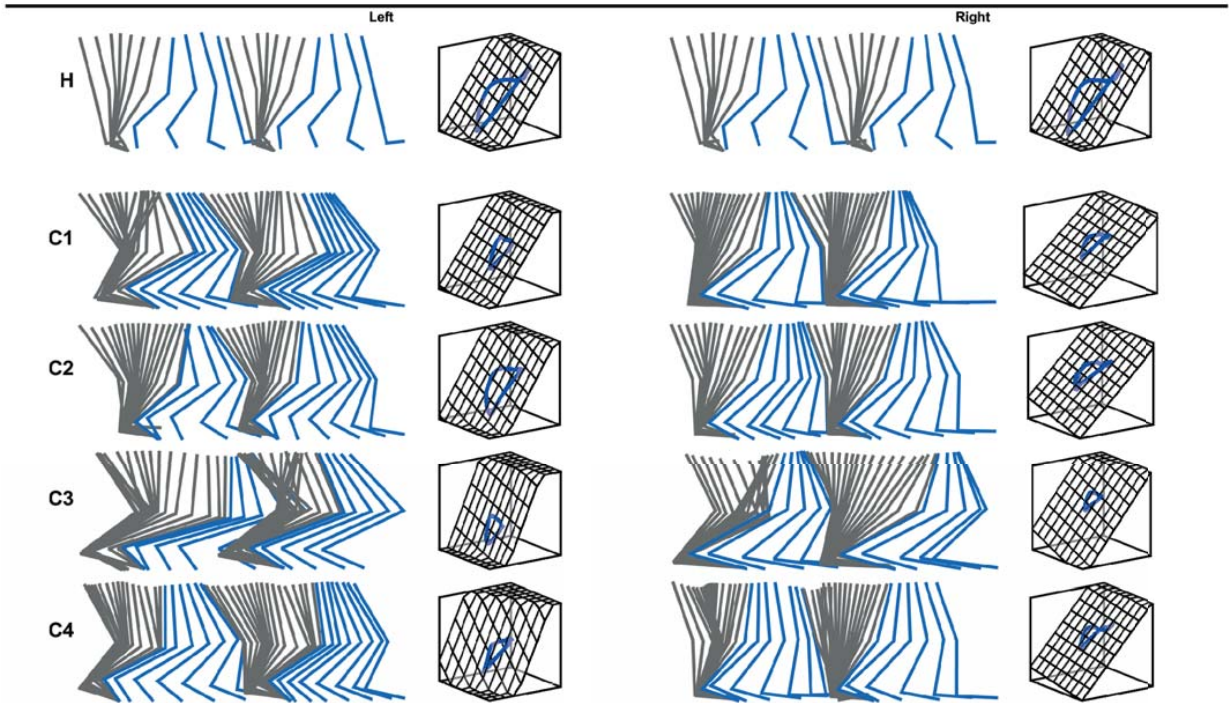

ÉCOLE POLYTECHNIQUE FÉDÉRALE DE LAUSANNE

Centre hospitalier universitaire vaudois

ALL VARIABLES USED FOR PCA

Variable	H		C1		C2		C3		C4	
	MEAN	SD	L	R	L	R	L	R	L	R
1 - D Cycle	1.1	0.1	2.1	2.1	2.1	2.1	2.8	2.5	2.1	2.1
2 - D Step	0.5	0.0	1.0	1.1	1.1	1.0	1.5	1.3	1.0	1.1
3 - P stance	63.6	1.7	72.7	79.0	74.2	71.5	77.3	79.6	68.3	75.8
4 - P swing	36.4	1.7	27.3	21.0	25.8	28.5	22.7	20.4	31.7	24.2
5 - P singleStance	36.3	1.8	20.7	26.9	28.7	25.5	18.9	24.8	22.9	31.3
6 - P doubleStance	27.4	3.0	52.6	52.2	45.8	46.0	58.3	55.0	44.9	44.5
7 - L StepLength	41.4	5.4	14.5	13.6	17.8	24.2	12.0	8.0	24.3	15.8
8 - L StrideLength	79.5	9.2	28.4	28.5	41.7	42.0	20.7	19.5	38.2	39.8
9 - L StepWidth	8.2	3.5	13.5	16.1	13.3	14.9	14.4	14.9	15.6	15.4
10 - V Stride	1.3	0.2	0.2	0.3	0.4	0.4	0.1	0.1	0.3	0.4
11 - L FootTrajectory	68.6	7.4	24.5	27.5	38.9	42.7	19.0	19.3	31.9	43.4
12 - A StepHeight	10.0	1.2	5.7	4.6	6.4	6.2	3.2	3.6	5.3	6.0
13 - A LateralMovement	31.5	19.9	17.8	17.2	24.0	21.1	20.3	21.2	30.5	20.1
14 - A HipVerticalMovement	3.0	0.7	2.2	1.7	3.2	2.4	2.3	2.6	2.1	2.5
15 - MIN AnkleFlex	-23.1	6.4	-12.4	-5.5	-25.1	-5.8	-23.5	0.4	-18.1	-5.5
16 - MAX AnkleFlex	3.5	4.1	4.8	6.8	3.1	21.1	1.0	10.5	6.0	11.1
17 - A AnkleFlex	26.6	4.1	17.3	12.2	28.2	26.8	24.4	10.1	24.2	16.6
18 - MIN KneeFlex	5.7	3.6	8.7	0.6	8.0	0.4	26.8	6.1	29.9	5.6
19 - MAX KneeFlex	64.8	3.7	55.7	35.5	61.1	36.6	60.0	33.6	57.2	38.5
20 - A KneeFlex	59.1	3.3	47.1	34.9	53.1	36.3	33.2	27.6	27.3	32.9
21 - MIN Femur	-13.2	3.8	-6.8	-12.5	-10.3	-16.8	-5.7	-10.9	0.4	-14.0
22 - MAX Femur	25.1	3.2	21.8	16.4	27.9	18.1	25.3	12.2	23.7	20.9
23 - A Femur	38.3	4.2	28.6	28.8	38.2	34.9	31.0	23.1	23.3	34.8
24 - MIN Tibia	-56.3	3.0	-44.7	-34.2	-46.6	-40.8	-47.3	-32.7	-49.8	-38.8
25 - MAX Tibia	19.3	3.1	-7.6	0.9	2.0	2.3	-24.5	-6.9	-10.9	3.0
26 - A Tibia	75.6	4.2	37.1	35.1	48.6	43.2	22.8	25.8	39.0	41.8
27 - MIN Foot	11.4	7.1	32.7	59.2	14.1	49.6	16.2	61.7	20.8	53.8
28 - MAX Foot	100.6	3.5	79.0	89.1	83.7	97.4	59.2	85.7	74.7	92.3
29 - A Foot	89.2	6.0	46.3	29.9	69.6	47.7	43.0	24.0	53.9	38.6
30 - MIN Leg	-27.9	2.9	-15.6	-17.9	-20.2	-24.6	-19.7	-17.0	-20.8	-22.1
31 - MAX Leg	21.3	2.1	7.8	8.2	15.4	9.4	1.0	2.2	7.5	9.7
32 - A Leg	49.2	3.8	23.3	26.1	35.6	34.0	20.7	19.2	28.3	31.8
33 - MAX V AnkleFlex	140.5	35.9	77.7	53.9	146.6	304.1	147.0	44.1	75.9	104.4
34 - MAX V KneeFlex	316.5	26.1	139.9	131.3	184.3	152.6	122.2	79.2	90.2	166.2
35 - MAX V Femur	187.6	15.9	79.3	70.8	126.2	91.2	86.8	46.1	57.1	111.8
36 - MAX V Tibia	368.4	18.2	102.0	149.4	188.3	131.4	78.9	79.9	91.7	164.7
37 - MAX V Foot	385.6	27.9	140.7	143.5	289.6	373.4	173.8	92.0	126.9	185.6
38 - MAX V Leg	191.6	15.7	64.0	100.7	110.4	89.3	65.9	59.3	62.8	115.9
39 - FFTphase FemurTibia	42.4	5.2	93.3	69.3	72.2	55.2	82.6	79.2	34.4	43.2
40 - FFTphase FemurFoot	54.5	5.2	101.5	81.9	91.3	57.1	104.5	103.3	53.8	59.2
41 - FFTphase FemurLeg	24.7	3.6	39.9	33.9	28.4	29.3	22.0	33.1	19.7	11.9
42 - FFTphase TibiaFoot	12.1	2.4	8.3	12.5	19.1	17.9	37.3	39.1	19.4	55.1
43 - FFTphase TibiaLeg	17.6	1.8	53.3	35.5	43.8	25.9	63.7	48.3	14.6	41.0
44 - FFTphase FootLeg	29.8	2.7	61.6	48.0	62.9	36.7	82.6	74.9	34.1	47.3
45 - FFTphase AnkleKnee	55.2	47.5	158.7	67.8	151.4	78.9	131.6	102.9	137.4	88.3
46 - FFTphase IpsiContra Femur	176.8	2.6	174.2	173.0	174.6	174.7	164.0	166.3	163.1	164.0
47 - FFTphase IpsiContra Tibia	177.4	2.0	161.5	159.2	158.8	159.9	110.2	101.9	88.6	117.4
48 - FFTphase IpsiContra Foot	176.8	2.7	164.1	164.0	150.0	143.7	151.5	151.3	128.8	126.1
49 - FFTphase IpsiContra Leg	178.0	1.5	173.5	174.5	172.9	174.6	146.0	156.0	166.0	165.4
50 - Lag FemurTibia	86.4	1.1	53.8	52.2	76.3	59.3	39.3	35.3	48.4	65.2
51 - Lag FemurFoot	84.7	1.1	51.4	22.4	45.3	30.2	27.2	23.5	41.3	69.7
52 - Lag FemurLeg	86.6	14.1	54.5	92.8	93.0	85.0	80.8	90.5	74.6	89.2
53 - Lag TibiaFoot	28.8	45.0	88.4	0.1	98.0	17.2	54.6	37.4	83.4	16.5
54 - Lag TibiaLeg	3.9	0.4	63.2	4.0	5.7	4.3	49.2	27.8	1.7	1.5
55 - Lag FootLeg	5.0	0.6	72.5	11.3	18.4	14.2	71.5	59.6	37.9	3.0
56 - Lag AnkleKnee Flex	72.3	7.9	18.4	51.6	49.4	52.5	38.7	46.5	36.0	51.7
57 - R FemurTibia	0.9	0.0	0.9	0.9	0.8	0.9	0.8	0.8	0.9	0.6
58 - R FemurFoot	0.9	0.0	0.9	0.8	0.8	0.8	0.9	0.9	0.9	0.7
59 - R FemurLeg	1.0	0.0	0.9	0.9	1.0	1.0	0.9	0.9	0.9	0.9
60 - R TibiaFoot	1.0	0.0	1.0	1.0	0.9	0.9	0.9	0.9	0.9	0.9
61 - R TibiaLeg	1.0	0.0	0.9	0.9	0.9	0.9	0.8	0.8	1.0	0.8
62 - R FootLeg	0.9	0.0	0.9	0.8	0.8	0.8	0.8	0.8	0.9	0.8
63 - R AnkleKnee Flex	0.8	0.0	0.8	0.9	0.8	0.8	0.9	0.8	0.8	0.7
64 - Lag Coord Femur	49.8	1.0	63.6	29.3	36.9	50.2	47.1	52.3	54.4	21.8
65 - Lag Coord Tibia	49.7	0.8	51.9	47.0	54.4	45.5	44.6	55.8	55.4	44.0
66 - Lag Coord Foot	49.6	1.1	51.3	47.8	59.4	40.2	55.0	54.7	46.0	52.0
67 - Lag Coord Leg	49.8	0.7	51.6	48.0	51.3	49.0	46.8	49.1	50.9	49.5
68 - Lag Coord Ankle Flex	50.0	5.5	29.5	64.2	34.4	66.2	61.8	34.8	55.1	35.7
69 - Lag Coord Knee Flex	49.6	0.9	35.1	56.0	57.3	42.8	33.8	76.1	58.7	49.8
70 - R Coord Femur	1.0	0.0	0.9	0.9	1.0	1.0	0.9	0.9	0.9	0.9
71 - R Coord Tibia	1.0	0.0	0.9	0.9	0.9	0.9	0.8	0.8	0.7	0.7
72 - R Coord Foot	1.0	0.1	0.9	0.9	0.9	0.9	0.9	0.9	0.7	0.8
73 - R Coord Leg	1.0	0.0	1.0	1.0	1.0	1.0	0.9	0.9	0.9	0.9
74 - R Coord Ankle Flex	0.9	0.1	0.8	0.7	0.7	0.7	0.8	0.8	0.7	0.7
75 - R Coord Knee Flex	1.0	0.0	0.9	0.9	0.9	0.9	0.9	0.9	0.8	0.7
76 - PC PathLength	0.9	0.0	0.8	0.7	0.7	0.7	0.7	0.7	0.9	0.7
77 - PC PathWidth	0.1	0.0	0.2	0.3	0.3	0.2	0.3	0.3	0.1	0.2
78 - PC Planarity	1.0	0.0	1.0	1.0	1.0	1.0	1.0	1.0	1.0	1.0
79 - PC Orientation Thigh	106.7	3.6	97.1	83.9	103.3	77.7	90.8	97.3	105.1	87.2
80 - PC Orientation Shank	41.6	4.8	38.5	128.6	36.3	100.7	32.8	72.9	47.0	99.4
81 - PC Orientation Foot	126.1	4.5	127.4	39.2	122.9	81.5	108.9	96.0	104.3	69.9

**Ce document a été imprimé au Centre d'impression EPFL,
imprimerie climatiquement neutre, certifiée myClimate.**